Lanthanide Nanoparticles in Immunodiagnostics

By

Johnathon Robert Lilley

A thesis submitted to

The University of Birmingham

For the degree of

DOCTOR OF PHILOSOPHY

School of Chemistry

University of Birmingham

College of Engineering and Physical Sciences

September 2017

i Abstract

This thesis shows the surface functionalisation of gold nanoparticles with surface active, luminescent Eu complexes and free light chain antibodies, to produce free light chain antibody functionalised gold nanoparticles which show characteristic, Eu luminescence.

We show how these particles can be used in the development of a novel FRET based assay whereby the Eu luminescence is quenched on addition of free light chain specific antibody, labelled with a suitable organic FRET acceptor for Eu luminescence as measured by lifetime measurements. We show how these particles can be used to develop a competitive immunoassay to measure the concentration of free light chain antibodies.

We also report the preparation of a novel functionalised dibenzoylmethane molecule with a thiol surface active group as to functionalise gold nanoparticles which can bind and sensitize Eu ions.

ii Acknowledgments

First and foremost, I would like to thank my supervisor Professor Zoe Pikramenou for giving me the opportunity to study in her group on this project which has been a great experience and learning curve and a fantastic yet challenging four years and for all her help and encouragement along the way. I would also like to extend my thanks to my second supervisor Professor Mark Drayson and Dr. Margaret Goodall for their help and assistance.

I would like to thank members of the office, Chris Stepanek, Sunil Claire, Sam Adams, Suleman Khan, Sajni Haria, Andrew Carrod all the masters and project students who turned up for making the workplace a good environment and being a fantastic bunch of both colleagues and friends. In particular I would like to mention both Shani Osborne and Siobhan King for both of their support and being great friends in and out of the office.

I would like to thank other people around the department for their friendship and support along the way including Greg O'Callaghan, William Britain, Louise Slope, Phil Jemmett, and everyone else who attends staff house fridays, and also other friends who have been in Birmingham for their pub based support. Also, all the other analytical and maintenance staff throughout the department for all their hard work.

Finally, to my family, the support of whom has been invaluable when things have not been going well, both in and out of the lab, and for constantly asking the question, '… So when exactly will you leave university?'.

iii Contents

iv Abbreviations

Ab	antibody
ABCN	1,1'-Azobis(cyclohexanecarbonitrile)
acac	acetylacetone
AF	Alexafuor
Ag	antigen
AuNP	gold nanoparticle
BJ	Bence Jones
bpy	bipyridine
BSA	bovine serum albumin
CEA	carcinoembryonic antigen
COSY	correlation spectroscopy
Cr	constant region
CTnI	cardiac troponin I
dcm	dichloromethane
DELFIA	dissociation enhanced lanthanide fluorescent assay
DLS	dynamic light scattering
DOTA	tetraazacyclododecane-1,4,7,10-tetraacetic acid
DPTA	diethylenetriaminepentaacetic acid
E2	estradiol
ELISA	enzyme-linked immunoabsorbant assay
ER-β	estrogen receptor β
F(ab)	antigen binding fragment
FCS	foetal calf serum
Fc	crystallisable fragment
FITC	fluorescein
FLC	free light chain
FRET	Förster resonance energy transfer
FWHM	full width at half maximum
HBsAg	hepatitis B surface antigen
HC	heavy chain
HMBC	heteronuclear multiple bond correlation
HPLC	high pressure liquid chromatography
HRP	horseradish peroxidaise
HSQC	heteronuclear single quantum coherence
I	emission intensity
ICPMS	inductively coupled plasma mass spectrometry
IgG	immunoglobin G
J	total angular momentum quantum number
$J(\lambda)$	spectral overlap integral
k^{FRET}	rate of Förster resonance energy transfer
L	total orbital angular momentum quantum number
LC	light chain
LFSE	ligand field stabilisation energy

Ln	lanthanide
LOD	limit of detection
MS	mass spectrometry
NIR	near infra-red
NMR	nuclear magnetic resonance
NP	nanoparticle
NSB	nonspecifc binding
PBS	phosphate buffered saline
PDI	polydispersity index
phen	phenanthroline
PMT	photomultiplyer tube
ppm	parts per million
ppy	phenylpyridine
PSA	prostate specific antigen
q	number of inner sphere coordinated water molecules
QD	quantum dot
r	donor – acceptor distance
RT	room temperature
S	total spin angular momentum quantum number
S_0	singlet ground state
S_1	first excited singlet state
SA	streptavidin
SPR	surface plasmon resonance
T_1	first excited triplet state
TBAOH	Tetrabutylammonium hydroxide
TEA	triethylamine
TEM	transmission electron microscopy
TFA	trifluoroacetic acid
TFS	TransFluoroSphere
TMP	3,3′,5,5′-tetramethylbenzidine dihydrochloride
TOF	time of flight
TR	time resolved
TSH	thyroid stimulating hormone
UCP	upconverting phosphor
UV	ultra violet
vis	Visible
Vr	variable region
ε	molar absorptivity
κ	Kappa
λ	Lambda
λ_{em}	emission wavelength
λ_{exc}	excitation wavelength
τ	lifetime of excited state
Φ	emission quantum yield
Φ_T	energy transfer efficiency

Compound numbers and names as discussed in text:

Compound Number / Name	**Structure**
1	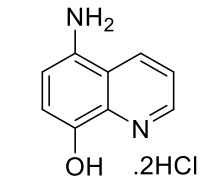
2	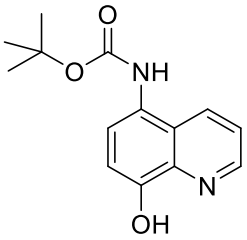
3	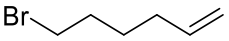
4	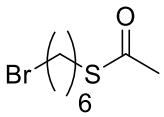
5	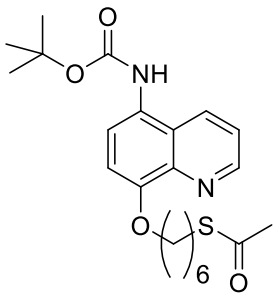
6	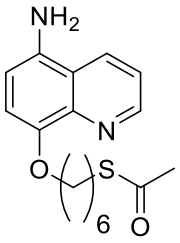

7	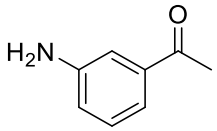
8	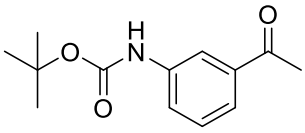
9	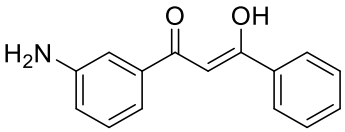
DTPA-bisanhydride	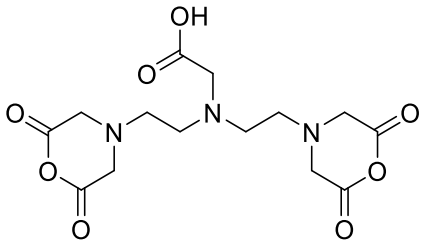
H_3QuinSAc	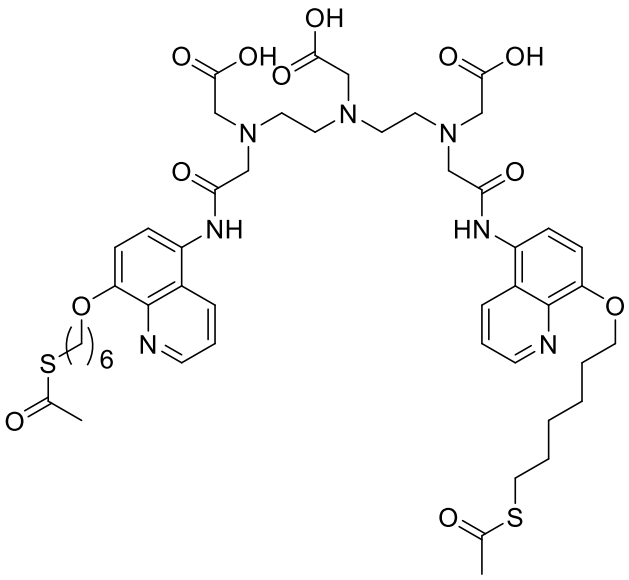

H_3SH	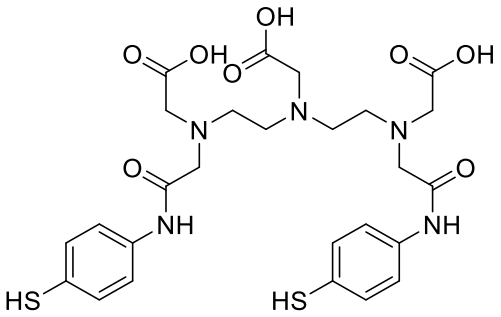
H_3QSH	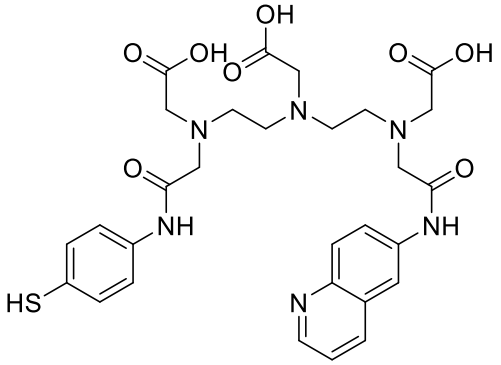
H_3Quin	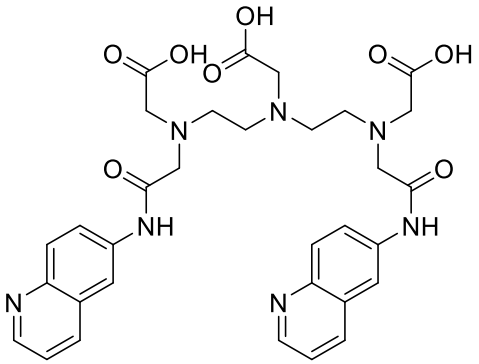
DBMSS	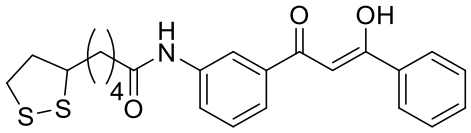

EuQuinSAc	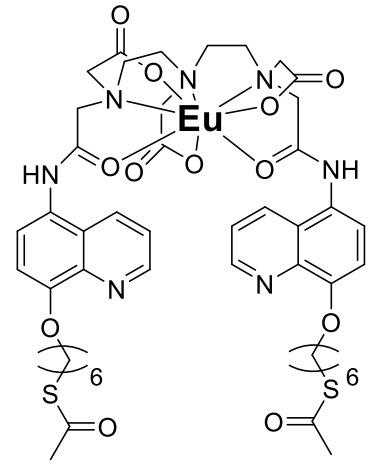
EuQSH	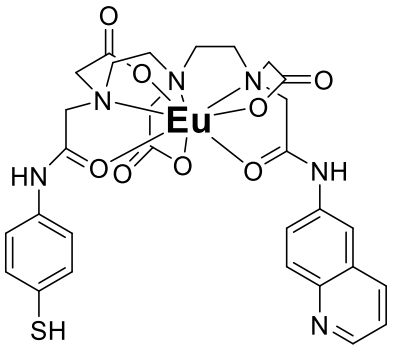
AF646	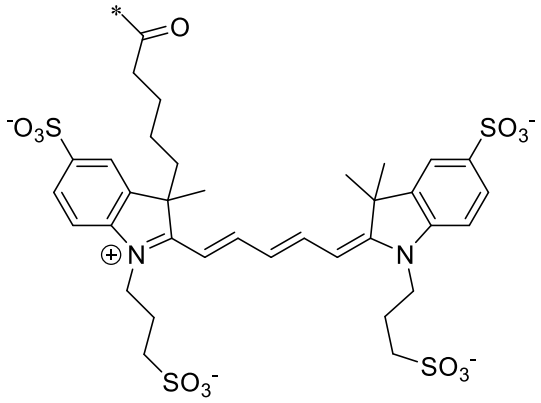

1 General Introduction

1.1 Immunoassays

Immunoassays are bioanalytical tests based on the highly specific antibody (Ab) – antigen (Ag) interaction and are among the most widely used biomedical diagnostic tools.[1] An antigen is a foreign species present in the body which induces an immune response. An antibody is a large protein which is produced by the immune system to bind to and neutralize antigens. The binding between an antibody and an antigen to form an immunocomplex (Figure 1.1.1.) is incredibly specific and as such the binding between the two is analogous to a 'lock and key' whereby each lock is specific to a given key.

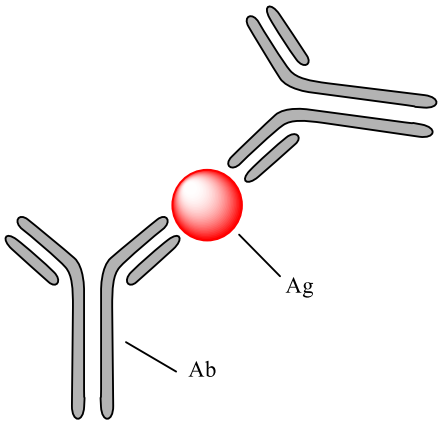

Figure 1.1.1.

The highly specific Ab – Ag interaction to form an immunocomplex.

Red circle, Ag.

In general, it is the concentration of antigen which is needed to be determined, although different biological analytes can also be determined *via* an immunoassay such as sugars, proteins or hormones.[2,3,4] The design of a biological detection system is different for each analyte, and several points must be considered when designing a successful and practical assay (Table 1.1.1.).

Table 1.1.1.

Considerations for the design of an immunoassay system.

Consideration	**Explanation**
Cost	The cost of running the assay must be financially feasible.
Required detection limits	The upper and lower detection range of the assay must be within a clinically relevant range for the analyte(s).
Readout time	The readout time of the assay should be relatively quick.
Complexity of performance	The assay should be quick and easy to perform.
Interference	The assay is required to be sensitive to only the analyte(s) in question.

These fundamental requirements should be balanced and considered for the design of the most appropriate assay for a given analyte.

Generally, immunoassays can be classed as either homogenous (solution based) or heterogeneous (surface based).[5] Heterogeneous assays have biomolecules attached to a surface whereupon a patient sample is added. The surface is washed, a detectable biomolecule is added, and the surface is washed again (Figure 1.1.2.). The signal from the detectable antibody is proportional to the concentration of analyte.

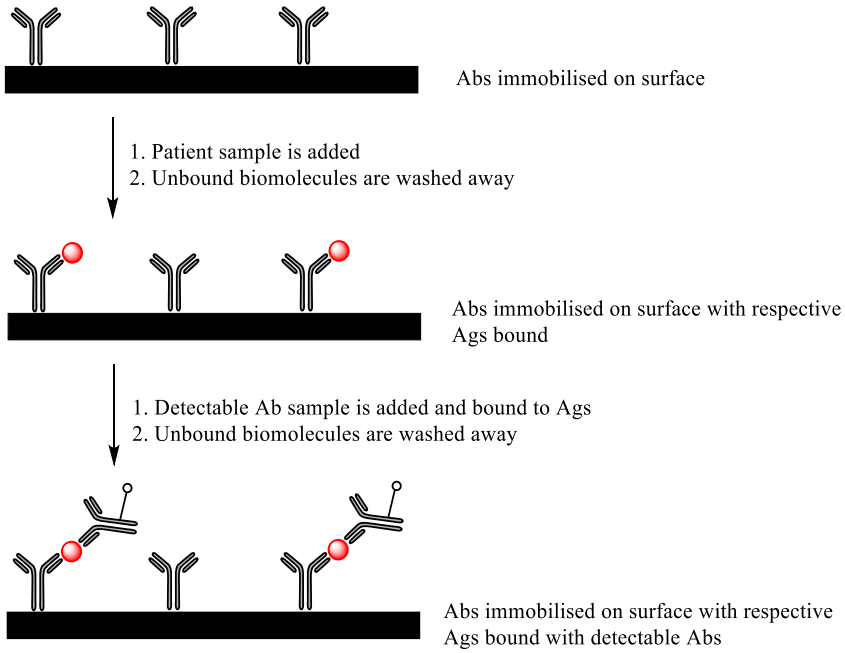

Figure 1.1.2.

General schematic of a heterogeneous immunoassay.

O*, detectable label.*

Several commercial heterogeneous assays are available on the marketplace, for example the DELFIA (dissociation enhanced lanthanide fluorescent assay) scheme (Figure 1.1.3.) which uses the optical properties of the lanthanides (Ln) for detection based on or the more widely known ELISA (enzyme-linked immunoabsorbant assay) (Figure 1.1.4.) which uses enzymatic action upon a dye for detection, both of which are commercially available.[6,7,8,9]

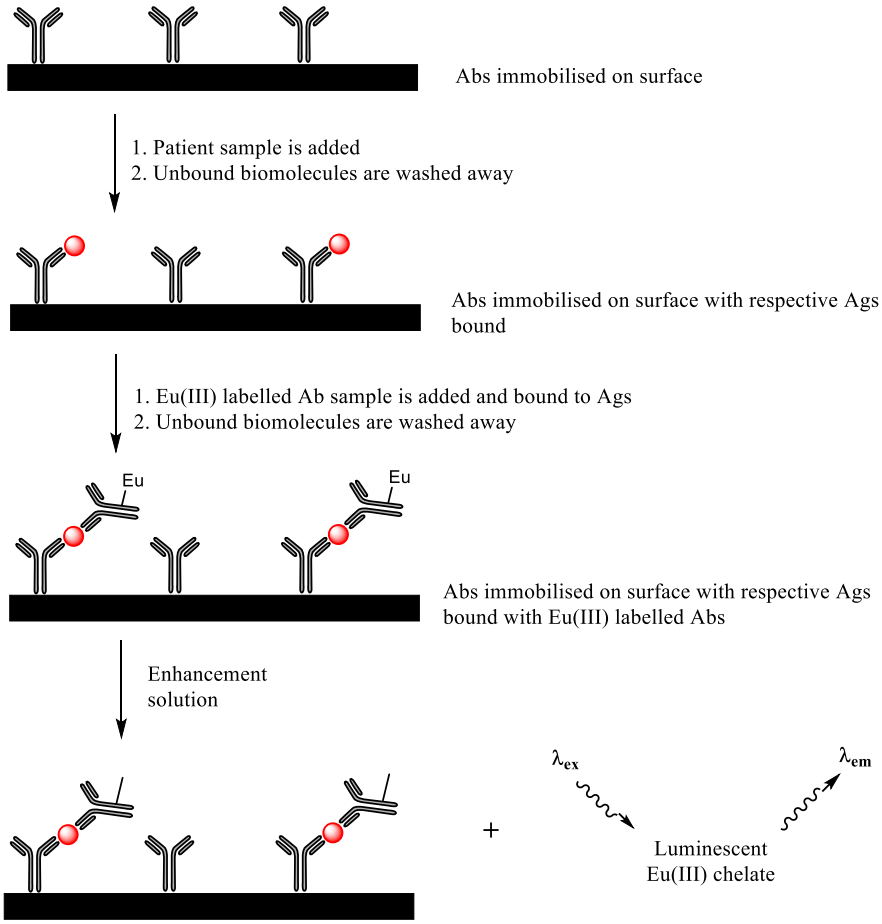

Figure 1.1.3.

General schematic of a DELFIA system.

The DELFIA system uses the specific luminescence signal from a Eu(III) ion to detect the concentration of antigen. On addition of the enhancement solution the previously non emissive Eu(III) ions become bound to a sensitizing chelate forming an emissive complex. The concentration of antigen present is directly proportional to the emission intensity observed from the Eu(III) chelate.

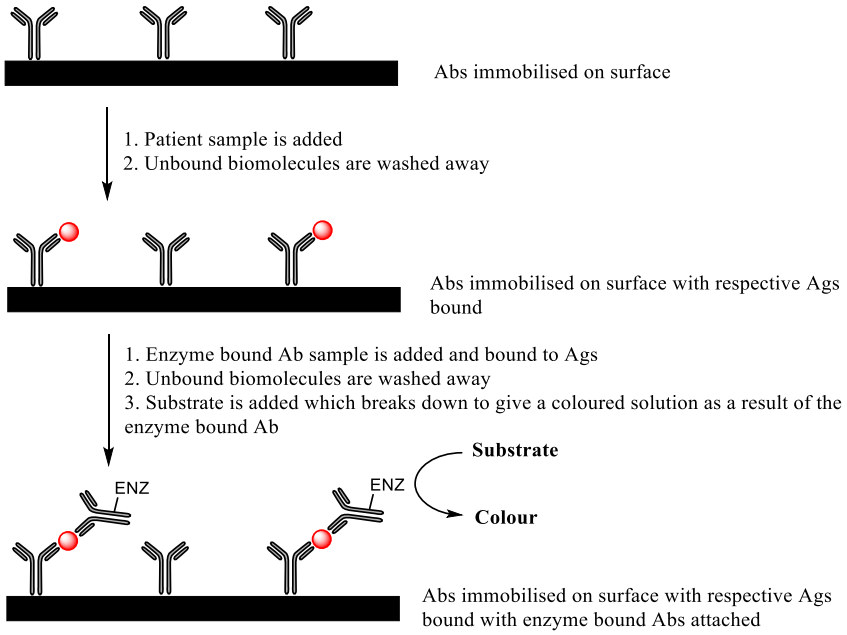

Figure 1.1.4.

General schematic of an ELISA system.

The ELISA system uses an enzymatic activity on a substrate to give a measured colour change to quantify the amount of the antigen present in the sample. The amount of measured enzymatic activity is directly proportional to the concentration of the antigen.

Homogenous assays have labelled antibodies in solution which come together to form an immunocomplex on specific binding to the particular antigen which results in a detectable signal. The concentration of the analyte is proportional to the signal which is measured (Figure 1.1.5.). These types of assays are discussed in much more detail in this thesis (Section 1.4.).

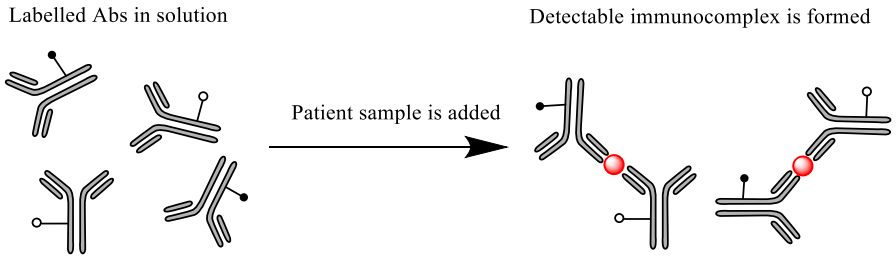

Figure 1.1.5.

General schematic of a homogeneous immunoassay.

O*, detectable label;* ●*, detectable label.*

As discussed earlier, the design of an immunoassay is governed by balancing the working considerations of the device. Generally speaking, heterogeneous systems show lower detection limits, but suffer from drawbacks associated with their performance cost, complexity and long readout times. Homogeneous systems, in comparison, are considered experimentally simple and give quick readout times. Indeed, a reliable experimental result can be obtained within ninety seconds using this type of system, although homogeneous assays suffer from a lack of sensitivity with respect to the limit of detection (LOD) of the analyte.[10]

Heterogeneous assay systems will always be limited by their experimental complexity, and whereby a large amount of work is done on these systems, which often involves the use of nanomaterials, the issue of complexity will always remain.[11,12,13,14] Research into homogenous systems is based around improving their detection limits as such to rival that of the surface based systems.

1.2 Förster resonance energy transfer

Förster resonance energy transfer (FRET) is a photochemical process discovered by German chemist Theodore Förster in 1946.[15] In its simplest definition, FRET is a coulombic distance dependant energy transfer between two chromophores, an energy donor in its excited state, and an energy acceptor (Figure 1.2.1.). Competing pathways with FRET include radiative and non-radiative decay of the donor in its excited state.[16]

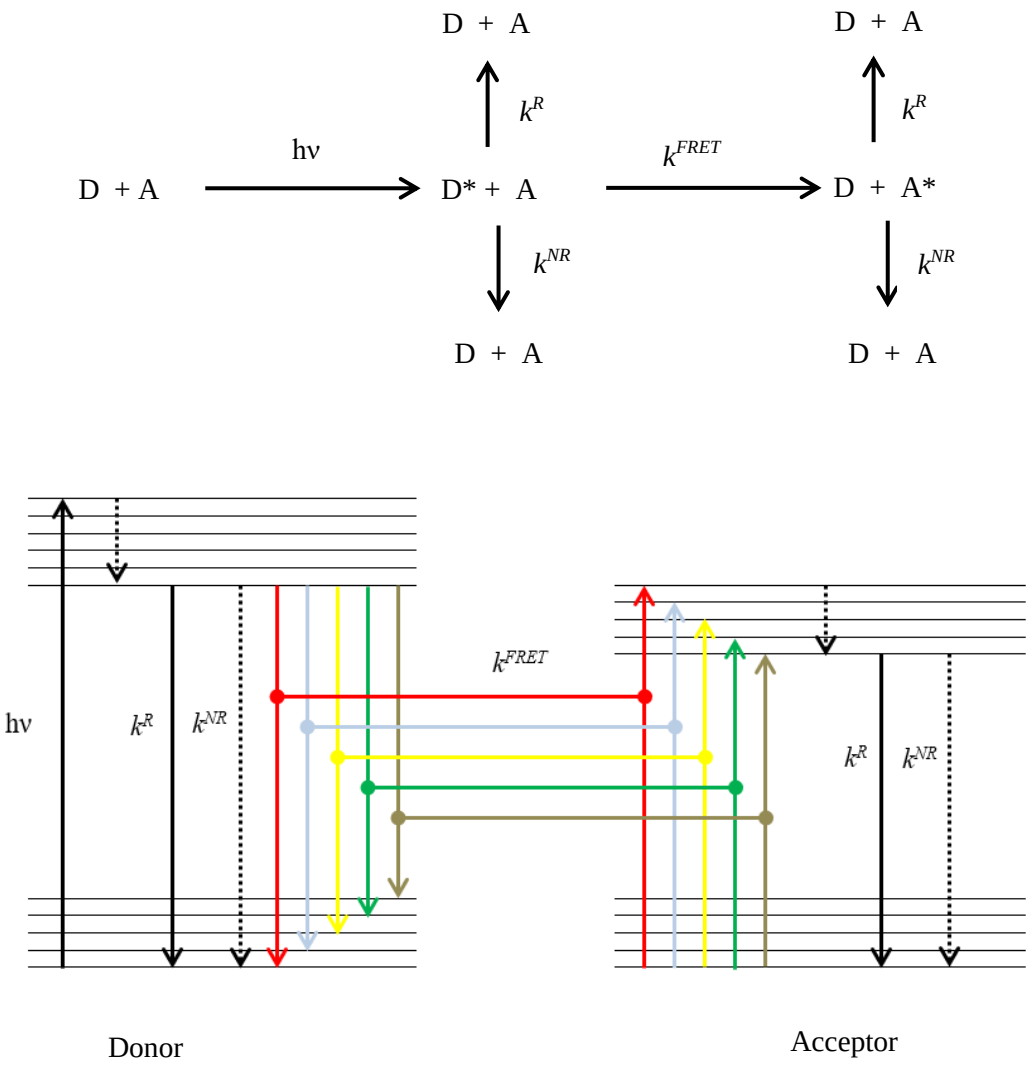

Figure 1.2.1.

Principle of a FRET system.

*D, Donor; A, Acceptor; hv, excitation wavelength; *, excited state; k^r, k^{nr}, k^{FRET}, radiative, non-radiative and FRET rates.*

For FRET to be active, the distance between the donor and the acceptor is usually required to be larger than 10 Å, to avoid short range interactions and shorter than 100 Å in space. k^{FRET} is proportional to the inverse of the donor – acceptor distance (r) to its sixth power (Equation 1.2.1.).

$$k^{FRET} \propto \frac{1}{r^6}$$

Equation 1.2.1.

Distance dependence of FRET.

k^{FRET}, FRET rate; r, donor – acceptor distance.

For FRET to occur, the emission spectrum of the energy donor must overlap with the absorption spectrum of the acceptor (Figure 1.2.2.). When these two spectra are overlaid, the region at which they overlap is known as the spectral overlap (J(λ)), and it is at this point where FRET is able to occur.

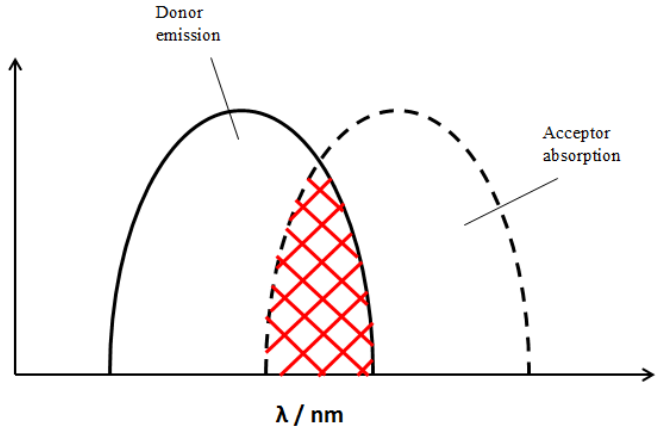

Figure 1.2.2.

Overlap of the donor emission spectrum and the acceptor absorption spectrum showing a spectral overlap. J(λ) where FRET can occur is indicated with the red lattice.

Each FRET pair has an associated R_0 value, defined as the distance between the two chromophores at which the energy transfer rate is 50% efficient. (Figure 1.2.3.). At this point k^{FRET} is equal to the sum of all the competing processes from the excited state of the donor.

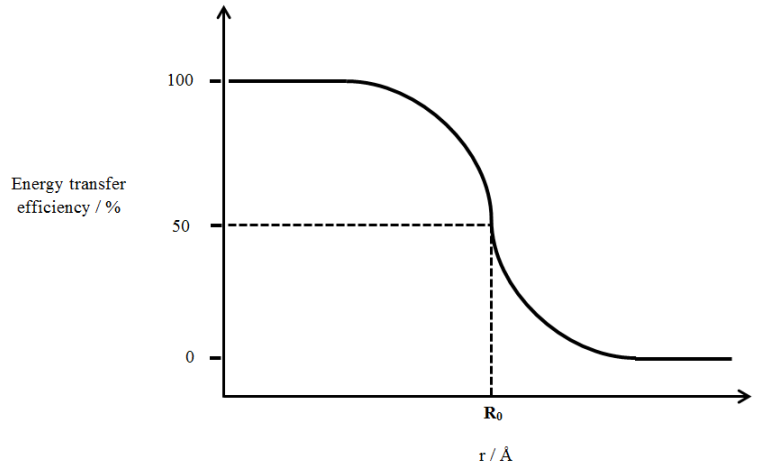

Figure 1.2.3.

Distance dependence of FRET with the R_0 value shown.

R_0 differs between each FRET pair and is dependent on the emission quantum yield (Φ) of the donor, the dipole orientation factor between the pair and J(λ) of the pair. R_0 can be worked out using these parameters mathematically (Equation 1.2.2.). Typical values for the R_0 parameter for common organic FRET pairs from Thermofischer Scientific are included (Table 1.2.1.).

$$R_0 = \left[\frac{9(ln10)\kappa^2\Phi_D}{128\pi^5 N_A n^4} J(\lambda)\right]^{\frac{1}{6}}$$

Equation 1.2.2.

Mathematical representation of R_0.

κ, dipole orientation factor; Φ_D, donor quantum yield; N_A, Avogadro constant; n, refractive index of solvent; J(λ), spectral overlap.

Table 1.2.1.

Typical R_0 values of common organic dyes as provided by Thermofischer scientific.[17]

Donor	**Acceptor**	**R_0 / Å**
Fluorescein (FITC)	Tetramethylrhodamine	55
IAEDANS	FITC	46
EDANS	Dabcyl	33
BODIPY FL	BODIPY FL	57
FITC	QSY 7 and QSY 9 dyes	61

J(λ) is dependent on the overlap of the donor emission and acceptor absorption spectra and the molar absorptivity (ε) of the acceptor, which can also be expressed mathematically (Equation 1.2.3.).

$$J(\lambda) = \int I_D(\lambda)\varepsilon_A(\lambda) \quad d\lambda$$

Equation 1.2.3.

Mathematical representation of J(λ).

I_D, normalised donor emission spectrum; ε_A, acceptor molar absorptivity.

FRET can be measured and monitored *via* steady state or time resolved (TR) emission spectroscopy measurements. It is more common in the literature to employ a method to quantify the quenching of the energy donor, although there are examples whereby a radiative energy acceptor is monitored for its steady state or time resolved emission spectra.[18,19]

The quenching of the energy donor by a suitable acceptor causes a decrease in the excited state lifetime (τ) of the donor, a decrease in the Φ of the donor and a decrease in the emission intensity (I) of the donor. It is the lifetime which will be considered in this thesis hence this section will concentrate on how FRET is monitored *via* excited state lifetime measurements.

The comparison of the excited state lifetime of the donor with and without the presence of an applicable energy acceptor can be used to determine the donor – acceptor distance of the pair using R_0 as a reference (Equation 1.2.4) and the energy transfer efficiency (Φ_T) between the donor and acceptor (Equation 1.2.5.). These equations are analogous with measurements of I and Φ of the energy donor.

$$r = \frac{R_0}{\left(\frac{\tau_D^0}{\tau_D} - 1\right)^{\frac{1}{6}}} \qquad \Phi_T = 1 - \frac{\tau_D}{\tau_D^0}$$

Equations 1.2.4. (Left) and 1.2.5. (Right)

Determination of r and Φ_T between a FRET pair.

τ_D , lifetime with quencher present; τ_D^0, lifetime without quencher present.

The combination of FRET pairs reported in the literature is vast, whereby common donors have traditionally included luminescent Ln complexes and organic dyes. More current trends are focused on luminescent nanoparticles (NPs) as donors such as upconverting phosphors (UCPs) and quantum dots (QDs), all of which are discussed in detail at a later section of this thesis (Section 1.5.). FRET acceptors have traditionally been organic dyes with a broad absorption spectrum and have now been extended to include QDs, gold NPs (AuNPs) and very current work has included graphene as an energy acceptor, which again are discussed at a later section of this thesis (Section 1.5.).[20]

Whilst the choice of energy donors and acceptors is broad, the fundamental requirements of the donor and the acceptor can be defined by common photophysical parameters (Tables 1.2.2. and 1.2.3.).

There are extensive examples of the use of FRET in homogeneous immunoassay technology which is explored in large detail in a later section of this thesis (Sections 1.4 and 1.5).

Table 1.2.2.

Photophysical considerations of a FRET donor.

Consideration	**Explanation**
Excited state lifetime (τ)	A long lived τ is advantageous for facile separation of the FRET signal from any background fluorescence signal which may be present.
Φ	A large emission quantum yield (Φ) is required so a larger amount of energy is available for the energy transfer process.
ε	A large molar absorptivity (ε) is required for the donor to have a large amount of initial energy absorbed.
Stokes shift	A large separation between the initial excitation wavelength (λ_{exc}) and emission wavelength (λ_{em}) leads to easier removal of background fluorescence.
Emission spectrum	A characteristic emission spectrum is easy to identify as the correct signal. A sharp emission signal can show a complete $J(\lambda)$ with a broad energy acceptor in comparison to a broad emission spectrum which is difficult to get an acceptor to show a full $J(\lambda)$ with.
Photobleaching	If a reusable device is proposed, the donor should not be susceptible to photobleaching.

Table 1.2.3.

Photophysical considerations of a FRET acceptor, assuming the acceptor is not required to show radiative emission.

Consideration	**Explanation**
$J(\lambda)$	The acceptor should show a large $J(\lambda)$ with the emission spectrum of the donor.
ε	A large ε leads to the acceptor being able to accept a larger amount of energy during the energy transfer.
λ_{exc}	The acceptor should show no absorption at the initial λ_{exc}.
Photobleaching	If a reusable device is proposed, the donor should not be susceptible to photobleaching.

1.3 Lanthanide chemistry

The Ln elements occupy the space on the periodic table between the 6s and 5d blocks. Research into this range of elements is extensive and ranges from taking advantage of their magnetic properties, such as the use of Gd(III) in magnetic resonance imaging (MRI) applications to their use in catalysis and small molecule activation.[21,22,23,24] The optical properties of the Ln elements are unique and as such they have been used in a large variety of devices and have been used broadly in biomedical and sensing applications.[25,26] Their optical properties are explored in detail in this work.

The Ln elements exist almost exclusively in their 3+ oxidation state as a result of the stabilisation exerted by the *4f*, *5d* and *6s* orbitals in this oxidation state, although other oxidation states of 4+ and 2+ have been reported, particularly of Eu and Sm.[27,28,29] In this 3+ oxidation state, as the series is crossed the electronic structure of the Ln(III) ions can be denoted as $[Xe]4f^n$ (Table 1.3.1.) As the series is crossed a contraction in the ionic radii of the elements is observed because of the poor shielding ability of the *f* orbitals.

Table 1.3.1.

Ionic radii and electronic structure of the Ln(III) ions as measured using EXAFS data.[30]

Element	**Ln(III) electronic structure**	**Ln(III) ionic radius / Å**
57 La	[Xe]	1.250
58 Ce	$[Xe]4f^1$	1.220
59 Pr	$[Xe]4f^2$	1.200
60 Nd	$[Xe]4f^3$	1.175
61 Pm	$[Xe]4f^4$	*Data not provided*
62 Sm	$[Xe]4f^5$	1.140
63 Eu	$[Xe]4f^6$	1.120
64 Gd	$[Xe]4f^7$	1.105
65 Tb	$[Xe]4f^8$	1.090
66 Dy	$[Xe]4f^9$	1.075
67 Ho	$[Xe]4f^{10}$	1.055
68 Er	$[Xe]4f^{11}$	1.040
69 Tm	$[Xe]4f^{12}$	1.025
70 Yb	$[Xe]4f^{13}$	1.010
71 Lu	$[Xe]4f^{14}$	0.995

The radial distribution function of the Ln(III) ions show a general trend of the valence *4f* electrons lying close to the nucleus in comparison to the shielding *6s* and *5d* orbitals and thus the *4f* orbitals can be essentially considered as spherical and core like, with no significant orbital overlap with any ligand orbitals. As a consequence of this behaviour, the bonding of the Ln(III) elements is dominated by ionic interactions between the ligand and the metal ion and the design of Ln(III) complexes is based around ionic interactions between hard donor ligands and the central metal ion. The coordination number of the Ln ion is variable. The most common coordination numbers are eight or nine which varies as a result of the contraction of the Ln(III) series, although lower and higher numbers can be achieved of four and twelve with bulky or small ligand systems.[31,32,33] Whilst the bonding of Ln(III) complexes is dominated by ionic interactions, crystal field effects cannot be completely overlooked and typical values for the ligand field stabilisation energy (LFSE) are in the order of the hundreds of cm^{-1}, although for transition metal complexes this value is typically much larger with LFSEs of thousands to tens of thousands cm^{-1}.[34,35]

Ln(III) ions, as before mentioned, display unique and useful optical properties and research into Ln(III) complexes as luminescent probes is prominent. The lack of orbital overlap between the Ln(III) ion and its surrounding environment results in the absorption and emission processes of the Ln series being due to the rearrangement of electrons within the *4f* orbitals of the metal. Thus, formal absorption and emission processes are sharp and characteristic in nature, as a result of transitions between well-defined *4f* energy levels.

The redistribution of electrons within *4f* orbitals is a forbidden process, because of the Laporte and orbital angular momentum selection rules and some transitions are further forbidden by the spin selection rule. As a result of this, *f–f* absorption processes are incredibly weak for the naked Ln(III) ion and the molar absorptivity is typically less than 10 M^{-1} cm^{-1} and only occur due to weak vibronic coupling.[36,37] This vibronic coupling can be increased as the symmetry of the *4f* orbitals is decreased, although the transition is still considered weak as a consequence of the lack of *4f* orbital overlap. These selection rules also govern the release of energy within the Ln(III) series, hence a radiative emission

process from a Ln(III) ion is often a triply forbidden process. This leads to only a small chance of a radiative transition occurring and the excited state lifetime of the metal ion being extended into the micro and milliseconds range. These *f–f* emission bands are characteristically sharp and are termed as hypersensitive transitions. These hypersensitive transitions are sensitive to the coordination environment of the Ln(III) ion, such as the $^5D_0 \rightarrow {}^7F_2$ transition within the Eu(III) ion which is particularly sensitive to the surroundings of the Eu(III) ion.

The spectroscopic energy levels of the Ln(III) series can be described with use of Hund's rules, which define the energy levels based on spin, orbital angular momentum and spin orbit coupling to give each Ln(III) ion a term symbol (Equation 1.3.1.) determined by the Russel-Saunders coupling scheme.[38]

$$^{(2S+1)}L_J$$

Equation 1.3.1.

General form of a spectroscopic term symbol.

S, total spin angular momentum quantum number; L, total orbital angular momentum; J, total angular momentum quantum number.

The observed emission bands of the Ln(III) ions are attributed to transitions between the lowest lying excited state and ground states of each Ln (Table 1.3.2.).

Table 1.3.2.

Main luminescent transitions of Ln(III) ions. 'J' indicates a range of transition levels.

Ln(III)	Emissive transitions
Eu(III)	$^5D_0 \rightarrow {}^7F_J$
Tb(III)	$^5D_4 \rightarrow {}^7F_J$
Dy(III)	$^4F_{9/2} \rightarrow {}^6H_J$
Sm(III)	$^4G_{5/2} \rightarrow {}^6H_J$
Nd(III)	$^4F_{3/2} \rightarrow {}^4I_J$
Yb(III)	$^2F_{5/2} \rightarrow {}^2F_{7/2}$
Er(III)	$^4S_{3/2} \rightarrow {}^4I_J$

For example, Eu(III) emission is a result of transitions from the $^5D_0$ excited state to the ^7F_J ground states of the Eu(III) ion, where J = 0 - 6 (Figure 1.3.1.).

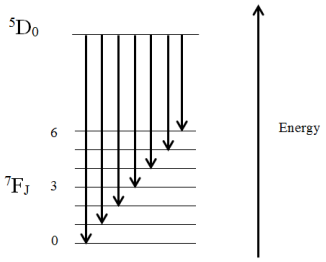

Figure 1.3.1.

Emission bands observed in the Eu(III) ion.

Of the Ln(III) ions, Eu(III), Tb(III), Dy(III) and Sm(III) all show luminescence in the visible region of the electromagnetic spectrum and Nd(III), Yb(III) and Er(III) are near infra-red (NIR) emitters. The photophysical properties of these ions have been extensively employed in a wide range of applications for their use as optical reporters in many biological and chemical systems.[39,40,41,42] Their incredibly long excited state lifetime allows for time-gated measurements whereby background fluorescent readings can be easily separated from the optical signal produced from the Ln(III) ion with time resolved methods (Figure 1.3.2.), while the sharp nature of the transitions leads to very characteristic steady state emission spectrum which can be easily recognised.

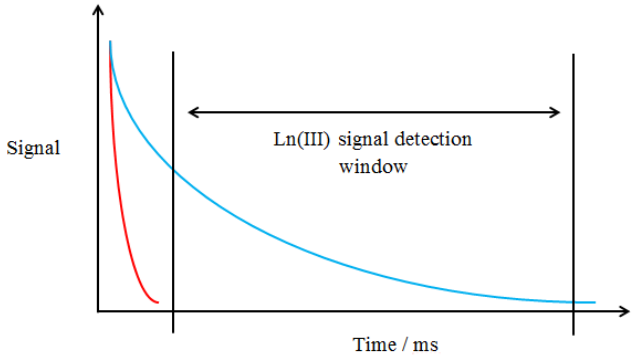

Figure 1.3.2.

Example of time-gated emission process.

Red curve, background fluorescence signal; blue curve, Ln(III) luminescent signal.

Despite these clear advantages associated with the use of the Ln(III) ions as optical probes, the series is not without its problems connected to their optical properties.

The forbidden nature of the rearrangement of electrons in the *4f* orbitals and the lack of LFSE effects leads to the absorption process within the metal ion to be inherently weak as previously discussed. This issue can be partially overcome with the careful design of organic chromophores which can indirectly transfer energy to the emissive state of a Ln(III) ion (Figure 1.3.3.). The organic chromophore is called a sensitizer and the process is known as sensitization.

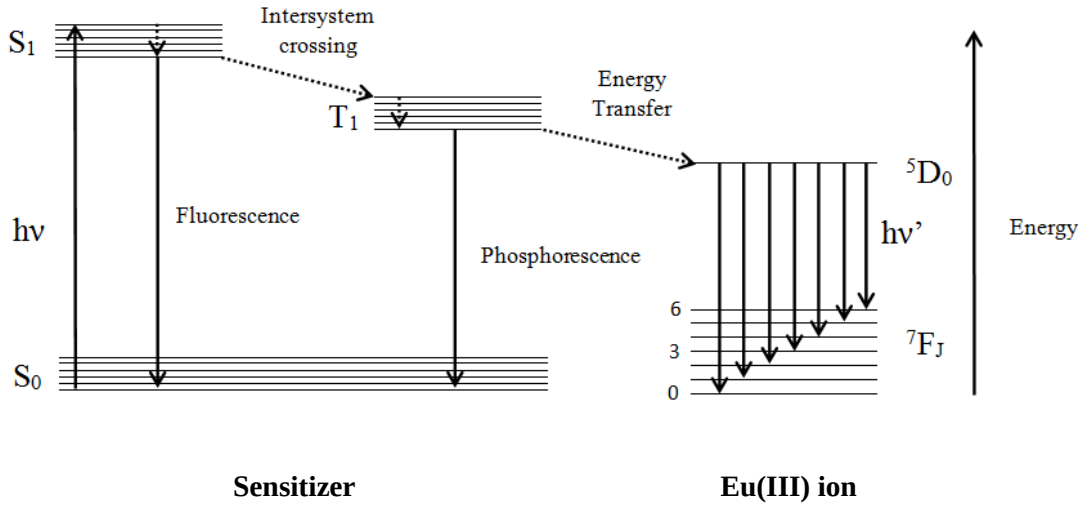

Figure 1.3.3.

Lanthanide sensitization process for Eu(III) ion.

S_0, ground state; S_1, first singlet excited state; hν, light; T_1, first triplet excited state.

Absorption of a photon to the first excited singlet state (S_1) of the sensitizer is observed, followed by intersystem crossing to a lower energy first excited triplet state (T_1) which can transfer energy to the Ln(III) ion. This process allows for population of the metal ion excited state, with an excitation wavelength in the UV (ultra-violet) region of the electromagnetic spectrum, showing the emission wavelength of the metal ion in the visible or NIR area of the spectrum. As such, the Stokes shift of this process can be incredibly large which is advantageous as, with careful sensitizer design, the optical signal from the Ln ion can be almost completely separated from the competing fluorescence and phosphorescence processes of the organic fluorophore.

The design of efficient sensitizing units for emissive Ln(III) ions is a very well-known and understood area of a research and common sensitizers for Eu(III) are included (Table 1.3.3.). Indeed, these sensitizers can be functionalised with a Ln binding site to produce a luminescent Ln complex.

Table 1.3.3.

Common organic sensitizing units for Eu(III).[43,44,45,46]

Name	**Structure**	**Absorption λ_{max} / nm**	**ε / M^{-1} cm^{-1}**
Dibenzoylmethane	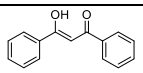	342	25,000
Bipyridine	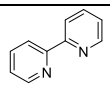	283	10,200
Quinoline		311	6,300
Acridone	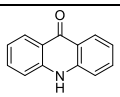	399	7,600

For efficient sensitization to be accomplised, the energy of the T_1 state of the sensitizer relative to the energy of the Ln(III) excited state should be carefully considered. Indeed, the ideal senzitizing unit for Eu(III) and Tb(III) requires the T_1 state of the sensitizer to be between 2500 – 3500 cm^{-1} higher in energy than the emisive state of the Ln(III) ion. If the T_1 is close in energy to the metal ion, a back energy transfer transition can occur, reducing the energy avaliable for radiative tranitisions from the Ln(III) ion. If the T_1 state is too high in energy, the state cannot populate the Ln(III) emissive state efficiently and can lead to radiative emission of the organic material or quenching from a ligand to metal charge transfer state from the metal. The ideal sensitizer allows long excitation wavelength of the chromafore to avoid simultaneous excitation of background biological molecules in a given system.

A further issue connected to the luminescent properties of the Ln(III) series is their weak luminescence in aqueous environements. The emissive state of the metal ion is efficiently quenched by vibrational oscilations of the O-H bond. This is also observed for N-H and C-H bonds but to a much lesser extent.

This quenching in aqueous and alcoholic solvents leads to a decrease in the emission quantum yield and the excited state lifetime of the metal ion or complex being studied. Evidence of this observation is the change in the emission quantum yield and the excited state lifetime of Ln complexes in a D_2O solvent when compared to a H_2O solvent (Figure 1.3.4.).

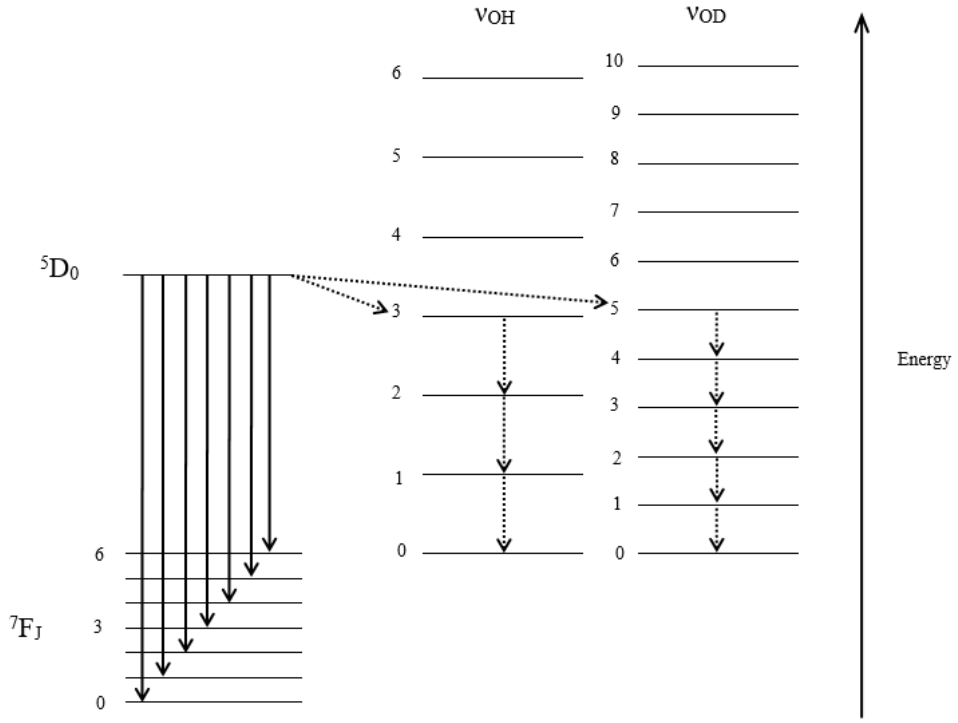

Figure 1.3.4.

Quenching of $^5D_0$ energy level of Eu(III) by O-H and O-D oscillators.

ν_{OH}, vibrational energy levels of OH oscillator; ν_{OD}, vibrational energy levels of OD oscillator.

This effect can be quantified with application of the Horrocks equation which compares the lifetime of the Ln(III) ion in deuterated solvent with non-deuterated solvent to give an estimate for the number of bound O-H oscillators (q) (Equation 1.3.2.).[47]

$$q = A(k_{OH} - k_{OD})$$

Equation 1.3.2.

Horrocks equation

q, Number of bound OH oscillators; k_{OH}, reciprocal lifetime in OH solvent; k_{OD}, reciprocal lifetime in OD solvent; A, quenching constant.

The quenching constant applied to this equation differs between the Ln(III) series depending on the quenching contribution the metal ion, and the quenching contribution of the solvent, for example the quenching effect exerted from a methanol molecule is *ca.* half as strong as the quenching exerted from a water molecule. Values of the A parameter in ms for Tb(III) and Eu(III) in water and MeOH are included (Table 1.3.4.).

Table 1.3.4.

A parameters for Eu(III) and Tb(III) in MeOH and water.[48,49]

Ln(III)	Solvent	A / ms
Eu(III)	Water	1.05
Tb(III)	Water	4.20
Eu(III)	MeOH	2.10
Tb(III)	MeOH	8.40

The Horrocks equation fails to take into account quenching from outer sphere O-H oscillators. The Parker-Beeby equation has been proposed whereby the quenching constant is revised and a second quenching constant, B is included to account for the outer sphere oscillators (Equation 1.3.3.). Revised quenching constants for the Parker-Beeby equation are included (Table 1.3.5.).

$$q = A'(k_{OH} - k_{OD} - B)$$

Equation 1.3.3.

Parker - Beeby equation

q, Number of bound OH oscillators; k_{OH}, reciprocal lifetime in OH solvent; k_{OD}, reciprocal lifetime in OH solvent; A', revised quenching constant; B, outer sphere quenching constant.

Table 1.3.5.

A' and B parameters for Eu(III) and Tb(III) in MeOH and water.[50]

Ln(III)	Solvent	A' / ms	B / ms^{-1}
Eu(III)	Water	1.20	0.25
Tb(III)	Water	5.00	0.06
Eu(III)	MeOH	2.40	0.25
Tb(III)	MeOH	10.00	0.06

Because of this quenching contribution, luminescent Ln(III) complexes are designed in a ‘cage like’ structure which physically hinders quenching O-H oscillators from deactivating the luminescent state of the metal ion. Common examples of these ‘cage like’ structures are shown, whereby the ligand can wrap around and protect a central Ln(III) cation (Figure 1.3.5.).

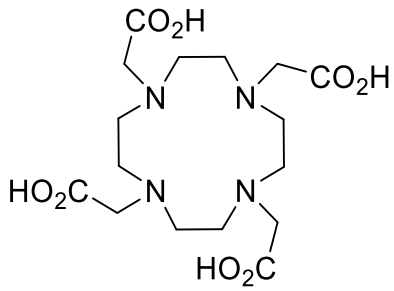

H_4DOTA
(tetraazacyclododecane-1,4,7,10-tetraacetic acid)

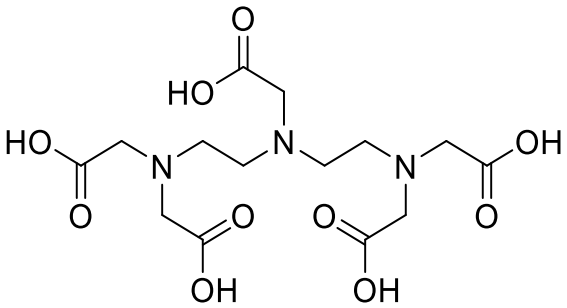

H_5DPTA
(diethylenetriaminepentaacetic acid)

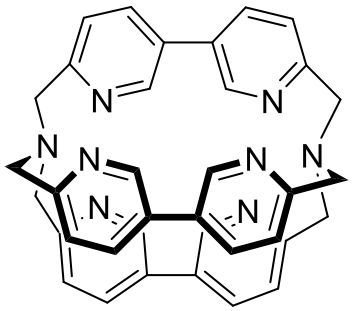

Cryptate

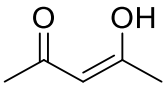

Hacac
(acetylacetone)

Figure 1.3.5.

Common ligands used to encapsulate and protect a Ln(III) ion.[51,52 53,54]

Since the bonding between Ln ions and a ligand is mainly electrostatic in nature the building of hard donor groups into a Ln(III) ligand is crucial to achieve a high binding constant and to ensure the metal ion does not ‘leach’ out of the complex. Popular hard donor ligands to encapsulate Ln(III) ions are N and O groups and negative carboxylate groups are particularly useful for charge balance with the positive metal ion, which can lead to a neutral complex.[55,56]

The design of a luminescent Ln complex is based on the successful combination of a suitable sensitizing unit and a protected Ln(III) binding site, both of which should be located close in space for efficient energy transfer to the metal ion. As such there are countless combinations of binding site and sensitizer which have been reported and the design of novel Ln complexes is an area which is constantly being improved.[57,58,59]

1.4 Lanthanides in immunoassays

The optical properties of luminescent Ln(III) chelates make for high quality donors in homogeneous FRET based immunoassay systems and in time resolved luminescence schemes. In the literature, there are plentiful examples of the use of both luminescent Ln(III) chelates and organic materials as FRET donors in immunoassay schemes.[60,61] Whilst both have been commonly reported, the optical properties of luminescent Ln(III) complexes have preferential properties when compared to organic fluorescent materials, and these properties can be easily compared. Whilst organic fluorescent materials can show larger emission quantum yields and molar absorptivity's, the luminescent properties of the Ln(III) series make for better FRET donors (Table 1.4.1.).

Table 1.4.1.

Comparison of organic fluorescence compared to Ln(III) luminescence as a FRET donor.

Consideration	**Luminescent Ln(III) chelate**	**Organic fluorescent material**
τ	Long, ranging into milliseconds range	Short, in the nanosecond range
Stokes shift	Large difference between sensitizer and Ln(III) emission	Very small, often absorption and emission spectrum overlap
Emission spectrum	Sharp line, very characteristic and easy for large J(λ) with FRET acceptor	Broad, difficult for a FRET acceptor to fully quench

The earliest publication involving the use of the optical properties of Ln(III) ions in an immunoassay scheme was in 1983 by Siitari *et al.* showing the detection of hepatitis B surface antigen (HBsAg) employing a luminescent Eu(III) labelling agent.[62] Anti HBsAg antibody was functionalised with the luminescent Eu(III) labelling agent and used in a sandwich assay format with anti HBsAg antigen immobilised on a surface (Figure 1.4.1.).

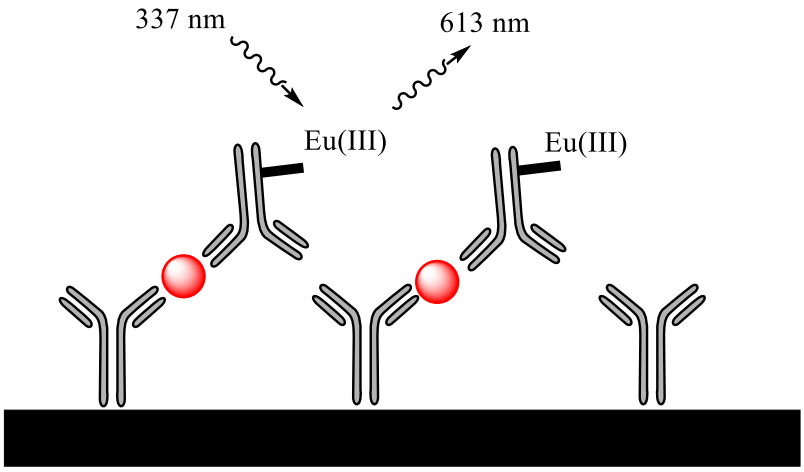

Figure 1.4.1.

Eu(III) functionalised anti HBsAg antibody assay for the time resolved detection of HBsAg.

Incubation of the functionalised antibodies and HBsAg led to formation of a surface immobilised immunocomplex which was detected *via* time resolved luminescence of the Eu(III) ion with excitation at 337 nm and emission at 613 nm. A 50 μs time delay between emission and excitation was used to eliminate any short-lived background fluorescence, ensuring the long-lived Eu(III) signal was the only optical signature being observed. A lower detection limit of 500 ng L^{-1} in terms of the concentration of analyte was achieved.

This publication has since inspired a huge amount of work into the use of luminescent Ln(III) chelates as the detectable label in an immunoassay scheme. As such, similar schemes using the visible emitting Ln(III) ions have been vastly studied using Eu(III), Sm(III), Tb(III) and Dy(III) encapsulated by ligands incorporating β-diketone or aromatic sensitizing units. Eu(III) and Tb(III) have longer lived excited stated lifetime values than the other visible emitting Ln(III) ions and so are more commonly used for their luminescent signals at 545 nm (Tb) and 614 nm (Eu) respectively. Recent work has been expanded to explore the area of multiplexed assays for the detection of multiple analytes simultaneously as well as the use of luminescent Ln nanomaterials.[63,64,65,66,67,68,69,70]

The success of using Eu(III) in the first heterogeneous time resolved luminescence assay was followed up ten years later with the first report of a homogeneous FRET assay with Eu(III) as an energy donor by Mathis in the detection of prolactin. Eu(III) cryptate functionalised anti prolactin antibody was used as the donor and XL665 functionalised anti prolactin antibody as the acceptor. Excitation at 337 nm led to excitation of the Eu(III) cryptate which when bound to analyte and acceptor labelled antibody in a sandwich assay format leads to an XL665 emission at 665 nm with a detection limit of 300 ng L^{-1} in terms of the concentration of prolactin (Figure 1.4.2.).[71]

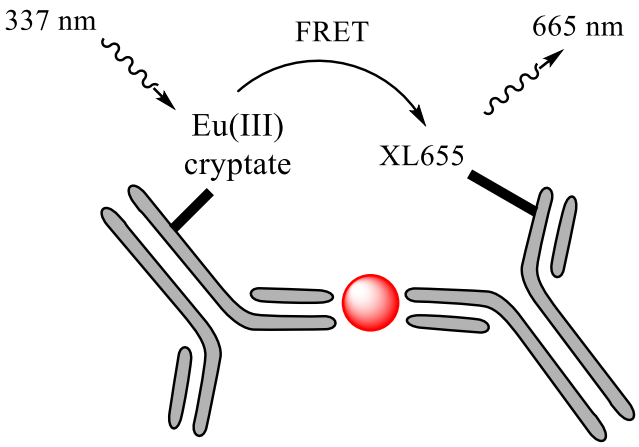

Figure 1.4.2.

First Eu(III) FRET assay developed by Mathis.

The use of a luminescent Ln(III) complex as a FRET donor with an organic acceptor group is widespread in the literature and the work started by Mathis has been the inspiration of many more similar FRET schemes involving luminescent Ln complexes as FRET donors in immunoassay schemes (Table 1.4.2.).

Table 1.4.2.

Selected examples of FRET assays whereby the donor is a single molecule luminescent Ln complex.[72,73,74]

Analyte	**FRET scheme used**	**LOD / ng L^{-1}**
Urinary albumin	Albumin-specific monoclonal antibody labelled with a stable fluorescent Eu chelate as donor and an albumin labelled with Cy5 as acceptor.	5.5×10^6
Interleukin-13	Anti-Interleukin-13 monoclonal antibody, Eu cryptate as donor and labelled different anti-Interleukin-13 monoclonal antibody labelled with XL665.	0.6
DNA Hybridisation	Two DNA probes are used each being complementary to the two different consecutive regions of a target DNA. The donor strand is labelled with a Tb(III) chelate and the acceptor strand with Cy5.	30 (pM)

This technology is outdated and has such been expanded to incorporate the use of luminescent Ln NPs as FRET donors whereby much lower detection limits can be achieved, when compared to single molecule methods, pushing the limits of conventional homogenous assay systems.

1.5 Nanoparticles in optical immunoassays

A NP is defined as a material which is between 1 and 100 nm in one dimension. Whilst this term allows particles to be more than 100 nm in a given dimension to be defined as a NP, a majority of the literature is focused on spherical particles.

The use of NPs in the literature is broad and a very widely studied area which has become enormous over the past twenty-five years. As such, the number of journals dedicated to publishing NP technology based research has risen from just one in 1990 to over 150 in 2012.[75] Inorganic NPs have been employed in a vast number of applications which range from medicinal applications and sensing to energy conversion devices.[76,77,78]

The reason for the vast amount of work dedicated to the applications of NPs is that it is possible to fine tune their properties for the application to which they are to be used. Indeed, NPs can be synthesised with very specific optical and electrochemical characteristics with variable surface to volume ratios.[79,80] Furthermore, the functionalisation of NPs is a very well-studied area hence molecules can be deposited on the surface of a particle which do not interfere with the core properties of the particles leading to a very specific set of properties for a given nanostructure.[81,82]

The use of NPs in immunoassay technology is an area which has become increasingly popular over recent years. The ease of functionalisation and controllable properties of NPs provides significant opportunity within the field of medical diagnostics. Indeed, the use of NPs within this field can lead to lower detection limits for analytes when compared to single molecule methods for both homogeneous and heterogeneous systems. The NP can be used as a scaffold for the immobilisation of biomolecules, or more commonly, as the detectable label itself within the system. Where the NP is used as the detectable label within the system, the amount of literature available is vast and reports of immunoassays based on colorimetric, electrochemical, optical and mass sensitive detection methods are common.[83,84,85,86,87,88] Indeed, it is the optical properties of NPs which are most widely studied, with

ca. 46% of all NP immunoassay publications being optical based between 2010 and 2013, and this is a continuing trend within the literature.[89] Within the field of optical NP based immunoassays, a majority of the literature is focused on the use of QDs and luminescent Ln NPs as the luminescent agent employed for their optical signatures.

1.5.1. Lanthanide doped nanoparticles in immunoassays

Luminescent Ln NPs can incorporate many luminescent Ln chelates inside a NP host, usually comprised of a polymer or silica host material. This leads to a much larger concentration of detectable Ln unit per biomolecule when compared to single molecule methods as previously described. Consequently, a large signal amplification is observed leading to a more sensitive assay, pushing the lower limit of detection down.[90] This type of technology started to trend in the literature in the early 2000's.

The first Ln based NPs developed were those whereby Ln(III) ions were encapsulated within a polymer host material with sensitising units. In 2001 Härmä *et al.* used polystyrene based NPs (*ca.* 100 nm) encapsulated with >30,000 Eu(III) ions and β-diketone units, for Eu(III) sensitization and coated with streptavidin (SA) for the detection of biotinylated prostate specific antigen (PSA) in a model assay system.[91] The PSA was detected *via* time resolved luminescence whereby the Eu(III) NP was excited at 340 nm to show emission at 615 nm, giving a lower detection limit of 0.4 ng L^{-1} of PSA. The same type of technology has more recently been employed for a polymer based assay with Eu(III) for cardiac troponin I (CTnI), whereby Eu(III) polystyrene NPs (*ca.* 100 nm) coated with anti CTnI antibodies were developed, showing a detection limit of 2 ng L^{-1} of CTnI *via* time resolved luminescence of the Eu(III) NP when bound to a surface *via* CTnI and surface immobilised anti CTnI antibodies (Figure 1.5.1.).[92]

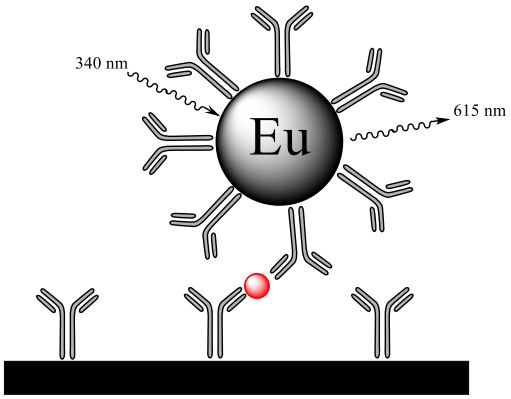

Figure 1.5.1.

Eu(III) doped polystyrene NP assay for the time resolved detection of CTnI.

Further examples of time resolved luminescent assay systems whereby luminescent Ln ions are doped into a polymer based host are included (Table 1.5.1.) which show generally lower detection limits when compared to single molecule methods.

Table 1.5.1.

Further selected examples of polymer based Ln NPs developed.[93,94,95,96,97]

Analyte	**NP and detection method used**	**LOD / ng L^{-1}**
α-fetoprotein	100 nm polystyrene NPs encapsulated with Eu(III) and β-diketone units coupled to anti α-fetoprotein Abs detected *via* TR luminescence.	0.04
PSA	50 nm Eu(III) chelate embedded polystyrene NPs functionalised with anti PSA Abs with differing amounts of acrylic acid present detected *via* TR luminescence.	1.6 (with 2.8% acrylic acid by mass)
Thyroid-stimulating hormone (TSH)	100 nm polystyrene NPs encapsulated with Eu(III) and β-diketone units coupled to anti TSH Abs detected *via* TR luminescence.	0.0012 (mIU I^{-1})
PSA	100 nm polystyrene NPs encapsulated with Eu(III) and β-diketone units functionalised with anti PSA Abs, detected *via* TR luminescence.	0.21
HBsAg	100 nm polystyrene NPs encapsulated with Eu(III) and β-diketone, functionalised with anti HBsAg Ab, detected *via* TR luminescence.	28

Despite their advantages of high sensitivity, Ln doped polymer based NPs have drawbacks associated with their usage, due to issues with leakage of the luminescent material and a tendency to agglomerate can arise, which somewhat limits their potential.[98]

As a solution to the problems associated with polymers as a host material, silica as the host material for luminescent Ln complexes for use in NP based immunoassays has been applied for their aqueous solubility without aggregation, surface biocompatibility and potential smaller particle size.

Yuan *et. al.* in 2004 were able to utilise these properties to detect HBsAg employing Eu(III) chelate doped silica NPs of 40 nm in diameter, developed from polymerised tetraothoorthosilicate, along with Eu(III) sensitizer BHHT, and functionalised with anti HBsAg antibody.[99] The HBsAg was detected with a lower detection limit of 74 ng L^{-1} *via* time resolved luminescence of the Eu(III) ion, exciting at 340 nm and observing the Eu(III) emission signal at 615 nm. A 0.2 ms time delay was used to eliminate any short lived background fluorescence from the observed signal to ensure the long lived Eu(III) NP was exclusively being observed. Yuan *et al.* extended their work using Tb(III) chelate doped silica nanoparticles with BPTA sensitizer, and functionalised with anti PSA antibody for the detection of PSA which was achieved with a lower detection limit of 7 ng L^{-1} *via* time resolved luminescence of the Tb(III) after exciting at 320 nm and observing the Tb(III) emission signal at 545 nm with a 0.2 ms time delay.[100]

Further examples of silica based Ln NPs are included (Table 1.5.2.). Whilst silica as a host material for Ln ions and their sensitizing units, is an improvement in comparison to the use of a polymer host material, the number of luminescent units encapsulated within the material is lower hence a slight loss in sensitivity can be observed when the two are compared.

Table 1.5.2.

Further selected examples of silica based Ln NPs developed.[101,102,103,104,105]

Analyte	**NP and detection method used**	**LOD / ng L^{-1}**
α-fetoprotein	45 nm silica NPs encapsulated with Tb(III) and BPTA, functionalised with anti α-fetoprotein Ab, detected *via* TR luminescence.	100
HBsAg	40 nm silica NPs encapsulated with BBCAP and Eu(III) / Tb(III) functionalised with anti HBsAg Ab, detected *via* TR luminescence.	35
CEA (Carcinoembryonic antigen) / HBsAg	40 nm silica NPs encapsulated with Eu(III) and BHHCT functionalised with either anti CEA Ab or anti HBsAg, detected *via* TR luminescence.	1.9 (for CEA) 23 (for HBsAg)
DNA	45 nm silica NPs encapsulated with Eu(III) quinolone complex and functionalised with complementary DNA strand, detected *via* TR luminescence.	0.08 (nM)
PSA	60 nm silica NPs encapsulated with Eu(III) / Tb(III) and PTTA, functionalised with anti PSA Ab, detected *via* TR luminescence.	210

Both polymer and silica doped Ln NPs can be used in FRET based assays whereby the Ln doped NPs are used as a detectable label with an appropriate FRET acceptor. The use of a polymer based Eu(III) chelate doped NP as a FRET donor was demonstrated by Valanne *et al.* in an assay for PSA. 100 nm polystyrene NPs containing Eu(III) with β-diketone and functionalised with anti PSA antibody were developed as a FRET donor. A 2 μm TransFluoSphere (TFS), containing multiple dyes with a spectral overlap with the Eu(III) emission signal, coated with anti PSA antibody was developed as the acceptor. As both the donor and the acceptor simultaneously bound PSA, FRET was observed between the Eu(III) NP and the TFS. Excitation of the Eu(III) NP at 340 nm led to emission from the TFS at 760 nm *via* FRET excitation of the TFS, showing a detection limit of 100 ng L^{-1} in terms of the concentration of PSA (Figure 1.5.2.).[106]

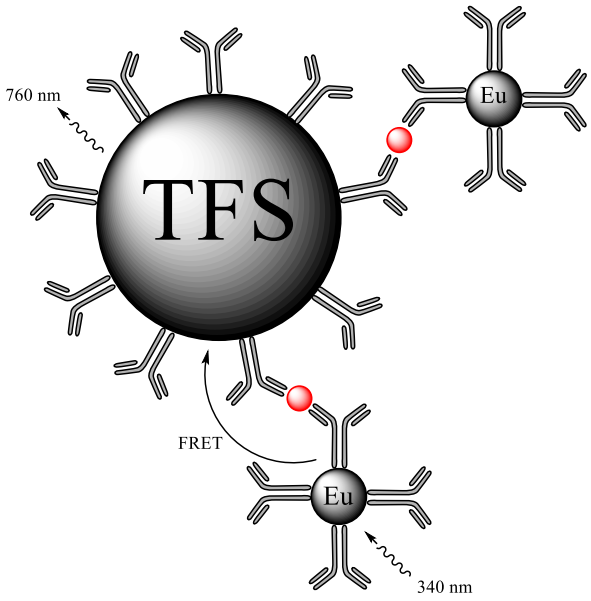

Figure 1.5.2.

FRET system schematic with Eu(III) doped polymer NP as the donor and a TFS sphere as the acceptor.

Indeed, further examples of Ln doped particles used in FRET assays from the literature show the potential from this type of system (Table 1.5.3.).

Table 1.5.3.

Selected examples of FRET assays whereby the donor is a luminescent Ln complex doped NP.[107,108,109,110]

Analyte	**FRET scheme used**	**LOD / ng L^{-1}**
Estradiol (E2)	100 nm polystyrene NPs encapsulated with Eu(III) and β-diketone units coupled to anti E2 Abs as the donor and anti E2 Abs functionalised with AlexaFluor (AF) 680 as the acceptor.	50 (pM)
BSA (Bovine serum Albumin)	90 nm polystyrene NPs encapsulated with Eu(III) as the donor and CdSe / ZnS QDs functionalised with SA as the acceptor. BSA acts a blocking reagent between the NPs and the QDs.	2.8×10^5 (In terms of conc. of QD)
E2	90 nm polystyrene NPs encapsulated with Eu(III) and β-diketone units coupled to anti E2 Abs as the donor and anti E2 Abs functionalised with AF680 as the acceptor.	70 (pM)
Caspase 3 inhibitors	A dual FRET system with 50 nm polystyrene NPs encapsulated with Eu(III), functionalised with AF680 loaded substrate as the donor. Complementary substrate labelled with QD as the acceptor.	N/A

1.5.2 Upconverting phosphors in immunoassays

The excitation of an organic chromophore for the sensitization of Ln(III) ions is a fully understood area and as discussed widely used in assay systems. Excitation in the UV area of the electromagnetic spectrum leads to a large background fluorescent signal from biological samples which requires time gated methods to distinguish from the required Ln signal, at which point some of the signal can be lost. A huge body of literature in the field of medical diagnostics is focused on the use of Ln NPs which can be excited *via* a two – photon process. UCPs show anti-Stokes behaviour with the absorption of low energy infrared radiation and emission in the visible area of the electromagnetic spectrum *via* a two – photon process. This allows for no excitation of background biomolecules involved, and the use of a NIR excitation wavelength is much more safe and more penetrating than that of excitation in the UV area of the spectrum, whilst the unique emissive properties of the Ln ion involved are retained.

UCPs are composed of Ln(III) ion pairs in crystals. Generally, Yb(III) ions which absorb light at 980 nm *via* a two – photon process are used as sensitizers, which can transfer the energy to other Ln(III) ions such as Er(III) (Figure 1.5.3.), Tm(III), Ho(III) and Tb(III).[111,112 113,114]

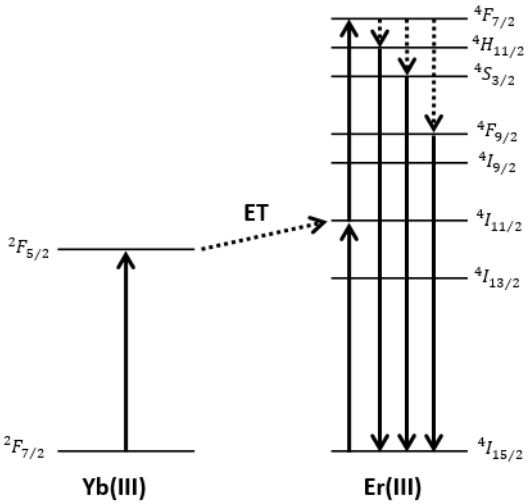

Figure 1.5.3.

Energy level diagram of a 50 nm $La_2(MoO_4)_3$ NP doped with Yb(III) and Er(III) with an λ_{exc} of 980 nm and emission at 519 nm, 541 nm, 653 nm.

Solid lines, excitation and emission processes; dashed lines, non-radiative emissive processes; ET, energy transfer.

UCPs have been applied to biomedical applications as the absorption of the Yb(III) ion at 980 nm and sharp line emission in the visible region results in virtually zero background interference from biological samples.[115] The first report of this type of luminescent reporter was in 1999 by Zijlmans *et. al.* where (Y.Yb.Er.)O_2S and (Y.Yb.Tm.)O_2S NPs between 0.2 and 0.4 µm were used in the detection of PSA and CD4 membrane antigen in tissue samples.[116]

UCPs can be applied in FRET based applications whereby the UCP is excited *via* the two – photon process at 980 nm is used as a FRET donor. In 2007, Kuningas *et. al.* used La_2O_2S:Yb(III),Er(III) NPs of 390 nm in the detection of E2 in a competitive assay format. The UCPs were functionalised with anti E2 F(ab) which binds to unlabelled E2 and E2 labelled with small molecule acceptor (Figure 1.5.4.). The acceptor labelled E2 competes for binding with the analyte hence the FRET signal is inversely proportional to the concentration of E2 in the patient sample. Excitation at 980 nm led to emission at 665 nm from the Er(III) ion and 740 nm from the acceptor with a lower detection limit of 60 ng L^{-1}.[117]

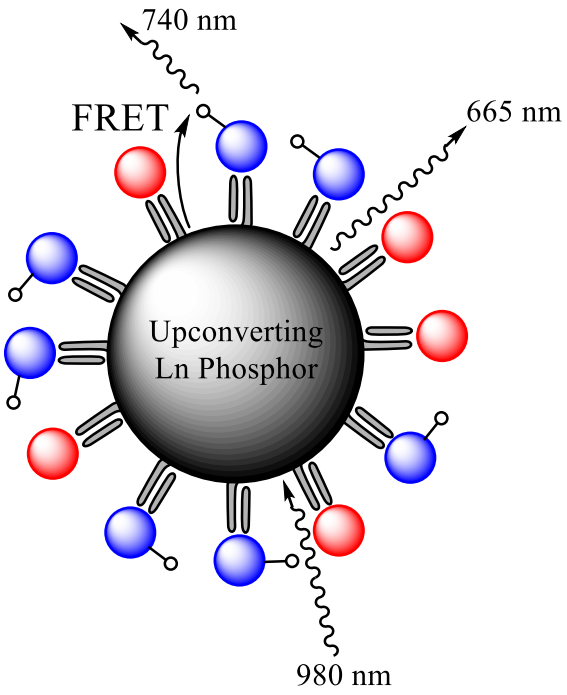

Figure 1.5.4.

Schematic of a competitive FRET immunoassay utilising a UCP donor.

=, Fab fragment; O*, acceptor label; red circle, analyte; blue circle, competing labelled analyte.*

Indeed FRET based UCPs have also been used with a variety of acceptors where $NaYF_4$:Yb,Er type particles as the UCP are among the most popular (Table 1.5.4.). The use of these types of nanocrystals are currently the most extensively used Ln FRET donors available in the literature and research into the usage and improvement of these materials is extensive.

Table 1.5.4.

Selected examples of FRET assays whereby the donor is a UCP.[118,119,120,121,122,123,124,125 126]

Analyte	**FRET scheme used**	**LOD / ng L^{-1}**
Avadin	$Na(Y_{1.5}Na_{0.5})F_6$:Yb,Er and $Na(Y_{1.5}Na_{0.5})F_6$:Yb,Tm of 50 nm, functionalised with biotin were used as FRET donors and 7 nm AuNPs functionalised with biotin were used as FRET acceptors.	0.5 (nM)
DNA	$NaYF_4$:Yb,Er functionalised with complementary DNA strand as the donor and TAMRA labelled with complementary DNA strand as the acceptor.	1.3 (nM)
E2	La_2O_2S:Yb(III),Er(III) functionalised with anti E2 Fab Ab as the FRET donor and E2 labelled with Oyster 556 as the acceptor.	0.4 (nM)
Goat IgG	50 nm $NaYF_4$:Yb,Er functionalised with anti goat IgG Ab as the donor and 20 nm AuNP functionalised with human IgG as the acceptor.	880
Biotin	22 x 24 x 32 nm $NaYF_4$:Yb,Er particles functionalised with SA as the acceptor and 16 nm CdTe based QD labelled with biotin as the acceptor.	2 (nM)
Glycated Haemoglobin	50 nm $NaYF_4$:Yb,Er functionalised with anti HbA1c Ab as the donor and HbA1c as the acceptor.	N/A
CEA	50 nm $NaYF_4$:Yb,Tm functionalised with CEA aptamer as the donor and PdNPs as the acceptor.	0.8
ATP	$NaYF_4$:Yb,Er functionalised with DNA as the donor and graphene oxide as the acceptor.	80 (nM)
DNA	30 nm $NaYF_4$:Yb,Er functionalised with complementary DNA strand as the donor and graphene oxide as the acceptor.	5 (pM)

Although these types of particles show virtually no background signal, the main disadvantage in this field is the low luminescent efficiency for smaller NPs which are of a desirable size for an immunoassay application where a smaller particle size shows the best FRET quenching which is possible.[127,128]

Whilst the use of Ln NPs as FRET donors is broad and has been applied to the detection of many analytes, with the inclusion of many luminescent chelates within a single nanostructure, a serious concern associated with the use of LnNPs as FRET donors, is the distance between the chromophores involved. The typical FRET range for a luminescent Ln complex to organic chromophore is <10 nm. Where LnNPs are used, particles of between 50 and 100 nm in diameter are often used, whereby Ln material deep within the large particle is outside the FRET range for an acceptor molecule bound to the surface, and this can be considered as lost signal which will not be quenched (Figure 1.5.5.).[129] A non-luminescent core would be advantageous to overcome this.

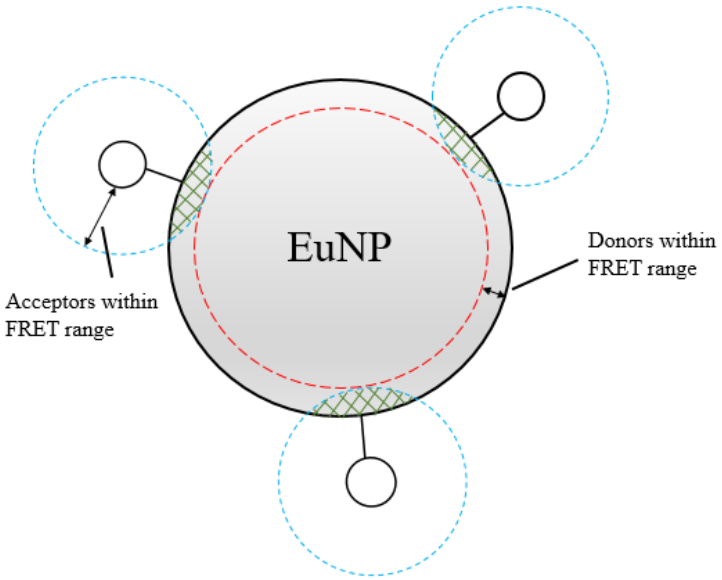

Figure 1.5.5.

Schematic showing the loss of signal from a doped Ln NP.

O, *acceptor label; dashed red line, area where Eu is within potential FRET range; dashed blue line, area where acceptor is within potential FRET range; green lattice, area where FRET is currently active.*

1.5.3 Quantum dots in immunoassays

As well as luminescent Ln NPs as FRET donors, another important class of NPs which can act as FRET donors are QDs. QDs are semiconductor NPs that have the capability to exhibit unique optical properties.[130] The semiconductor cores most commonly consist of CdSe or CdTe materials and are surrounded by one or more shells such as ZnS and CdS with a higher band gap and are often surrounded by a polymer and surface ligands (Figure 1.5.6.).[131,132,133,134]

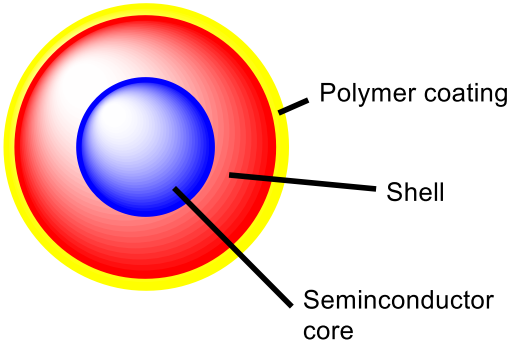

Figure 1.5.6.

Generic QD structure.

The optical properties of QDs are highly tunable and depend on both the size and composition of the core and the surrounding shells. As such QDs can be designed to have an extremely high molar absorptivity (10^6 M^{-1} cm^{-1}), exhibit sharp emission spectra and have a high emission quantum yield, with a large Stokes shift which makes them ideal candidates for labelling in immunodiagnostics, especially as their absorption properties can be tuned to avoid background excitation of biomolecules present.[135,136]

The optical properties of QDs have made them ideal for use in FRET systems. Whilst QDs can be used as energy acceptors, using luminescent Lns as donors, a clear majority of the literature is focussed on QDs as energy donors.[137,138]

Wei *et. al.* were able to use the luminescent properties of QDs in a homogeneous FRET assay for estrogen receptor β (ER-β) in a sandwich assay format. QD 565 which has a core of CdSe and a ZnS shell were functionalised with anti ER-β antibody and used as a FRET donor whereby the FRET acceptor was anti ER-β antibody labelled with organic dye AF568 which shows a large spectral overlap with the emission spectrum of QD 565. As the immunocomplex formed, excitation at 476 nm led to emission from the dye at between 590 and 720 nm *via* fluorescence microscopy, leading to a lower detection limit of 2.65 ng L^{-1} based on the concentration of ER-β present.[139]

The use of QDs as FRET donors in the literature is plentiful, whereby common energy acceptors have included organic dyes, AuNPs and black hole quenchers (Table 1.5.5.). QDs also have a large potential for simultaneous detection of analytes with the ability to excite many different QDs with the same excitation wavelength.[140,141]

Table 1.5.5.

Selected examples of FRET assays whereby the donor is a QD.[142 143,144,145]

Analyte	**FRET scheme used**	**LOD / ng L^{-1}**
CEA	CdTe based QDs immobilised on 100 nm SiO_2 and functionalised with anti CEA Ab as the donor and AuNP functionalised with anti CEA Ab as the acceptor.	300
Glucose	CdTe based QDs functionalised with concanavalin A as the donor and 13 nm AuNP functionalised with β-cyclodextrin as the acceptor.	50 (nM)
Thrombin	QD 565 functionalised with a DNA aptamer beacon is the donor and DNA intercalating dye BOBO-3 is the acceptor.	1 (nM)
Renin	SA functionalised QD as the donor and biotin functionalised peptide conjugated to Cy5, which is cleaved up action from analyte, as the acceptor.	25 (pM)

Despite their advantages, QDs suffer from drawbacks. Namely the blinking effect which is common with the use of QDs whereby the emission has "on or off" states which can somewhat limit their use as the optical signal is not constant.[146] The excited state lifetime of the QD is short in the nanosecond range which can cause issues associated with eliminating the optical signal from background fluorescence, although the tunable nature of the excitation wavelength can help avoid the use of dangerous excitation wavelengths in the experimental setup. Also, similarly to Ln NPs, often a large size of the QD can lead to a large distance between the donor and the acceptor leading to a poor FRET signal as the coatings required to tune the properties of the material can often be relatively thick leading to a poor chromophore separation. Also, the toxicity of QDs is a downfall to these materials, when safer alternatives, such as Ln NPs, can be used.[147,148]

1.5.4 Nanoparticles as FRET acceptors

Whilst much of the literature in the area of NPs in FRET assays is dominated by the use of the NP as a FRET donor from their tunable and exciting emissive properties, there have been reports of nanoparticles as FRET acceptors. As afore mentioned, QDs have found application as FRET acceptors, although this is uncommon. AuNPs have been widely reported at FRET donors due to their high fluorescence quenching capability because of their surface plasmon resonance (SPR) absorption band which is both highly absorbing and broad, meaning a broad range of emission wavelengths can be quenched. Indeed, the spherical nature of the AuNP means that the FRET signal is no longer limited by the dipole orientation factor as the AuNP has no defined dipole.[149] Where the AuNP is used as a FRET acceptor, common donors are organic dyes and QDs, both of which have a short lived excited state lifetime.

The high quenching capability of AuNPs was demonstrated by Chen *et. al.* in a competitive FRET assay for IgM molecules. Anti IgM antibodies were conjugated to AuNPs of 13 nm in diameter and IgM molecules were conjugated to FITC molecules, the emission which shows a large spectral overlap with the SPR band of 13 nm AuNPs. As the FITC labelled IgM were incubated with varying concentrations of anti IgM antibody labelled AuNP, upon excitation at 490 nm, the emission intensity of the FITC was decreased as the concentration of anti IgM antibody labelled AuNP was increased by monitoring the emission siganl of the FITC at 520 nm, as a result of FRET quenching from the SPR band of the AuNP. This was able be taken forward to develop a competitive FRET based assay for IgM molecules to show a lower detection limit for IgM of 42 nM (Figure 1.5.7.).[150]

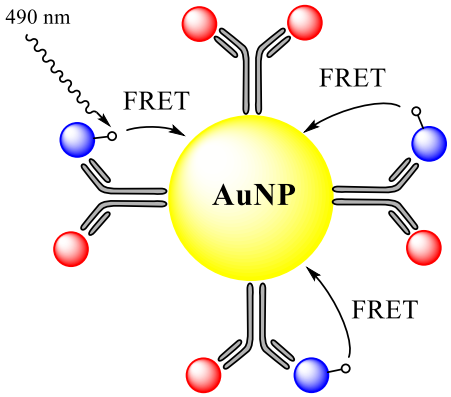

Figure 1.5.7.

Schematic of a competitive FRET immunoassay utilising AuNP acceptor.

O*, FITC label; red circle, IgM; blue circle, competing labelled IgM.*

Indeed, the use of the SPR band of AuNPs as a FRET quencher is common and have been applied to many assay systems in the literature (Table 1.5.6.).

Table 1.5.6.

Selected examples of FRET assays whereby the acceptor is an AuNP.[151,152 153,154]

Analyte	**FRET scheme used**	**LOD / ng L^{-1}**
CTnI	Anti CTnI Abs functionalised with Cy3 dye as the donor and 20 nm AuNP functionalised with anti CTnI Abs as the acceptor.	700
DNA methylation	FITC labelled DNA as the donor and gold nanorods of 10 x 10 x 30 nm as the acceptor.	0.25 (U mL^{-1})
CEA	DNA modified fluorescent polymer NP of 50 nm functionalised with DNA as the donor and AuNP of 13 nm functionalised with DNA as the acceptor.	100
DNA hybridisation	Silica particles of 50 nm doped with FITC functionalised with complementary DNA strand as the donor and 13 nm AuNPs functionalised with a complementary DNA strand as the acceptor.	3 (pM)

1.6 Free light chain assays

Immunoglobin G (IgG) type antibodies are comprised of four individual units to make up a whole antibody, which is typically a 'Y' shape with two antigen binding sites. These units are made of heavy chains (HCs) and light chains (LCs). Each IgG antibody has two HCs and two LCs (Figure 1.6.1.).[155]

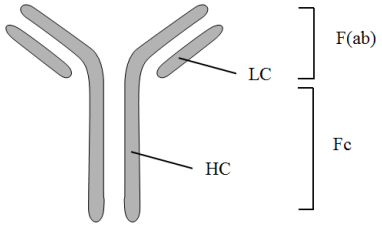

Figure 1.6.1.

IgG structure with HC and LC regions shown.

F(ab), Ag binding fragment region; Fc, crystallisable region.

Whilst IgG is the most common antibody in humans providing most resistance against invading antigens, other structures can be found. These are IgD and IgE which also have a 'Y' shape as well as dimer IgA and pentamer IgM (Figure 1.6.2.). Similarly, all of these contain HC and LC units.

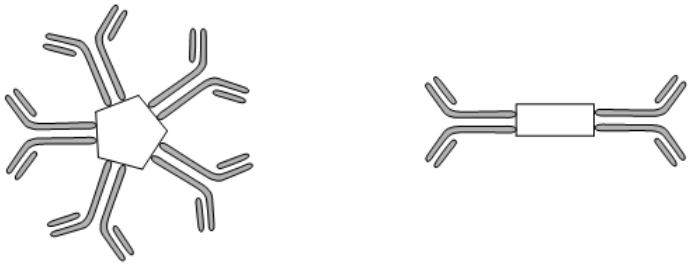

Figure 1.6.2.

Schematic of IgM (left) and IgA (right) Abs.

Each IgG is comprised of two antigen binding fragment (F(ab)) units and one crystallisable fragment (Fc). The LC antibodies are located on the (F(ab)) and are connected to the HC with disulphide bonds (Figure 1.6.3.). An IgG molecule is *ca.* 150 kDa in size.

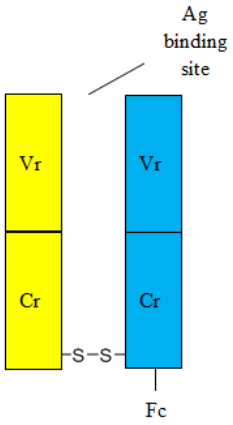

Figure 1.6.3.

General F(ab) structure with LC highlighted in yellow and HC highlighted in blue.

Vr, variable region; Cr constant region.

There are two types of LC in mammalian species, so called Kappa (κ) and Lambda (λ) chains. Each LC is comprised of *ca.* 210 – 220 amino acids, is *ca.* 25 kDa in size and is made up of a variable region (V_r) which sits at the antigen binding site of the antibody, and a constant region (C_r) which is bound to a HC in an antibody molecule.[156,157] Each type of LC chain antibody has an identical C_r amino acid sequence and the amino acid sequence of the V_r differs. As such many LC antibodies have been sequenced and reported.[158,159,160]

Antibodies are made and developed in bone marrow cells and are released into the serum for use. During this production process LC antibodies are produced in a small excess to HC antibodies. LC and HC units become joined to form whole Ig units which leaves a small concentration of LC antibody which is also released in the serum (Figure 1.6.4.). The unbound LCs are called free light chains (FLCs) and known as Bence Jones (BJ) proteins if they are present in the urine.[161]

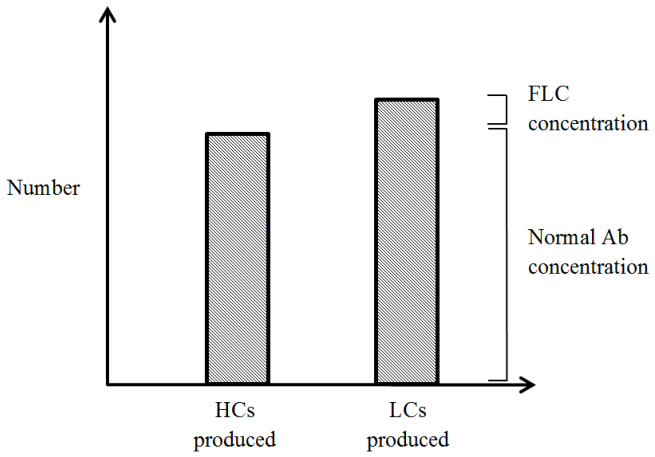

Figure 1.6.4.

Graph of HC production against LC production in an apparently healthy individual. Not to scale.

In an apparently healthy individual the concentration of κ and λ FLC in the blood is 3.3 – 19.4 mg L^{-1} (κ) and 5.7 – 26.3 mg L^{-1} (λ) and a κ : λ ratio of between 0.26 : 1.65.[162] The quantification of the concentration of both κ and λ FLC in the serum or urine is crucial in the diagnosis of multiple myeloma and can be used in the aid of other BJ related disorders including multiple sclerosis, systemic lupus erythematosus and others.[163,164,165]

Currently there is no known cure for myeloma. Many patients die within months of diagnosis of this condition, with symptoms such as bone pain, tiredness and renal failure, and the patient will also become much more susceptible to infection.[166] The five year survival rate of myeloma in the UK is currently 47.0% after the initial diagnosis and the ten year survival rate is 32.5%.[167] As such, early diagnosis of this condition is crucial to delivering the care and treatment to patients in aid of them surviving the disease as long and as comfortably as possible.

Myeloma is a cancer of the bone marrow which leads to a large excess of cancerous bone marrow to be produced. These clonal bone marrow cells are also involved in the production of antibodies and as a result a large overproduction of antibodies is observed, and a large FLC concentration is present in the serum (Figure 1.6.5.). This FLC concentration varies depending on the time course of the disease from the normal concentrations to of 30 – 40 times larger than the normal serum concentration. A patient diagnosed with myeloma will see an increase in the concentration of only one type of LC, hence the κ : λ ratio is an important measurement to make a successful diagnosis of either a κ or a λ myeloma.

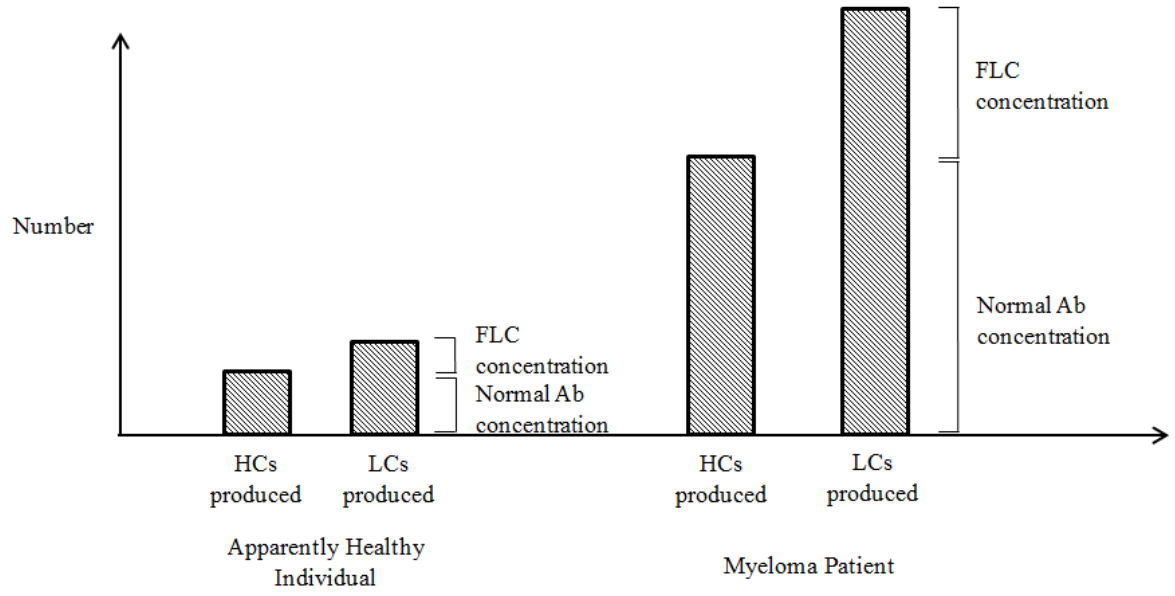

Figure 1.6.5.

Graph of HC production against LC production in an apparently healthy individual against a myeloma patient. Not to Scale.

Until the 1970s diagnosis of myeloma was particularly challenging as researchers were looking at quantifying the concentration of BJ protein in the urine.[168] This led to a barrier to this research as the kidneys play a role in keeping proteins within the body and not letting them seep into the urine and it is not until the FLC concentration is large in the serum that experimentalists were detecting these proteins within the urine, as the kidneys reabsorption mechanisms are overcome.[169,170] Because of this issue, it is serum FLC assays that are now generally used, although the first commercial serum FLC assays were based around electrophoresis and radioimmunoassay methods which were experimentally difficult and

lacked the sensitivity to give an early myeloma diagnosis. Indeed, the detection ranges of electrophoresis type assays were typically between 500 and 2000 mg L^{-1} which are well above normal serum levels of FLC.[171,172,173]

In 2001, a breakthrough in the area of serum FLC assays was published by Bradwell *et. al.* whereby the concentration of κ and λ FLCs were measured separately *via* a turbidimetric immunoassay and this is currently the only US food and drug administration approved method of FLC concentration determination used today.[174] The assay is able to determine the concentration of FLC in the serum between 3.6 – 172 mg L^{-1} for κFLC and 5.6 – 268 mg L^{-1} for λFLC, both of which are lower than the normal serum concentrations of FLC concentration, showing an increase in the sensitivity of *ca*. 500 times in comparison to electrophoresis methods previously used.

A large research effort is made towards the quantification of the concentration of both of κ and λ FLCs, and several new assays have been developed and commercialised, often using methods to quantify the concentration of both κ and λ FLCs.[175,176] In 2013 a multiplex Luminex assay was developed by Campbell *et. al.* whereby Luminex beads coated with anti FLC antibody were developed which show competitive binding between FLC in a patient sample and FLC functionalised with biotin. SA functionalised with organic dye phycoerythrin was used for detection showing detection ranges of 5.3 – 413.9 mg L^{-1} for κFLC and 2.5 – 406.5 mg L^{-1} for λFLC, both of which are within the normal serum concentrations of FLC.[177] This is rivalled with the development of Seralite which uses a dipstick method to quantify the concentration of κ and λ FLCs simultaneously using anti FLC antibody functionalised AuNPs to bind FLCs as a patient sample flows over the NPs in a portable device, showing detection ranges of between 7.9 – 790 mg L^{-1} for κFLC and 7.8 – 780 mg L^{-1} for λFLC again within the normal serum concentrations of FLC.[178,179]

1.7 Thesis aims and objectives

The aim of this thesis is to develop a novel, homogeneous FRET based assay for the quantification of FLCs using nanoparticles in a cheap and easy to run assay format, which in turn can be used to diagnose LC related disorders, such as multiple myeloma and others.

Our approach is to develop a system whereby the FRET donor is a luminescent Eu(III) complex which has advantages over organic FRET donors with its large Stokes shift, sharp line emission spectrum and long lived τ. This complex is to be attached to the surface of a AuNP, along with LC material which can show competitive binding with FLC in a patient sample with anti FLC antibody. The anti FLC antibody is tagged with an organic dye which acts as a FRET acceptor, developing a system whereby the FRET is 'on' if no competitive binding occurs and 'off' if competitive binding occurs, as measured *via* quenching of the Eu(III) complex (Figure 1.7.1.).

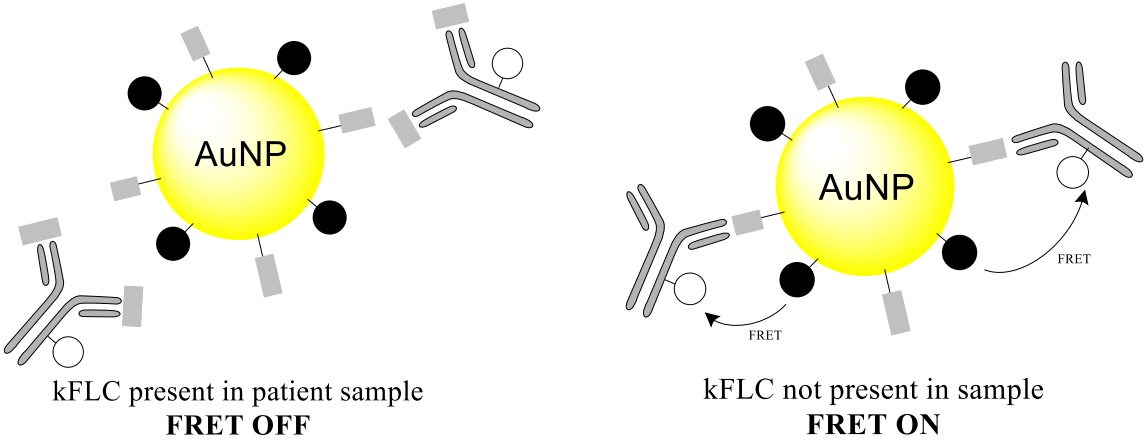

Figure 1.7.1.

FRET assay design as discussed in this thesis.

O, *FRET acceptor;* ●, *FRET donor;* ▭, *LC either in sample or bound to AuNP.*

The use of Ln NPs in assay technology is a popular area of research whereby lower detection limits can be reached for both surface and solution based assays. This homogeneous system is designed to be facile for the experimentalist to perform with no lengthy washing procedures, whilst also being cheap to run whereby only a small amount of material is required to get an assay readout. This system competes with current technology based on luminescent Ln NPs in homogeneous assay schemes as the luminescent Ln reporter is bound to the surface, and not buried deep within a large nanomaterial, which can be 100 nm, far out of the FRET range for a surface bound acceptor (Section 1.5). The advantage of the surface bound donor molecule in our system is the distance between the donor and the acceptor is reduced and so all within the range for FRET to occur and signal from unquenched Eu(III) reporters is no longer an issue.

1.8 Referenced material

1 J. L. Bock, *Am. J. Clin. Pathol.*, 2000, **113**, 628 – 646.

2 S. Song, N. Liu, Z. Zhao, E. N. Ediage, S. Wu, C. Sun, S. D. Saeger and A. Wu, *Anal. Chem.*, 2014, **86**, 4995–5001.

3 X. Sun, Y. Zhang, D. Zheng, S. Yue, C. Yang and Z. Xu, *Biosens. Bioelectron.*, 2017, **92**, 81 – 86.

4 M. Tschöp, H. M. Behre, E. Nieschlag, R. A. Dressendörfer and C. J. Strasburger, *Clin. Chem. Lab. Med.*, 1998, **36**, 223 – 230.

5 I. A. Darwish, *Int. J. Biomed. Sci.*, 2006, **2**, 217 – 235.

6 PerkinElmer DELFIA kit information, http://www.perkinelmer.co.uk/lab-products-and-services/application-support-knowledgebase/delfia/delfia-trf-assays.html, (Acsessed online April 2017).

7 N. Kim and S. Son, *J. Fluoresc.*, 2016, **26**, 1715 – 1721.

8 Thermofisher ELISA kit information, https://www.thermofisher.com/uk/en/home/life-science/protein-biology/protein-biology-learning-center/protein-biology-resource-library/pierce-protein-methods/overview-elisa.html, (Accessed online April 2017).

9 C. C. Capule and J. Yang, *Anal. Chem.*, 2012, **84**, 1786 – 1791.

10 T. Kreisig, R. Hoffmann and T. Zuchner, *Anal. Chem.*, 2011, **83**, 4281 – 4287.

11 Y. Wu, W. Guo, W. Peng, Q. Zhao, J. Piao, B. Zhang, X. Wu, H. Wang, X. Gong and J. Chang, *ACS Appl. Mater., Interfaces*, 2017, **9**, 9369 – 9377.

12 X. Huang, R. Chen, W. Lai and Y. Xiong, *Anal. Chem.*, 2016, **88**, 1951 – 1958.

13 S. Wang, Z. Chen, J. Choo and L. Chen, *Anal. Bioanal. Chem.*, 2016, **408**, 1015–1022.

14 C. Hsu, H. Huang, W. Chen, W. Nishie, H. Ujiie, K. Natsuga, S. Fan, H. Wang, J. Y. Lee, W. Tsai, H. Shimizu and C. Cheng, *Anal. Chem.*, 2014, **86**, 4605 – 4610.

15 T. Förster, *Naturwissenschaften*, 1946, **33**, 166 – 175.

16 B. Valeur, *Molecular fluorescence: Principles and applications*, Wiley-VCH, Weirheim, 1st edition, 2001, ch. 9, 247 – 271.

17 Thermofisher information on common FRET pairs for organic dyes, https://www.thermofisher.com/uk/en/home/references/molecular-probes-the-handbook/technical-notes-and-product-highlights/fluorescence-resonance-energy-transfer-fret.html, (Accessed online April 2017).

18 A. R. Clapp, I. L. Medintz, J. M. Mauro, B. R. Fisher, M. G. Bawendi and H. Mattoussi, *J. Am. Chem. Soc.*, 2004, **126**, 301 – 310.

19 K. Boeneman, J. B. Delehanty, J. B. Blanco-Canosa, K. Susumu, M. H. Stewart, E. Oh, A. L. Huston, G. Dawson, S. Ingale, R. Walters, M. Domowicz, J. R. Deschamps, W. R. Algar, S.DiMaggio, J.

Manono, C. M. Spillmann, D. Thompson, T. L. Jennings, P. E. Dawson and I. L. Medintz, *ACS Nano.*, 2013, **7**, 3778 – 3796.

20 J. Shi, F. Tian, J. Lyu and M. Yang, *J. Mater. Chem. B*, 2015, **3**, 6989 – 7005.

21 P. Verwilst, S. Park, B. Yoon and J. S. Kim, *Chem. Soc. Rev.*, 2015, **44**, 1791 – 1806.

22 M. Bottrill, L. K. Wok and N. J. Long, *Chem. Soc. Rev.*, 2006, **35**, 557 – 571.

23 K. R. D. Johnson and P. G. Hayes, *Chem. Soc. Rev.*, 2013, **42**, 1947 – 1960.

24 F. T. Edelmann, *Chem. Soc. Rev.*, 2013, **42**, 7657 – 7672.

25 R. D. Teo, J. Termini and H. B. Gray, *J. Med. Chem.*, 2016, **59**, 6012 – 2024.

26 S. Comby, E. M. Surender, O. Kotova, L. K. Truman, J. K. Molloy and T. Gunnlaugsson, *Inorg. Chem.*, 2014, **53**, 1867 – 1879.

27 N. Kaltsoyannis and P. Scott, *The f elements*, Oxford science publications, New York, 1st edition, 1999, ch. 2 and ch. 3, 6 – 32.

28 L. A. Ekanger, D. R. Mills, M. M. Ali, L. A. Polin, Y. Shen, E. M. Haacke and M. J. Allen, *Inorg. Chem.*, 2016, **55**, 9981 – 9988.

29 M. Szostak, N. J. Fazakerley, D. Parmar and D. J. Procter, *Chem. Rev.* 2014, **55**, 5959 – 6039.

30 P. D'Angelo, A. Zitolo, V. Migliorati, G. Chillemi, M. Duvail, P. Vitorge, S. Abadie and R. Spezia *Inorg. Chem.*, 2011, **50**, 4572 – 4579.

31 J. G. Bünzli, *J. Coord. Chem.*, 2014, **67**, 3706 – 3733.

32 J. Jiang, W. Liu, K. Poon, D. Du, D. P Arnold and D. K. P. Ng, *Eur, J. Inorg. Chem.*, 2000, 205 – 209.

33 T. A. Beineke and J. Delgaudio, *Inorg. Chem.*, 1968, **7**, 715 – 721.

34 M. Zbiri, C. A. Daul and T. A. Wesolowski, *J. Chem. Theory Comput.*, 2006, **2**, 1106 – 1111.

35 P. Atkins, T. Overton, J. Rourke, M. Weller and F. Armstrong, *Shriver and Atkins Inorganic chemistry*, Oxford university press, New York, 5th edition, 2010, ch. 20, 473 – 506.

36 S. V. Eliseevaa and J. G. Bünzli, *Chem. Soc. Rev.*, 2010, **39**, 189 – 227.

37 J. G. Bünzli, *Coord. Chem. Rev.*, 2015, **293**, 19 – 47.

38 J. G. Bünzli, *Chem. Rev.*, 2010, **110**, 2729 – 2755.

39 R. D. Teo, J. Termini and H. B. Gray, *J. Med. Chem.*, 2016, **59**, 6012−6024.

40 J. G. Bünzli and C. Piguet, *Chem. Soc. Rev.*, 2005, **34**, 1048 – 1077.

41 J. M. Zwier, H. Bazin, L. Lamarque and G. Mathis, *Inorg. Chem,*. 2014, **53**, 1854 – 1866.

42 A. J. Amoroso and S. J. A. Pope, *Chem. Soc. Rev.*, 2015, **44**, 4723 – 4742.

43 J. Zawadiak and M. Mrzyczek, *Spectrochimica Acta Part A*, 2010, **75**, 925 – 929.

44 K. Nakamoto *J. Phys. Chem.*, 1960, **64**, 1420 – 1425.

45 D. Sutherland and C. Compton, *J. Org. Chem.*, 1952, **17**, 1257 – 1261.

46 U. Steiner, D. Woll and S. Walbert, WO 2003074542 A2, 2003.

47 W. D. W. Horrocks and D. R. Sudnick, *J. Am. Chem. Soc.*, 1979, **101**, 334 – 340.

48 R. C. Holz, C. A. Chang and W. D. Horrocks, *Inorg. Chem.*, 1991, **30**, 3270 – 3275.

49 N. Sabbatini and M. Guardigli, *Coord. Chem. Rev.*, 1993, **123**, 210 – 228.

50 A. Beeby, I. M. Clarkson, R. S. Dickins, S. Faulkner, D. Parker, L. Royle, A. S. de Sousa, J. A. G. Williams and M. Woods, *J. Chem. Soc., Perkin Trans. 2*, 1999, 493 – 503.

51 N. Viola-Villegas and R. P. Doyle, *Coord. Chem. Rev.*, 2009, **253**, 1906 – 1925.

52 K. L. Nash, D. Brigham, T. C. Shehee and A. Martin**,** *Dalton Trans*., 2012, **41**, 14547 – 14556.

53 T. Güden-Silber, C. Doffek, C. Platas-Iglesias and M. Seitz, *Dalton Trans.*, 2014, **43**, 4238 – 4241.

54 A. N. Gusev, M. Hasegawa, T. Shimizu, T. Fukawa, S. Sakurai, G. A. Nishchymenko, Victor F. Shulgin, S. B. Meshkova and W. Linert, *Inorg. Chim. Acta.*, 2013, **406**, 279 – 284.

55 J. Garcia and M. J. Allen, *Eur. J. Inorg. Chem.*, 2012, **29**, 4550 – 4563.

56 P. D. Bernardoa, A. Melchiorb, M. Tolazzib and P. L. Zanonatoa, *Coord. Chem. Rev.*, 2012, **256**, 328 – 351.

57 L. Jiang, J. Zheng, W. Chen, J. Ye, L. Mo, Z. Li, L. Hu, C. Zhang and S. Dai, *J. Phys. Chem. C,* 2017, **121**, 5925 – 5930.

58 D. M. Weekes, C. F. Ramogida, M. G. Jaraquemada-Peláez, B. O. Patrick, C. Apte, T. I. Kostelnik, J. F. Cawthray, L. Murphy and C. Orvig, *Inorg. Chem.*, 2016, **55**, 12544 – 12558.

59 A. Mohamadi and L.W. Miller, *Bioconjug. Chem.*, 2016, **27**, 2540 – 2548.

60 D. Geißler, S. Linden, K. Liermann, K. D. Wegner, L. J. Charbonnière and N. Hildebrandt, *Inorg. Chem.*, 2014, **53**, 1824 – 1838.

61 R. Roy, S. Hohng and T. Ha, *Nat. Methods.* 2008, **5**. 507 – 516.

62 H. Siitari, I. Hemmila, E. Soini and T. Lovgren and V. Koistinen, *Nature*, 1983, **301**, 258 – 260.

63 J. Vuori, S. Rasi, T. Takala and K. Vaananen, *Clin. Chem.*, 1991, **37**, 2087 – 2092.

64 R. Liang, Y, Yang, J. Zhou, T. Liu, X. Xu, Q. Liang, Z. Chen, Z. Dong and Y. Wu, *J. Fluoresc.*, 2017, **27**, 309 – 316.

65 F. Wua and C. Zhang, *Anal. Biochem.*, 2002, **311**, 57 – 67.

66 H. Kimura, M. Mukaida, G. Wang, J. Yuan and K. Matsumoto, *Forensic Sci. Int.*, 2000, **113**, 345 – 351.

67 Q. Wang, K. N. Nono, M. Syrjänpää, L. J. Charbonniere, J. Hovinen and H. Harmä, *Inorg. Chem.*, 2013, **52**, 8461 – 8466.

68 F. Wu, S. Han, C. Zhang and Y. He, *Anal. Chem.*, 2002, **74**, 5882 – 5889.

69 R. C. Morton and E. P. Diamandis, *Anal. Chem.*, 1990, **62**, 1841 – 1845.

70 J,.Yuan, K. Matsumoto and H. Kimura, *Anal. Chem.*, 1998, **70**, 596 – 601.

71 G. Mathis, *Clin. Chem.* 1993, **39**, 1953 – 1959.

72 Q. Qin, O. Peltola and K. Pettersson, *Clin. Chem.*, 2003, **49**, 1105 – 1113.

73 K. Enomoto, A. Araki, T. Nakajima, H. Ohta, K. Dohi, M. Preaudat, P. Seguin, G. Mathis, R. Suzuki, G. Kominami and H. Takemoto, *J. Pharm. Biomed. Anal.*, 2002, **28**, 73 – 79.

74 S. Sueda, J. Yuan, and K. Matsumoto, *Bioconjug. Chem*. 2002, **13**, 200 – 205.

75 S. E. Lohse and C. J. Murphy, *J. Am. Chem. Soc.*, 2012, **134**, 15607 – 15620.

76 S. Lal, S. E. Clare and N. J. Halas, *J. Acc. Chem. Res.*, 2008, **41**, 1842 – 1851.

77 M. Grzelczak, J. Perez-Juste, P. Mulvaney and L. M. Liz-Marza, *Chem. Soc. Rev.*, 2008, **37**, 1783 − 1791.

78 P. V. Kamat, *Acc. Chem. Res.*, 2012, **45**, 1906 – 1915.

79 N. L. Rosi and C. A. Mirkin, *Chem. Rev.*, 2005, **105**, 1547 – 1562.

80 K. L. Kelly, E. Coronado, L. L. Zhao and G. C. Schatz, *J. Phys. Chem. B*, 2003, **107**, 668 – 677.

81 R. Thiruppathi, S. Mishra, M. Ganapathy, P. Padmanabhan and B. Gulyás, *Adv. Sci*., 2016, **4**, 1600279 **–** 1600293.

82 E. Harrison, J. A. Coulter and D. Dixon, *Nanomed.*, 2016, **11**, 851 – 865.

83 L. Xiao, A. Zhu, Q. Xu, Y. Chen, J. Xu and J. Weng, *ACS Appl. Mater. Interfaces*, 2017, **9**, 6931 – 6940.

84 X. Wei, Z. Chen, L. Tan, T. Lou and Y. Zhao, *Anal. Chem.*, 2017, **89**, 556 – 559.

85 H. Zhang, H. Dong, G. Yang, H. Chen and C. Cai, *Anal. Chem.*, 2016, **88**, 11108 – 11114.

86 F. Qu, M. Yang and A. Rasooly, *Anal. Chem.*, 2016, **88**, 10559 – 10565.

87 X. Lin, X. Wang, L. Liu, Q. Wen, R. Yu and J. Jiang, *Anal. Chem.*, 2016, **88**, 9881 – 9884.

88 R. Du, L. Zhu, J. Gan, Y. Wang, L. Qiao and B. Liu, *Anal. Chem.*, 2016, **88**, 6767 – 6772

89 D. Tang, Y. Cui and G. Chen, *Analyst*, 2013, **138**, 981 – 990.

90 Y. Xu and Q. Li, *Clin. Chem.*, 2007, **53**, 1503 – 1510.

91 H. Harma, T. Soukka and T. Lovgren, *Clin. Chem.*, 2001, **43**, 561 – 568.

92 M. Jarvenpaa, K. Kuningas, I. Niemi, P. Hedberg, N. Ristiniemi, K. Pettersson and T. Lovgren, *Clin. Chim. Acta.*, 2012, **414**, 70 – 75.

93 T. Matsuya, S. Tashiro, N. Hoshino, N. Shibata, Y. Nagasaki and K. Kataoka, *Anal. Chem.*, 2003, **75**, 6124 – 6132.

94 P. Huhtinen, M. Kivela, T. Soukka, H. Tenhu, T. Lovgren and H. Harma, *Anal. Chim. Acta.*, 2008, **630**, 211 – 216.

95 A. Pelkkikangas, S. Jaakohuhta, T. Lövgren and H. Härmä, *Anal. Chim. Acta.*, 2004, **517**, 169 – 176.

96 T. Soukka, K. Antonen, H. Härmä, A. Pelkkikangas, P. Huhtinen and T. Lövgren, *Clin. Chim. Acta.*, 2003, **328**, 45 – 58.

97 A. Valanne, S. Huopalahti, R. Vainionpää, T. Lövgren and H. Härmä, *J. Virol. Methods*, 2005, **129**, 83 – 90.

98 F. Wang, W. B. Tan, Y. Zhang, X. Fan and M. Wang, *Nanotech.*, 2006, **17**, R1 – R13.

99 Z. Ye, M. Tan, G. Wang and J. Yuan, *J. Mater. Chem.*, 2004, **14**, 851 – 856.

100 Z. Ye, M. Tan, G. Wang and J. Yuan, *Anal. Chem.*, 2004, **76**, 513 – 518.

101 Z. Ye, M. Tan, G. Wang and J. Yuan, *Talanta*, 2005, **65**, 206 – 210.

102 H. Zhang, Y. Xu, W. Yang and Q. Li, *Chem. Mater.*, 2007, **19**, 5875 – 5881.

103 M. Tan, G. Wang, X. Hai, Z. Ye and J. Yuan, *J. Mater. Chem.* 2004, **14**, 2896 – 2901.

104 Y. Chen, Y. Chi, H. Wen and Z. Lu, *Anal. Chem.*, 2007, **79**, 960 – 965.

105 H. Jiang, G. Wang, W. Zhang, X, Liu, Z. Ye, D. Jin, J. Yuan and Z. Liu, *J. Fluoresc.*, 2010, **20**, 321 – 328.

106 A. Valanne, H. Lindroos, T. Lovgren and T. Soukka, *Anal. Chim. Acta.*, 2005, **539**, 251 – 256.

107 L. Kokko, T. Kokko, T. Lövgren and T. Soukka, *Anal. Chim. Acta.*, 2008, **606**, 72 – 79.

108 H. Harma, S, Pihlasalo, P. J. Cywinski, P. Mikkonen, T. Hammann, H. G. Löhmannsröben and P. Hanninen, *Anal. Chem.* 2013, **85**, 2921 – 2926.

109 L. Kokko, K. Sandberg, T. Lövgren and T. Soukka, *Anal. Chim. Acta.*, 2004, **503**, 155 – 162.

110 A. Valanne, P. Malmi, H. Appelblom, P. Niemela and T. Soukka, *Anal. Biochem*. 2008, **375**, 71 – 81.

111 G. Yi, B. Sun, F. Yang, D. Chen, Y. Zhou and J. Cheng, *Chem. Mater.* 2002, **14**, 2910 – 2914.

112 S. Heer, O. Lehmann, M. Haase and H. Gudel, *Angew. Chem. Int. Ed.*, 2003, **42**, 3179 – 3182.

113 I. Etchart, I. Hernandez, A. Huignard, M. Berard, W. P. Gillin, R. J. Curry and A. K. Cheetham, *J. Mater. Chem.*, 2011, **21**, 1387 – 1394.

114 C. H. Yang, Y. X. Pan, Q. Y. Zhang and Z. H. Jiang, *J. Fluoroesc.* 2007, **17**, 500 – 504.

115 A. Bednarkiewicz, M. Nyk, M. Samoc and W. Strek, *J. Phys. Chem. C.*, 2010, **114**, 17535 – 17541.

116 H. J. Zijlmans, J. Bonnet, J. Burton, K. Kardos, T. Vail, R. S. Niedbala and H. J. Tanke, *Anal. Biochem.*, 1999, **267**, 30 – 36.

117 K. Kuningas, H. Pakkila, T. Ukonaho, T. Rantanen, T. Lovgren and T. Soukka, *Clin. Chem.*, 2007, **53**, 145 – 146.

118 L. Wang, R. Yan, Z. Huo, L. Wang, J. Zeng, J. Bao, X. Wang, Q. Feng and Y. Li, *Angew. Chem. Int. Ed.*, 2005, **44**, 6054 – 6057.

119 P. Zhang, S. Rogel, K. Nguyen and D. Wheeler, *J. Am. Chem. Soc.*, 2006, **128**, 12410 – 12411.

120 K. Kuningas, T. Ukonaho, H. Pa1kkila, T. Rantanen, J. Rosenberg, T. Lovgren and T. Soukka, *Anal. Chem.*, 2006, **78**, 4690 – 4696.

121 M. Wang, W. Hou, C. Mi, W. Wang, Z. Xu, H. Teng, C. Mao and S. Xu, *Anal. Chem.*, 2009, **81**, 8783 – 8789.

122 L. Mattsson, K. D. Wegner, N. Hildebrandt and T. Soukka, *RSC Adv.*, 2015, **5**, 13270 – 13277.

123 E. Jo, H. Mun and M. Kim, *Anal. Chem.*, 2016, **88**, 2742 – 2746.

124 H. Li, L. Shi, D. Sun, P. Li and Z. Liu, *Biosens. Bioelectron.*, 2016, **86**, 791 – 798.

125 C. Liu, Z. Wang, H. Jia and Z. Li, *Chem. Commun.*, 2011, **47**, 4661 – 4663.

126 P. Alonso-Cristobal, P. Vilela, A. El-Sagheer, E. Lopez-Cabarcos, T. Brown, O. L. Muskens, J. Rubio-Retama and A. G. Kanaras, *ACS Appl. Mater. Interfaces*, 2015, **7**, 12422 – 12429.

127 F. Wang, R. Deng, J. Wang, Q.Wang, Y. Han, X. Chen and X. Liu, *Nat. Mater.*, 2011, **10**, 968 – 973.

128 V. Muhr, C. Würth, M. Kraft, M. Buchner, A. J. Baeumner, U. Resch-Genger and T. Hirsch, *Anal. Chem.*, 2017, **89**, 4868 – 4874.

129 A.Valanne, J. Suojanen, J. Peltonen, T. Soukka, P. Hanninen and H. Harma, *Analyst*, 2009, **134**, 980 – 986.

130 R. Gill, M. Zayats and I. Willner, *Angew. Chem. Int. Ed.*, 2008, **47**, 7602 – 7625.

131 M. Bruchez. Jr, M. Moronne, P. Gin, S. Weiss and A. P. Alivisatos, *Science*, 1998, **281**, 2013 – 2016.

132 B. O. Dabbousi, J. Rodriguez-Viejo, F. V. Mikulec, J. R. Heine, H. Mattoussi, R. Ober, K. F. Jensen and M. G. Bawendi, *J. Phys. Chem. B*, 1997, **101**, 9463 – 9475.

133 M. Green, P. Williamson, M. Samalova, J. Davis, S. Brovelli, P. Dobson and F. Cacialli, *J. Mater. Chem.*, 2009, **19**, 8341 – 8346.

134 Z. Ning, M. Molnar, Y. Chen, P. Friberg, L. Gan, H. Agren and Y. Fu., *Phys. Chem. Chem. Phys.*, 2011, **13**, 5848 – 5854.

135 L. D. True and X. Gao, *J. Mol. Diagn.*, 2007, **9**, 7 – 11.

136 T. Jamieson, R. Bakhshi, D. petrova, R. Pocock, M. Imani and A. M. Seifalian, *Biomat.*, 2007, **28**, 4717 – 4732.

137 L. J. Charbonniere, N. Hildebrandt, R. F. Ziessel and H. Lohmannsroben, *J. Am. Chem. Soc.*, 2006, **128**, 12800 – 12809.

138 K. D. Wegner, Z. Jin, S. Linden, T. L. Jennings and N. Hildebrandt, *ACS Nano*, 2013, **7**, 7411 – 7419.

139 Q. Wei, M. Lee, X. Yu, E. K. Lee, G. H. Seong, J. Choo and Y. W. Cho, *Anal. Biochem.* 2006, **358**, 31 – 37.

140 J. Liu, J. H. Lee and Y. Lu, *Anal. Chem*., 2007, **79**, 4120 – 4125.

141 W. R. Algar and U. J. Krull, *Anal. Chem.*, 2009, **81**, 4113 – 4120.

142 J. Qian, C. Wang, X. Pan and S. Liu, *Anal. Chim. Acta.*, 2013, **763**, 43 – 49.

143 B. Tang, L. Cao, K. Xu, L. Zhuo, J. Ge, Q. Li and L. Yu, *Chem. Eur. J*., 2008, **14**, 3637 – 3644.

144 C. Chi, Y. Lao, Y. Li and L. Chen, *Biosens. Bioelectron.*, 2011, **26**, 3346 – 3352.

145 Y. Long, L. Zhang, Y. Zhang and C. Zhang, *Anal. Chem.*, 2012, **84**, 8846 – 8852.

146 V. Rombach-Riegraf, P. Oswald, R. Bienert, J. Peterson, M. P. Domingo, J. Pardo, P. Graber and E. M. Galvez, *Biochem. Biophys. Res. Commun.*, 2013, **30**, 260 – 264.

147 N. Hildebrandt, *ACS Nano*, 2011, **5**, 5286 – 5290.

148 W. R. Algar, A. J. Tavares and U. J. Krull, *Anal. Chim. Acta.*, 2010, **673**, 1 – 25.

149 P. P. Hu, L. Q. Chen, C. Liu, S. J. Zhen, S. J. Xiao, L. Peng, Y. F. Lia and C. Z. Huang, *Chem. Commun.*, 2010, **46**, 8285 – 8287.

150 J. Chen, Y. Huang, S. Zhao, X. Lu and J. Tian, *Analyst*, 2012, **137**, 5885 – 5890.

151 S. Mayilo, M. A. Kloster, M. Wunderlich, A. Lutich, T. A. Klar, A. Nichtl, K. Kurzinger, F. D. Stefani and J. Feldmann, *Nano Lett.*, 2009, **9**, 4558 – 4564.

152 G. L. Wang, H. Q. Luo and N. B. Li, *Analyst*, 2014, **139**, 4572 – 4577.

153 Z. Lin, G. Zhang, W. Yang, B. Qiua and G. Chen, *Chem. Commun.*, 2012, **48**, 9918 – 9920.

154 F. Gao, P. Cui, X. Chen, Q. Ye, M. Li and L. Wang, *Analyst*, 2011, **136**, 3973 – 3980.

155 C. A. Janeway, P. Travers and M. Walport, *Immunobiology: The Immune System in Health and Disease*, Garland Science, New York, 5th edition, 2001.

156 R. S. Abraham, R. J. Clark, S. C. Bryant, J. F. Lymp, T. Larson, R. A. Kyle and J. A. Katzmann, *Clin. Chem.*, 2002, **48**, 655 – 657.

157 A. R. Bradwell, H. D. Carr-Smith, G. P. Mead and M. T. Drayson, *Clin. and Appl. Immunol. Rev.*, 2002, **3**, 17 – 33.

158 C. P. Milstein and E. V. Deverson, *Biochem. J.* 1971, **123**, 945 – 958.

159 J. Svasti and C. Milstein, *Biochem. J.* 1972, **128**, 427 – 444.

160 G. P. Smith, *Biochem. J.* 1978, **171**, 337 – 347.

161 C. A Hutchison, T. Plant, M. Drayson, P. Cockwell, M. Kountouri, K. Basnayake, S. Harding, A. R Bradwell and G. Mead, *BMC Nephrology*, 2008, **9**, 11 – 19.

162 J. A. Katzmann, R. J. Clark, R. S. Abraham, S. Bryant, J. F. Lymp, A. R. Bradwell and R. A. Kyle, *Clin. Chem.*, 2002, **48**, 1437 – 1444.

163 B. Kaplan, B. M. Aizenbud, S. Golderman, R. Yaskariev and B. A. Sela, *J. Neuroimmunol.* 2010, **229**, 263 – 271.

164 R. Aggarwal, W. Sequeira, R. Kokebie, R. A. Mikolaitis, L. Fogg, A. Finnegan, A. Plass, J. A. Block and M. Jolly, *Arthritis care and Res.*, 2011, **63**, 891 – 898.

165 J. A. Brebner and R. A. Stockley, *F1000 Medicine Reports*, 2013, **5**, 4 – 10.

166 NHS Information on the symptoms of myeloma, http://www.nhs.uk/conditions/Multiple-myeloma/Pages/Introduction.aspx, (Accessed online May 2017).

167 Cancer research UK information on the survival rates of myeloma, http://www.cancerresearchuk.org/health-professional/cancer-statistics/statistics-by-cancer-type/myeloma/survival#heading-Zero, (Accessed online May 2017).

168 E. Jenner, *Clinica Chimica Acta*, 2014, **427**, 15 – 20.

169 P. G. Hill, J. M. Forsyth, B. Rai and S. Mayne, *Clin. Chem.*, 2006, **52**, 1743 – 1748.

170 M. Korpysz, M. Morawska, A. Burska and H. Donica, *Curr. Issues Pharm. Med. Sci.*, 2014, **27**, 165 – 170.

171 M. A. Jenkins, *Clin. Biochem. Rev.*, 2009, **30**, 119 – 122.

172 D. F. Keren and L. Schroeder, *Clin. Chem. Lab. Med.*, 2016, **54**, 947 – 961.

173 M. V. Bhole, R. Sadler and K. Ramasamy, *Annals of Clin. Biochem.*, 2014, **51**, 528 – 542.

174 A. R. Bradwell, H. D. Carr-Smith, G. P. Mead, L. X. Tang, P. J. Showell, M. T. Drayson and R. Drew, *Clin. Chem.*, 2001, **47**, 673 – 680.

175 T. Nakano and A. Nagata, *J. of Immunol. Methods*, 2004, **293**, 183 –189.

176 R. Lakshminarayanan, Y. Li, K. Janatpour, L. Beckett and I. Jialal., *Am. J. Clin. Pathol.*, 2007 **127**, 746 –751.

177 J. P. Campbell, M. Cobbold, Y. Wang, M. Goodall, S. L. Bonney, A. Chamba, J. Birtwistle, T. Plant, Z. Afzal, R. Jefferis and M. T. Drayson, *J. Immunol. Methods*, 2013, **391**, 1 – 13.

178 J. P. Campbell, J. L. J. Heaney, M. Shemar, D. Baldwin, A. E. Griffin, E. Oldridge, M. Goodall, Z. Afzal, T. Plant, M. Cobbold, R. Jefferis, J. F.M. Jacobs, C. Hand and M. T. Drayson, *Clin. Chem. Lab. Med.*, 2017, **55**, 424 – 434.

179 Abingdon health information on Seralite, https://www.abingdonhealth.com/medical-diagnostics/b-cell-dyscrasias/seralite/, (Accessed online May 2017).

2 Preparation of luminescent light chain functionalised gold nanoparticles for FRET assays

2.1 Introduction

The first uses of colloidal gold can be traced back to the middle ages with their use as red pigments in stained glass windows, although it was not until the 1950s that Turkevich *et. al*. reported the first synthesis of colloidal gold.[1,2] Since then, the study into the properties and uses of AuNPs has been vast and as such AuNPs have been used in a plethora of applications due to their aqueous solubility, easy functionalisation and inert, non-toxic nature, whereby monodisperse particles with a tuneable diameter can be produced, whereby the optical properties of the particle are dependent on the size of the particle.[3] The uses of AuNPs is vast and ranges from medical diagnostics as previously discussed (Section 1.5), to energy conversion devices, intercellular imaging and many others.[4,5,6]

2.1.1 Lanthanide functionalised AuNPs

AuNPs offer a unique opportunity to incorporate multiple molecular scale luminophores into a single nanoscale architecture for signal detection without engaging in lengthy synthetic procedures for the incorporation of multiple labels. Indeed, it is possible to functionalise the surface of AuNPs with luminescent probes to retain the optical properties of the probe being used and this has been shown for transition metal and Ln based probes, both of which have found use in intercellular imaging applications.[7,8] Indeed, as well as luminescent Ln functionalised AuNPs, researchers have explored the possibility of Gd(III) functionalised AuNPs for their application within the field of MRI imaging, by increasing the relaxation rate of water molecules.[9,10,11]

Luminescent Ln functionalised AuNPs were first reported in 2006 by Lewis *et. al.* who synthesised a luminescent Eu complex with a DTPA bis-amide backbone, with a dual phenylamide based sensitizer with terminal thiol groups. This complex was able to be deposited on the surface of 13 nm AuNPs *via* the strong Au – S bond (Figure 2.1.1).[12] The luminescent Ln functionalised AuNPs were found to retain the characteristic sharp line emission spectrum of $^5D_0$ to the ground states of ^7F_J (J = 0 – 4) from the Eu(III) ion *via* excitation of the phenyl based sensitizer at 280 nm.

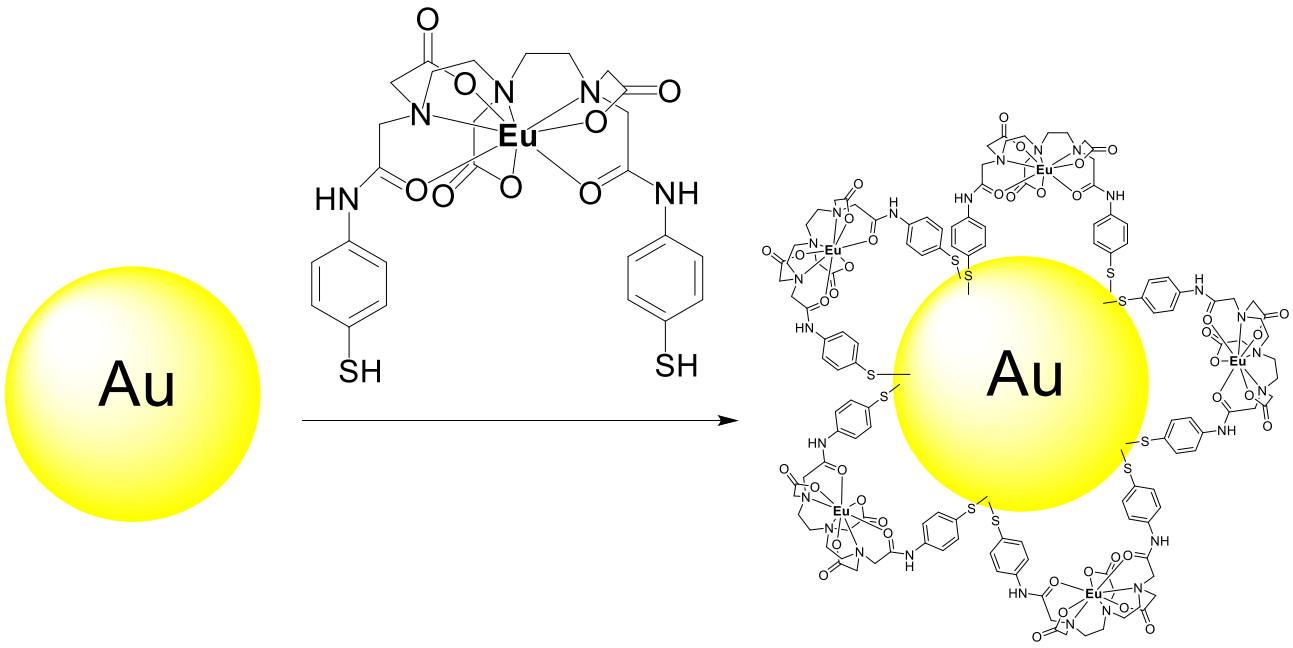

Figure 2.1.1.

Functionalisation of AuNP with surface active luminescent Eu(III) complex as developed by Davies.

Around the same time, Ipe *et. al.* were able to functionalise AuNPs with thiol modified dipyridyl units which bind and sensitize both Tb(III) and Eu(III) ions, similarly, showing strong *f–f* luminescence from both Ln(III) ions (Figure 2.1.2.).[13]

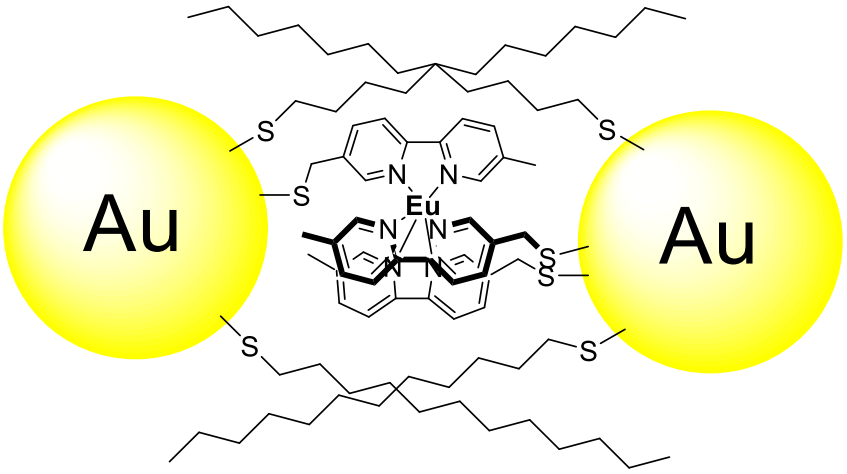

Figure 2.1.2.

Functionalisation of AuNP with surface active luminescent Eu(III) complex as developed by Ipe.

Research into the use of luminescent Ln functionalised AuNPs has not been vast and few publications exist in this area, although their use as both imaging probes and within sensing applications has been reported. In 2012 Davies *et. al.* reported the use of a luminescent Ln probe functionalised AuNPs for imaging of human platelets. AuNPs were coated with both a luminescent Eu(III) quinoline based probe and a pH responsive peptide whereby at pH < 6.5 the peptide structure becomes altered and inserts itself across a cell membrane. The particles were imaged using an excitation wavelength of 340 nm, showing Eu(III) luminescence within the platelets.[14] Gunnlaugsson *et. al.* have developed a range of AuNPs functionalised with Eu(III), Tb(III) and Yb(III) in DOTA complexes with terminal thiol groups for a range sensing applications including small molecules and BSA, as well as pH responsive AuNPs all of which are based on the sensitized luminescence of the Ln cation involved (Figure 2.1.3.).[15,16,17]

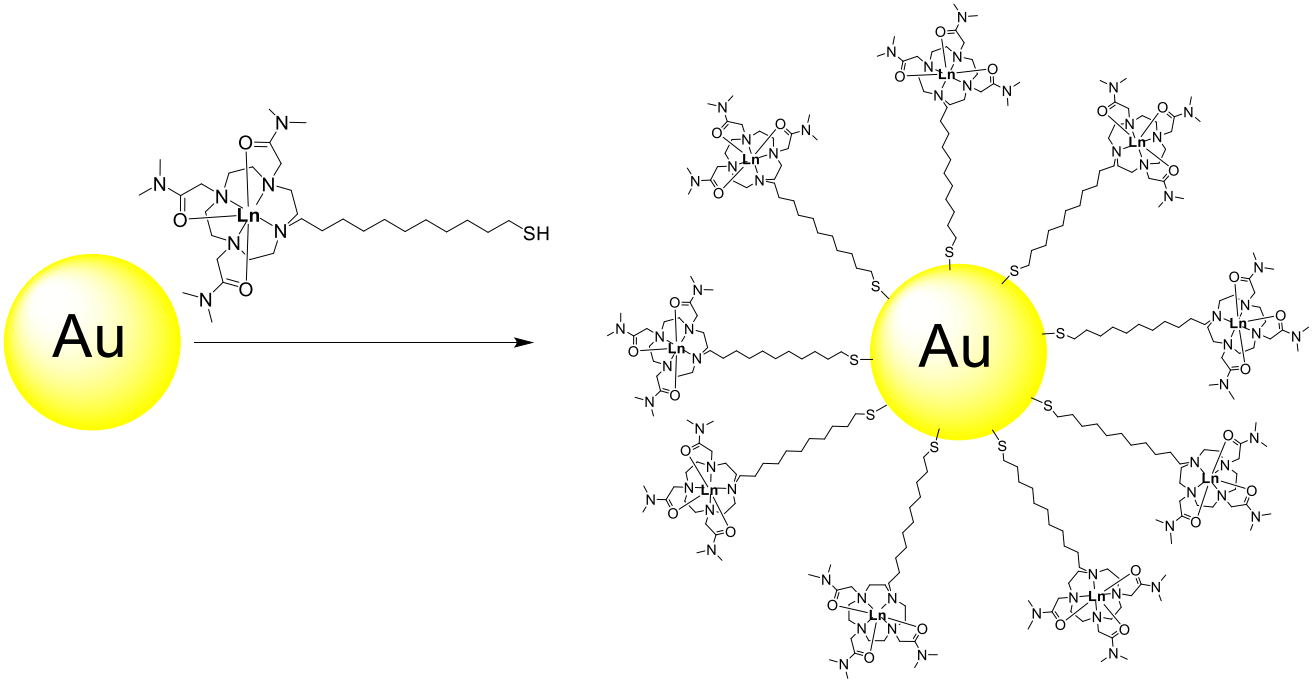

Figure 2.1.3.

Functionalisation of AuNP with surface active Ln(III) complex as developed by Gunnlaugsson for sensing applications.

Whilst the reports of Ln NPs as the luminescent agent in both surface and solution based luminescence bioassay schemes is a well understood area, the use of a Ln capped AuNP as the detectable label has yet to be explored in either type of system. Whilst Ln based NPs, are excellent candidates for FRET donors in solution based assays which can show lower detection limits than single molecule based methods, as previously discussed a large proportion of the luminescent reporter is buried deep within the particle, too deep for the reporter to experience a FRET quench from a surface bound acceptor (Section 1.5.). A surface bound luminescent reporter would effectively remove this large distance between the chromophores, hence bringing all of the FRET donor into usage.

In 2012 Pihlasalo *et. al.* developed a system whereby the determination of protein was achieved *via* FRET from the surface of a NP. Polystyrene NPs of 60 nm in diameter were prepared and γ-globulin proteins were functionalised with either luminescent Eu(III) complex or organic dye AF680, which shows a large ΔJ with the emission spectrum of the Eu(III) ion. The labelled proteins were adsorbed to the polystyrene NPs, whereby the emission of the Eu(III) was quenched *via* FRET by the AF680 using an excitation wavelength of 340 nm. On addition of competing proteins, the labelled γ-globulin proteins were displaced and the FRET turned 'off' as the donor and acceptor become separated (Figure 2.1.4.). A lower detection limit of 2.6 ng of protein was achieved and was also able to be applied to cell counting.[18] This report highlights the possibility of using a surface bound luminescent Ln complex as a FRET donor.

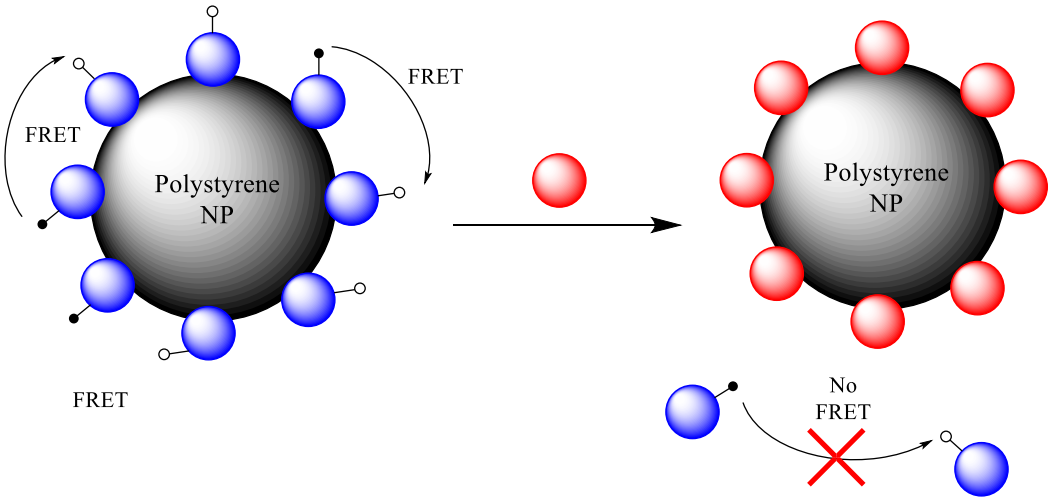

Figure 2.1.4.

FRET assay for determination of protein concentration.

red circle, analyte; blue circle, competing labelled analyte, O, *AF680;* ●, *luminescent Eu complex.*

It was also shown in a recent report that FRET is active between organic fluorophores on the surface of a silica NP whereby FITC is used as an energy donor to a rhodamine B energy acceptor in a study evaluating the effect of the concentration the energy donor and energy acceptor on the observed FRET signal between the two.[19]

2.1.2 Antibody functionalised AuNPs in immunoassays

AuNPs have been used extensively within immunoassay schemes. Indeed, as previously discussed, AuNPs have found use in homogeneous assay schemes as FRET acceptors (Section 1.5.), and the use of AuNPs as a scaffold upon which to immobilise biomolecules, such as antibodies, is common within immunoassay schemes. The use of antibody functionalised AuNPs within immunoassay schemes is common and can lead to lower detection limits in comparison to the use of single molecule methods. Mitchell *et. al.* were able to show how a surface based SPR assay for progesterone was able to be improved with the use of AuNP functionalised antibodies over single antibodies. It was found that the lower detection limit without the AuNP present was 20.1 pg mL^{-1} which was improved to 8.6 pg mL^{-1} with the inclusion of the colloidal gold into the system.[20] A similar effect was observed in an SPR assay for testosterone.[21] Indeed, other NPs have also been used to scaffold antibodies in immunoassay schemes, although AuNPs are the most widely used for their properties as previously discussed such as silica.[22,23]

As such, many methods have been developed for the conjugation of antibodies to AuNPs. These can be done by the experimentalist themselves, or several commercial sources are available which provide functionalised AuNPs to which the experimentalists antibodies can be simply added to develop antibody functionalised AuNPs.[24,25] Where the experimentalist performs the conjugation themselves, AuNPs can be functionalised with antibodies in a variety of ways (Figure 2.1.6.). These include adsorption onto the AuNP surface, covalently linked *via* click chemistry or EDC coupling with lysine residues on the antibody, coupling to the sugar units on the on the Fc area of an IgG using boronic acid chemistry, or using AuNPs and antibodies functionalised with SA and biotin, taking advantage of their strong bond.[26,27,28,29,30,31,32]

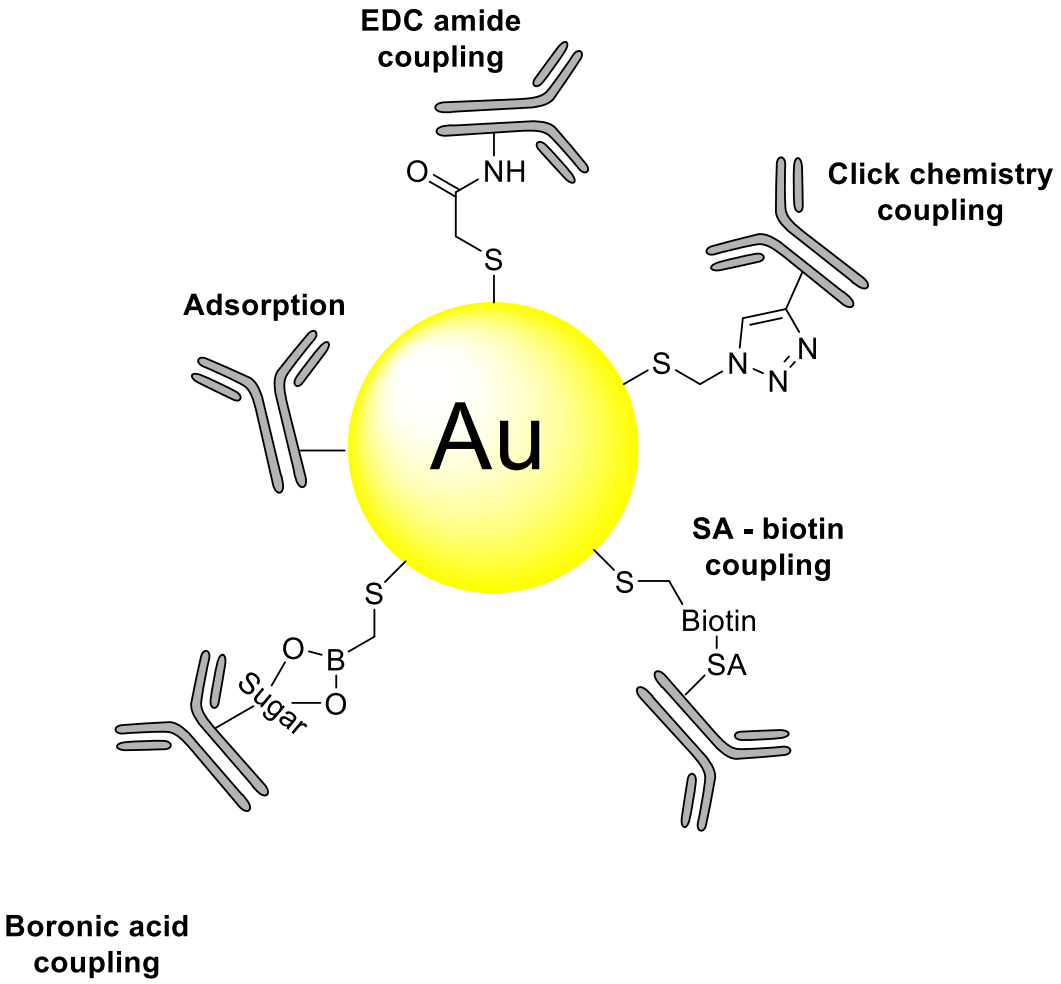

Figure 2.1.6.

Methodologies for functionalising AuNPs with antibodies.

2.2 Chapter outline

This chapter shows the surface functionalisation of AuNPs with surface active, luminescent Eu complexes and LCs, to produce LC functionalised AuNPs which show characteristic Eu luminescence and are used a FRET donor. These particles are then incubated with anti FLC antibody modified with a suitable FRET acceptor for Eu(III) luminescence and it is demonstrated how FRET can be observed between the pair, measured by excited state lifetime measurements (Figure 2.2.1.).

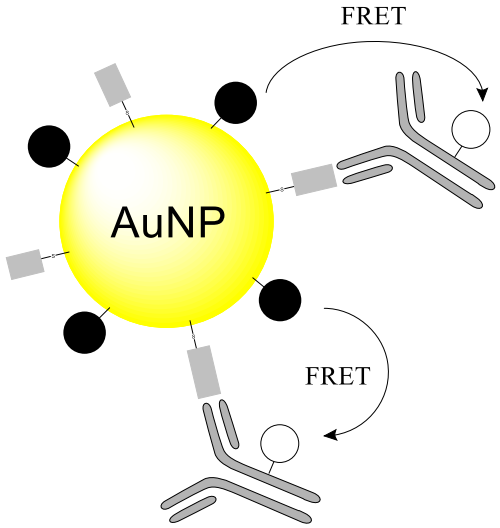

Figure 2.2.1.

General schematic of FRET between the functionalised AuNPs with FLC and Eu complex and anti FLC Ab conjugated to FRET acceptor.

O*, acceptor label;* ●*, Eu donor label; grey rectangle, FLC.*

This chapter reports the synthesis, of surface active Eu complexes, their photophysical properties and their functionalisation onto AuNPs. It is then reported how AuNPs can be dual functionalised with the surface active Eu complexes and FLCs whilst retaining their characteristic *f-f* luminescence and how these particles can be used in a homogenous FRET based assay.

2.3 Synthesis of surface active Eu complexes

For the surface active luminescent europium complexes, **EuQSH** and **EuQuinSAc** (Figure 2.3.1.) were chosen.

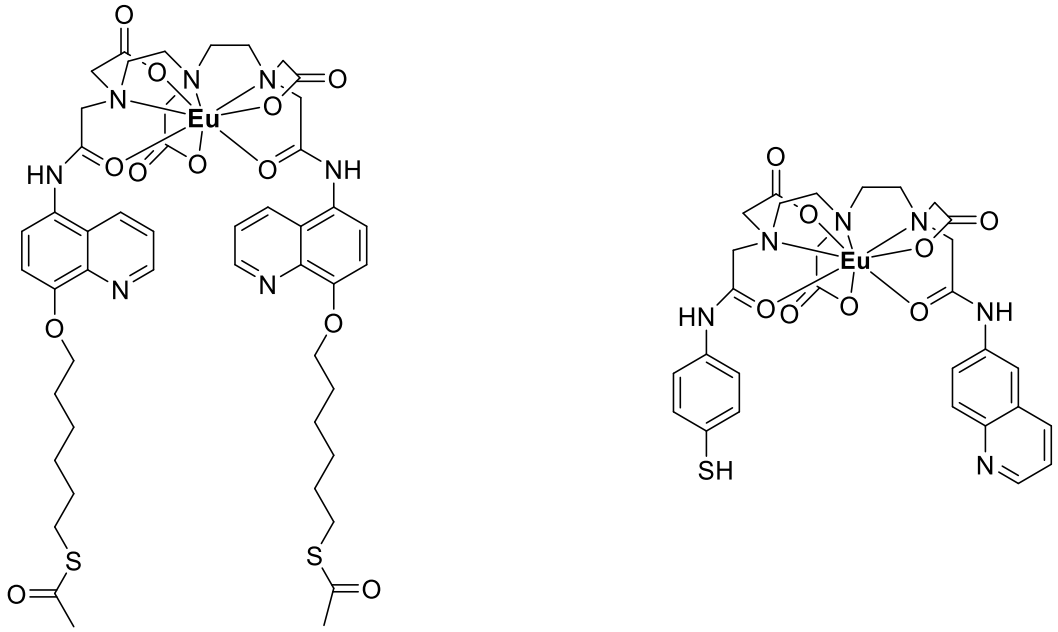

Figure 2.3.1.

*Left: Structure of **EuQuinSAc**; Right: Structure of **EuQSH**.*

EuQuinSAc incorporates a DTPA-bisamide backbone with a quinoline sensitizing unit, attached to a six carbon aliphatic linker which is terminated with thioester groups. The quinoline group is known to be an effective sensitizer for Eu(III) with a T_1 state of *ca.* 22,000 cm^{-1} which can lead to an emission Φ of 4% in terms of Eu(III) luminescence.[33] The DTPA-bisamide backbone gives thermodynamically stable Ln(III) complexes with hard donor atoms (N and O) and carboxylates with a binding constant of *ca*. 10^{15}. On binding Eu(III) the arms become preorganised for binding to a surface which is achieved with the thioester surface active group.

EuQSH is a similar design with the use of a DTPA-bisamide backbone with a quinoline sensitizer incorporated into the design and a terminal sulphur group for attachment to a gold surface.[34,35]

EuQuinSAc was synthesised *via* the following scheme for the ligand **H_3QuinSAc** (Figure 2.3.2.) followed by the inclusion of Eu(III) into to form **EuQuinSAc**.

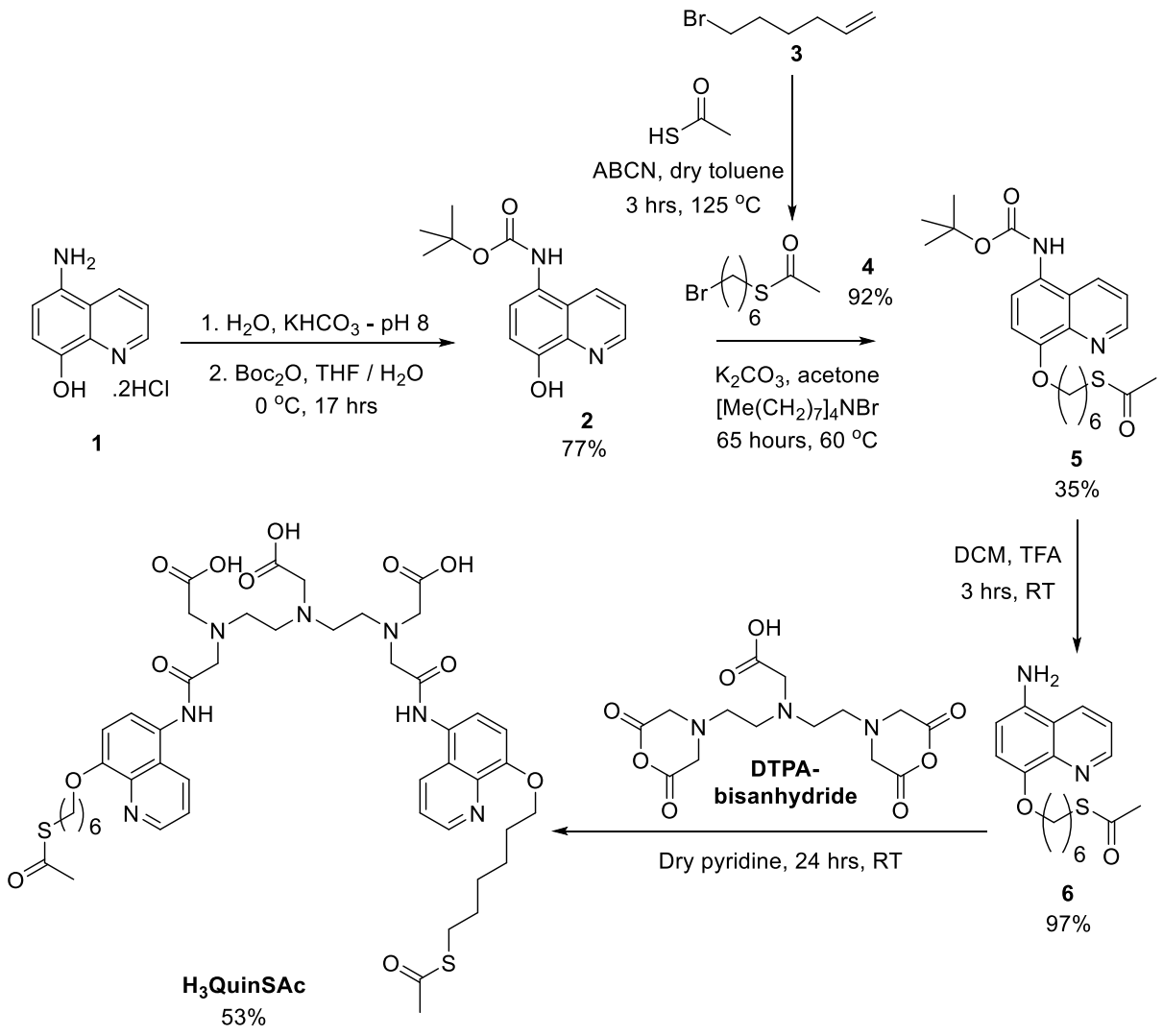

Figure 2.3.2.

*Synthetic scheme for **H_3QuinSAc** adopted.*

The synthesis of **H_3QuinSAc** proceeded *via* an improvement of a synthesis previously achieved within the Pikramenou group which commenced by protection of the amine with a Boc protecting group on substituted quinoline **1** to generate N-Boc protected amine **2**. The reaction was carried out at 0 ^{0}C to encourage formation of the N-Boc protected amine over the O-Boc protected compound. This is an improvement on previous attempts which were low yielding due to O-Boc formation. The protection step was followed by Williamson ether synthesis of **5**, from the reaction of **2** with aliphatic carbon linker **4**, which was previously prepared *via* a radical reaction of **3** with thioacetic acid in the presence of

radical initiator ABCN. The N-Boc protected Williamson ether product, **5** was then treated with TFA in dry DCM to yield deprotected amine **6** which was used in the production of **H_3QuinSAc** *via* dual acylation with DTPA-bisanhydride in dry pyridine. The synthesis was performed in an overall yield of 11% based on the starting moles of **1**. Characterisation data for compounds **2**, **4**, **5** and **6** and **H_3QuinSAc** are found in the appendix.

H_3QuinSAc was characterised by ^{1}H nuclear magnetic resonance (NMR) spectroscopy, ^{13}C NMR spectroscopy, and mass spectrometry (MS) with signals confirming the product at *m/z* = 994.9 $[M + H]^+$ and 498.0 $[M + H]^{2+}$ where an electrospray ionisation technique was used.

H_3QSH was synthesised *via* dual acylation of DTPA-bisanhydride with 6-aminoquinoline and 4-aminothiophenol which produced three acylation products (Figure 2.3.3.). The asymmetric product **H_3QSH** was separated from the others (**H_3SH** and **H_3Quin**) *via* preparative high pressure liquid chromatography (HPLC) running a water / acetone gradient. Using this method **H_3Quin** was found to elute first followed by **H_3QSH** and the last to elute being **H_3SH**, as seen *via* comparison of the HPLC traces at 210 nm and 336 nm and confirmed with MS where an electrospray ionisation technique was used.

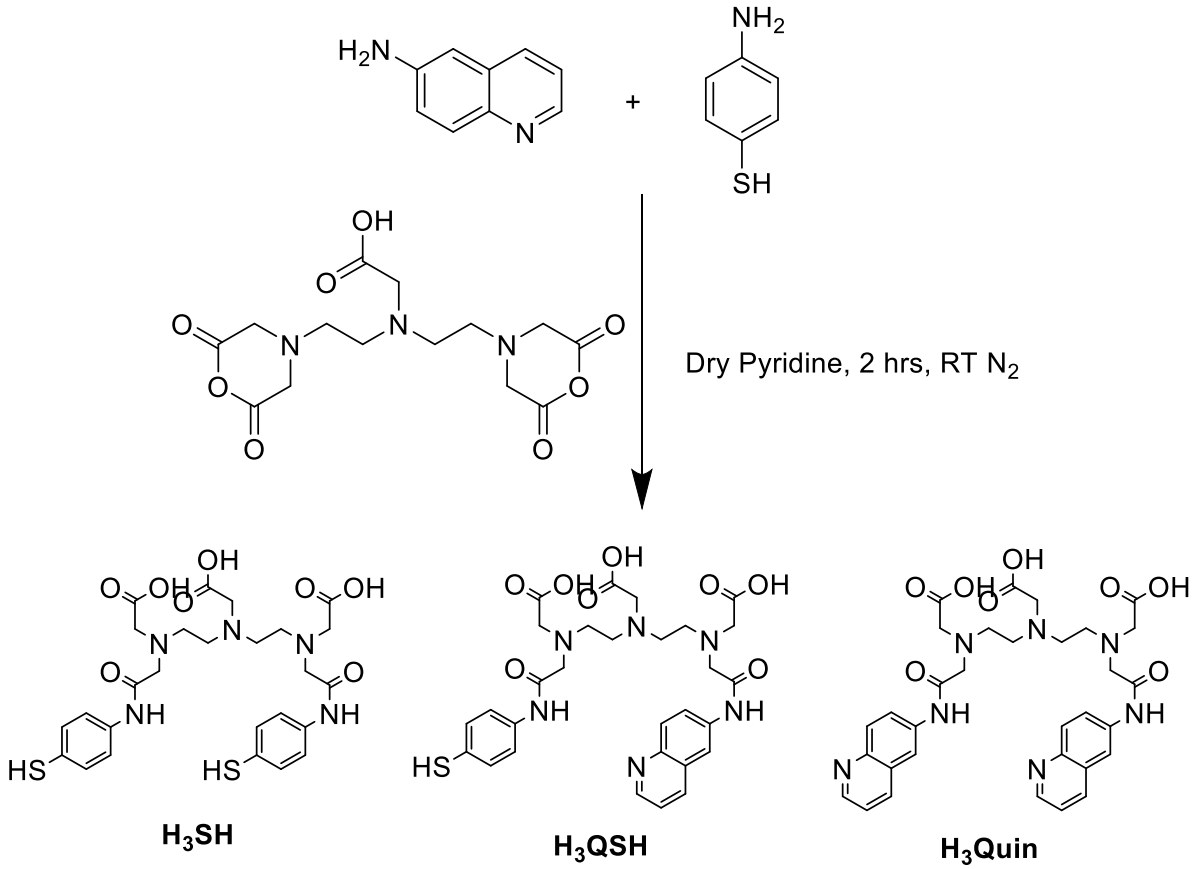

Figure 2.3.3.

*Synthetic scheme for **H_3QSH** adopted.*

H_3QSH was characterised with ^{1}H NMR data, ^{13}C NMR data, and MS with peaks confirming the product at *m/z* = 627.3 $[M + H]^+$ and 649.2 $[M + Na]^+$. Characterisation data for **H_3QSH** are found in the appendix.

The UV Vis spectra of **H_3QuinSAc** and **H_3QSH** were recorded (Figure 2.3.4.).

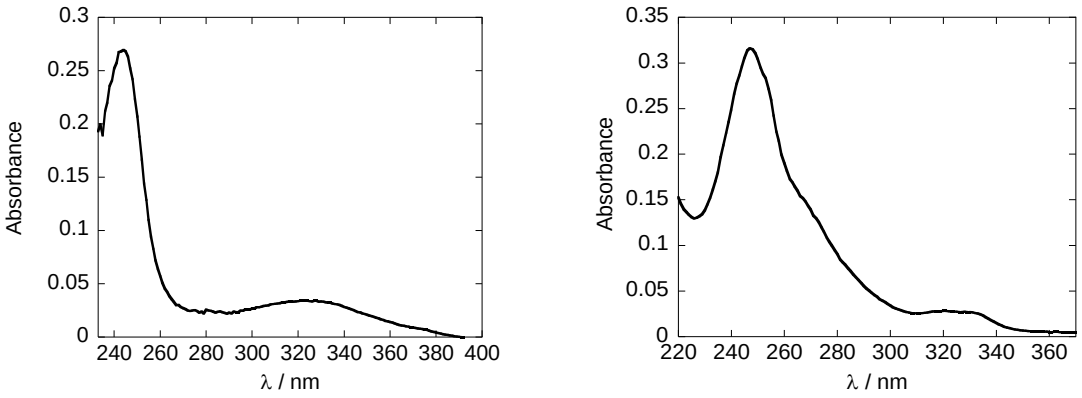

Figure 2.3.4.

*Left: UV Vis spectrum of **H_3QuinSAc** (4 µM in THF : Water (1 : 1)), Right: UV Vis spectrum of **H_3QSH** (8 µM in MeOH).*

The absorption spectrum of **H_3QuinSAc** shows two distinct bands with λ_{max} at 244 nm (ε = 67000 M^{-1} cm^{-1}) and 321 nm (ε = 9000 M^{-1} cm^{-1}) arising from $S_0 \rightarrow S_2$ and $S_0 \rightarrow S_1$ transitions both $\pi \rightarrow \pi^*$ in nature from the quinoline groups. That of **H_3QSH** shows less distinct bands with λ_{max} at 247 nm (ε = 39000 M^{-1} cm^{-1}) and 320 nm (ε = 3000 M^{-1} cm^{-1}) both again arising from $\pi \rightarrow \pi^*$ transitions from the quinoline group and the phenyl group will contribute to the band observed at 247 nm.

EuQuinSAc was prepared by the addition of $EuCl_3.6H_2O$ into a solution of deprotonated **H_3QuinSAc** in (1 : 1) by volume THF : water (Figure 2.3.5.).

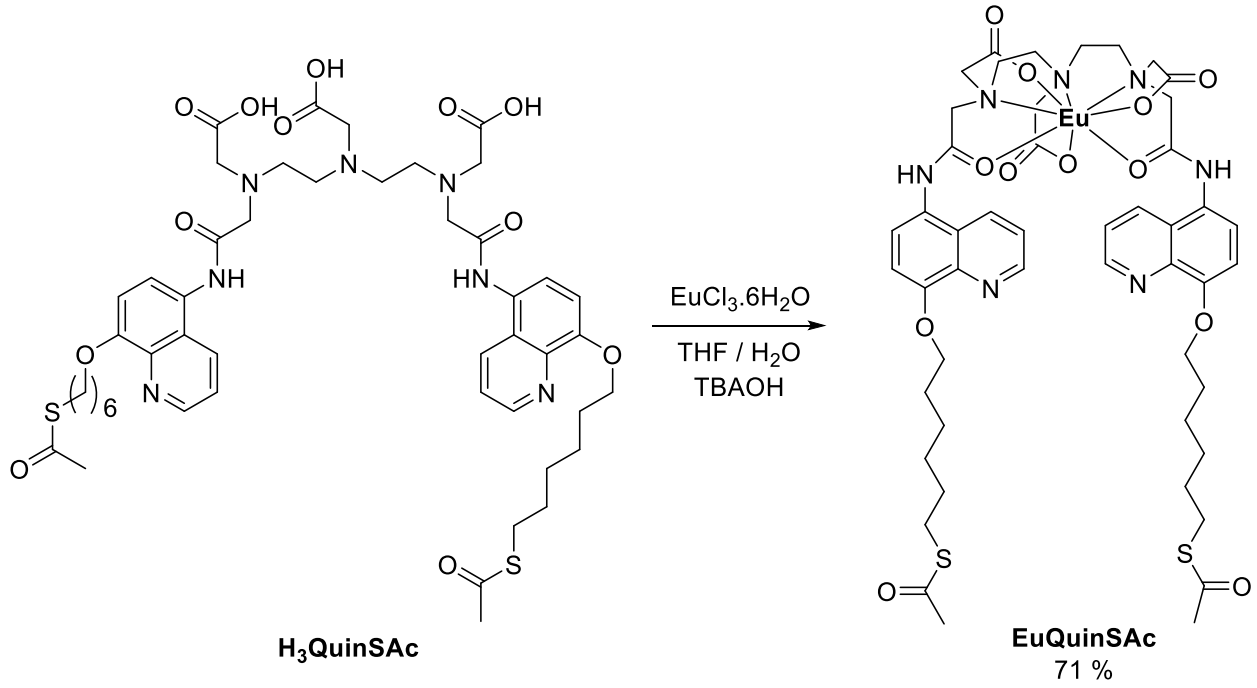

Figure 2.3.5.

*Preparation of **EuQuinSAc** from **H_3QuinSAc.***

EuQuinSAc was isolated after trituration with acetone with MS, using an electrospray ionisation, data showing peaks at *m/z* : 1144.4 $[M + H]^+$ and 572.7 $[M + H]^{2+}$ and 242 from residual $[N(Bu)_4]^+$ which was removed *via* trituration with MeCN, leaving the peaks arising from **EuQuinSAc** in the MS with the typical Eu(III) isotope pattern. The peaks arising from the MS of **H_3QuinSAc** (*m/z* = 994.9 $[M + H]^+$ and 498.0 $[M + H]^{2+}$) were not observed.

EuQSH was prepared in a similar fashion by the addition of $EuCl_3.6H_2O$ into a solution of deprotonated **H_3QSH** in (1 : 1) by volume THF : water (Figure 2.3.6.).

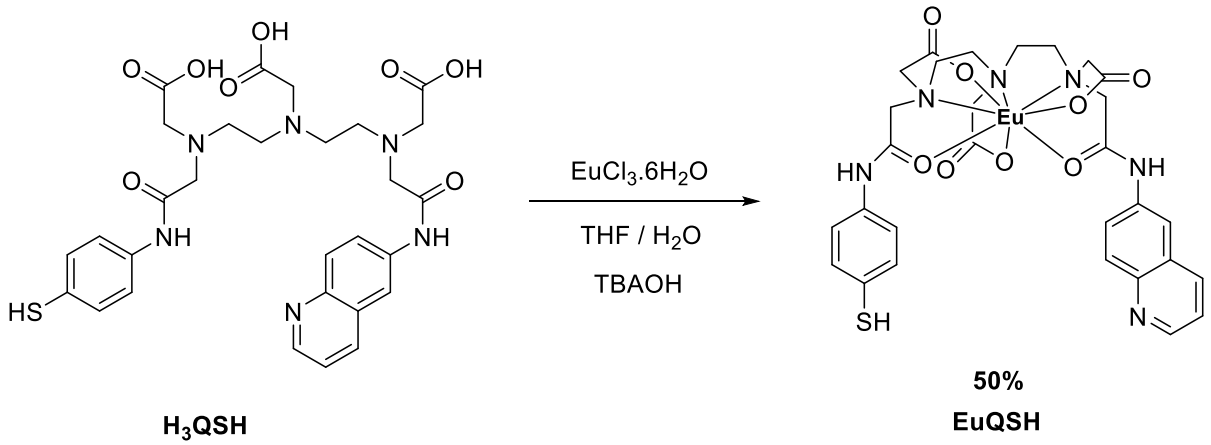

Figure 2.3.6.

*Preparation of **EuQSH** from **H_3QSH***

EuQSH was isolated after trituration with MeCN and characterised *via* MS data showing peaks at *m/z* : 797.1 $[M + Na]^+$ with the typical Eu(III) isotope pattern. Similarly to the **EuQuinSAc** preparation, residual $[N(Bu)_4]^+$ was required to be removed *via* trituration with MeCN and peaks corresponding to the ligand (*m/z* : 627.3 $[M + H]^+$ and 649.2 $[M + Na]^+$) were not observed.

2.4 Photophysical properties of EuQSH and EuQuinSAc

The photophysical properties of both **EuQuinSAc** and **EuQSH** were recorded using UV Vis spectroscopy and emission spectroscopy (Figures 2.4.1. and 2.4.2.).

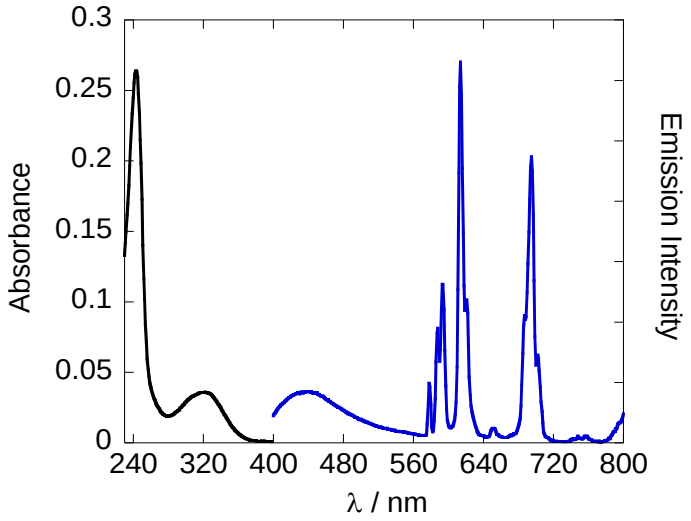

Figure 2.4.1.

Combined UV Vis (Black) and emission (Blue) spectra of ***EuQuinSAc*** *(4 µM in MeOH, λ_{exc} = 320 nm) corrected for PMT response.*

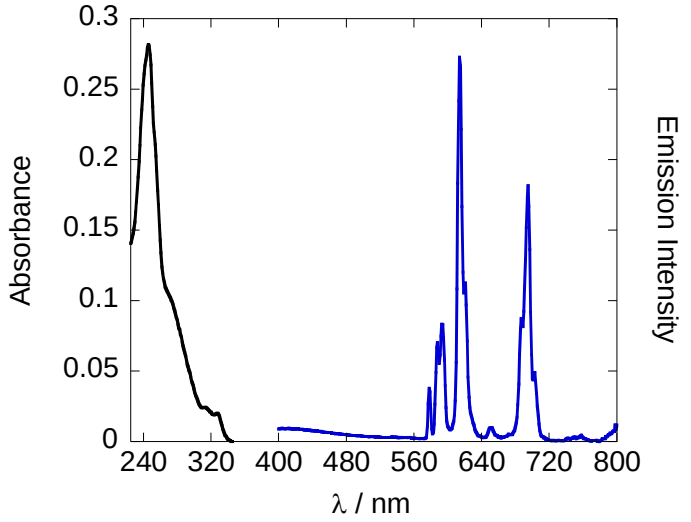

Figure 2.4.2.

Combined UV Vis (Black) and emission (Blue) spectra of ***EuQSH*** *(8 µM in MeOH, λ_{exc} = 315 nm), corrected for PMT response.*

The emission spectra of both **EuQSH** and **EuQuinSAc** show the characteristic Eu(III) *f-f* luminescence from the $^5D_0$ to the ground states of ^7F_J (J = 0 – 5), whereby the J = 2 band at 614 nm is the most prominent in both cases. **EuQuinSAc** shows a small amount of ligand fluorescence from the quinoline π^* groups at 440 nm which suggests the energy transfer process from the T_1 state of the quinoline does not transfer all the energy from this state to the Eu(III) ion. The absorption profile of **EuQuinSAc** matches that of **H_3QuinSAc** whereby two distinct bands at 243 nm (ε = 66000 M^{-1} cm^{-1}) and 321 nm (ε = 9000 M^{-1} cm^{-1}) arising from $S_0 \rightarrow S_2$ and $S_0 \rightarrow S_1$ transitions both $\pi \rightarrow \pi^*$ in nature from the quinoline groups. Similarly, a small amount of ligand fluorescence is observed for **EuQSH** although this is less in comparison to **EuQuinSAc**, perhaps due to the presence of one quinoline group instead of two. The absorption spectrum of **EuQSH** shows two distinct bands at 246 nm (ε = 35000 M^{-1} cm^{-1}) from a mixture of the thiophenyl and quinoline groups and 320 nm (ε = 3000 M^{-1} cm^{-1}) from the quinoline group. Excitation spectra of both compounds monitoring the emission of the compounds at 614 nm (Figure 2.4.3.) confirms that sensitized luminescence from the quinoline groups is active in both cases.

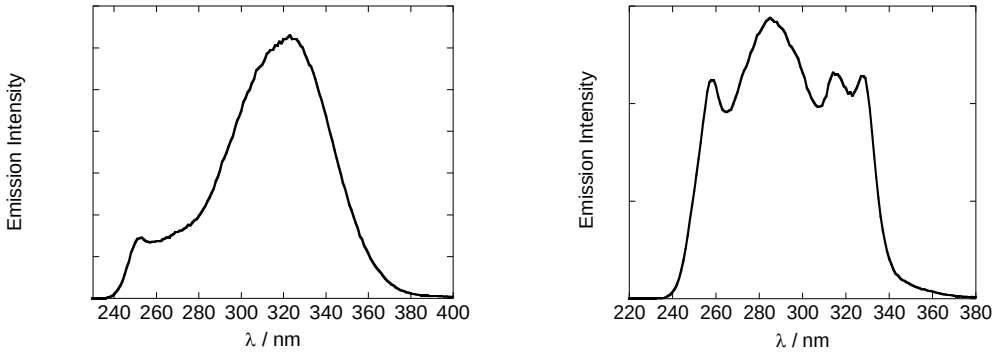

Figure 2.4.3.

*Left: Excitation spectra of **EuQuinSAc** in MeOH, monitoring the emission at 614 nm; Right: Excitation spectra of **EuQSH** in MeOH monitoring the emission at 614 nm.*

Lifetime data of **EuQSH** and **EuQuinSAc** in both H_2O and D_2O water and emission quantum yield data in MeOH as measured by integrating sphere were recorded (Table 2.4.1.).

Table 2.4.1.

*Lifetime and Φ data for **EuQSH** (λ_{exc} = 315 nm) and **EuQuinSAc** (λ_{exc} = 320 nm).*

Sample	**τ (H_2O) / µs**	**τ (D_2O) / µs**	**τ (MeOH) / µs**	**Φ (MeOH) / %**
EuQSH	580 (χ^2 = 1.0)	1850 (χ^2 = 1.1)	860 (χ^2 = 1.3)	4.0
EuQuinSAc	180 (42%), 450 (58%) (χ^2 = 1.3)	1090 (χ^2 = 1.3)	540 (χ^2 = 1.2)	1.0

The emission quantum yield data for *f-f* emission for both **EuQSH** and **EuQuinSAc** is comparable to other Eu complexes which have been reported utilising a quinoline sensitizing unit. The emission quantum yield is fairly low (< 10%) in both cases due to energy loss in the energy transfer process between the T_1 state of the organic sensitizing unit and the $^5D_0$ level of the Eu(III) ion. Indeed, both complexes show ligand fluorescence from the π* state of the quinoline group showing a competing pathway is active with the energy transfer process, in particular from **EuQuinSAc** with a large ligand emission being observed, hence a lower emission quantum yield.

The excited state lifetime in deuterated solvents is higher than the non-deuterated analogue as a result of the quenching effect from the O-H vibration which is less efficient for O-D oscillations. **EuQuinSAc** in water shows bi exponential decay behaviour. Use of the Parker-Beeby equation for both compounds in D_2O and H_2O suggest q values of 1.1 ± 0.5 for **EuQuinSAc** (using the long component) and 1.0 ± 0.5 for **EuQSH**, showing that each complex has one bound deactivating solvent molecule.

2.5 Synthesis of AuNPs

The synthesis of the AuNPs used for this work was achieved *via* the well-known citrate reduction of $HAuCl_4$ to prepare stable spherical particles of uniform size and shape (**Cit@Au**) in a simple one-pot synthesis at a concentration of 1.6 nM. The surface of the AuNPs is coated with citrate ions which can be easily displaced for the functionalisation of the surface of the gold. The NPs are characterised *via* UV Vis spectroscopy and transmission electron microscopy (TEM) (Figures 2.5.1. and 2.5.2.).

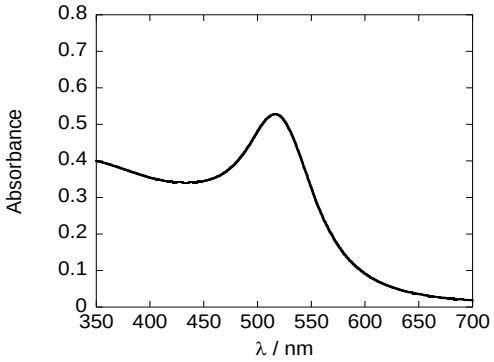

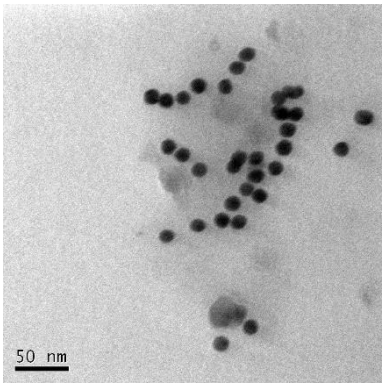

Figures 2.5.1. (Left) and 2.5.2. (Right)

Left; UV Vis spectrum of 1.6 nM ***Cit@Au*** *as synthesised, Right; TEM image of* ***Cit@Au*** *as synthesised.*

The UV Vis spectrum of **Cit@Au** shows a broad band with a λ_{max} of 516 nm which is the characteristic absorption band of AuNPs known as the SPR band resulting from charge separation within the NP causing a dipole oscillation.[36] This characteristic band of **Cit@Au** is sensitive to both the surface chemistry and the size of the NP. Changes in the SPR absorption band can be used to assess changes in either the surface chemistry or size of the gold colloid. The TEM image shows the particles of a spherical and uniform size distribution at a size of *ca.* 12 nm. **Cit@Au** is also characterised *via* (Dynamic light scattering) DLS which can be used to size spherical NPs *via* light scattering (Table 2.5.1.) and zeta potential measurements for an indication of the stability of NPs.

Table 2.5.1.

DLS sizing data for ***Cit@Au***.

Sample	**Intensity distribution / nm**	**Number distribution / nm**	**PDI**
Cit@Au	18 ± 3	12 ± 3	0.1

DLS data is given in both intensity distribution and number distribution. The intensity distribution can be a somewhat misleading measurement which is weighted toward the measurement of larger particles as the scattering response is proportional to the square of the molecular weight of the particle, hence the presence of any agglomeration or aggregation can be measured. This is corrected for the number distribution whereby the size given is proportional to the scattering intensity whereby the presence of any small number of large aggregates is not picked up and a more accurate particle size is established.[37] The polydispersity (PDI) index measurement gives a measure of how uniform the size and shape of the particles are. A value of 0.1 indicates that the particles are uniform in size and shape, which is confirmed with TEM images of the particles.

The zeta potential measurement gives a measure of the stability of the particles by passing an electrical current through the particles, causing the particles to migrate through solution based on their surface charge. For colloidal gold, a zeta potential measurement of lower than – 30 mV is considered to give stable particles. The zeta potential of **Cit@Au** gives a value of – 36 ± 16 mV which shows that stable particles have been formed, whereby the anionic coating is from the negative charge of the citrate ions.[38]

2.6 Functionalisation of AuNPs with Eu complexes

The functionalisation of **Cit@Au** can be monitored *via* perturbations of the SPR wavelength of the NP. Herein the deposition of **EuQSH** and **EuQuinSAc** onto **Cit@Au** for the preparation of **EuQS@Au** and **EuQuinSAc@Au** is shown (Figure 2.6.1.).

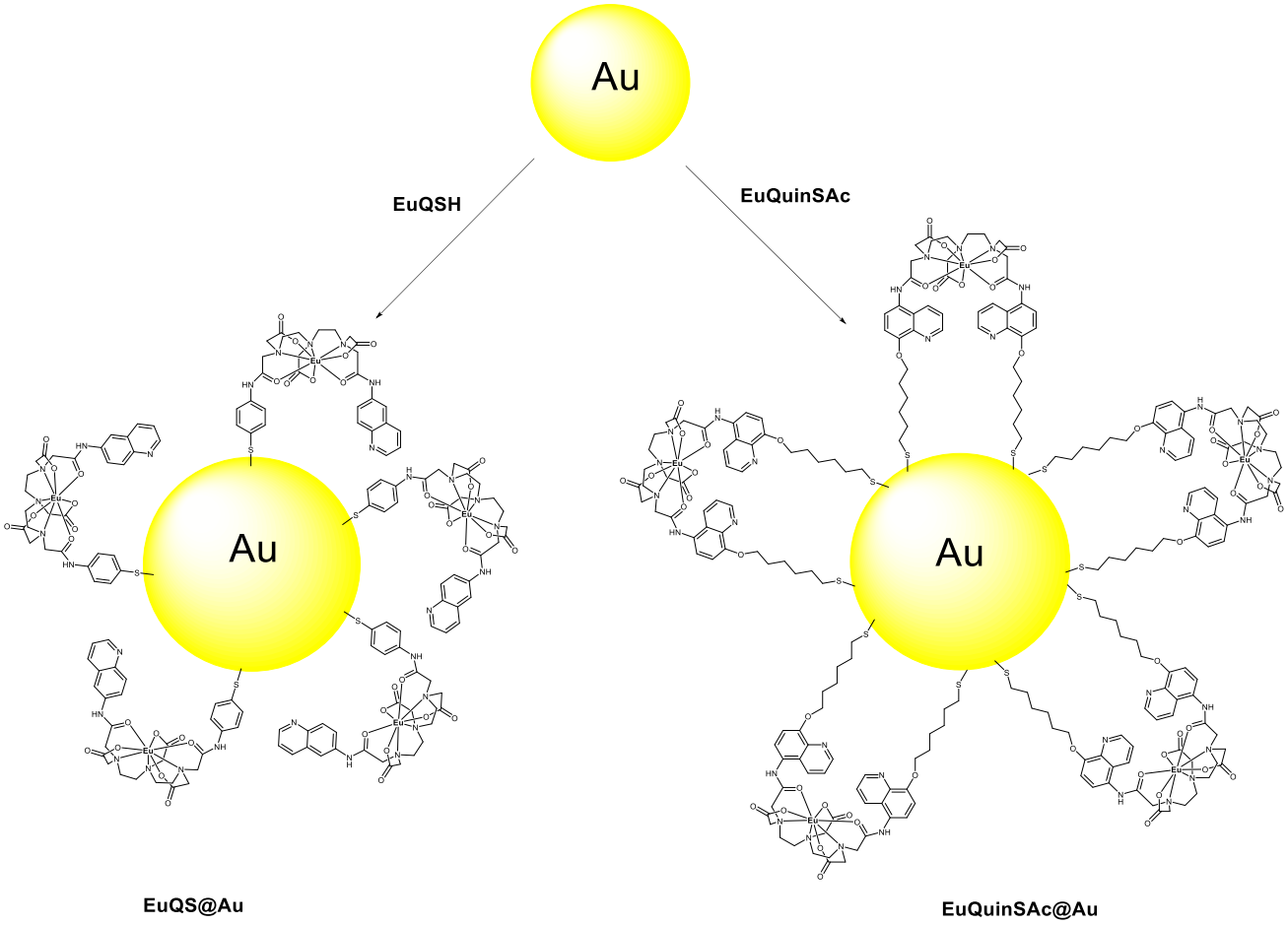

Figure 2.6.1.

*Preparation of **EuQuinSAc@Au** and **EuQS@Au** with the functionalisation of **Cit@Au.***

The SPR wavelength of **Cit@Au** is altered whilst the **EuQSH** or **EuQuinSAc** complexes are deposited onto the gold surface, as monitored *via* UV Vis spectroscopy (Figures 2.6.2. and 2.6.3.). The nanoparticle surface is considered to be fully functionalised with **EuQSH** or **EuQuinSAc** at the point that no further bathochromic shift can be observed. At this point, an excess of Eu complex is present and this is removed with the use of size exclusion chromatography, using Sephadex G15, whereby the large size difference between the functionalised AuNP and the probe allow the two to be separated. It

is interesting to note that citrate stabilised AuNPs, do not pass through the Sephadex, or indeed particles which only have a partial coating of Eu(III) complex on the surface, which is possibly a result of the interaction of the surface citrate anions with the sugar. In all cases the SPR wavelength recorded is worked out *via* the full width at half maximum (FWHM) of the curve, at a point where the curve resembles a parabolic shape (see general experimental, Section 6).

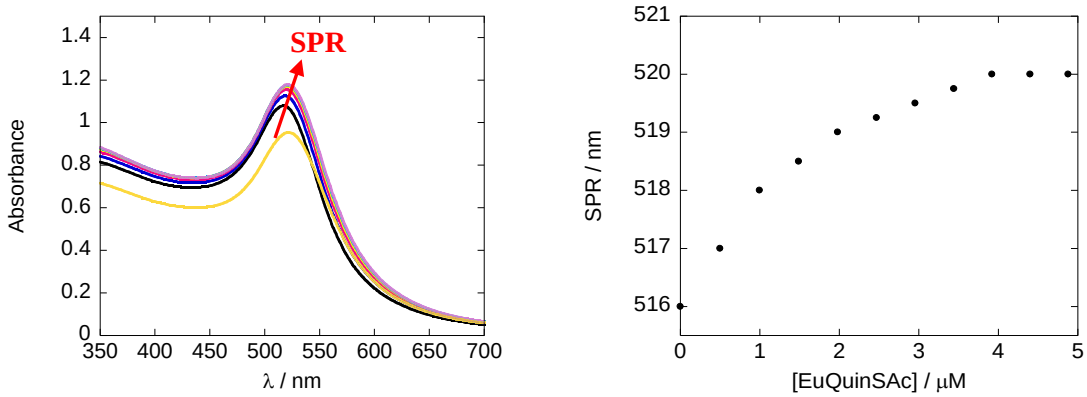

Figure 2.6.2.

Change in SPR wavelength of ***Cit@Au*** *(3.2 nM in water, 2 mL) as a methanolic solution of* ***EuQuinSAc*** *(0.2 mM in MeOH, 5 μL aliquots) is titrated in to a final concentration of 4.87 μM. The yellow curve is post Sephadex chromatography to show that no aggregation occurs from the purification method.*

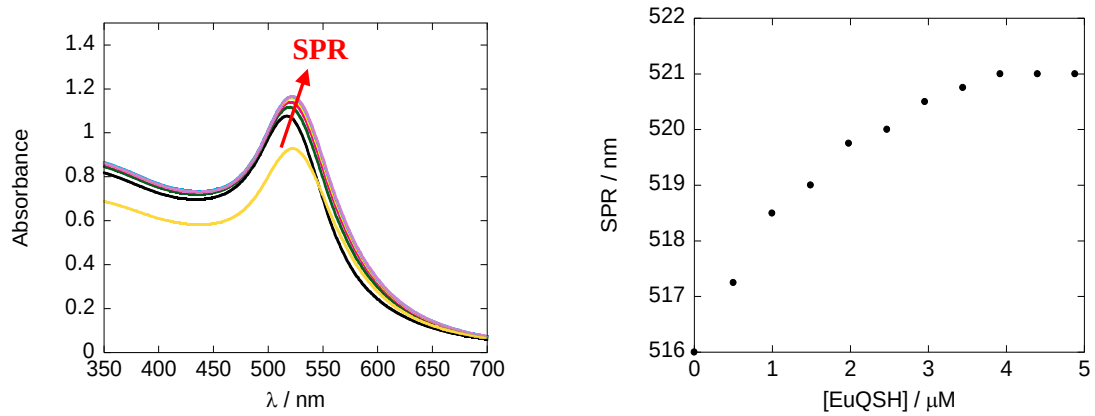

Figure 2.6.3.

Change in SPR wavelength of ***Cit@Au*** *(3.2 nM in water, 2 mL) as a methanolic solution of* ***EuQSH*** *(0.2 mM in MeOH, 5 μL aliquots) is titrated in to a final concentration of 4.87 μM. The yellow curve is post Sephadex chromatography to show that no aggregation occurs from the purification method.*

Both **EuQSH** and **EuQuinSAc** show positive shifts in the SPR wavelength of the NP as the surface is functionalised with the Eu complexes which reaches a saturation point at 521 nm for **EuQS@Au** and 520 nm for **EuQuinSAc@Au** indicating the surface is fully functionalised at this concentration of *ca.* 3800 nM. This suggests *ca.* 1200 Eu complexes per particle in both cases, although a more accurate method of determining the surface coverage of the AuNP is described at a later section. The absorption spectrum for both show the SPR wavelength of the NP is unaltered post purification which shows that the NP is unaltered during the Sephadex column chromatography. Particles were further characterised with TEM (Figure 2.6.4.) and DLS data (Table 2.6.1.).

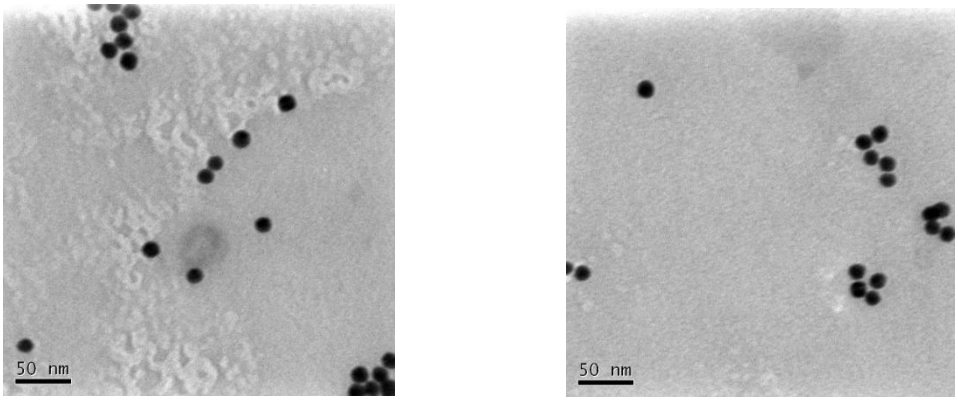

Figure 2.6.4.

*Left: TEM image of **EuQuinSAc@Au**; Right: TEM image of **EuQS@Au.***

Table 2.6.1.

*DLS characterisation data for **EuQS@Au** and **EuQuinSAc@Au**.*

Sample	**Intensity distribution / nm**	**Number distribution / nm**	**PDI**
EuQS@Au	23 ± 10	12 ± 4	0.3
EuQuinSAc@Au	24 ± 11	12 ± 3	0.5

TEM images of both sets of particles show that both **EuQS@Au** and **EuQuinSAc@Au** are spherical in nature and of uniform morphology with a diameter of *ca.* 12 nm for both **EuQS@Au** and **EuQuinSAc@Au** as averaged over five particles in the image in each case which agrees with the DLS data for the Eu coated AuNPs. Indeed, this is in agreement with the UV Vis spectroscopy data which

shows that particle stability is maintained after both the addition of the Eu probes and from the action of the size exclusion column. A change in zeta potential from – 36 mV (**Cit@Au**) to – 11 ± 4 mV (**EuQS@Au**) shows that the AuNP surface has been functionalised with respect to **Cit@Au**. The positive change in the zeta potential suggests that particle stability is lost when the particles are coated with Eu probes in comparison to the negative citrate anions.

An advantage to using NPs as a support for luminescent probes is that the luminescent properties of the NP are independent of the nanostructure and hence the luminescent properties of both **EuQS@Au** and **EuQuinSAc@Au** are expected to mirror that of **EuQSH** and **EuQuinSAc**. The emission spectra of the probes demonstrates this (Figure 2.6.5.).

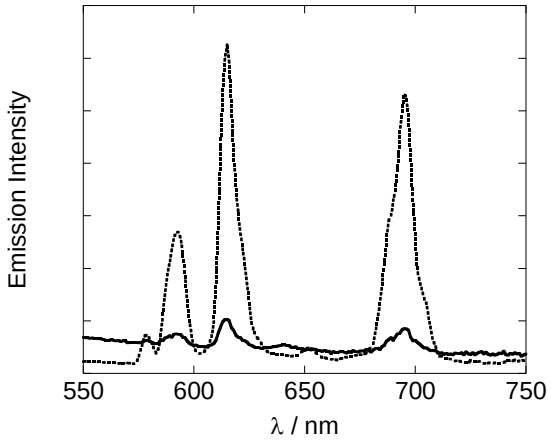

Figure 2.6.5.

*Emission spectra of **EuQuinSAc@Au** (——) vs **EuQS@Au** (-----), both (2.7 nM in water, λ_{exc} = 320 nm) corrected for PMT response.*

The steady state emission spectra of both **EuQuinSAc@Au** and **EuQS@Au** show the same Eu(III) *f-f* luminescence from the $^5D_0$ to the ground states of ^7F_J (J = 0 – 5), whereby the J = 2 band at 614 nm is the most prominent in both cases. The excited state lifetime of **EuQS@Au** is 580 μs which is comparable to the free probe in water. The time resolved signal from **EuQS@Au** shows bi-exponential behaviour whereby a short component of 2 μs is observed which can be attributed to scattering from the presence of the AuNP and the long component is the signal from the Ln ion. The signal from

EuQuinSAc@Au is difficult to distinguish from the scattering signal. The optical signal from **EuQS@Au** is much stronger in intensity than that of **EuQuinSAc@Au**. The steady state emission spectra suggests that **EuQuinSAc@Au** is quenched to a much larger degree than that of **EuQS@Au** in aqueous environments.

Whilst the amount of Eu(III) complex on the surface of the colloid can be estimated *via* the changes in the SPR wavelength of the particle *via* UV Vis spectroscopy, this method has a high level of error associated with it. Inductively coupled plasma mass spectrometry (ICPMS) is a highly accurate analytical technique whereby metal ions are dissolved in acidic solution and their concentration measured *via* the characteristic MS of the metal ions. Indeed, this technique can be used to determine the concentration of both Au and Eu in solution, which can in turn give the ratio of Au : Eu and hence the amount of metal complex loading per AuNP. This was used for analysis of **EuQS@Au** and **EuQuinSAc@Au** (Table 2.6.2.) whereby NPs were digested into ultrapure aqua regia for analysis.

Table 2.6.2.

*ICPMS data for **EuQS@Au** and **EuQuinSAc@Au**.*

Sample	**Eu complexes per particle**
EuQS@Au	800
EuQuinSAc@Au	850

The ICPMS data shows that the fully functionalised AuNPs have *ca.* 800 (**EuQS@Au**) or 850 (**EuQuinSAc@Au**) luminescent probes per particle. These results are similar to those reported in the literature whereby Davies *et. al.* found that 1335 **EuQuinSAc** molecules could be deposited on the surface of 13 nm AuNPs.[39] Osborne *et. al.* used a similar technique to determine the amount of $[Ru(bpy)_3]^{2+}$ based probes on the surface of 13 nm AuNPs treated with a Zonyl FSA® fluorinated surfactant, and that between 550 and 700 transition metal probes were deposited onto the surface of surfactant modified AuNPs.[40]

2.7 Functionalisation of AuNPs with FLCs

All FLCs are composed of a V_r and a C_r (Section 5.6), whereby the C_r for each FLC is terminated with a sulphur containing cysteine group, ordinarily used for binding the LC to the Fc region of an antibody. Cysteine has been shown to bind to a AuNP surface *via* the strong Au – S bond.[41,42,43] As well as the terminal sulphur containing cysteine amino acid, all twenty naturally occurring amino acids can have been shown to interact with a AuNP surface *via* N – Au and O – Au bonds, and non-covenant hydrogen bonding, albeit with different strengths and orientations, depending on the amino acid in question.[44,45] There are many established methods for the conjugation of biomolecules to NP based materials, some of which are described in an earlier section of this thesis. Indeed, the use of EDC facilitated amide coupling to lysine residues of a protein, or simple adsorption are amongst the most common reported in the literature. Whilst the conjugation of a wide variety of biomolecules to AuNPs has been reported, as far as we are aware, the functionalisation of AuNPs with FLC material has never been studied. In the first instance examination of whether binding to the surface of the gold colloid is a possibility whilst maintaining NP stability *via* their natural amino acid groups was carried out.

κstandard and λstandard are FLC samples which were isolated from patients who have either κ or λ myeloma respectively. As previously discussed, the C_r for all human κFLCs are identical with V_r chains differing between each type of κFLC. The C_r for all λFLCs are identical, with V_r chains differing between each type of λFLC. κFLCs and λFLCs have a different C_r. Herein the deposition of κstandard and λstandard onto **Cit@Au** is described for the preparation of **κstandard@Au** and **λstandard@Au** (Figure 2.7.1.) *via* displacement of the citrate ions on the gold surface as measured by a change in the absorption spectrum of the NP as the proteins bind to the gold surface (Figures 2.7.2. and 2.7.3.). Coated NPs were again purified *via* size exclusion chromatography. The positive bathochromic shift in the UV Vis spectra of **Cit@Au** as either type of FLC is titrated into the solution showed that the method of adsorption of the FLC onto the AuNP surface was successful. Particles were examined *via* TEM (Figure 2.7.4.) and DLS (Table 2.7.1.).

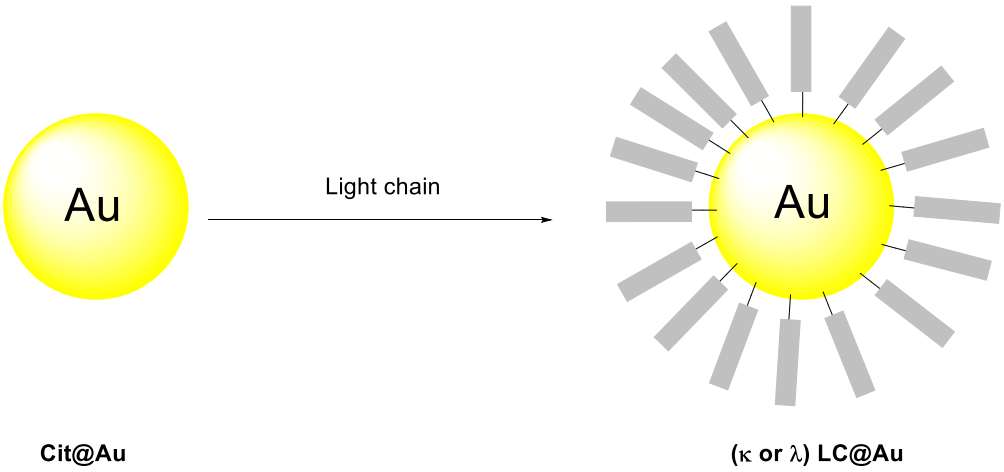

Figure 2.7.1.

*Preparation of **LC@Au** with the functionalisation of **Cit@Au**.*

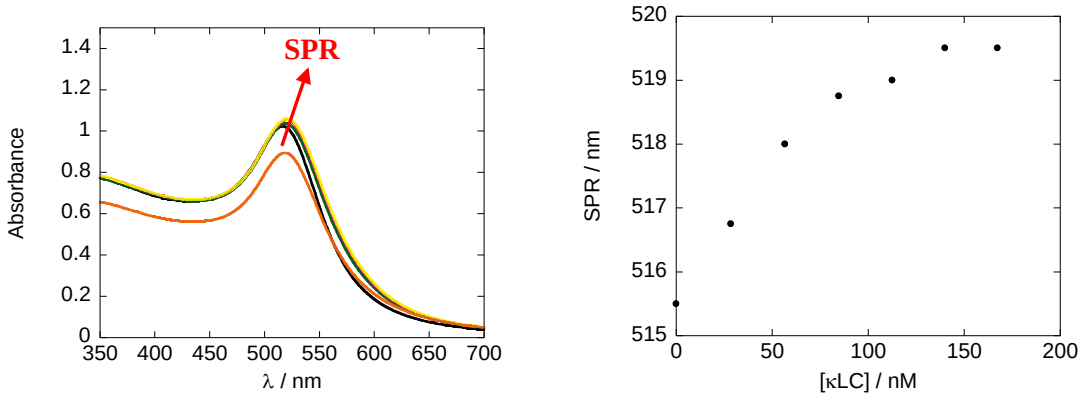

Figure 2.7.2.

*Change in SPR wavelength of **Cit@Au** (3.2 nM in water, 2 mL) as a solution of κstandard (8 µM in 0.001 M PBS, 8 µL aliquots) is titrated to a final concentration of 170 nM (48 µL). The orange curve is post size exclusion chromatography to show that no aggregation occurs from the purification method.*

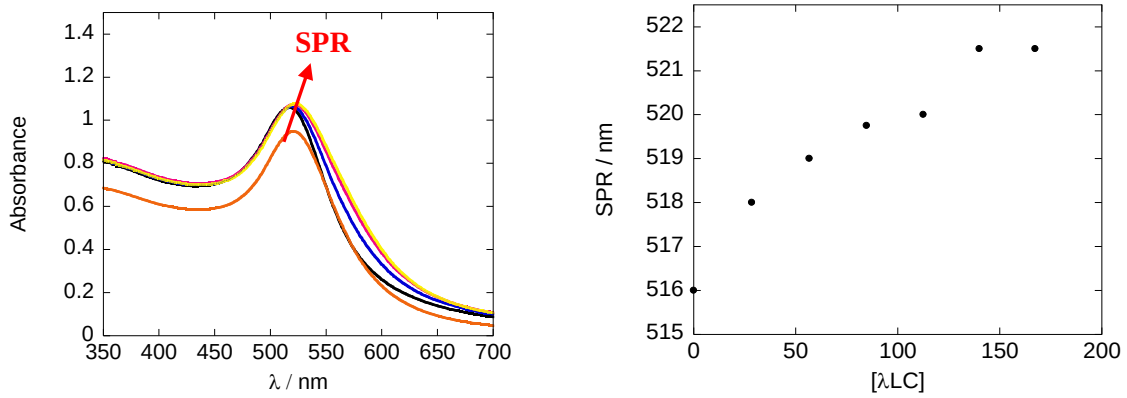

Figure 2.7.3.

Change in SPR wavelength of ***Cit@Au*** *(3.2 nM in water, 2 mL) as a solution of λstandard (8 μM in 0.001 M PBS, 8 μL aliquots) is titrated to a final concentration of 170 nM (48 μL). The orange curve is post size exclusion chromatography to show that no aggregation occurs from the purification method.*

Table 2.7.1.

DLS characterisation data for ***κstandard@Au*** *and* ***λstandard@Au****.*

Sample	**Intensity distribution / nm**	**Number distribution / nm**	**PDI**
κstandard@Au	52 ± 38	15 ± 4	0.2
λstandard@Au	47 ± 26	17 ± 4	0.3

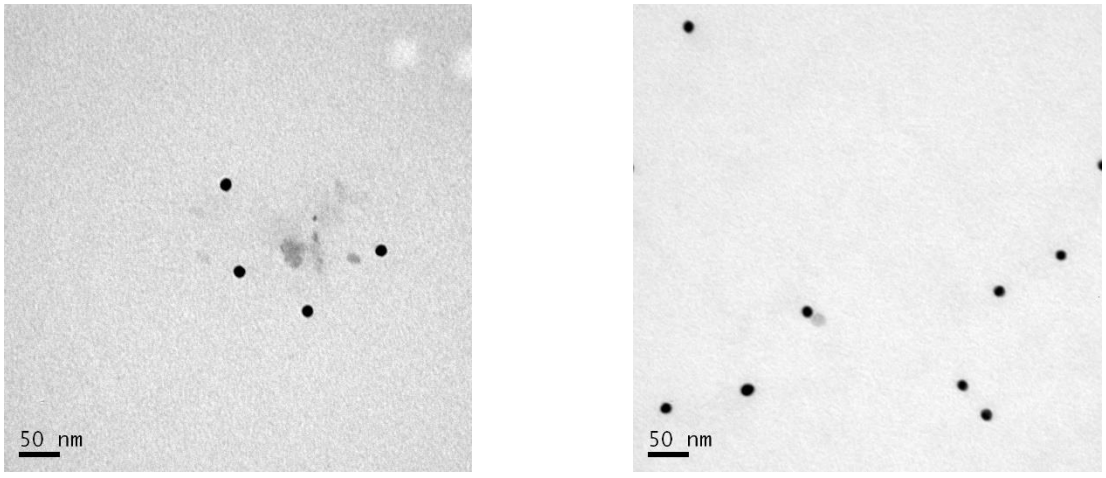

Figure 2.7.4.

Left: TEM image of ***κstandard@Au****; Right: TEM image of* ***λstandard@Au***

The change in the UV Vis spectrum of **Cit@Au** as either κstandard or λstandard is added shows that between 30 and 40 LCs can be functionalised onto **Cit@Au**, and that the concentration of surface bound LC is between two and three mg L^{-1}. This concentration of surface bound LC is comparable to that of the normal serum concentrations of FLC in an apparently healthy individual (Section 1.6).

TEM images of both sets of particles show that both **κstandard@Au** and **λstandard@Au** are spherical in nature and of uniform morphology with a diameter of *ca.* 15 nm for **κstandard@Au** and *ca.* 17 nm for **λstandard@Au** which agrees with the DLS data for the FLC coated AuNPs. The increase in size of the particles is attributed to LC binding hence a larger hydrodynamic diameter is observed. The larger particle size for **λstandard@Au** is attributed to the tendency of λFLC to dimerise.

The functionalisation of **Cit@Au** with both surface active, luminescent Eu(III) complex and FLC can be combined to develop particles functionalised with both luminescent material and LC material. **EuQSH** and **EuQuinSAc** can be grafted onto a AuNP surface and retain the luminescent properties of the complex, whilst both κFLC and λFLC can be deposited onto the surface of AuNPs at a concentration which is comparable to that of normal serum concentrations of FLCs in an apparently healthy individual.

Herein the combination of these ideas is shown with the deposition of **EuQSH** onto **Cit@Au** for a partial coating of Eu(III) complex onto the gold colloid, followed by κstandard (Figure 2.7.5.). In both cases the surface functionalisation of the AuNP was monitored *via* UV Vis spectroscopy (Figure 2.7.6.) *via* shifts of the SPR wavelength of the AuNP. Previous work within the research group of Professor Pikramenou by Dr Alison Savage has showed how a similar method involving AuNPs coated with Eu complex and peptide sequences could be used to develop luminescent AuNPs coated with Eu complex and peptides.

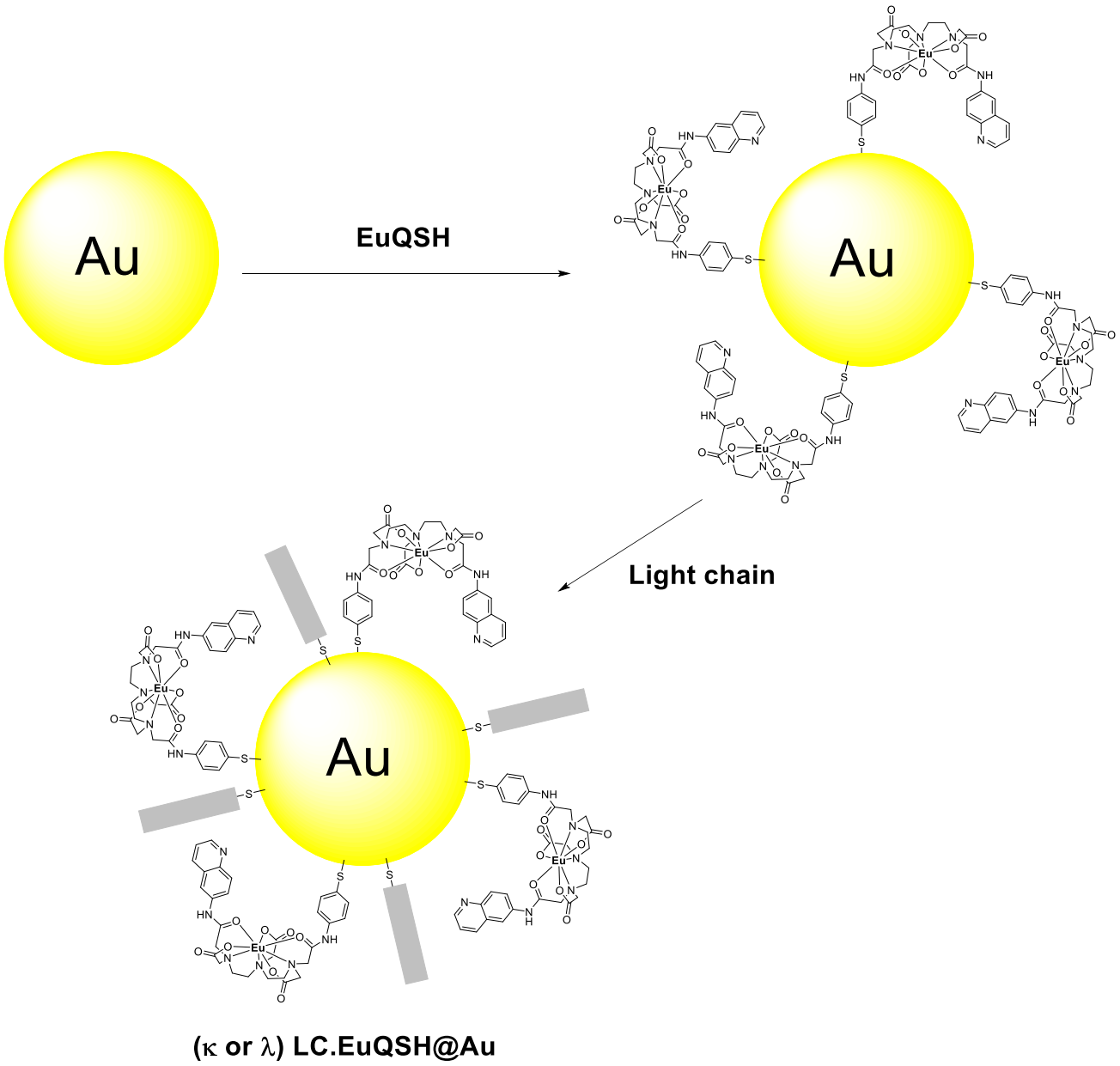

Figure 2.7.5.

*Preparation of **LC.EuQS@Au** with the functionalisation of **Cit@Au** with **EuQSH** then LC.*

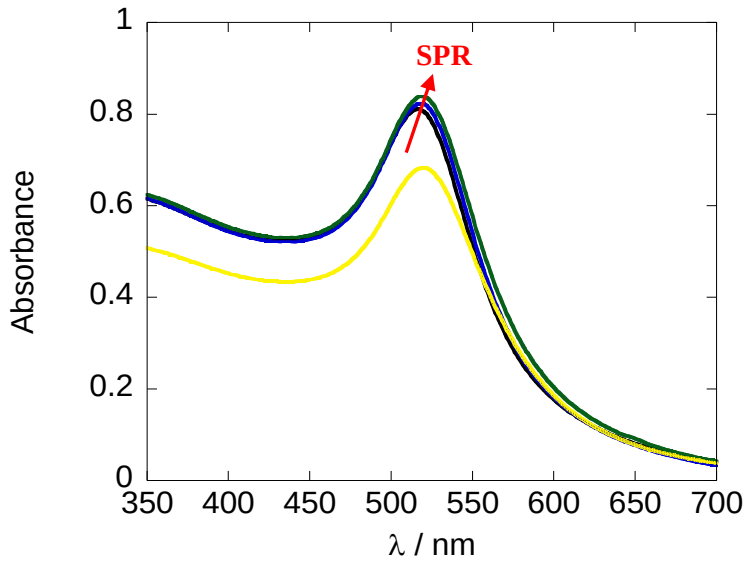

Figure 2.7.6.

Change in SPR wavelength of ***Cit@Au*** *(3.2 nM in water, 2 mL) as a methanolic solution of* ***EuQSH*** *(0.2 mM, 10 μL) is added in to a final concentration of 1 μM, followed by the addition of a solution of κstandard (5 μL, 20 μM in 0.001 M PBS) to a final concentration of 60 nM. The yellow curve is post chromatography to show that no aggregation occurs from the purification method.*

The initial addition of **EuQSH** to **Cit@Au** shows a bathochromic shift in the SPR wavelength of the AuNPs of 2 nm from 516 nm to 518 nm, because of partial surface functionalisation of **Cit@Au** with **EuQSH**. The afore mentioned, partially functionalised **Cit@Au** do not pass through a size exclusion column and indeed, this is the case for this partially coated gold colloid species. An identical UV Vis spectrum is obtained after the sample is left for fifteen minutes indicating that any extra bathochromic shift observed is not due to excess **EuQSH** in the sample. The addition of κstandard at 60 nM into the solution results in a further bathochromic shift of 1 nm from 518 nm to 519 nm as a result of surface modification of partially coated **Cit@Au** with κLC, again at a concentration which is comparable to that of normal serum concentrations of FLCs. Particles were purified *via* size exclusion chromatography to produce **κstandard.EuQS@Au** and characterised *via* DLS (Table 2.7.2.), TEM (Figure 2.7.3.), zeta potential data and steady state emission spectroscopy (Figure 2.7.4.).

Table 2.7.2.

DLS characterisation data for ***κstandard.EuQS@Au***

Intensity distribution / nm	**Number distribution / nm**	**PDI**
56 ± 54	14 ± 4	0.4

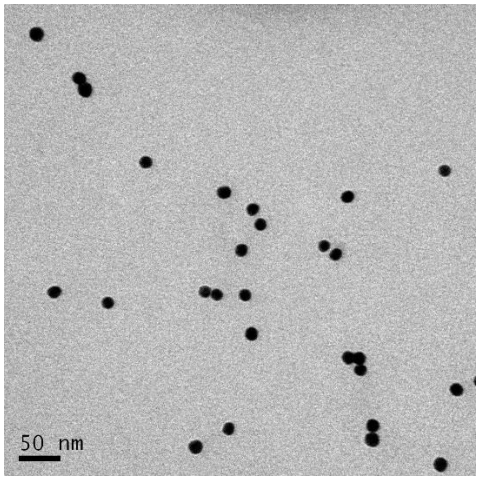

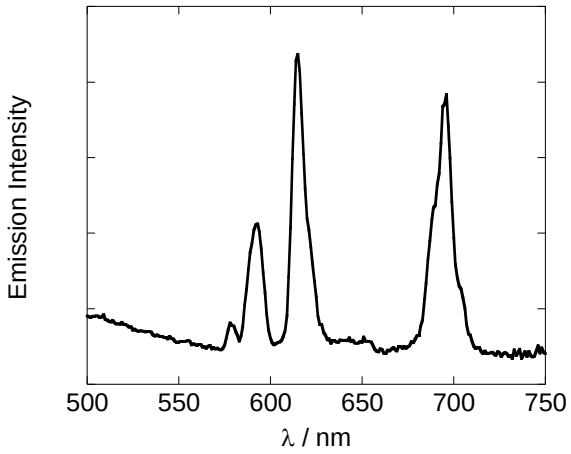

Figures 2.7.3. (Left) and Figures 2.7.4. (Right).

Left: TEM image of ***κstandard.EuQS@Au****; Right: Emission spectrum of* ***κstandard.EuQS@Au****,* λ_{exc} *= 320 nm, corrected for PMT response.*

TEM images of **κstandard.EuQS@Au** particles show that the particles are spherical in nature and of uniform morphology with a diameter of *ca.* 15 nm which agrees with the DLS data for the LC and **EuQSH** coated AuNPs. The particles show a zeta potential of – 23 ± 6 mV which shows a change in the surface chemistry of **κstandard.EuQS@Au** when compared to that of **EuQS@Au**. Indeed, the emission spectrum shows emission from the surface bound **EuQSH** complexes due to sensitized luminescence and show a lifetime of 580 μs (Figure 2.7.5.), comparable to that of **EuQSH** in water. ICPMS data shows that these partially Eu coated **κstandard.EuQS@Au** particles have *ca.* 250 **EuQSH** luminescent complexes per particle, which shows **κstandard.EuQS@Au** are *ca.* 30% coated with **EuQSH** when compared to that of fully coated **EuQS@Au**.

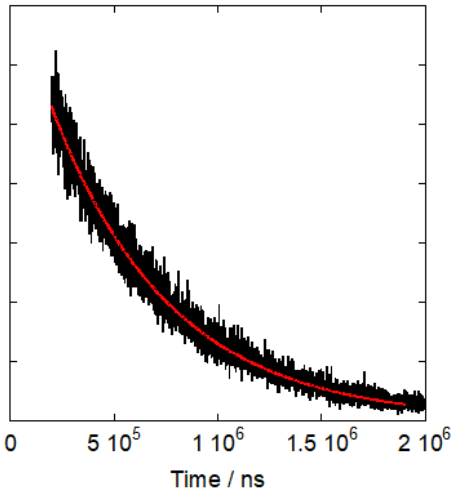

Figure 2.7.5.

Lifetime curve of ***κstandard.EuQS@Au****,* λ_{exc} *= 320 nm and* λ_{em} *= 614 nm.*

This method can be also be applied to the loading of **Cit@Au** with both κstandard and λstandard and **EuQuinSAc** in all cases whereby a partial coating of Eu(III) is achieved followed by the addition of LC and monitored *via* UV Vis spectroscopy (Figures 2.7.6., 2.7.7. and 2.7.8.) and characterised with TEM (Figure 2.7.9., 2.7.10. and 2.7.11.). In all cases Eu(III) luminescence is observed from the particles when excited at 320 nm, albeit much stronger from the **EuQSH** coated particles in comparison to the **EuQuinSAc** probe. Indeed, positive bathochromic shifts are observed in all cases as both Eu complex both Eu complex and LC is added.

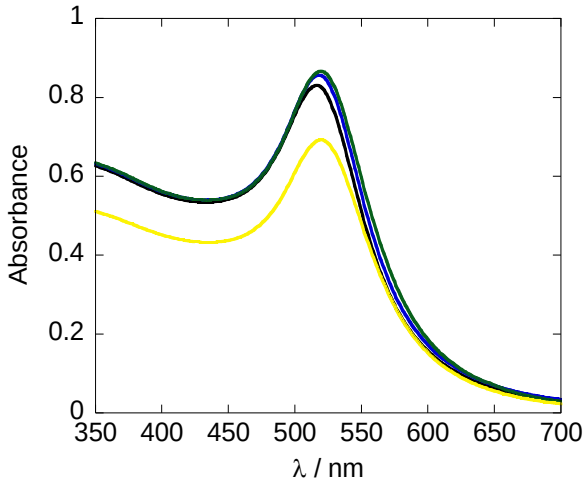

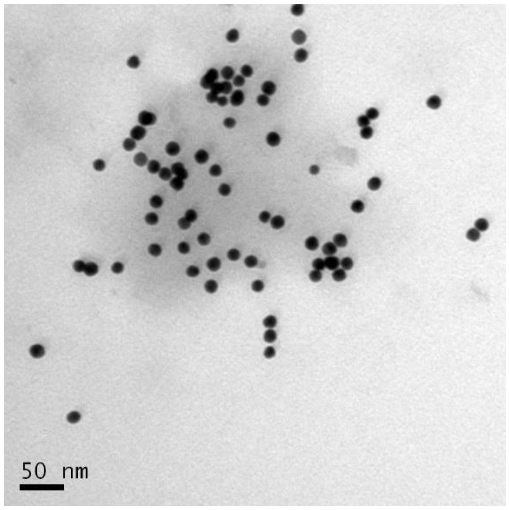

Figures 2.7.6. (Left) and Figures 2.7.9. (Right).

Left; Change in SPR wavelength of ***Cit@Au*** *(3.2 nM in water, 2 mL) as a methanolic solution of* ***EuQuinSAc*** *(0.2 mM, 10 μL) is added in to a final concentration of 1 μM, followed by the addition of a solution of κstandard (5 μL, 20 μM in 0.001 M PBS) to a final concentration of 60 nM. The yellow curve is column chromatography to show that no aggregation occurs from the purification method; Right: TEM image of* ***κstandard.EuQuinSAc@Au****.*

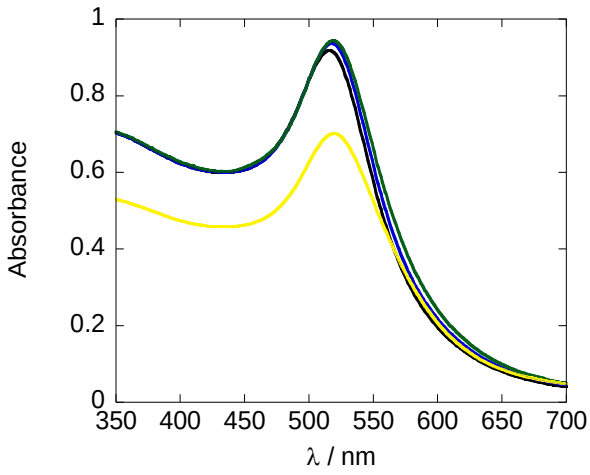

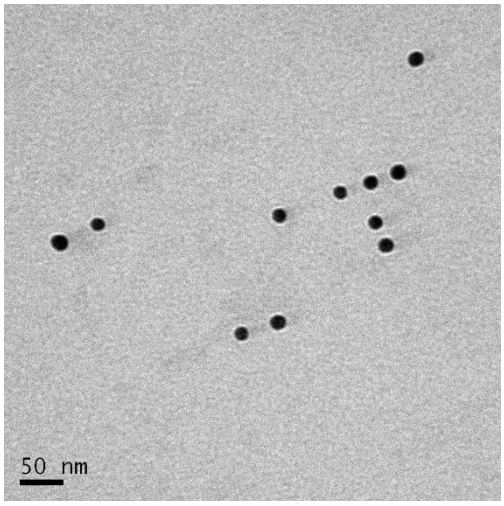

Figures 2.7.8. (Left) and Figures 2.7.10. (Right).

Left: Change in SPR wavelength of ***Cit@Au*** *(3.2 nM in water, 2 mL) as a methanolic solution of* ***EuQuinSAc*** *(0.2 mM, 10 μL) is added in to a final concentration of 1 μM, followed by the addition of a solution of λstandard (5 μL, 20 μM in 0.001 M PBS) to a final concentration of 60 nM. The yellow curve is post column chromatography to show that no aggregation occurs from the purification method; Right: TEM image of* ***λstandard.EuQuinSAc@Au****.*

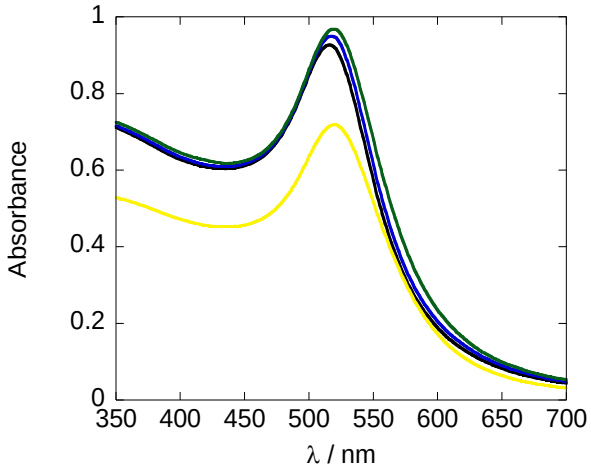

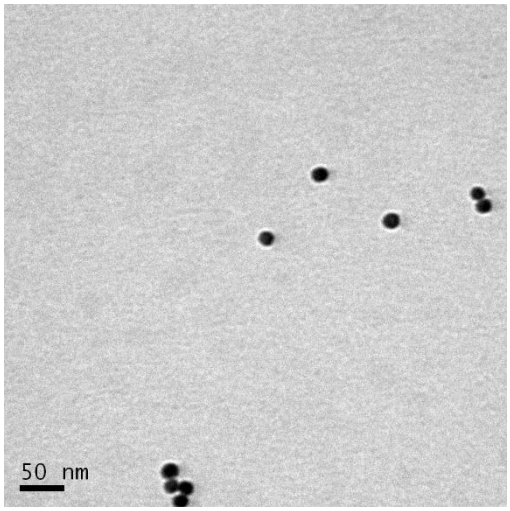

Figures 2.7.9. (Left) and Figures 2.7.11. (Right).

Left: Change in SPR wavelength of ***Cit@Au*** *(3.2 nM in water, 2 mL) as a methanolic solution of* ***EuQSH*** *(0.2 mM, 10 μL) is added in to a final concentration of 1 μM, followed by the addition of a solution of λstandard (5 μL, 20 μM in 0.001 M PBS) to a final concentration of 60 nM. The yellow curve is post column chromatography to show that no aggregation occurs from the purification method; Right: TEM image of* ***λstandard.EuQS@Au****.*

Both κstandard and λstandard can be dual coated onto **Cit@Au** with Eu complex to develop particles which show *f-f* luminescence whereby **EuQSH** is more emissive than **EuQuinSAc** on **Cit@Au**, and the V_r for each κLC is different.

The binding of pure κLC samples onto **Cit@Au** as well as **EuQSH** complex was examined, whereby the V_r sequence for each κLC is identical in each case. Two sets of pure κLC were examined and their properties are included (Table 2.7.3.).

Table 2.7.3.

properties of κnew and κfur.

κLC Sample	**Details**	**Monomer Size / Kda**	**Monomer : Dimer Ratio**
κnew	Pure, synthetic κLC Sample	24	50 : 50
κfur	Pure, κLC Sample isolated from patient sample	20	75 : 25

Indeed, the dual coating of κLC samples and **EuQSH** were also successful whereby similarly the surface of **Cit@Au** was partially coated with luminescent Eu complex followed by addition of κFLC sample as monitored *via* UV Vis (Table 2.7.4.) and purified *via* Sephadex column chromatography.

Table 2.7.4.

*Data for **κnew.EuQS@Au** and **κfur.EuQS@Au**.*

κLC Sample	**SPR λ / nm**	**DLS Number distribution / nm**	**PDI**	**Eu : Au ratio by ICPMS**
κnew.EuQS@Au	519	14 ± 4	0.3	100
κfur.EuQS@Au	519	16 ± 5	0.3	100

2.8 Functionalisation and properties of BUCIS04-AF647

To act as a FRET acceptor, the organic molecule Alexa Fluor® 647 (**AF647**) (Figure 2.8.1.) was used which shows a large J(λ) with the emission spectrum of **EuQSH** (Figure 2.8.2.).

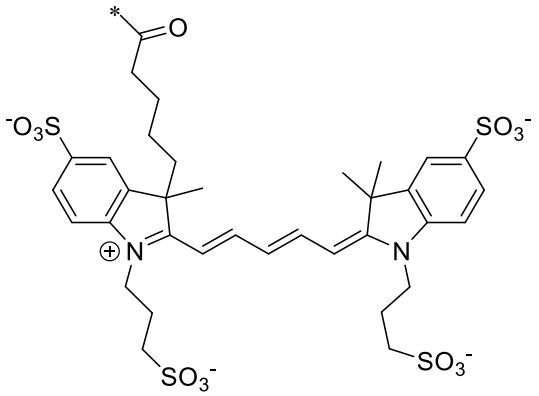

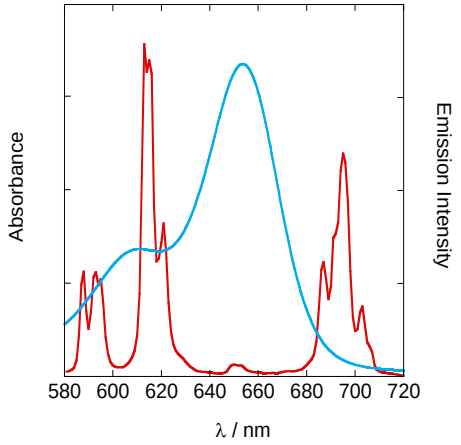

Figures 2.8.1. (Left) and Figures 2.8.2. (Right).

*Left: Structure of **AF647**; Right: Absorption spectrum of **AF647** (Blue) and **EuQSH** emission spectrum (Red).*

AF647 is a suitable FRET acceptor for Eu(III) as seen from the large J(λ) between the absorption spectrum of **AF647** and the emission spectrum of **EuQSH**, in particular the band observed at 614 nm from the $^5D_o \rightarrow {}^7F_2$ band. The absorption spectrum of **AF647** shows a λ_{max} at 650 nm with a large molar extinction coefficient of 240,000 M^{-1} cm^{-1} which enhances its suitability as a FRET acceptor. The emission spectra of **AF647** shows a broad band, typical of organic fluorescence centered at 668 nm showing red emission with an emission quantum yield of 0.33 and a lifetime of 1.0 ns as measured by ATDBio.[46] The lifetime of **EuQSH** is *ca*. five orders of magnitude larger than that of **AF647** which is important for this system as any signal observed from the emission of the **AF647** dye can be sufficiently eliminated with time resolved measurements and the huge difference in the lifetime means that one acceptor can quench multiple donors, as the acceptor is almost instantaneously deexcited after excitation *via* FRET allowing the acceptor to quench a further Eu(III) ion.

AF647 was conjugated to anti-κFLC mAb, **BUCIS04**, which is an IgG structure, known to specifically bind the κFLC C_r using a Fluoraprobe 647 kit as supplied by Life Technologies, for the preparation of the FRET acceptor **BUCIS04-AF647**. The conjugate was shown to be successful using a conjugate check and go kit as supplied by Life Technologies which uses a lateral flow assay technique to bind antibodies. The lateral flow assay flows the sample through a nitrocellulose membrane which contains a test line consisting of Proteins A and G, both of which are known to bind and show high affinity for the Fc region of many IgG molecules. As the sample flows through the membrane towards the absorbent pad the IgG binds to the test line causing the sample to be seen on the test line visually as an effect of the **AF647** dye (Figure 2.8.3.).

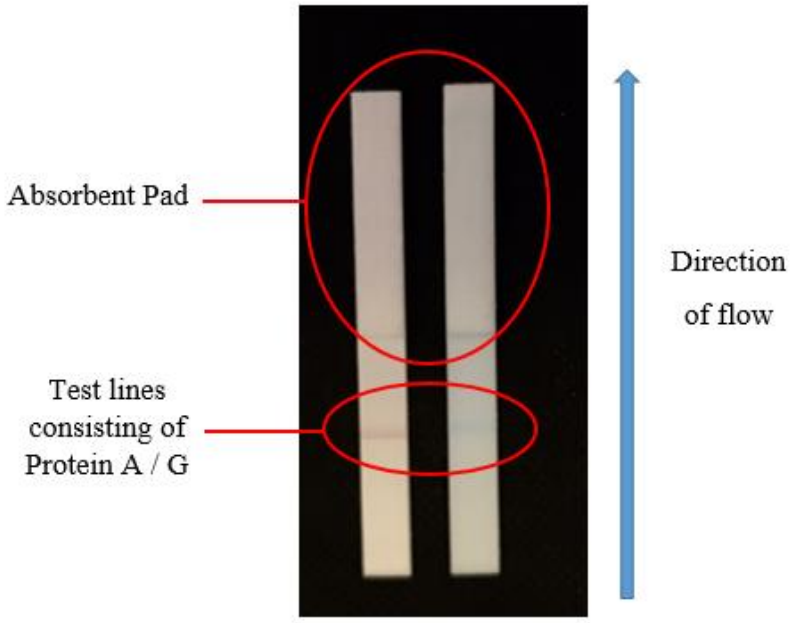

Figure 2.8.3.

Left stick: Positive control using a AuNP antibody conjugate as supplied by Life Sciences run in the presence of 1% BSA. Right stick: ***BUCIS04-AF647*** *conjugate run at a concentration of 60 ug / mL in the presence of 1% BSA.*

The lateral flow assay for the **BUCIS04-AF647** shows a blue band on the test line consisting of proteins A and G as confirmed with the immunogold positive control. The blue band is a result of the colour of the **AF647** dye, which shows that this dye is attached to the IgG which is in turn bound to the protein A / G test line of the lateral flow assay, confirming the success of the **BUCIS04-AF647** conjugation.

The activity of the **BUCIS04-AF647** conjugate was examined to ensure that **BUCIS04** was still active for the binding of κFLC post conjugation to the organic fluorophore *via* an ELISA assay with κnew immobilized on the surface of a 96 well plate. After varying concentrations of **BUCIS04-AF647** were incubated with the surface immobilized κnew, goat anti mouse IgG horseradish peroxidase (HRP), followed by a solution of 3,3′,5,5′-tetramethylbenzidine dihydrochloride (TMP) were added whereby the ELISA signal was obtained by the catalytic reaction of HRP and TMB followed by treatment with dilute H_2SO_4 which shows an absorption signal at 450 nm. The concentration of **BUCIS04-AF647** is directly proportional to the absorbance of the TMP dye as measured at 450 nm (Figure 8.3.4.).

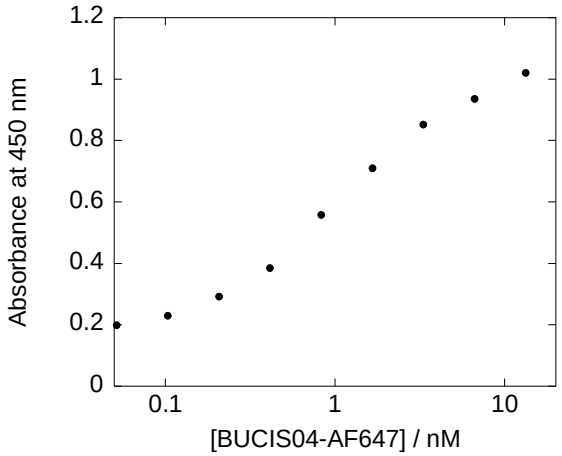

Figure 2.8.4.

*ELISA assay of **BUCIS04-AF647** against surface immobilized κnew as measured via the absorbance signal obtained with TMP and HRP.*

The ELISA assay shows that **BUCIS04** remains active against κnew as the organic fluorophore is attached down to a concentration of *ca*. 0.1 nM with this experimental setup, which showed the same absorbance as the background control. A further control showing the ELISA signal was not affected by the **AF647** showed the same absorbance as the background buffer signal as the absorbance of **AF647** is negligible at 450 nm. Whilst **BUCIS04-AF647** shows activity at this concentration, the same experimental setup with **BUCIS04** shows that antibody activity is lost post conjugation and concentrations lower than 0.01 nM of **BUCIS04** continue to show activity.

The combination of the lateral flow assay and the ELISA assay show that **BUCIS04-AF647** is successfully conjugated and that the antibody is still functional down to concentrations of 0.1 nM, albeit not as active as non-functionalised **BUCIS04**.

2.9 FRET Assay

The large J(λ) between the emission spectrum of **κLC.EuQS@Au** samples and the absorption spectrum of **BUCIS04-AF647** allow for a FRET signal from the two species to be observed, in particular from the $^7F_2 \leftarrow {}^5D_o$ band at 614 nm but also from the bands arising from $^7F_0$, $^7F_1$, and $^7F_3$, although the emission intensity is strongest from the $^7F_2$ transition. The signal can be measured *via* time resolved emission spectroscopy considering the long lived lifetime of the Eu(III) donor which is quenched as an effect of the organic dye as the two come together close in space, given that FRET is a distance dependent process (Section 1.2).

It has been shown that FLCs can be bound to their respective antibody in a variety of buffered solutions including tris HCl and PBS, both of which the stability of the particles were examined in *via* UV Vis.[47,48] **κstandard.EuQS@Au** shows a broadening and positive shift of 7 nm in the SPR wavelength of the particles when suspended in PBS which shows that the particles become destabilised as an effect of the salt and therefore inappropriate to be used in the FRET assay. This is not observed for tris HCl buffer at pH 8.0 whereby the SPR wavelength of **κstandard.EuQS@Au** is identical in and out of buffered solution.

The effect **BUCIS04-AF647** on **κstandard.EuQS@Au** was measured for particle stability *via* UV Vis spectroscopy to examine any perturbations in the SPR wavelength of the functionalised gold colloid (Figure 2.9.1.) in both aqueous and tris HCl buffered solution.

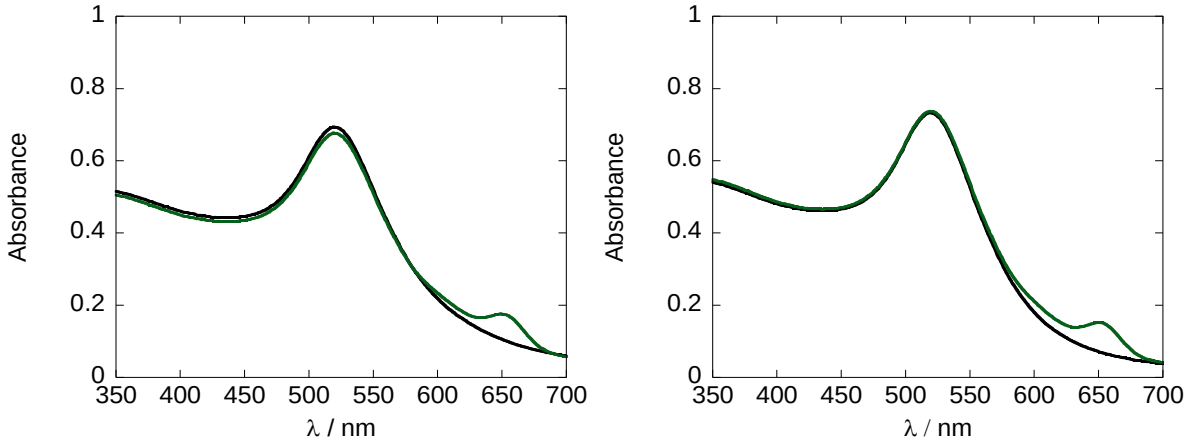

Figure 2.9.1.

Left, Change in SPR wavelength of ***κstandard.EuQS@Au*** *(2.7 nM, 2 mL) upon incubation with* ***BUCIS04-AF647*** *(1.0 mg / mL, 8 µL) to a concentration of 20 nM, green curve) in tris HCl buffered aqueous solution; Right: Change in SPR wavelength of* ***κstandard.EuQS@Au*** *(2.7 nM, 2 mL) upon incubation with* ***BUCIS04-AF647*** *(1.0 mg / mL, 8 µL) to a concentration of 20 nM in aqueous solution.*

On addition of **BUCIS04-AF647** at 20 nM the SPR wavelength of **κstandard.EuQS@Au** remains constant and no broadening or λ_{max} perturbation is observed which shows that particle stability is maintained and the surface of the functionalised AuNP is unaltered, as measured *via* UV Vis, in both aqueous and tris HCl buffered solution. The band observed at *ca.* 650 nm is from the absorption of the **AF647** dye.

The addition of 100 nM of **BUCIS04-AF647** into **κLC.EuQS@Au** at 2.7 nM a concentration comparable to that of the surface bound κLC shows a drop in the lifetime of the Eu(III) ion for all κLC samples which can be attributed to a FRET process occurring from **EuQSH** to the **AF647** dye with a λ_{exc} of 320 nm, monitoring emission at 614 nm, from the $^7F_2 \leftarrow {}^5D_o$ emission band of the Eu(III) ion (Table 2.9.1.), (Figures 2.9.1., 2.9.2. and 2.9.3.). Indeed, addition of non-functionalised **BUCIS04** at the same concentration shows no change in the lifetime of the Eu(III) ion showing that the observed FRET signal is a result of quenching from the **AF647** dye. Steady state measurements of the system were not possible as **AF647** shows a slight absorption at 320 nm, leading to a broad emission signal from the **AF647** dye centered at 665 nm.

Table 2.9.1.

Lifetime data for addition of ***BUCIS04-AF647*** *(1.0 mg / mL, 4 µL) into* ***κLC.EuQS@Au,*** ***κnew.EuQS@Au*** *or* ***κfur.EuQS@Au*** *(2.7 nM, 200 µL),* λ_{exc} *= 320 nm,* λ_{em} *= 614 nm.*

AuNP sample / 2.7 nM	**Tris HCl / µM**	**BUCIS04-AF647 / nM**	**τ / µs**	**χ^2**
κstandard.EuQS@Au	0	0	570	1.3
κstandard.EuQS@Au	50	0	560	1.2
κstandard.EuQS@Au	0	100	520	1.3
κstandard.EuQS@Au	50	100	490	1.3
κnew.EuQS@Au	0	0	570	1.1
κnew.EuQS@Au	50	0	560	1.1
κnew.EuQS@Au	0	100	520	1.1
κnew.EuQS@Au	50	100	480	1.1
κfur.EuQS@Au	0	0	570	1.1
κfur.EuQS@Au	50	0	560	1.1
κfur.EuQS@Au	0	100	540	1.1
κfur.EuQS@Au	50	100	510	1.1

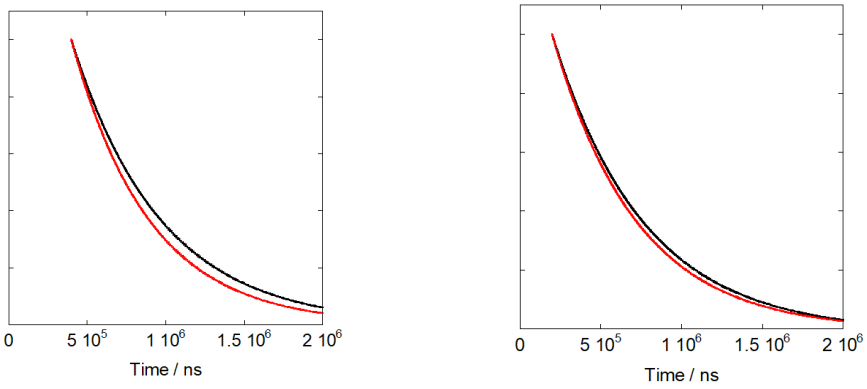

Figure 2.9.1

Left: Normalised lifetime plot for ***κstandard.EuQS@Au*** *(2.7 nM, 200 µL) in tris HCl buffer (Black) showing the addition of* ***BUCIS04-AF647*** *(1.0 mg / mL, 4 µL) (Red); Right: Normalized lifetime plot for* ***κstandard.EuQS@Au*** *(2.7 nM, 200 µL) (Black) showing the addition of* ***BUCIS04-AF647*** *(1.0 mg / mL, 4 µL) (Red).*

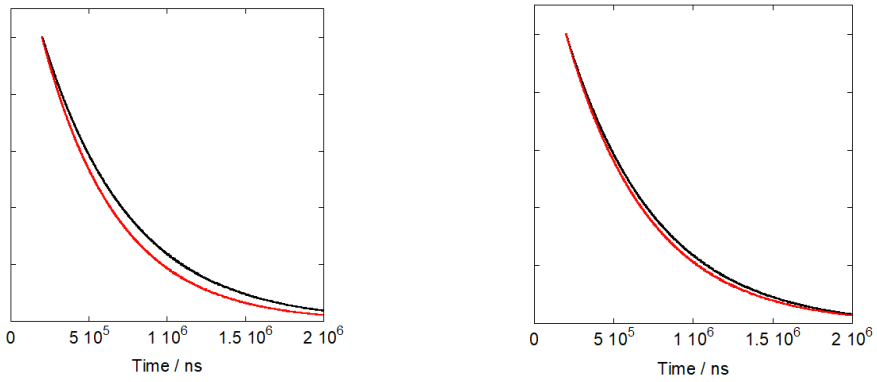

Figure 2.9.2.

Left: Normalised lifetime plot for ***κnew.EuQS@Au*** *(2.7 nM, 200 µL) in tris HCl buffer (Black) showing the addition of* ***BUCIS04-AF647*** *(1.0 mg / mL, 4 µL) (Red); Right: Normalized lifetime plot for* ***κnew.EuQS@Au*** *(2.7 nM, 200 µL) (Black) showing the addition of* ***BUCIS04-AF647*** *(1.0 mg / mL, 4 µL) (Red).*

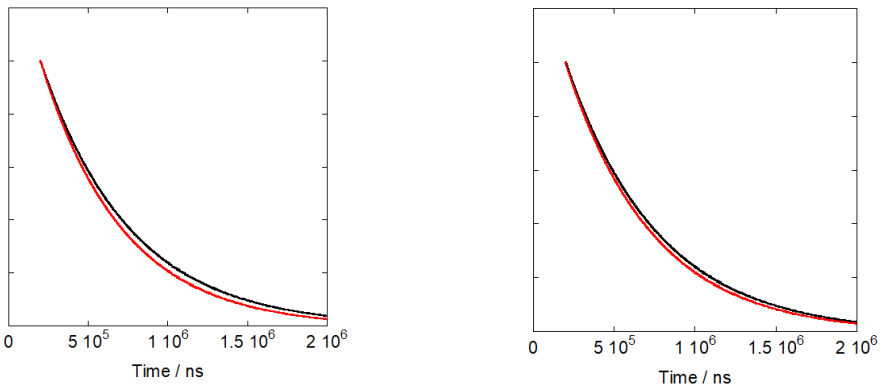

Figure 2.9.3.

Left: Normalised lifetime plot for ***κfur.EuQS@Au*** *(2.7 nM, 200 µL) in tris HCl buffer (Black) showing the addition of* ***BUCIS04-AF647*** *(1.0 mg / mL, 4 µL) (Red); Right: Normalized lifetime plot for* ***κfur.EuQS@Au*** *(2.7 nM, 200 µL) (Black) showing the addition of* ***BUCIS04-AF647*** *(1.0 mg / mL, 4 µL) (Red).*

For all examined **κLC.EuQS@Au** samples, as **BUCIS04-AF647** is added at 100 nM, in all cases a FRET signal is observed which is seen *via* a decrease in lifetime of the Eu(III) ion. Indeed, the Φ_T between the FRET pair can be estimated in all cases by comparing the lifetime of the Eu(III) ion with and without the FRET signal being active (Section 1.2.). The FRET pair of **EuQSH** and **AF647** has never before been reported, hence the value of R_0 is estimated based on the FRET pairing between a terpryridine sensitized Eu complex and **AF647**, used in a DNA assay, to be 58 Å. Values for the energy transfer efficiency for the FRET pair are included (Table 2.9.2.).[49]

Table 2.9.2.

FRET efficiency data for the addition of ***BUCIS04-AF647*** *into* ***κLC.EuQS@Au****.*

AuNP sample / 2.7 nM	**Tris HCl / μM**	**BUCIS04-AF647 / nM**	**Φ_T**
κstandard.EuQS@Au	0	100	0.09
κstandard.EuQS@Au	50	100	0.14
κnew.EuQS@Au	0	100	0.09
κnew.EuQS@Au	50	100	0.14
κfur.EuQS@Au	0	100	0.05
κfur.EuQS@Au	50	100	0.09

The observed FRET signal from the dual coated particles show that the average distance from the Eu(III) donors to the **AF647** acceptor is *ca.* 9 nm and the energy transfer efficiency is *ca*. 10% efficient, although this is variable based on the κLC sample used. This result implies that FRET is not observed between all Eu(III) ions and every acceptor as the gold colloids used are 12 nm in diameter, whereas the FRET range is 9 nm (Figure 2.9.4.). Whilst FRET is active in this novel nanoparticle system, the energy transfer efficiency, although low, is comparable to the literature. Harma *et. al.* report energy transfer efficiencies of between 0.13 and 0.15 for the FRET signal between Eu loaded luminescent polystyrene NPs and QDs in an assay for BSA.[50] Whilst similar energy transfer efficiencies have been reported, Casanova *et. al*. reported the FRET transfer efficiency between the FRET pair of luminescent

Ln-doped Oxide NPs and Cy5 dye to be up to 0.80, which was variable based on the donor : acceptor ratio.[51]

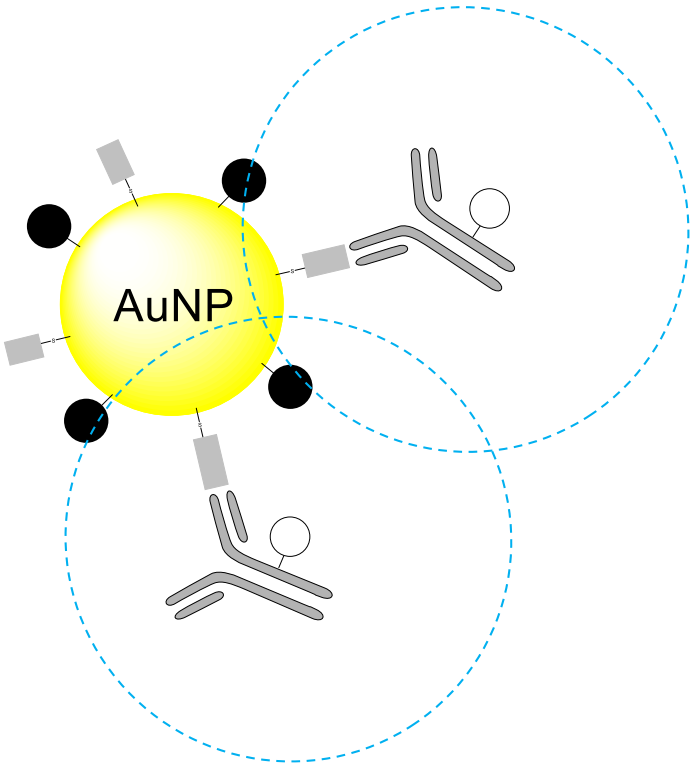

Figure 2.9.4.

Schematic showing distances with FRET assay, Not to scale.

O, *acceptor label; dashed blue line, area where acceptor is within potential FRET range;* ●, *Eu donor label.*

Homogenous FRET assays are designed to be much easier and quicker on the experimentalist to perform without the need for complex washing procedures as are necessary for surface based assay systems. In a clinical environment, it would be required for this assay to be easy to perform for the experimentalist, upon an automated system, designed to achieve accurate and reliable results. It was able to be shown show how this system thus far, can be run on a PHERAstar® multimode plate reader, whereby 96 wells can be examined in quick succession for the Eu(III) excited state lifetime. Using a time resolved fluorescence (TRF) optic module to gather lifetime data, it is shown how this system can be applied from an emission spectrometer to a clinically relevant system. Indeed, lifetime data from the PHERAstar® multimode plate reader shows the addition of **BUCIS04-AF647** into

κstandard.EuQS@Au and how the excited state lifetime of **κstandard.EuQS@Au** can be monitored (Table 2.9.3.), (Figure 2.9.5.).

Table 2.9.3.

*Lifetime data for addition of **BUCIS04-AF647** (20 µL, 100 µg / mL in PBS) into **κstandard.EuQS@Au** (110 µL 2.7 nM), λ_{exc} = 337 nm, λ_{em} = 615 nm using the TRF optic module, in the presence of tris HCl*

AuNP sample / 2.7 nM	**BUCIS04-AF647 / nM**	**τ / µs**
κstandard.EuQS@Au	0	550
κstandard.EuQS@Au	100	500

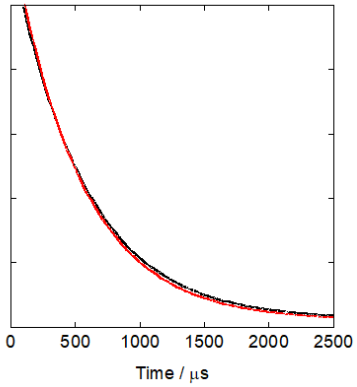

Figure 2.9.5.

*Normalised lifetime plot for **κstandard.EuQS@Au** (2.7 nM, 100 µL) in tris HCl buffer (Black) showing the addition of **BUCIS04-AF647** (20 µL, 100 µg / mL in PBS) to a concentration of 100 nM (Red).*

It has been shown that this system can be operated in a clinical setting *via* a multimodal plate reader. Indeed, this is promising for a clinical environment, whereby 96 pieces of data can be gathered in quick succession, effectively removing any experimental complexity as is involved with heterogeneous assay systems. Whilst this was possible with this plate reader, the PHERAstar® instrument is not optimized for this system. Indeed, the TRF optic module has an excitation wavelength of 337 nm which is not ideal for the excitation of **EuQSH** as can be shown *via* its excitation spectrum (Section 2.4) and leads to a weak signal being observed.

2.10 Concluding Remarks

The synthesis of Eu(III) complexes with built in surface active groups for binding to a gold surface and sensitizers based on quinoline groups, which are known to population the emissive energy level of Eu(III) *via* its T_1 energy level have been reported which shown Eu(III) luminescence. These were able to be attached to the surface gold nanoparticles to develop luminescent nanostructures which display Eu(III) luminescence and for the case of **EuQS@Au**, show a long lived excited state lifetime of 580 µs.

This was taken forward and the surface of a gold nanoparticle was able to be functionalised with LC samples *via* their natural amino acid groups and it was able to be shown how the surface of a gold nanoparticle can be decorated with both Eu(III) complex and LC sample simultaneously, whilst maintaining Eu(III) luminescence from the particles, and the excited state lifetime of 580 µs.

It was possible to use these particles to show a FRET signal between the surface bound Eu(III) ions and the organic dye **AF647**, which was bound to κLC specific antibody, **BUCIS04**, as monitored *via* the excited state lifetime of the Eu(III) ion. Upon addition of the energy acceptor, a quench in the Eu(III) lifetime of *ca.* 10% can be measured whilst maintaining particle stability. Whilst a FRET signal can be observed, this is lower than that of many similar systems within the literature, whereby a quench of up to 80% has been reported.

2.11 Referenced material

1 K. L. Kelly, E. Coronado, L. L. Zhao and G. C. Schatz, *J. Phys. Chem. B*, 2003, **107**, 668 – 677.

2 J. Turkevich, P. C. Stevenson and J. Hillier, *Discuss. Faraday Soc.*, 1951, **11**, 55 – 75.

3 M. Grzelczak, J. Pérez-Juste, P. Mulvaney and L. M. Liz-Marzán, *Chem. Soc. Rev.*, 2008, **37**, 1783 – 1791.

4 M. Notarianni, K. Vernon, A. Chou, M. Aljada, J. Liu and N. Motta, *Solar Energy*, 2014, **106,** 23 – 37.

5 E. Boisselier and D. Astruc, *Chem. Soc. Rev.*, 2009, **38**, 1759 – 1782.

6 Y. Yeh, B. Creran and V. M. Rotello, *Nanoscale*, 2012, **4**, 1871 – 1880.

7 N. J. Rogers, S. Claire, R. M. Harris, S. Farabi, G. Zikeli, I. B. Styles, N. J. Hodges and Z. Pikramenou, *Chem. Commun.*, 2014, **50**, 617 – 619.

8 S. A. M. Osborne and Z. Pikramenou, *Faraday Discuss.*, 2015, **185**, 219 – 231.

9 M. Milne, P. Gobbo, N. McVicar, R. Bartha, M. S. Workentin and R. H. E. Hudson, J. *Mater. Chem. B*, 2013, **1**, 5628 – 5635.

10 C. Alric, J. Taleb, G. L. Duc, C. Mandon, C. Billotey, A. L. Meur-Herland, T. Brochard, F. Vocanson, M. Janier, P. Perriat, S. Roux and O. Tillement, *J. Am. Chem. Soc.*, 2008, **130**, 5908 – 5915.

11 L. Moriggi, C. Cannizzo, E. Dumas, C. R. Mayer, A. Ulianov and L. Helm *J. Am. Chem. Soc.*, 2009, **131**, 10828 – 10829.

12 D. J. Lewis, T. M. Day, J. V. MacPherson and Z. Pikramenou, *Chem. Commun.*, 2006, 1433 – 1435.

13 B. I. Ipe, K. Yoosaf, and K. G. Thomas, *J. Am. Chem. Soc.*, 2006, **128**, 1907 – 1913.

14 A. Davies, D. J. Lewis, S. P. Watson, S. G. Thomas and Z. Pikramenou, *Proc. Natl. Acad. Sci.*, 2012, **109**, 1862 – 1867.

15 J. Massue, S. J. Quinn and T. Gunnlaugsson, *J. Am. Chem. Soc.*, 2008, **130**, 6900 – 6901.

16 S. Comby and T. Gunnlaugsson, *ACS Nano*, 2011, **5**, 7184 – 7197.

17 L. K. Truman, S. Comby and T. Gunnlaugsson, *Angew. Chem. Int. Ed.*, 2012, **51**, 9624 – 9627.

18 S. Pihlasalo, P. Puumala, P. Hanninen and H. Harma, *Anal. Chem.*, 2012, **84**, 4950 – 4956.

19 A. Dhir and A. Datta, *J. Phys. Chem. C*, 2016, **120**, 20125 – 20131.

20 J. S. Mitchell, Y. Wu, C. J. Cook and L. Main, *Anal. Biochem.*, 2005, **343**, 125 – 135.

21 J. S. Mitchell and T. E. Lowe, *Biosens. and Bioelectron.*, 2009, **24**, 2177 – 2183.

22 C. Tsai, C. Chen, Y. Hung, F. Chang and C. Mou, *J. Mater. Chem.*, 2009, **19**, 5737 – 5743.

23 M. T. Hurley, Z. Wang, A. Mahle, D. Rabin, Q. Liu, D. S. English, M. R. Zachariah, D. Stein and P. DeShong, *Adv. Funct. Mater.*, 2013, **23**, 3335 – 3343.

24 Information from Innova Biosciences on InnovaCoat® GOLD Nanoparticles & Conjugation Kits, https://www.innovabiosciences.com/gold-conjugation-kits.html, (Accessed online May 2017).

25 Information from abcam on GOLD conjugation kits, http://www.abcam.com/gold-conjugation-kit-40nm-20-od-ab154873.html, (Accessed online May 2017).

26 Y. Liu, L. Zhang, W. Wei, H. Zhao, Z. Zhou, Y. Zhang and S. Liu, *Analyst*, 2015, **140**, 3989 – 3995.

27 I. H. El-Sayed, X. Huang and M. A. El-Sayed, *Nano Lett.*, 2005, **5**, 829 – 834.

28 A. J. Di Pasqua, R. E. Mishler, Y. Ship, J. C. Dabrowiak and T. Asefa, *Mater. Lett.*, 2009, **63**, 1876 – 1879.

29 S. Liang, C. Li, C. Zhang, Y. Chen, L. Xu, C. Bao, X. Wang, G. liu, F. Zhang and D. Cui *Theranostics*, 2015, **5**, 970 – 984.

30 C. Finetti, L. Sola, M. Pezzullo, D. Prosperi, M. Colombo, B. Riva, S. Avvakumova, C. Morasso, S. Picciolini and M. Chiari, *Langmuir*, 2016, **32**, 7435 – 7441.

31 A. W. Scott, V. Garimella, C. M. Calabrese and C. A. Mirkin, *Bioconjug. Chem.*, 2017, **28**, 203 – 211.

32 A. K. Adak, B. Li, L. Huang, T. Lin, T. Chang, K. C. Hwang and C. Lin, *ACS Appl. Mater. Interfaces*, 2014, **6**, 10452 – 10460.

33 D. J. Lewis, F. Moretta, A. T. Holloway and Z. Pikramenou, *Dalton Trans.*, 2012, **41**, 13138 – 13146.

34 K. Wright, PhD thesis, University of Birmingham, 2013.

35 A. Savage, PhD thesis, University of Birmingham, 2013.

36 X. Huang and M. A. El-Sayed, *J. of Adv. Research*, 2010, **1**, 13 – 28.

37 Information from Malvern on the interpretation of DLS data, http://www.biophysics.bioc.cam.ac.uk/wpcontent/uploads/2011/02/DLS_Terms_defined_Malvern.pdf (Accessed online May 2017).

38 J. D. Clogston and A. K. Patri, *Met. Mol. Biol.*, 2011, **697**, 63 – 70.

39 A. Davies, D. J. Lewis, S. P. Watson, S. G. Thomas and Z. Pikramenou, *Proc. Natl. Acad. Sci.*, 2012, **109**, 1862 – 1867.

40 S. A. M. Osborne and Z. Pikramenou, *Faraday Discussions*, 2015, **185**, 219 – 231.

41 C. P. Milstein and E. V. Deverson, *Biochem. J.*, 1971, **123**, 945 – 958.

42 J. Svasti and C. Milstein, *Biochem. J.* 1972, **128**, 427 – 444.

43 A. H. Pakiari and Z. Jamshidi, *J. Phys. Chem. A*, 2007, **111**, 4391 – 4396.

44 F. Ramezani, M. Amanlou and H. Rafii-Tabar, *Amino Acids*, 2014, **46**, 4, 911 – 920.

45 M. Hoefling, F. Iori, S. Corni and K. Gottschalk, *Langmuir*, 2010, **26**, 8347 – 8351.

46 Information on Alexa Fluor® organic dye series from atdbio, http://www.atdbio.com/content/34/Alexa-dyes (Acsessed online May 2017).

47 J. P. Campbell, M. Cobbold, Y. Wang, M. Goodall, S. L. Bonney, A. Chamba, J. Birtwistle, T. Plant, Z. Afzal, R. Jefferis and M. T. Drayson, *J. Immunol. Methods*, 2013, **391**, 1 – 13.

48 A. R. Bradwell, H. D. Carr-Smith, G. P. Mead, L. X. Tang, P. J. Showell, M. T. Drayson and R. Drew, *Clin. Chem.*, 2001, **47**, 673 – 680.

49 V. Laital and I. Hemmilä, *Anal. Chem.*, 2005, **77**, 1483 – 1487.

50 H. Harma, S, Pihlasalo, P. J. Cywinski, P. Mikkonen, T. Hammann, H. L. Löhmannsröben and P. Hanninen, *Anal. Chem.* 2013, **85**, 2921 – 2926.

51 D. Casanova, D. Giaume, T. Gacoin, J. Boilot and A. Alexandrou, *J. Phys. Chem. B*, 2006, **110**, 19264 – 19270.

3 Introduction of blocking agents into FRET assay

3.1 Introduction

Commercial immunoassay systems such as ELISA or DELFIA and others on the market place are reliant on the specific interaction between antibody and antigen. For the most effective readout from a given system, it is crucial to eliminate any background interference from the system. Background interference is often a result of non-specific binding (NSB) within the system whether it be NSB between biomolecules or within the actual system itself.

To combat this, immunoassay systems are designed with components to inhibit NSB from both non-specific protein interactions and from binding to other assay components used during detection. Indeed, the ideal NSB blocking agent would accomplish this whilst showing no cross reactivity with assay components, and without disrupting bonds between biomolecule and the surface involved. NSB blocking reagents can generally be grouped into two categories (Table 3.1.1.) and can be used to block on a variety of surfaces including polymer based surfaces, silica and gold.[1,2]

Table 3.1.1.

NSB blocking reagents and their properties.[3,4,5,6,7,8,9,10,11]

Category	**General Properties**	**Examples**
Detergent	• Disrupt ionic and hydrophobic biomolecule – surface bonds • Inhibition of enzyme – substrate reactions • Inexpensive and stable • Can disrupt non-covalent biomolecule – surface bonds	Tween 20, Triton – X 100, Zonyl FSA
Protein	• Block non-occupied sites on the surface • Can be used to 'space out' surface bound biomolecules	BSA, Foetal calf serum (FCS)

Whilst detergent and protein NSB blocking agents are the most commonly employed, other polymer based blocking agents have been used such as polyethylene glycol, polyvinyl alcohol and polyvinylpyrrolidone, which can be used to coat hydrophobic surfaces.[12,13,14] Indeed, the inclusion of NSB blocking agents into a model ELISA system is included to highlight the necessity of eliminating background interference from a biological diagnostic device (Figure 3.1.1.).

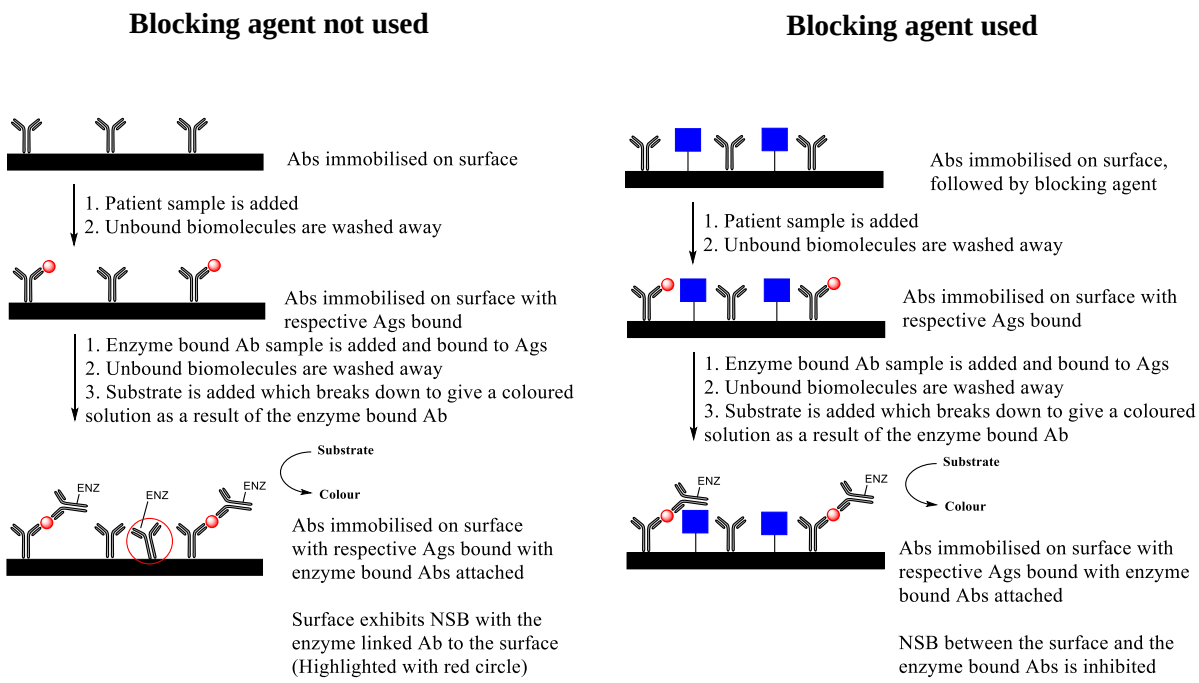

Figure 3.1.1.

Model ELISA assay showing the NSB within a system.

Blue square, Blocking agent.

NSB within a system can lead to assay readouts whereby a false readout is observed. Indeed, in the model ELISA system, the concentration of the antigen is directly proportional to the enzymatic action on the substrate. When the system exhibits NSB, a false positive readout in the concentration of antigen is measured as a result of the enzyme linked antibody binding to the surface, continuing to show activity upon addition of the substrate (Figure 3.1.2.).

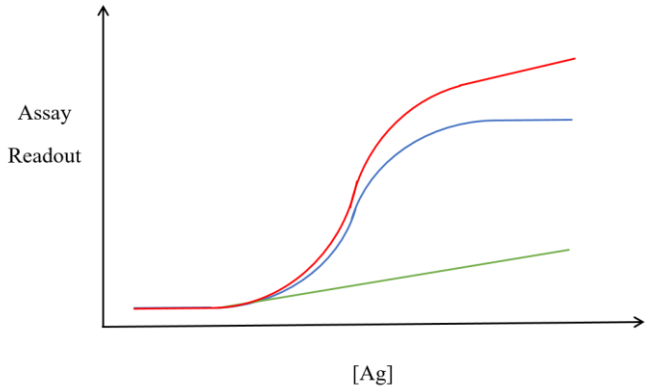

Figure 3.1.2.

False positive result observed if NSB is not controlled from model ELISA assay.

Green line, NSB signal; Blue line, specific binding signal; Red line, signal observed.

In general, finding the most efficient and best NSB blocking agent combination is exhaustive and empirical testing is required to both choose and optimise the blocking of NSB within a given system, which can often consist of a combination of protein and detergent based blocking agents.

3.2 Chapter Outline

All immunoassay systems are developed with the use of a NSB blocking agent or combination of blocking agents to minimise NSB and get the best assay readout possible from the system. With the FRET assay with **κnew.EuQS@Au** and **BUCIS04-AF647** for κFLC, with the introduction of NSB blocking agents we can get the best signal possible from the assay (Figure 3.2.1.).

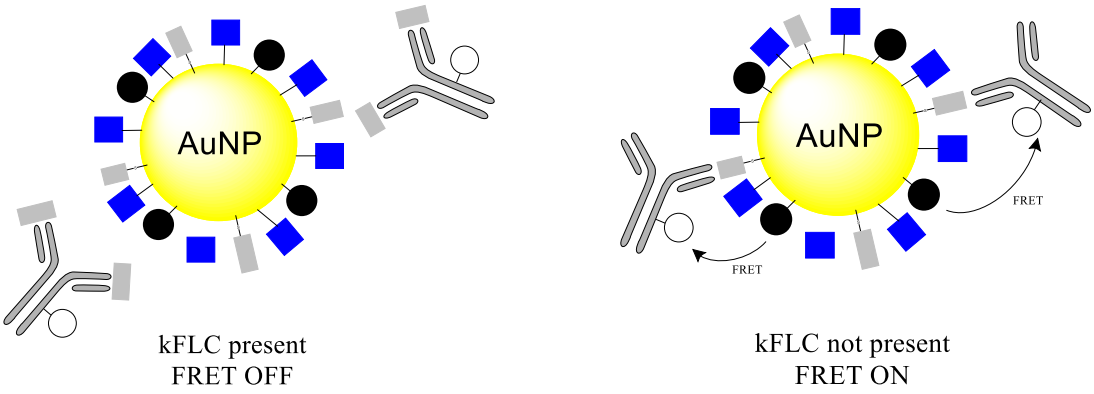

Figure 3.2.1.

General schematic of FRET assay between ***κnew.EuQS@Au*** *and* ***BUCIS04-AF647*** *for κFLC with the inclusion of NSB blocking agents.*

Herein, the effect of NSB blocking agents on **κnew.EuQS@Au** are examined, and how this can be used for a competitive assay for the detection of κnew.

3.3 NSB interaction

As previously discussed, AuNPs are widely employed in bioassay applications for their aqueous solubility, non-toxic nature and their ease of functionalisation. Whilst the ease of functionalisation is useful for the deposition of biomolecules and other material when working with gold colloids, this can lead to issues with unwanted biomolecules showing a level of interaction with the gold surface involved. In the field of medical diagnostics, as discussed, NSB can lead to false and inaccurate results.[15,16]

Indeed, an unwanted interaction between **EuQS@Au** and **BUCIS04-AF647** can be observed as measured *via* lifetime measurements, whereby a quench in the lifetime of **EuQS@Au** is observed upon incubation with **BUCIS04-AF647** (Table 3.3.1.) (Figure 3.3.1.).

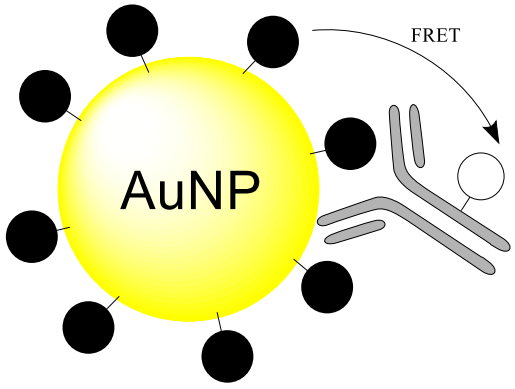

Figure 3.3.1.

Schematic showing NSB interaction between ***EuQS@Au*** *and* ***BUCIS04-AF647****, Not to scale.*

Table 3.3.1.

Lifetime data showing the affect of ***BUCIS04-AF647*** *(1.0 mg / mL, 4 µL), upon the lifetime of* ***EuQS@Au*** *(200 µL, 2.7 nM).*

AuNP sample / 2.7 nM	**Tris HCl / µM**	**BUCIS04-AF647 / nM**	**τ / µs**	**χ^2**
EuQS@Au	0	0	580	1.1
EuQS@Au	50	0	580	1.1
EuQS@Au	0	100	550	1.1
EuQS@Au	50	100	530	1.1

Upon incubation of **EuQS@Au** at 2.7 nM with **BUCIS04-AF647** at 100 nM in both tris HCl buffered and non buffered solution leads to a decrease in the Eu lifetime. Since FRET is a distant dependent interaction which can occur up to *ca.* 10 nm, when the two chromophores become close in space, this can be considered a NSB interaction between **EuQS@Au** and the **AF647** dye. The nature of the interaction is unclear, but a likely cause is the interaction of amino acid residues from **BUCIS04-AF647** showing an interaction with the gold surface.

Whilst the comparison of the FRET between **AF647** and **EuQS@Au** cannot be directly compared with that of **AF647** and **κnew.EuQS@Au** due to the different AuNP surface functionalisation, clearly this interaction cannot be ignored. To combat this interaction within the system with **κnew.EuQS@Au** and **BUCIS04-AF647**, the addition of blocking agents to the system are examined in an attempt to block out this interaction.

3.4 Protein blocking agents

The use of non-reactive proteins as a blocking agent is common. Indeed, it is necessary to use proteins which show no cross reactivity with the reagents involved to be a successful blocking reagent. The use of BSA as a blocking agent at between 1 and 3% is common as it is a non-reactive protein, which shows no activity with human IgG. Another common protein based blocking agent is FCS (Foetal calf serum), of which BSA is a major component, also comprising of other serum based proteins, which is also typically used between 1 and 3%. FCS is also comprised of calf FLCs, which are secreted into calf serum which are of a different structure to human FLC, hence no cross reactivity between **BUCIS04-AF647** and calf FLC is observed.

We examine the effect of the addition of both BSA and FCS, each at 1% on the SPR wavelength of **EuQS@Au** which is sensitive any changes or functionalisation of its surface *via* UV Vis (Figure 3.4.1.). It was necessary to add in the blocking reagent at the lower concentration to minimise any particle aggregation, which could be observed when higher concentrations of the blocking agent were added to functionalised gold colloids.

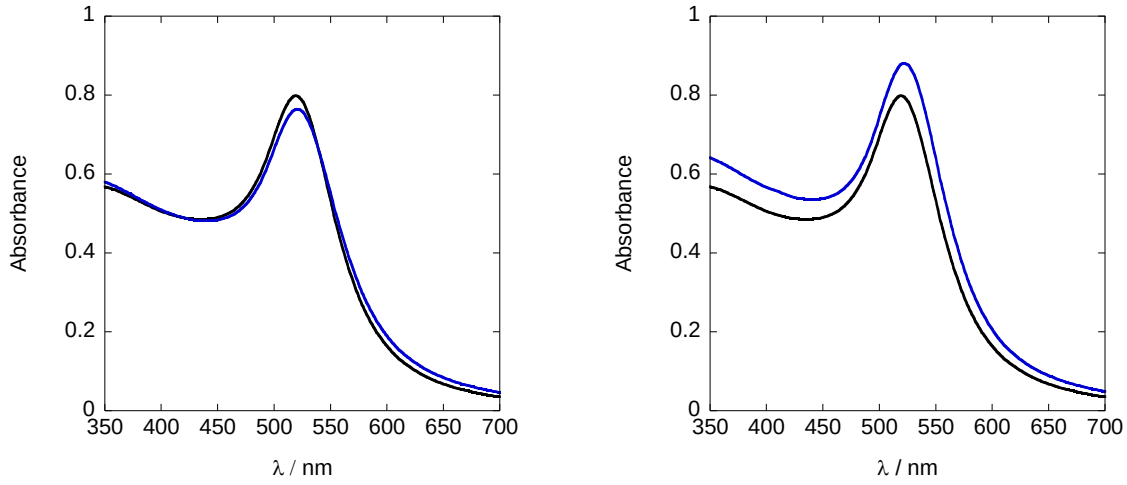

Figure 3.4.1.

*Left: **EuQS@Au**, (2 ml, 2.7 nM) in water (Black curve), **EuQS@Au**, (2 ml, 2.7 nM) in water in 1% BSA solution after 30 minutes incubation (Blue curve); Right: **EuQS@Au**, (2 ml, 2.7 nM) in water (Black curve), **EuQS@Au**, (2 ml, 2.7 nM) in water in 1% FCS solution after 30 minutes incubation (Blue curve).*

The incubation of both BSA and FCS at 1% to **EuQS@Au** show perturbations in the SPR wavelength of the functionalised gold colloids. A bathochromic shift of 2 nm is seen for the addition of BSA and that of 3 nm for FCS. We attribute the positive change in the SPR wavelength to the proteins acting as blocking agents and blocking any remaining sites on the AuNP where NSB can occur. Eu(III) luminescence is observed from the blocking agent modified particles.

Incubation of protein blocking reagent treated **EuQS@Au** with **BUCIS04-AF647** was examined *via* excited state lifetime measurements (Table 3.4.1.).

Table 3.4.1.

*Lifetime data showing the effect of **BUCIS04-AF647** (1.0 mg / mL, 4 µL), upon the lifetime of protein blocking agent modified **EuQS@Au** (200 µL, 2.7 nM).*

Blocking Agent Present	**Tris HCl / µM**	**BUCIS04-AF647 / nM**	**τ / µs**	χ^2
BSA	0	0	570	1.1
BSA	50	0	570	1.1
BSA	0	100	560	1.1
BSA	50	100	550	1.0
FCS	0	0	570	1.1
FCS	50	0	580	1.1
FCS	0	100	560	1.1
FCS	50	100	550	1.1

The incubation of both BSA and FCS into **EuQS@Au** show that as **BUCIS04-AF647** is added at 100 nM, the FRET signal is decreased in comparison to raw **EuQS@Au** without the use of a blocking agent showing the effect of the blocking agent. Despite this, a small FRET signal is measured in both cases as seen with the slight decrease in Eu(III) lifetime.

3.5 Detergent blocking agents

The use of detergent based blocking agents is common, and indeed in many surface based techniques, detergent based species are often included in washing buffers during operation to inhibit NSB as much as is possible. Detergent blocking agents are generally used at a much lower concentration to their protein counterparts, and as such, the use of detergent based blocking agents at between 0.01 – 0.1% is common. Tween 20 is a nonionic surfactant which is commonly used as a blocking agent in biological systems, which has been shown to have an interaction with surface of a gold colloid.[17,18] Fluorinated surfactant Zonyl has also been shown to have an interaction with the surface of AuNPs by our group and others.[19,20]

The effect of the addition of both Tween 20 and Zonyl® FSA surfactants, each at 0.05 % on the SPR wavelength of **EuQS@Au** was examined, which is sensitive any changes or functionalisation of its surface *via* UV Vis (Figure 3.5.1.).

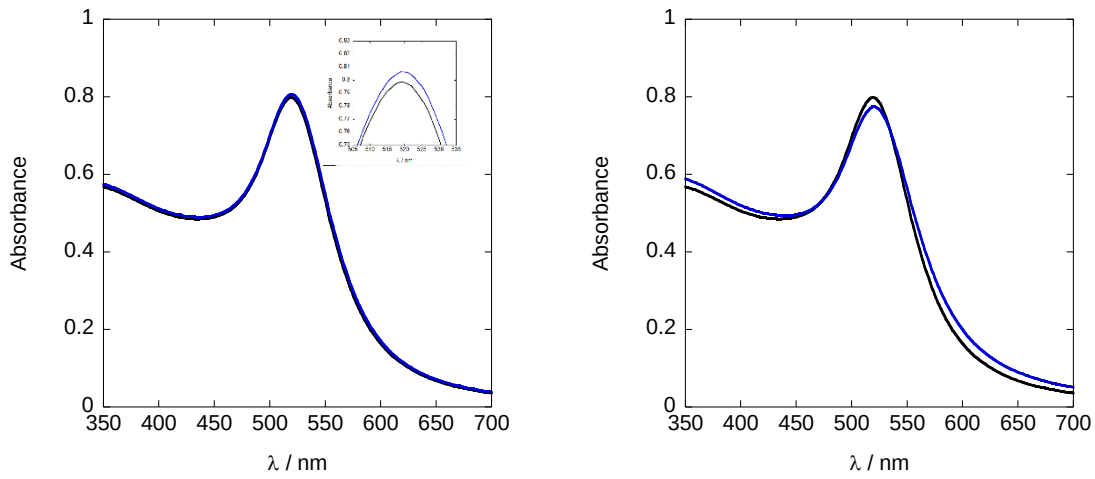

Figure 3.5.1.

Left: ***EuQS@Au****, (2 ml, 2.7 nM) in water (Black curve),* ***EuQS@Au****, (2 ml, 2.7 nM) in water in 0.05% Tween 20 solution after 30 minutes incubation (Blue curve); Right:* ***EuQS@Au****, (2 ml, 2.7 nM) in water (Black curve),* ***EuQS@Au****, (2 ml, 2.7 nM) in water in 0.05% Zonyl FSA solution after 30 minutes incubation (Blue curve).*

No SPR λ_{max} perturbation is observed for the addition of Tween 20 or for Zonyl® FSA, although a slight decrease in intensity and broadening is seen for the addition of Zonyl® FSA. Both samples continue to show Eu(III) luminescence both in and out of tris HCl buffered solution.

Incubation of detergent blocking reagent treated **EuQS@Au** with **BUCIS04-AF647** was examined *via* excited state lifetime measurements (Table 3.5.1.).

Table 3.5.1.

*Lifetime data showing the affect of **BUCIS04-AF647** (1.0 mg / mL, 4 µL), upon the lifetime of detergent blocking agent modified **EuQS@Au** (2.7 nM, 200 µL).*

Blocking Agent Present	**Tris HCl / µM**	**BUCIS04-AF647 / nM**	**τ / µs**	**χ^2**
Tween 20	0	0	580	1.1
Tween 20	50	0	580	1.2
Tween 20	0	100	540	1.1
Tween 20	50	100	520	1.1
Zonyl® FSA	0	0	570	1.0
Zonyl® FSA	50	0	570	1.1
Zonyl® FSA	0	100	540	1.1
Zonyl® FSA	50	100	520	1.0

The incubation of both Tween 20 and Zonyl® FSA into **EuQS@Au** show that as **BUCIS04-AF647** is added at 100 nM, the FRET signal is similar in comparison to raw **EuQS@Au** without the use of a blocking agent, showing that detergent based blocking agents are inappropriate for the gold nanoparticle FRET assay.

3.6 Competition assay for κnew

Whilst the NSB signal between **EuQS@Au** and **BUCIS04-AF647** was not fully eliminated, the FRET assay for the detection of κnew with **κnew.EuQS@Au** was examined with the addition of protein blocking agents. The incubation of **κnew.EuQS@Au** with BSA and FCS, each at 1%, on the SPR wavelength of **κnew.EuQS@Au** *via* UV Vis was recorded (Figure 3.6.1.).

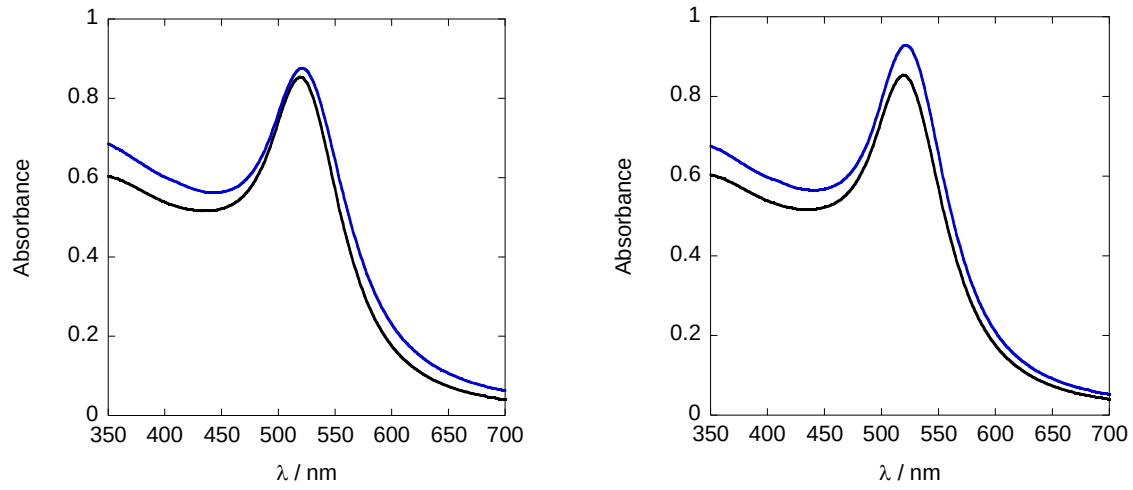

Figure 3.6.1.

*Left: **κnew.EuQS@Au**, (2 ml, 2.7 nM) in water (Black curve), **κnew.EuQS@Au**, (2 ml, 2.7 nM) in water in 1% BSA solution after 30 minutes incubation (Blue curve); Right: **κnew.EuQS@Au**, (2 ml, 2.7 nM) in water (Black curve), **κnew.EuQS@Au**, (2 ml, 2.7 nM) in water in 1% FCS solution after 30 minutes incubation (Blue curve).*

The incubation of both BSA and FCS at 1% to **κnew.EuQS@Au** show perturbations in the SPR wavelength of the functionalised gold colloids. A bathochromic shift of 2 nm is seen for the addition of BSA and that of 3 nm for FCS.

Incubation of protein blocking reagent treated **κnew.EuQS@Au** with **BUCIS04-AF647** was examined *via* lifetime measurements (Table 3.6.1.) and shows that FRET between **κnew.EuQS@Au** incubated with blocking agents and **BUCIS04-AF647** is active.

Table 3.6.1.

*Lifetime data showing the affect of **BUCIS04-AF647** (1.0 mg / mL, 4 µL), upon the lifetime of protein blocking agent modified **κnew.EuQS@Au** (2.7 nM 200 µL).*

Blocking Agent Present	**Tris HCl / µM**	**BUCIS04-AF647 / nM**	**τ / µs**	**χ^2**
BSA	0	0	580	1.1
BSA	50	0	570	1.1
BSA	0	100	510	1.1
BSA	50	100	500	1.1
FCS	0	0	580	1.1
FCS	50	0	550	1.2
FCS	0	100	490	1.1
FCS	50	100	460	1.2

On addition of **BUCIS04-AF647** at 100 nM into protein incubated **κnew.EuQS@Au**, FRET is observed as seen by a decrease in the lifetime of the Eu(III) ion. Indeed, as previously observed, the FRET signal is larger in the presence of tris HCl buffered solution and the energy transfer efficiency is similar to **κnew.EuQS@Au** without the presence of the blocking agent of between 10 and 15%. In both cases, the presence of the blocking agent slightly affects the excited state lifetime of the Eu(III) ion from the incubation period.

For the competitive assay it was decided chose to incubate the κnew sample for detection with **BUCIS04-AF647** prior to adding this premixed sample into **κnew.EuQS@Au**. It was necessary to ensure that the active sites of **BUCIS04-AF647** had bound to the κnew sample to allow no binding of **BUCIS04-AF647** to **κnew.EuQS@Au** (Figure 3.6.2.). The FRET assay is successful for the detection of κnew at high concentrations as measured by lifetime data (Table 3.6.2.).

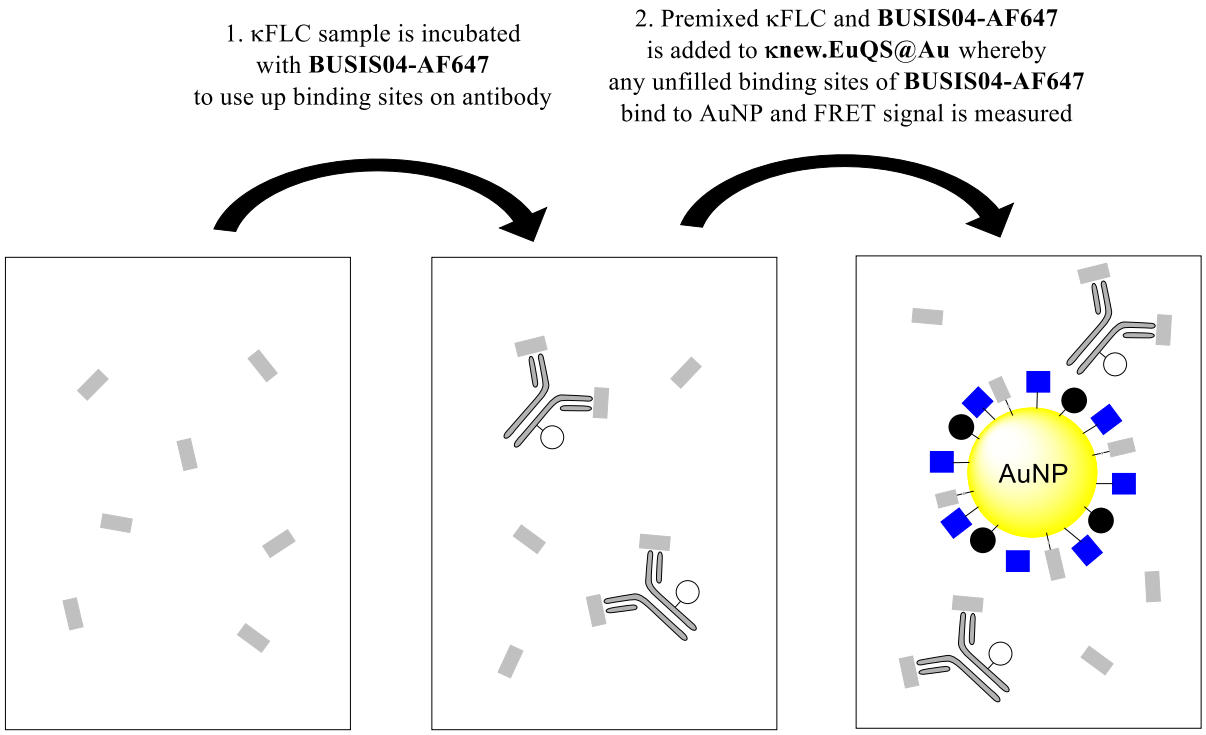

Figure 3.6.2.

*FRET assay for detection of κnew using **BUCIS04-AF647** and **κnew.EuQS@Au**. Not to scale.*

Table 3.6.2.

*Lifetime data after addition of premixed κnew (4.9 mg / ml in PBS 5 μL) and **BUCIS04-AF647** (1.0 mg / mL, 4 μL), into **κnew.EuQS@Au** (200 μL, 2.7 nM).*

Blocking Agent Present	**Tris HCl / μM**	**BUCIS04-AF647 / nM**	**κnew / μM**	**τ / μs**	**χ^2**
None	0	100	0	520	1.1
None	50	100	0	480	1.1
None	0	100	45	550	1.1
None	50	100	45	550	1.1
1% BSA	0	100	0	510	1.1
1% BSA	50	100	0	500	1.1
1% BSA	0	100	45	550	1.1
1% BSA	50	100	45	540	1.1
1% FCS	0	100	0	490	1.1
1% FCS	50	100	0	460	1.2
1% FCS	0	100	45	550	1.1
1% FCS	50	100	45	500	1.0

In all cases, the FRET signal without the presence of κnew at 45 μM is larger, which shows competition between κnew and **κnew.EuQS@Au**. In all cases, a degree of NSB continues to be an issue whereby the Eu(III) lifetime is not completely unaffected by the addition of **BUCIS04-AF647** premixed with the analyte as seen by the Eu(III) lifetime showing a slight decrease upon the addition of premixed analyte and **BUCIS04-AF647**.

3.7 Concluding remarks

A major issue relating to immunoassay technology where a surface is used for heterogeneous systems or indeed homogeneous systems using nanotechnology is NSB, whereby a small, unwanted interaction between a biomolecule and one of the surfaces involved happens and leads to a false positive result being obtained and hence a potential incorrect diagnosis. Because of this, NSB blocking agents are added to physically block out biomolecules from showing NSB to a surface.

It was found that indeed a large NSB signal is seen between Eu functionalised AuNPs and FRET acceptor **BUCIS04-AF647** with a decrease in the Eu(III) excited state lifetime on incubation of **EuQS@Au** with **BUCIS04-AF647**. To combat this interaction, it was found that non-reactive proteins BSA and FCS were able to partially block this NSB and this was taken forward to use these to block any NSB between **BUCIS04-AF647** and **κnew.EuQS@Au**. Whilst the NSB was not fully controlled with the addition of BSA or FCS at 1% it was possible to see competitive binding between **κnew.EuQS@Au** and **κnew** sample.

3.8 Referenced material

1 R. P. Bagwe, L. R. Hilliard, and W. Tan, *Langmuir*, 2006, **22**, 4357 – 4362.

2 E. Güven, K. Duus, M. C. Lydolph, C. S. Jørgensen, I. Laursen, G. Houen, *J. Immunol. Methods*, 2014, **403**, 26 – 36.

3 J. G. Kenna, G. N. Major and R. S. Williams, *J. Immunol. Methods*, 1985, **85**, 409 – 419.

4 I. Buchwalow, V. Samoilova, W. Boecker and M. Tiemann, *Sci. Rep.*, 2011, **1**, 1 – 6.

5 B. S. Munge, J. Fisher, L. N. Millord, C. E. Krause, R. S. Dowd and J. F. Rusling, *Analyst*, 2010, **135**, 1345 – 1350.

6 D. J. Rodda and H. Yamazaki, *Immunol. Invest.*, 1994, **23**, 421 – 428.

7 Y. Xiao and S. N. Isaac, *J. Immunol. Methods*, 2012, **384**, 148 – 151.

8 P. A. Lalor and P. A. Revell, *J. Immunol. Methods*, 1989, **122**, 149 – 150.

9 B. Zhang, X. Wang, F. Liu, Y. Cheng and D. Shi, *Langmuir*, 2012, **28**, 16605 −16613.

10 B. A. Kairdolf, M. C. Mancini, A. M. Smith and S. Nie, *Anal. Chem.*, 2008, **80**, 3029 – 3034.

11 Q. He, J. Zhang, J. Shi, Z. Zhu, L. Zhang, W. Bu, L. Guo and Y. Chen, *Biomaterials*, 2010, **31**, 1085 – 1092.

12 M. Zheng, F. Davidson and X. Huang, *J. Am. Chem. Soc.*, 2003, **125**, 7790 – 7791.

13 E. L. Bentzen, I. D. Tomlinson, J. Mason, P. Gresch, M. R. Warnement, D. Wright, E. Sanders-Bush, R. Blakely and S. J. Rosenthal, *Bioconjugate Chem.*, 2005, **16**, 1488 – 1494.

14 P. G. M. van Gageldonk, C. von Hunolstein, F. R. M. van der Kli and G. A. M. Berbers, *Clin Vaccine Immunol.* 2011, **18**, 1183 – 1186.

15 P. Sandström, M. Boncheva and B. Åkerman, *Langmuir*, 2003, **19**, 7537 – 7543.

16 E. C. Dreaden, L. A. Austin, M. A. Mackey and Mostafa A. El-Sayed, *Ther. Deliv.*, 2012, **3** 457 – 478.

17 Y. Shih, C. Ke, C. Yu, C. Lu and W. Tseng, *ACS Appl. Mater. Interfaces*, 2014, **6**, 17437 – 17445.

18 C. Lin, C. Yu, Y. Lin and W. Tseng, *Anal. Chem.*, 2010, **82**, 6830 – 6837.

19 J. Lin, C. Chang, Z. Wu and W. Tseng, *Anal. Chem.*, 2010, **82**, 8775 – 8779.

20 J. Lin, C. Chang and W. Tseng, *Analyst*, 2010, **135**, 104 – 110.

4 Preparation of novel gold nanoparticles which bind and sensitize lanthanides

4.1 Introduction

A major drawback of the use of sensitized luminescence for the population of the emissive energy state of the Ln ion, especially for imaging applications, is that a high energy excitation wavelength is often required to excite the organic based sensitizing unit, often in the ultraviolet area of the electromagnetic spectrum. High energy wavelengths are not only dangerous and damaging to tissue, but also do not penetrate deep, thus are not transmitted far into the body.[1] Indeed, UCPs can be used in intercellular imaging to avoid this as the excitation wavelength used is a two – photon process often at 980 nm, which requires high power lasers to achieve sufficient signal from the emissive Ln ion.[2,3] As a result, whilst the emissive properties of the Ln are favoured for imaging type applications, it is organic and transition metal based probes such as $[Ru(bpy)_3]^{2+}$ and $Ir(ppy)_3$ which are often used, despite their emissive properties being less favoured for this type of application, resulting from their excitation wavelength in the visible area of the electromagnetic spectrum.[4,5,6,7] Although organic fluorescent probes can show high quantum yields, their excited state lifetime is short and often less than 10 nanoseconds, which means that time gated measurements are not possible and their broad emission signal is often difficult to identify from background fluorescence. Transition metal probes show longer lifetimes extending into the hundreds of nanoseconds range meaning that time gated measurements are possible, although their optical signal is broad and not as characteristic as the Ln series.

Whilst the structures of new luminescent Ln complexes can appear complicated, the two basic requirements of a luminescent Ln complex are the same. A suitable Ln binding site which can protect the central Ln ion from quenching oscillations present in aqueous and alcoholic solvents is required, along with a suitable organic sensitizing unit which can successfully transfer energy to the Ln ion *via* its T_1 state. Indeed, reports of new sensitizer – binding site combinations are common.[8,9]

β-diketone units such as acac in their anionic form can be used to bind to Ln and other metal ions and form stable complexes (Figure 4.1.1.). As such Ln β-diketone systems have found applications as chiral shift reagents, antibody labels, electroluminescent materials, and others.[10,11,12,13,14,15]

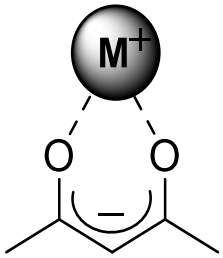

Figure 4.1.1.

Structure of anionic β-diketone binding to a metal ion.

The aryl functionalised β-diketone, DBM can be used in the same fashion for binding to Ln ions, including Eu which can commonly form stable complexes of $Eu(DBM)_3$ *via* coordination from the β-diketone unit in its deprotonated form (Figure 4.1.2.). Excess coordination sites are filled with coordinating solvent molecules. $Eu[(DBM)_4]^-$ salts have also been reported.[16]

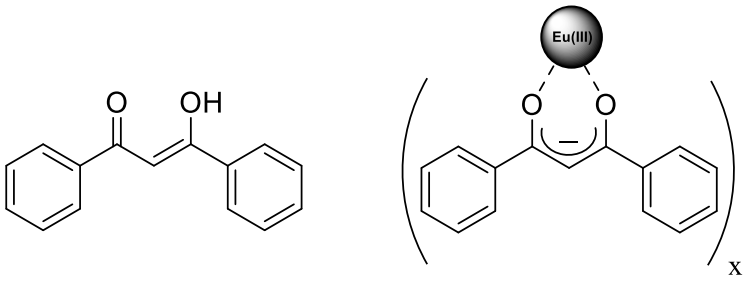

Figure 4.1.2.

Structures of DBM (Left) and $Eu(DBM)_x$ where x can be 3 or 4 (Right).

For the efficient sensitization of Eu(III), DBM is one of the most widely used and popular units to bind and sensitize Eu(III) ions, which has been studied since the 1940s, showing characteristic *f-f* luminescence from the Eu(III) ion. The $^5D_0 \rightarrow {}^7F_2$ band is particularly prominent in comparison to other Eu(III) complexes due to the symmetrical nature of the complex.[17] It is possible to excite $Eu(DBM)_3$

derivatives up to 400 nm in the long wave ultraviolet area of the electromagnetic spectrum, an improvement on harsh wavelengths traditionally used for the absorption of light within a luminescent Ln complex.[18,19]

Many derivatives of the classical $Eu(DBM)_3$ have been synthesised in attempts to increase the luminescence of the original complex. Basset *et. al.* developed complexes whereby two benzoyl β-diketonate sites joined by a 1,3-phenylene spacer unit were synthesised, allowing two binding sites for Lns to be coordinated, thus making the complex twice as luminescent as $Ln(DBM)_3$ (Figure 4.1.3.).[20] Indeed, taking advantage of the extra coordination sites on $Ln(DBM)_3$ is also common whereby the use of phenanthroline (phen) is common which can provide extra sensitization, whilst further protecting the complex from quenching solvent oscillations (Figure 4.1.4.).[21,22] Changes in sensitizer, and the use of fluorinated ligands to protect from quenching C-H oscillations have also been studied.[23,24]

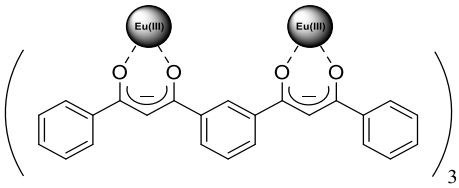

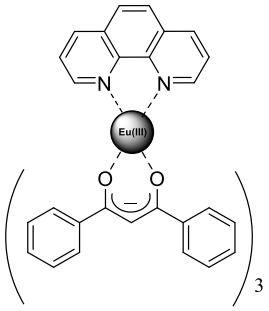

Figures 4.1.3. (Left) and 4.1.4. (Right)

New strategies to improve the luminescence of Eu DBM complexes.

The use of Ln DBM complexes combined with NP technology is fairly common and using these type of complexes as dopants within both silica and polymer based luminescent Ln NPs is popular, as previously discussed (Section 1.5), in the preparation of highly luminescent NPs showing strong *f-f* luminescence, which can be in used in bioassay applications.

Ln based DBM complexes and their derivatives have been used for functionalised surfaces and NPs. Indeed, in 2009 Gulino *et. al.* showed how a self-assembled monolayer of a luminescent Eu(III)

complex could be attached to a silica surface. A [Eu(DBM)$_3$(phen)] complex with a terminal Si(OMe)$_3$ complex was synthesised, whereby incubation with a glass surface allowed the complex to be grafted onto the surface (Figure 4.1.5.).[25] Indeed, after copious washing of the surface to remove excess complex, Eu(III) luminescence was observed with an excitation wavelength of 340 nm. A similar system was developed by Armelao *et. al.* whereby a silica surface was again functionalised with a Eu(III), DBM complex and showed *f-f* emission.[26] Unpublished work within the Pikramenou group performed by Dr Suleman Khan has shown how DBM and other small organic molecules can be used to make luminescent NPs and surfaces *via* coordination to a silica functionalised DTPA molecule bound to a silica surface (Figure 4.1.6.). Coordination of DBM into the DTPA cavity allows sensitization of the Ln ion and luminescence can be observed. This was also shown for a **EuQuinSAc** functionalised Au surface whereby coordination of DBM into the DTPA cavity allowed for a luminescent enhancement of the central Eu(III) ion *via* extra sensitization from the DBM unit as well as the dual quinoline sensitizer present.

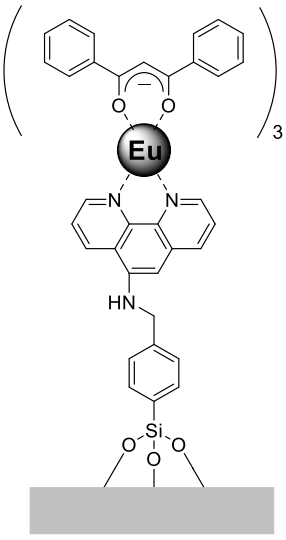

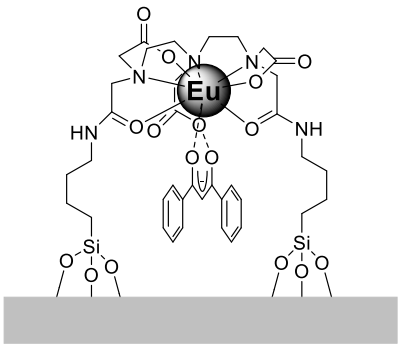

Figures 4.1.5. (Left) and 4.1.6. (Right)

Left: Development of luminescent Eu(III) self assembling monolayers on a glass surface; Right: Development of luminescent Eu(III) self assembling monolayers on a glass surface or silica NP.

The combination of AuNPs and DBM is yet to be studied and is the focus of this piece of work, whereby the favourable properties of AuNPs are combined with a Ln DBM complex.

4.2 Chapter outline

This chapter is concerned with the preparation of a functionalised DBM molecule with a thiol surface active group as to functionalise AuNPs with a DBM group, which can bind and sensitize Eu(III) ions (Figure 4.2.1.).

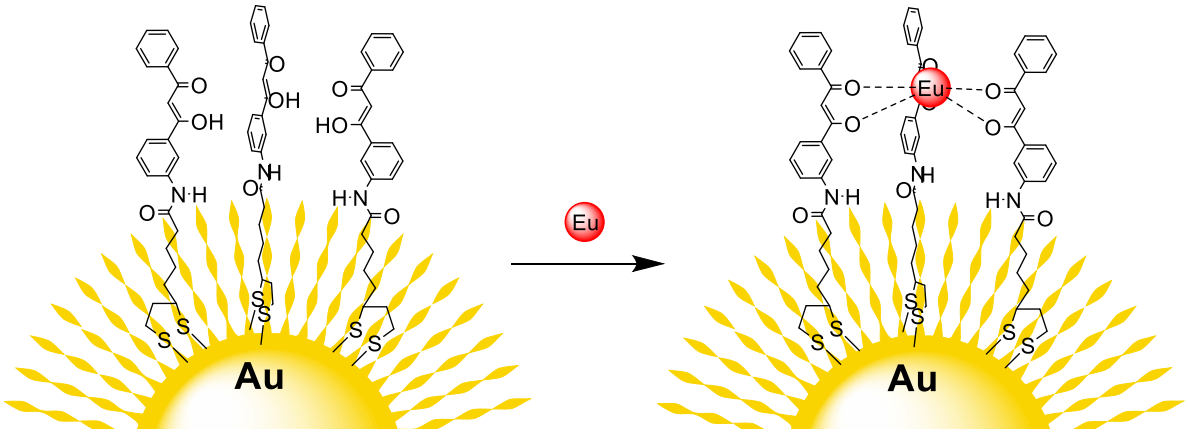

Figure 4.2.1.

General schematic of surface active DBM unit on AuNPs, binding Eu(III) ions.

Herein, the synthesis of a surface active DBM group, its photophysical properties and the surface functionalisation of AuNPs with the DBM unit are reported. The functionalised AuNPs are then shown to successfully bind and sensitize Eu(III) ions on the surface on the AuNP to develop novel luminescent AuNPs.

4.3 Synthesis of DBMSS

The molecule **DBMSS** was chosen as the synthetic target (Figure 4.3.1.). **DBMSS** contains the afore mentioned DBM unit for the binding and sensitization of Eu(III) ions and is functionalised with a thioctic acid side chain which is terminated with thiol groups for binding to a AuNP surface *via* the strong Au – S bonding moiety.

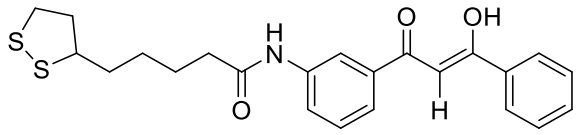

Figure 4.3.1.

*Structure of **DBMSS**.*

The synthesis of **DBMSS** was achieved in a three step synthesis *via* two intermediates from amino functionalised acetophenone, **7** (Figure 4.3.2.).

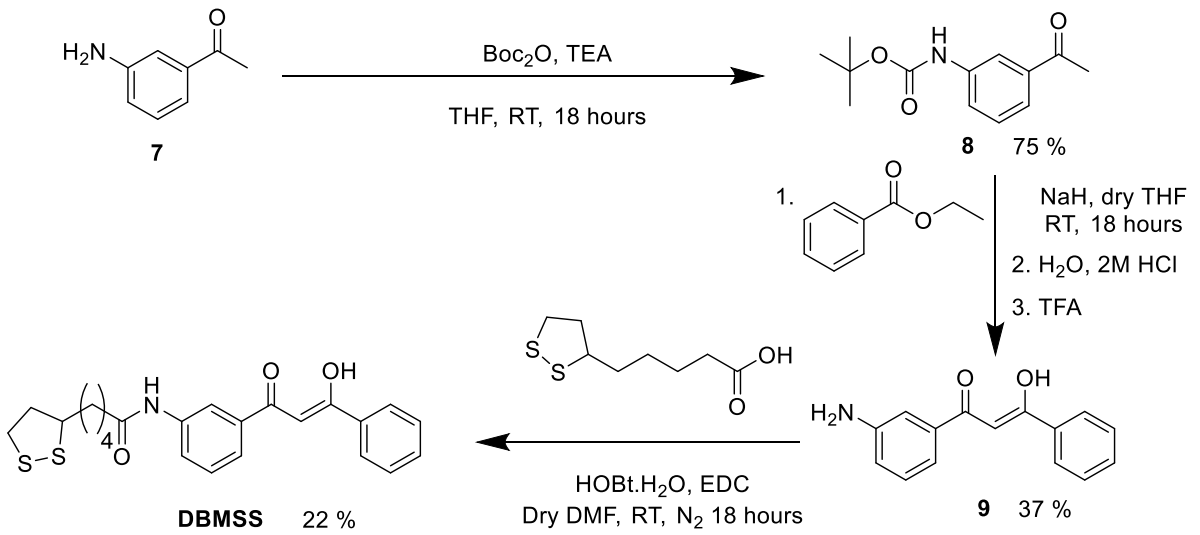

Figure 4.3.2.

*Synthetic scheme for **DBMSS**.*

The synthesis of the ligand was achieved *via* Boc protection of amine **7** to produce **8** which was then used in a one pot Claisen condensation with ethyl benzoate and subsequent removal of the protecting group with TFA to yield amine functionalised DBM molecule **9**, which could be used in an amide coupling reaction with thioctic acid to include the sulphur terminus on the target **DBMSS** in an overall 6% yield with respect to the starting amount of **7**. Characterisation spectra for compounds **8** and **9** are found in the appendix attached to this chapter.

Indeed, the preparation of amine functionalised DBM derivative **9**, allows the possibility of easy functionalisation of DBM derivatives *via* amide coupling with further functional groups, allowing the facile preparation of functionalised DBM molecules.

The identity of the product was confirmed with NMR spectroscopy and MS. MS of **DBMSS** shows a peak with *m/z:* 450.1 which is assigned to $[M + Na]^+$. Peaks with *m/z* values corresponding to compound **3** or thioctic acid were not observed. The ^1H NMR spectrum of **DBMSS** (Figure 4.3.3.) shows the expected number of resonances and was assigned using 2D COSY NMR spectroscopy (Figures 4.3.4. and 4.3.5.).

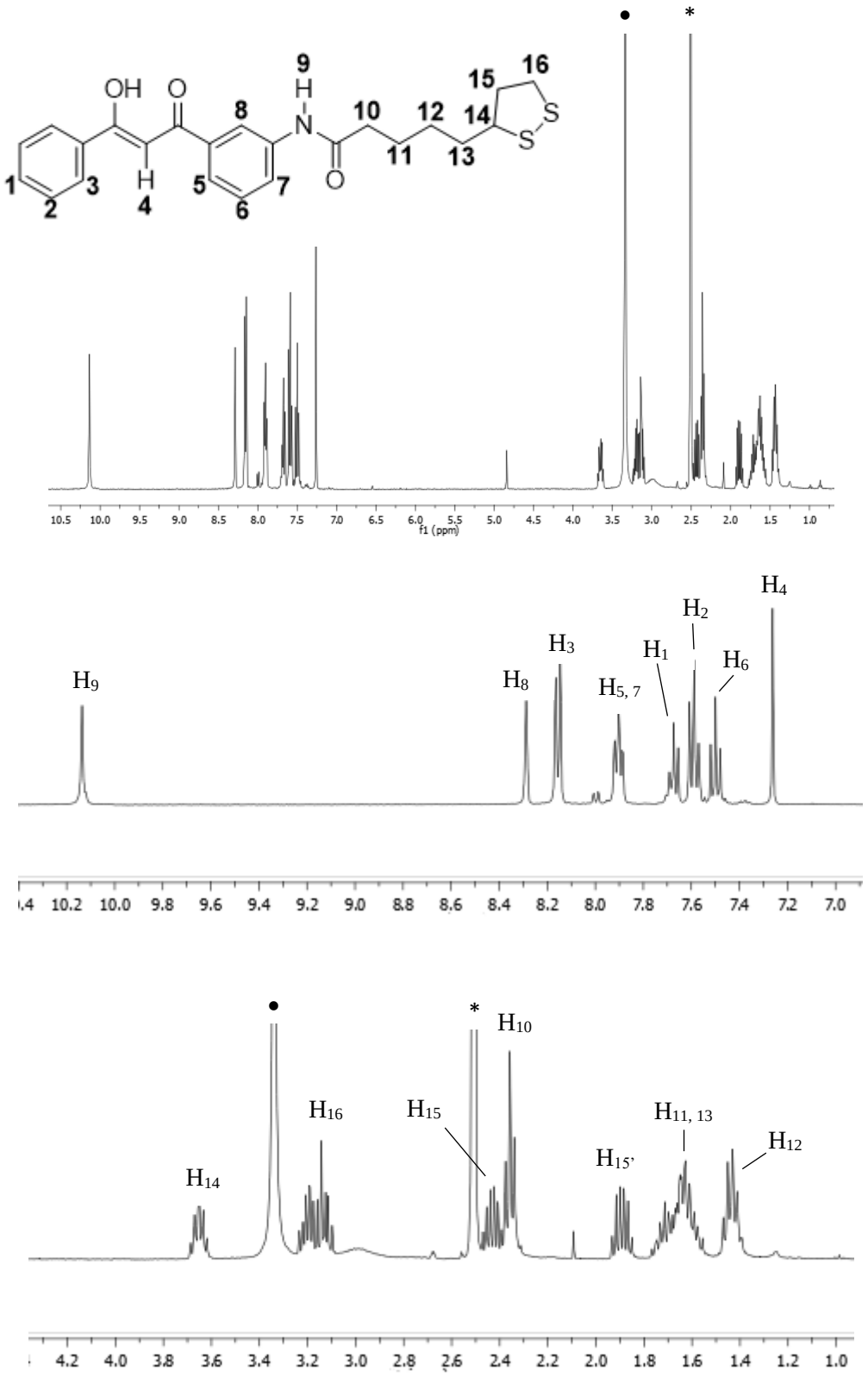

Figure 4.3.3.

*^{1}H NMR spectrum of **DBMSS** in d_6-DMSO. Aliphatic and aromatic reigions are presented separately.*

**, residual solvent resonance; •, water.*

The ^{1}H NMR spectrum of **DBMSS** confirms the formation of the product. The signal observed at 10.1 ppm is a singlet from the amide group (H_9) which is a new resonance in comparison to amine substituted DBM, **9**, whereby the signal corresponding to the amine group is no longer observed. The singlet at 7.3 ppm is a result of the central β-diketone proton (H_4) which is characteristic of this type of resonance of an aryl β-diketone. The relative integration of this resonance is one, which shows that this molecule exists primarily in its enol tautomer. The aromatic region of the spectrum shows the expected nine protons and each ring was assigned *via* COSY NMR spectroscopy, showing the coupling of protons on each substituted benzyl ring. Resonances at 8.2 ppm, 7.7 ppm and 7.6 ppm were found to couple to each other and all show splitting patterns indicating a ^{3}J value of 7.3 Hz and are assigned to protons H_3, H_1 and H_2. Signals on the next ring showed a signal shifted downfield at 8.3 ppm as a triplet which is assigned to H_8, as a result of its proximity to electron withdrawing groups of the amide and carbonyls of the β-diketone unit. H_5 and H_7 are overlapping signals at 7.9 ppm. The remaining aromatic proton is H_6 which appears as a triplet at 7.5 ppm. The aliphatic region of the spectrum shows the presence of the thioctic acid linker which integrates with the aliphatic area of the spectrum. This area of the spectrum is analogous with others who have reported similar compounds with a thioctic acid linker.[27] Peaks at 3.6 ppm, 3.1 – 3.2 ppm, 2.4 ppm and 1.8 ppm are from the five membered ring with the disulphide bond and are assigned to H_{14}, H_{16} and H_{15}, where H_{15} is split into two resonances at 2.4 ppm and 1.8 ppm. Protons in the four carbon chain show a triplet at 2.4 ppm from H_{10} which is shifted downfield in relation to the rest of the chain due to its proximity to the amide group, which are seen as a multiplet between 1.8 and 1.5 ppm with a relative integration of four showing protons H_{11} and H_{13} and finally a signal at 1.4 ppm corresponding to H_{12}.

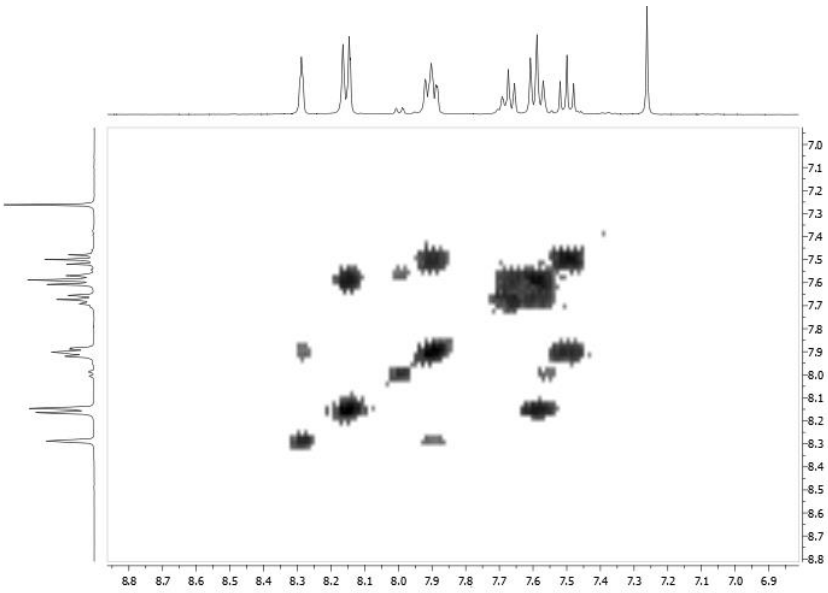

Figures 4.3.4.

*^{1}H COSY NMR spectrum of **DBMSS** in d_6-DMSO for the aromatic region.*

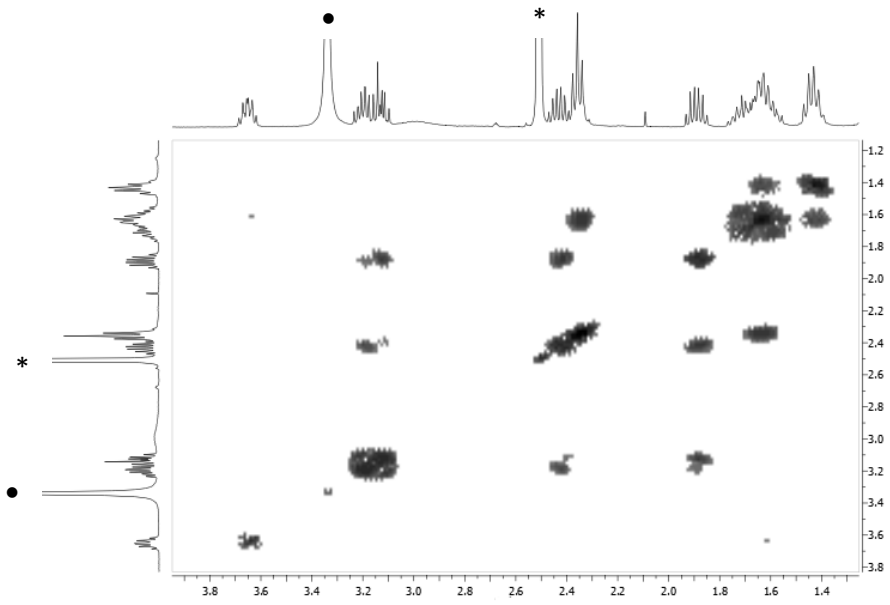

Figure 4.3.5.

*^{1}H COSY NMR spectrum of **DBMSS** in d_6-DMSO for the aliphatic region.*

**, residual solvent resonance; •, water.*

The identity was further confirmed *via* ^{13}C NMR spectroscopy (Figure 4.3.6.).

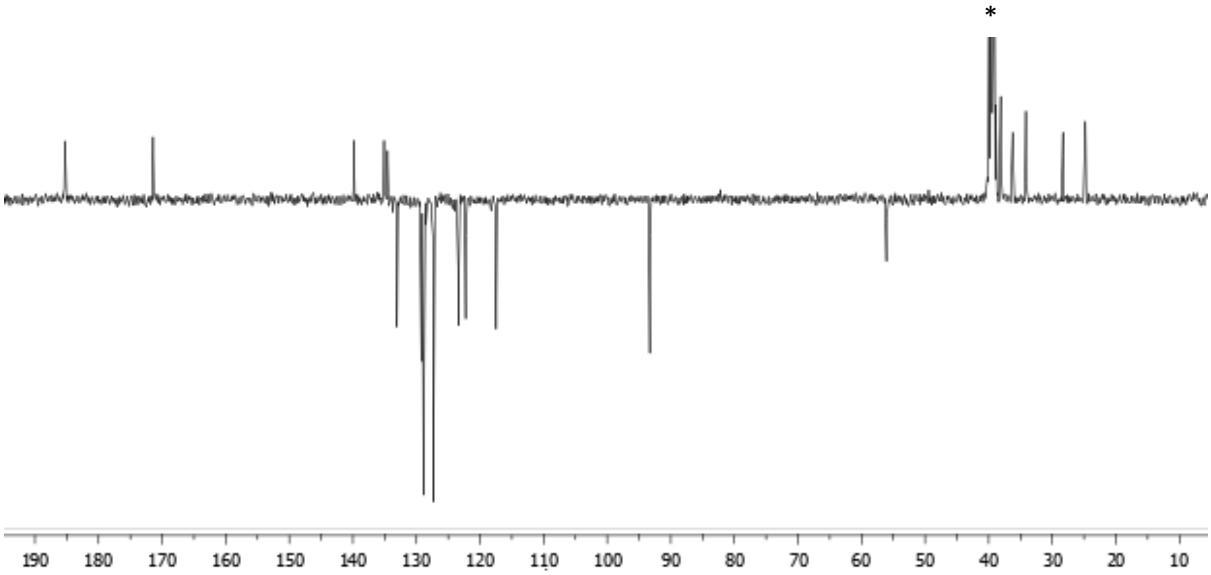

Figure 4.3.6.

*^{13}C NMR spectrum of **DBMSS** in d_6-DMSO.*

**, residual solvent resonance*

The ^{13}C NMR spectrum of **DBMSS** further confirms the presence of **DBMSS**. From an expected 21 ^{13}C resonances, 20 are observed and the remaining resonance is seen to be overlapping with the excess solvent at 39.5 ppm. Two resonances are observed at 185.3 and 185.2 ppm which are attributed to carbonyl resonances making up the β-diketone unit. The other carbonyl resonance at 171.4 ppm corresponds to the amide carbon. The aromatic region of the spectrum between 145 and 115 ppm show the expected ten signals, of which the three phenyl ring substitutions are observed. The signal at 93.3 ppm is from the centre of the β-diketone unit which shows a resonance meaning only one proton is attached to this carbon which gives further proof to the molecule existing in its enol form. The remainder of the resonances observed between 60 and 20 ppm show the thioctic acid linker unit in the molecule with the expected seven resonances.

4.4 Photophysical properties of DBMSS and lanthanide binding

The UV Vis spectrum of **DBMSS** (Figure 4.4.1.) in methanol shows a spectrum similar to that of DBM.

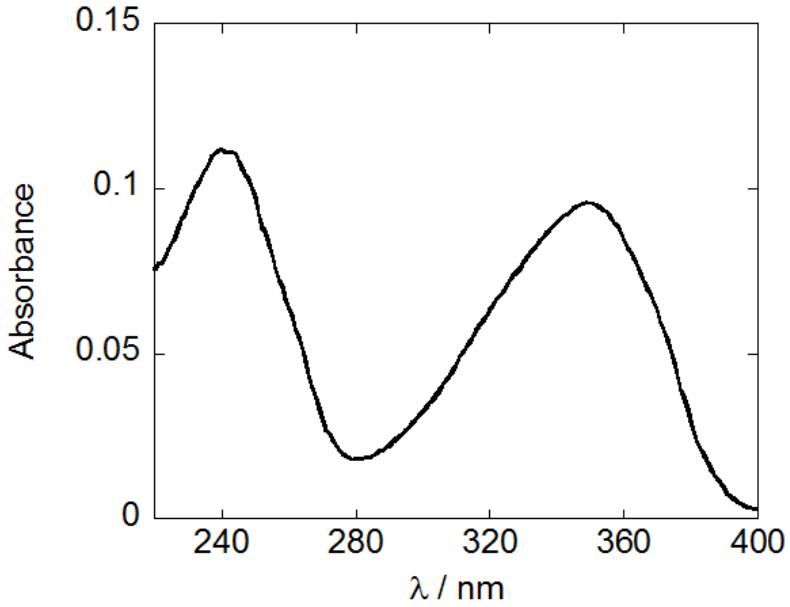

Figure 4.4.1.

*UV Vis spectrum of 4.8 µM **DBMSS** in MeOH.*

The UV Vis spectrum in MeOH of **DBMSS** shows two intense bands with λ_{max} values of 350 nm (ε = 19900 M^{-1} cm^{-1}) and 240 nm (ε = 23200 M^{-1} cm^{-1}). These bands can be attributed to $S_1 \leftarrow S_0$ and $S_2 \leftarrow S_0$ absorption bands both $\pi^* \leftarrow \pi$ in nature from the aryl groups. This is comparable with other functionalised DBM molecules synthesised in the literature.[28]

Eu(III) was able to be successfully coordinated into the ligand by addition of $EuCl_3.6H_2O$ into a solution of deprotonated **DBMSS** *via* treatment with TEA. To examine the binding between the Eu(III) ion and **DBMSS**, Eu(III) was titrated into the ligand, whilst the subsequent *f-f* emission signal was monitored (Figure 4.4.2.), with an excitation wavelength of 350 nm. Indeed, such is the weakly absorbing nature of the Eu(III) ion, in particular at 350 nm, the emission signal observed can be exclusively attributed to sensitization from the **DBMSS** ligand. Indeed, after the coordination of Eu(III) into **DBMSS,** the excitation spectrum shows how the emissive Eu(III) state can be populated and confirms that sensitized luminescence of the Eu(III) ion as a result of the **DBMSS** unit is active (Figure 4.4.2.).

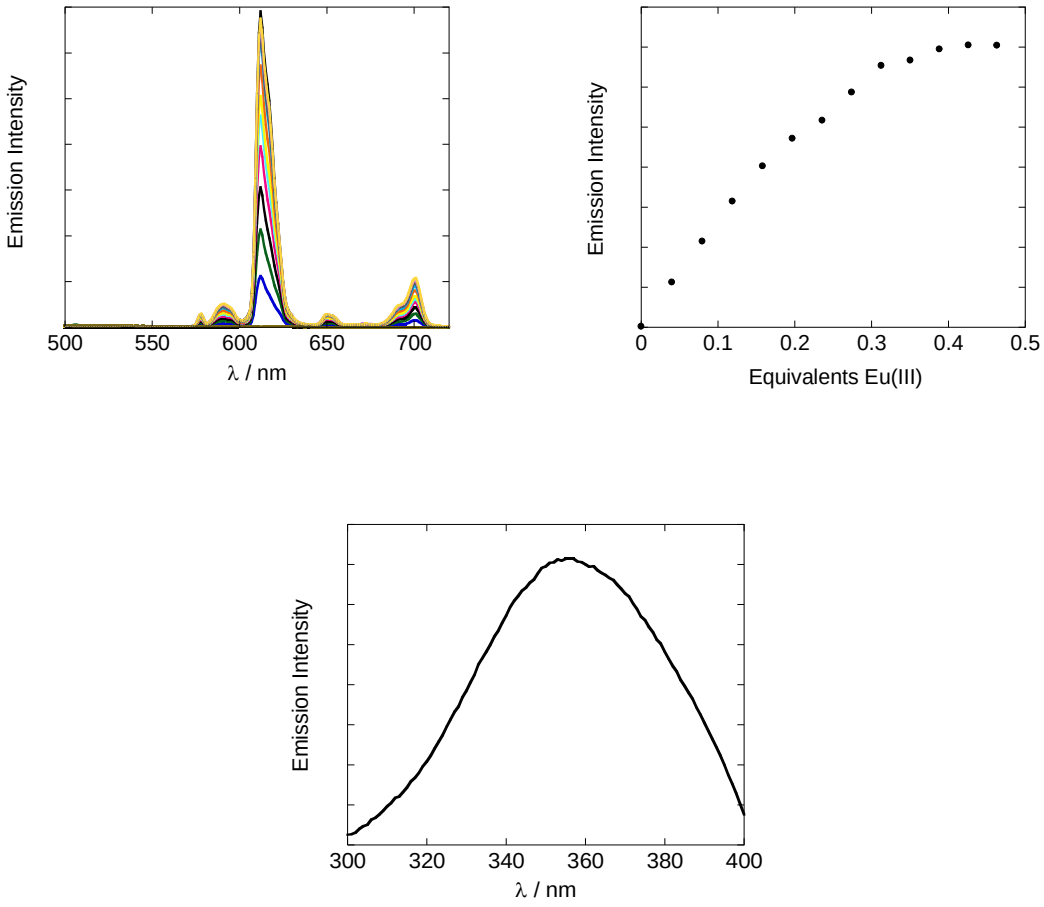

Figure 4.4.2.

Top left: Emission titration of $EuCl_3.6H_2O$ (0.8 mM, 6 µL aliquots) into a solution of ***DBMSS*** *(60 µM in MeOH, 2 ml) with 0.05% TEA to a final concentration of 28 µM (72 µL) λ_{exc} = 350 nm, Emission spectra corrected for PMT response; Top right: Growth of Eu(III) emission peak as integrated between limits of 607 and 621 nm; Bottom: Excitation spectrum of* ***DBMSS*** *after final addition of $EuCl_3.6H_2O$, monitoring the emission at 614 nm.*

As Eu(III) is introduced into the system the characteristic Eu(III) emission spectra is observed from the $^5D_o \rightarrow {}^7F_J$ energy levels whereby the J = 2 transition is the most intense transition at 612 nm. Indeed, the J = 2 transition is more intense in comparison to other transitions for the **DBMSS** system than for the DTPA quinoline sensitized Eu(III) complexes which show an increase in symmetry of the **DBMSS** ligand and the subsequent complex in comparison to **EuQuinSAc** and **EuQSH**. The emission of the Eu(III) ceases to rise when the ratio of **DBMSS** : Eu(III) reaches 3 : 1 which shows the formation of a **Eu(DBMSS)$_3$** complex.

The excitation spectrum shows that sensitized emission of the Eu(III) ion as a result of the **DBMSS** unit is active and the Eu(III) emission can be observed up to *ca.* 380 nm. As the use of invasive high energy wavelengths, is often used in the sensitization of Ln complexes, excitation up to this wavelength is an advantage, especially when combined with the properties of AuNPs. Lifetime studies of the methanolic solution of mixed **DBMSS** and $EuCl_3.6H_2O$ gave rise to biexponential decay behaviour, whereby the long lived Ln lifetime is present with values of 100 μs (45%) and 240 μs (55%) (χ^2 = 0.9) and that in the deuterated solvent analogue was 170 μs (33%) and 450 μs (67%) (χ^2 = 1.1). Use of the Parker-Beeby equation on the long component of each lifetime shows four solvent molecules are bound to the central Eu(III) ion. The coordination number of Eu(III) is usually high between eight and ten, hence this result confirms three **DBMSS** units are coordinated to the central metal ion as a β-diketone unit is bidentate *via* its two oxygen atoms.

4.5 Functionalisation of gold nanoparticles with DBMSS

To create luminescent AuNPs with **DBMSS** and Eu(III), it was decided to functionalise the surface of AuNPs with **DBMSS**, from which excess **DBMSS** could be removed, followed by coordination of Eu(III) ions into the functionalised AuNPs. This methodology was adopted to ensure that only Au surface immobilised **DBMSS** units were involved in the Eu(III) coordination. Indeed, this methodology has been applied in a similar system whereby Savage *et. al.* showed the addition of Eu(III) into Ln binding peptides, which were immobilised on 13 nm AuNPs.[29]

The addition of **DBMSS** in methanolic solution to **Cit@Au,** synthesised as previously described, gives rise to a large change in the SPR wavelength of **Cit@Au** (Figure 4.5.1.).

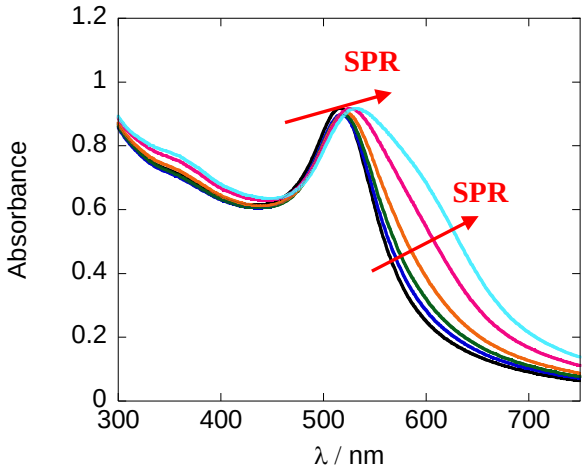

Figure 4.5.1.

Change in SPR wavelength of ***Cit@Au*** *(3.2 nM in water, 2* mL*) as a methanolic solution of* ***DBMSS*** *(0.2 mM in MeOH, 10 µL aliquots) is titrated in to a final concentration of 4.87 µM (50 µL).*

The large perturbation in the UV Vis spectrum of **Cit@Au** observed shows a widening and large shift in the nanomaterial SPR wavelength which is characteristic of AuNPs which have become destabilised and aggregated, which shows that the addition of **DBMSS** to **Cit@Au** causes destabilised particles. Attempts to functionalise the AuNP with **DBMSS** at different concentrations of **DBMSS** also resulted in NP aggregation.

The stability of AuNPs can be improved *via* functionalisation of the gold colloid with commercial surfactant or polymer.[30,31] Indeed, the increased stability and necessity for a surfactant molecule in the preparation of $[Ru(bpy)_3]^{2+}$ coated AuNPs has been shown due to the charge of the complex with the use of Zonyl®, Triton™ and Tween® functionalised AuNPs.[32,33] Herein, it is shown how the stability of **Cit@Au** can be improved with a preloading of fluorinated polymer Zonyl® FSA (Figure 4.5.2.) to the surface of the AuNP whereby the **DBMSS** probe is expected to bind to the surface after the Zonyl® FSA has been preloaded onto the NP.

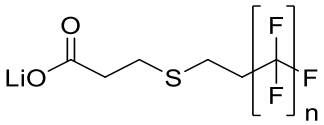

Figure 4.5.2.

Structure of Zonyl® FSA

The interaction of Zonyl® FSA leads to a small change in the SPR wavelength of the AuNP of 1 nm (Figure 4.5.3.) and excess Zonyl® FSA was removed *via* centrifugation in the development of **Z@Au**, after which DLS and were recorded (Table 4.5.1.). Particle size and morphology was further determined *via* TEM (Figure 4.5.4.).

Table 4.5.1.

*NP characterisation data for **Z@Au**.*

Sample	**Intensity distribution / nm**	**Number distribution / nm**	**PDI**
Cit@Au	18 ± 3	12 ± 3	0.1
Z@Au	25 ± 3	15 ± 3	0.1

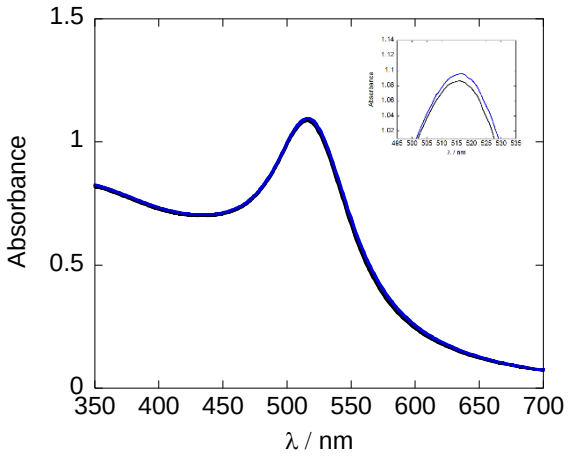

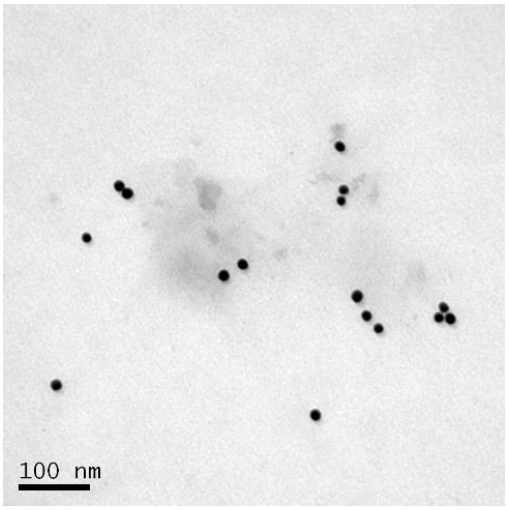

Figures 4.5.3. (Left) and 4.5.4. (Right).

Left; Change in SPR upon addition of Zonyl® FSA (50 ng / mL) into ***Cit@Au****, the Blue curve represents the addition of the surfactant, Right; TEM image of* ***Z@Au*** *after removal of excess Zonyl® FSA.*

The increased stability of the NPs is highlighted with a negative change in zeta potential of the particles from – 30 mV to – 50 mV. DLS sizing suggests that the particles are 15 nm which shows an increase in relation to **Cit@Au** which is in agreement with the TEM data which show the particles are *ca.* 15 nm and of a spherical morphology.

The surface of **Z@Au** was successfully functionalised with **DBMSS** in the production of **DBMSS.Z@Au** (Figure 4.5.5.).

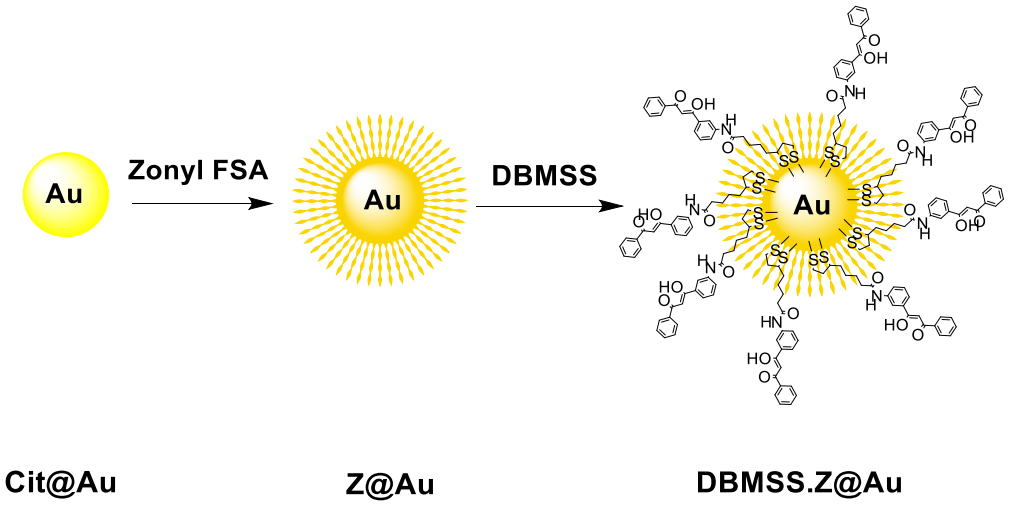

Figure 4.5.5.

Preparation of ***DBMSS.Z@Au*** *with the functionalisation of* ***Cit@Au*** *with Zonyl® FSA followed by* ***DBMSS.***

The surface functionalisation of **Z@Au** was monitored *via* UV Vis spectroscopy (Figure 4.5.6.). Excess **DBMSS** was removed *via* size exclusion chromatography using Sephadex G15 taking into account the large difference between the functionalised NP and **DBMSS**, whereby the SPR wavelength is unaltered showing that no aggregation occurs from the purification method.

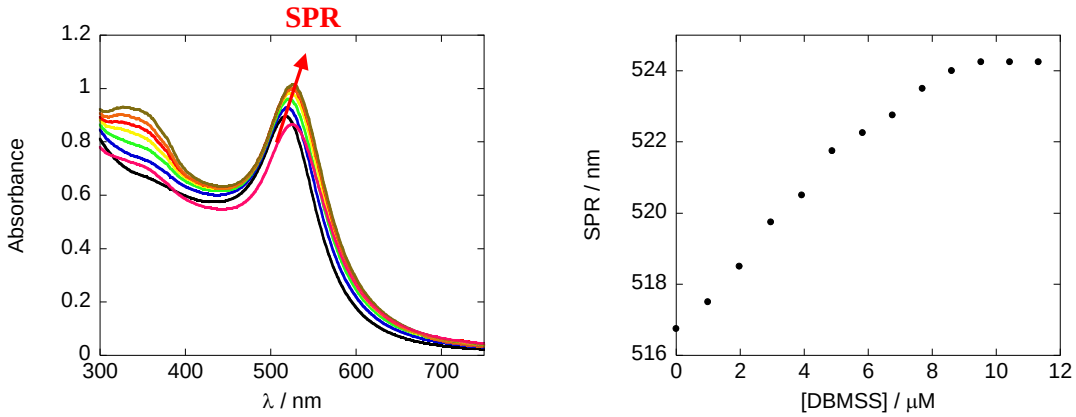

Figure 4.5.6.

Change in SPR wavelength of ***Z@Au*** *(3.2 nM in water, 2* mL*) as a methanolic solution of* ***DBMSS*** *(0.2 mM, 10 μL aliquots in MeOH) is titrated in to a final concentration of 11.32 μM (120 μL). The pink curve is post chromatography.*

A positive shift in the SPR wavelength of the AuNP is observed as the surface is functionalised with **DBMSS** which reaches saturation point at 524 nm showing an overall SPR wavelength shift of 7 nm with respect to **Z@Au**. This SPR wavelength is the same post chromatography hence the particles are not destabilised during the purification process. The SPR wavelength of the particles are not widened with the fluorinated surfactant present hence the particles are stabilised whilst functionalised with **DBMSS** and the use of Zonyl® FSA was successful in stabilising the particles. The growing band observed at 350 nm is from the absorption by the aryl β-diketone unit from **DBMSS** which appears less intense post purification as a result of the excess **DBMSS** being removed. The concentration at which saturation point is reached suggests *ca*. 2000 **DBMSS** units per particle, although the error associated with this measurement *via* UV Vis spectroscopy data is large.

Post chromatography the particles were examined with DLS (Table 4.5.2.). Particle size and morphology was determined with TEM (Figure 4.5.7.).

Table 4.5.2.

*DLS characterisation data for **DBMSS.Z@Au** after Sephadex G15.*

Intensity distribution / nm	**Number distribution / nm**	**PDI**
24 ± 4	15 ± 4	0.2

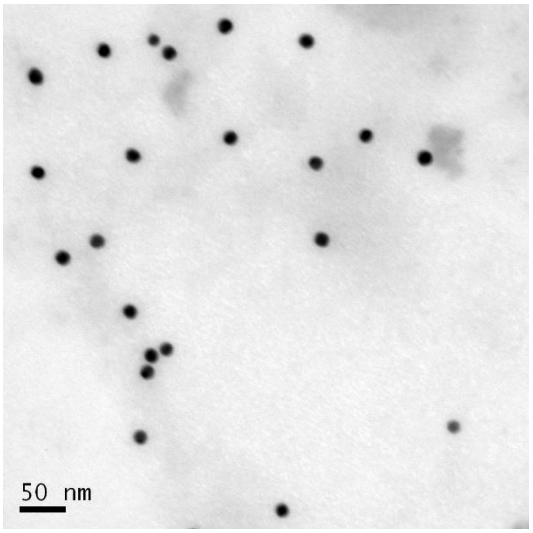

Figure 4.5.7.

TEM image of ***DBMSS.Z@Au*** *after Sephadex G15.*

DLS sizing suggests that the particles are *ca.* 15 nm which is in agreement with the TEM data which show that the **DBMSS** functionalised AuNPs are *ca.* 15 nm and of a spherical morphology.

4.6 Loading of lanthanides into DBMSS functionalised AuNPs

DBMSS functionalised AuNPs, were able to show the binding and sensitization of Eu(III) ions. An aqueous solution of $EuCl_3.6H_2O$ was titrated into **DBMSS.Z@Au**, in the presence of TEA, in the preparation of **Eu.DBMSS.Z@Au** (Figure 4.6.1.).

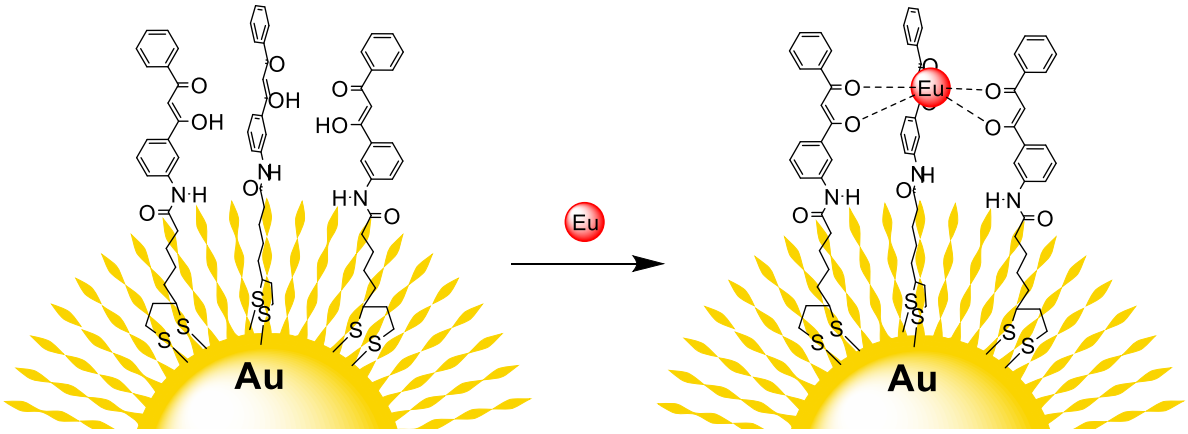

Figure 4.6.1.

Preparation of ***Eu.DBMSS.Z@Au*** *from* ***DBMSS.Z@Au***

The process was monitored *via* emission spectroscopy whereby as the Eu(III) ion binds to **DBMSS.Z@Au**, sensitized emission from the aryl β-diketone unit was observed (Figure 4.6.2.). Indeed, after the coordination of Eu(III) the excitation spectrum shows how the emissive Eu(III) state can be populated and confirms that sensitized emission of the Eu(III) ion as a result of the **DBMSS** unit is active (Figure 4.6.2.).

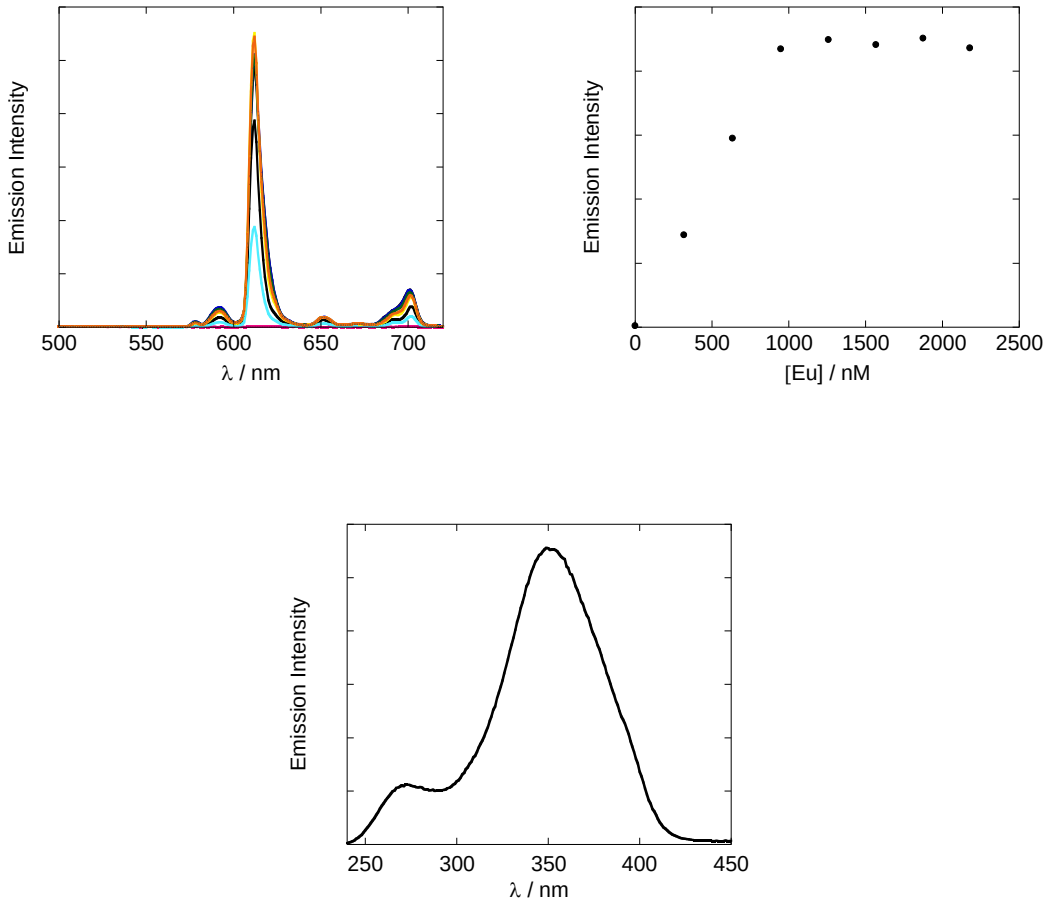

Figure 4.6.2.

Top left: Emission titration of $EuCl_3.6H_2O$ (0.08 mM, 2 µL aliquots) into a solution of ***DBMSS.Z@Au*** *(2.7 nM in water) with 0.05% TEA to a final concentration of 2.18 µM of $EuCl_3.6H_2O$ (14 µL), λ_{exc} = 350 nm, Emission spectra corrected for PMT response; Top right: Growth of Eu(III) emission peak as integrated between limits of 607 and 621 nm; Bottom, Excitation spectrum of* ***DBMSS.Z@Au*** *after final addition of $EuCl_3.6H_2O$, monitoring the emission at 614 nm.*

The incubation of Eu(III) in **DBMSS.Z@Au** shows an increase in the characteristic Eu(III) luminescence signal, which shows a plateau at *ca.* 950 nM as the particles binding sites for Eu(III) are all occupied and no further Eu sensitization is observed. Control experiments of incubating Eu(III) with **Z@Au** showed no luminescence hence the optical signal observed can be attributed to the **DBMSS** unit on the surface of the AuNP. This would suggest a binding of *ca.* 350 Eu ions per particle, although there is a large error associated with this estimation. The previous estimation of *ca.* 2000 **DBMSS** units per particle would suggest that some of the **DBMSS** units on the AuNP are unoccupied given that the ratio of **DBMSS** : Eu(III) is 3 : 1. With this approximation, it can be estimated that around half the binding sites on the Au surface are not filled. The excitation spectrum shows that the emissive Eu(III) state can be populated up to *ca.* 380 nm and confirms that sensitized emission of the Eu(III) ion as a result of the **DBMSS** unit is active. This is an improvement on the previously presented quinoline sensitized luminescent AuNPs of **EuQS@Au** and **EuQuinSAc@Au**, as the particles can be excited at a much less harsh wavelength, and the initial absorption from the ligand is much larger with respect to their molar absorptivity values. The lifetime of **DBMSS.Z@Au** in the presence of Eu(III), in water was found to be biexponential showing a 30 μs (30%) and 130 μs (70%) (χ^2 = 1.0). Whilst this is shorter than that observed for **EuQS@Au** complexes, the **Eu.DBMSS.Z@Au** type particles can still be used in time resolved luminescence type applications such as acting as a FRET donor.

The **DBMSS.Z@Au** particles were found not to show any destabilisation from the Ln(III) ion during the binding process as monitored *via* UV Vis spectroscopy (Figure 4.6.4.) and DLS (Table 4.6.1.). The TEM image of **Eu.DBMSS.Z@Au** (Figure 4.6.5.) also shows that there is no change in the size or morphology of the AuNPs when functionalised with Eu ions.

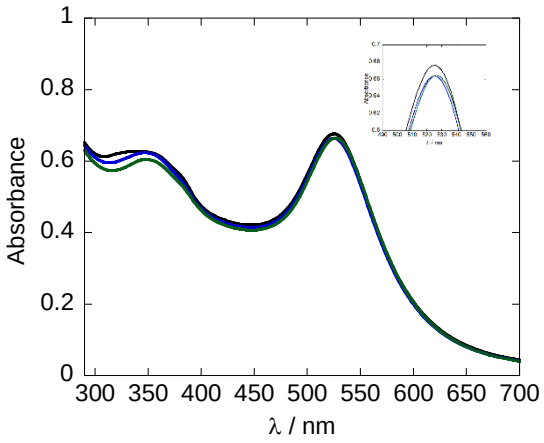

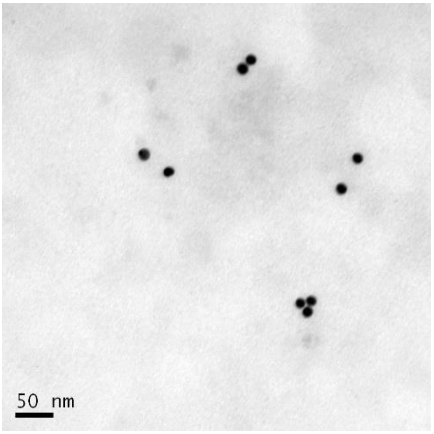

Figures 4.6.4. (Left) and 4.6.5. (Right)

Left, Change in SPR wavelength as ***DBMSS.Z@Au*** *(2.7 nM in water) is incubated with TEA (0.05%), blue curve, followed by addition of* $EuCl_3.6H_2O$ *(0.08 mM, 40 µL)1.7 µM, green curve; Right, TEM image of* ***Eu.DBMSS.Z@Au****.*

Table 4.6.1.

DLS characterisation data for ***Eu.DBMSS.Z@Au.***

Intensity distribution / nm	**Number distribution / nm**	**PDI**
18 ± 3	15 ± 3	0.3

4.7 Concluding remarks

The preparation and characterisation of a novel substituted DBM ligand with a thioctic acid group has been reported. This ligand was found to form a 3 : 1 complex with Eu(III) and the energy level of the T_1 state showed efficient excitation of the Eu(III) excited state and show *f-f* emission. **DBMSS** was deposited on the surface of surfactant modified AuNPs and retains its luminescence, showing excitation up to *ca*. 380 nm on the surface of the AuNP when coordinated to Eu(III).

The **DBMSS** system rivals the previously reported Eu coated AuNPs as the ligand shows a much stronger absorption of light at 350 nm (ε = 19900 M^{-1} cm^{-1}) and three ligands coordinate to the central metal ion in comparison to **EuQSH** with absorption at 320 nm (ε = 3000 M^{-1} cm^{-1}) and **EuQuinSAc** at 321 nm (ε = 9000 M^{-1} cm^{-1}). The τ of **Eu.DBMSS.Z@Au** in aqueous solvent is lower than that of **EuQS@Au** showing biexponential behaviour with a long component of 130 µs, in comparison to a single component of 580 µs observed for **EuQS@Au**, resulting from quenching oscillations from the solvent whereby four quenching oscillators are present for the **DBMSS** system in comparison to one for **EuQSH**. Despite this lower τ, **Eu.DBMSS.Z@Au** continues to show the long lived Ln τ to act as a FRET donor.

It is envisaged that **Eu.DBMSS.Z@Au** will be able to be dual loaded onto AuNP with LC antibodies and used in a FRET assay as previously described (Section 2.9), again using **BUCIS04-AF647** as a suitable FRET acceptor of Eu(III) emission at 614 nm. The necessity for **Cit@Au** to be modified with Zonyl® FSA may alter how the biomolecule interacts with the LC antibody meaning different conjugation methods may need to be explored.

As well as use as a FRET donor, the strong luminescence observed from **Eu.DBMSS.Z@Au**, and the 4 coordinated water molecules into the **DBMSS** system paves the way for a possible dual contrast imaging agent with Eu(III) showing luminescence and Gd(III) increasing the relaxation rate of coordinated water molecules.

4.8 Referenced material

1 L. Prodi, E. Rampazzo, F. Rastrelli, A. Speghini and N. Zaccheroni, *Chem. Soc. Rev.*, 2015, **44**, 4922 – 4952.

2 L. C. Ong, L. Y. Ang, S. Alonso and Y. Zhang. *Biomaterials*, 2014, **35**, 2987 – 2989.

3 Y. Chien, Y. Chou, S. Wang, S. Hung, M. Liau, Y. Chao, C. Su and C. Yeh, ACS Nano., 2013, **7**, 8516 – 8528.

4 F. Oltolina, L. Gregoletto, D. Colangelo, J. Gómez-Morales, J. M. Delgado-López and M. Prat *Langmuir*, 2015, **31**, 1766 – 1775.

5 J. Zhang, Y. Fu, C. V. Conroy, Z. Tang, G. Li, R. Y. Zhao and G. Wang, *J. Phys. Chem. C*, 2012, **116**, 26561 – 26569.

6 R. Zhang, Z. Ye, Y. Yin, G. Wang, D. Jin, J. Yuan and J. A. Piper, *Bioconj. Chem.*, 2012, **23**, 725 – 733.

7 Y. Liu, P. Zhang, X. Fang, G. Wu, S. Chen, Z. Zhang, H. Chao, W. Tanc and L. Xu, *Dalton Trans.*, 2017, **46**, 4777 – 4785.

8 C. Y. Chow, S. V. Eliseeva, E. R. Trivedi, T. N. Nguyen, J. W. Kampf, S. Petoud and V. L. Pecoraro *J. Am. Chem. Soc.*, 2016, **138**, 5100 – 5109.

9 D. Kovacs, X. Lu, L. S. Mészáros, M. Ott, J. Andres and K. E. Borbas, *J. Am. Chem. Soc.*, 2017, **139**, 5756 – 5767.

10 W. D. Horrocks and J. P. Sipe, *J. Am. Chem. Soc.*, 1971, **93**, 6800 – 6804.

11 R. E. Sievers and R. E. Rondeau, *J. Am. Chem. Soc.*, 1971, **93**, 1522 – 1524.

12 H. Jang, C. Shin, B. Jung, D. Kim, H. Shim and Y. Do, *Eur. J. Inorg. Chem.*, 2006, 718 – 725.

13 Y. Zheng, L. Fu, Y. Zhou, J. Yu, Y. Yu, S. Wang and H. Zhang *J. Mater. Chem.*, 2002, **12**, 919 – 923.

14 H. Tsukube and S. Shinoda, *Chem. Rev.*, 2002, **102**, 2389 – 2403.

15 R. V. Deun, D. Moors, B. D. Fréa and K. Binnemans, *J. Mater. Chem.*, 2003, **13**, 1520 – 1522.

16 D. Zhou, C. Huang, G. Yao, J. Bai and T. Li, *J. Alloys Compd.*, 1996, **235**, 156 – 162.

17 S. I. Weissman, *J. Chem. Phys.*, 1942, **10**, 214 – 217.

18 Y. Jinghe, R. Xuezhen, Z. Huabin and S. Ruiping, *Analyst*, 1990, **115**, 1505 – 1508.

19 L. Sun, Z. Wang, J. Z. Zhang, J. Feng, J. Liu, Yin Zhao and Liyi Shi, *RSC Adv.*, 2014, **4**, 28481 – 28489.

20 A. P. Bassett, S. W. Magennis, P. B. Glover, D. J. Lewis, N. Spencer, S. Parsons, R. M. Williams, L. D. Cola, and Z. Pikramenou, *J. Am. Chem. Soc.*, 2004, **126**, 9413 – 9424.

21 C. Malba, U. P. Sudhakaran, S. Borsacchi, M. Geppi, F. Enrichi, M. M. Natile, L. Armelao, T. Finotto, R. Marin, P. Rielloa and A. Benedetti, *Dalton Trans.*, 2014, **43**, 16183 – 16196.

22 A. K. Singh, S. K. Singh, H. Mishra, R. Prakas, and S. B. Rai, *J. Phys. Chem. B*, 2010, **114**, 13042 – 13051.

23 A. I. S. Silva, V. F. C. Santos, N. B. D. Lima, Al. M. Simas and S. M. C. Gonçalves, *RSC Adv.*, 2016, **6**, 90934 – 90943.

24 L. Lin, H. Tang, Y. Wang, X. Wang, X. Fang and L. Ma, *Inorg. Chem.*, 2017, **56**, 3889 – 3900.

25 A. Gulino, F. Lupo, G. G. Condorelli, A. Motta and I. L. Fragalà, *J. Mater. Chem.*, 2009, **19**, 3507–3511.

26 L. Armelao, D. B. Dell'Amico, L. Bellucci, G. Bottaro, L. Labella, F. Marchetti and S. Samaritani., *Inorg. Chem.*, 2016, **55**, 939 – 947.

27 S. J. Adams, D. J. Lewis, J. A. Preece and Z. Pikramenou, *ACS Appl. Mater. Interfaces*, 2014, **6**, 11598 – 11608.

28 J. Hubaud, I. Bombarda, L. Decome, J. Wallet and E. M. Gaydou, *J. Photochem. and Photobiol. B: Biol.*, 2008, **92**, 103 – 109.

29 A. C. Savage and Z. Pikramenou, *Chem. Commun.*, 2011, **47**, 6431 – 6433.

30 P. Nativo, I. A. Prior and M. Brust, *ACS Nano*, 2008, **2**, 1639 – 1644.

31 H. Yuan, A. M. Fales and T. Vo-Dinh, *J. Am. Chem. Soc.*, 2012, **134**, 11358 – 11361.

32 S. A. M. Osborne and Z. Pikramenou, *Farad. Discuss.*, 2015, **185**, 219 – 231.

33 N. J. Rogers, S. Claire, R. M. Harris, S. Farabi, G. Zikeli, I. B. Styles, N. J. Hodges and Z. Pikramenou, *Chem. Commun.*, 2014, **50**, 617 – 619.

5 Conclusions and further work

5.1 Thesis Conclusions

This thesis has shown how AuNPs can be capped with luminescent Eu(III) complexes to produce AuNPs which show the characteristic Eu(III) luminescence with a long lived excited state lifetime and this was shown for two Eu(III) complexes based on DTPA derivatives. These were grafted onto the surface of AuNPs alongside LC material to continue to show Eu(III) luminescence.

On addition of anti-κFLC mAb, **BUCIS04** which was conjugated to a suitable FRET acceptor for Eu(III) **AF647**, it was possible to observe FRET between **κLC.EuQS@Au** and **BUCIS04-AF647** as measured *via* excited state lifetime measurements, whilst maintaining particle stability. This FRET signal was found to be low and between 10 – 15% of the energy was found to have been transferred when the **BUCIS04-AF647** was incubated with **κLC.EuQS@Au** at 100 nM and 2.7 nM respectively. Indeed, it was also found that the inclusion of the gold surface leads to problems associated with NSB of biomolecules with the AuNP as seen *via* a FRET quench between **EuQS@Au** and **BUCIS04-AF647** as measured *via* excited state lifetime measurements. To block out this unwanted interaction, various different blocking agents were incubated with **EuQS@Au** prior to the addition of **BUCIS04-AF647**. Blocking agents based on detergent species were found to have no affect on the NSB although both non-reactive proteins BSA and FCS, both at 1%, showed a slight improvement of the signal by resisting a drop in the excited state lifetime of **EuQS@Au** at 2.7 nM when **BUCIS04-AF647** was added at 100 nM, although this NSB was not completely removed from the system.

It was able to be shown that competitive binding can be seen between κnew and **κnew.EuQS@Au** when **BUCIS04-AF647** was mixed with κnew at 45 µM, to use up the binding sites on **BUCIS04-AF647,** before incubation with **κnew.EuQS@Au**, although the NSB is still an issue in this system.

5.2 Further Work

Although **EuQuinSAc** and **EuQSH** both show Eu(III) luminescence and can be grafted onto the surface of the AuNP, the use of the quinoline sensitizing unit is not ideal. Indeed, excitation of the molecules at 320 and 315 nm respectively give molar absorptivity's of less than 10000 in each case. To improve on these, **DBMSS** was developed which shows a λ_{max} of 350 nm (ε = 19900 M^{-1} cm^{-1}) to which three of these bind an Eu(III) ion. Despite **Eu.DBMSS.Z@Au** requiring the use of a surfactant species and the excited state lifetime of **Eu.DBMSS.Z@Au** being lower that **EuQS@Au**, it would be advantageous to develop similar ligands to **DBMSS** (Figure 5.2.1.).. Examples of such are the fluorinated analogue of **DBMSS** to remove quenching C-H oscillations, or a ligand incorporating two binding sites which would, in theory, show enhanced luminescence due to more luminescent material.

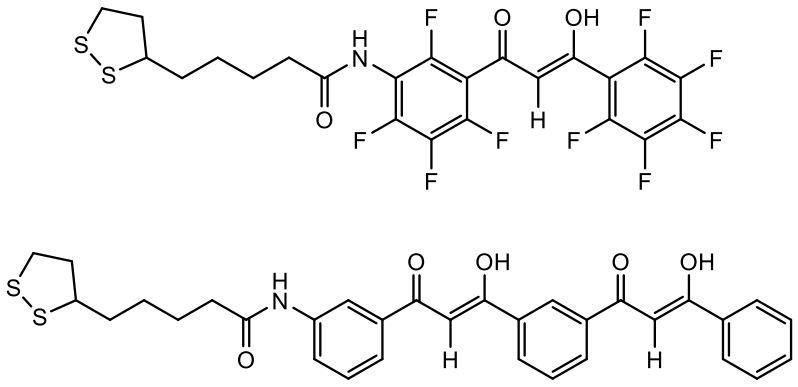

Figure 5.2.1.

*Potential new synthetic targets further to **DBMSS***

The quenching nature of water molecules to **Eu.DBMSS.Z@Au,** could be turned into an advantage with the incorporation of Gd(III) into these sites for MRI applications, and leads the way to a potential dual mode imaging agent with Gd(III) for MRI and Eu(III) for luminescence using nanotechnology.

The inclusion of **DBMSS** over **EuQSH** in the AuNP FRET assay would be an advantageous step due to the favoured properties of the **DBMSS** over **EuQSH**, although the biexponential excited state lifetime of **Eu.DBMSS.Z@Au** could potentially prove problematic.

The initial FRET signal from the incubation of **κLC.EuQS@Au** and **BUCIS04-AF647** at 2.7 nM and 100 nM respectively leads to a quench of between 10 – 15% whilst maintaining particle stability. This figure is low in comparison to many systems in the literature, which can be as high as 80% energy transfer. To improve on this figure would be advantageous to achieve the maximum FRET quench possible. Indeed, the concentration of **κLC.EuQS@Au** at 2.7 nM is difficult experimentally to change with higher concentrations causing issues with particle stability and lower concentrations causing issues with a lower optical signal. The incubation of larger concentrations of **BUCIS04-AF647** with **κLC.EuQS@Au** leads to a larger FRET signal being observed, although nanoparticle aggregation is also observed. In terms of the NSB observed in the system, it was possible to eliminate this partially with the addition of non-reactive proteins BSA and FCS, both at 1%, although particle stability is not maintained above these concentrations, which may indeed fully eliminate any NSB.

The stability of AuNPs can be improved upon with the functionalisation of the AuNP with polymers or surfactants, which was seen with a change in the zeta potential of **Cit@Au** – 30 mV to – 50 mV on functionalisation with a fluorinated polymer Zonyl® FSA (Section 4.5.). Indeed, the incorporation of a nanoparticle stabilising unit into the system, prior to functionalisation with Eu complex and LC, may allow for larger concentrations of biomolecule to be incubated with the particles. Indeed, this would be a large advantage to the system as more **BUCIS04-AF647** could be incubated with **κLC.EuQS@Au**, possibly showing a much larger FRET signal, and indeed, a larger protein blocking agent may also be achieved, further inhibiting NSB. The addition of a stabilising unit to the system could cause potential problems relating to the binding of the LC to the AuNP, given that a lot of polymers and surfactants have also been used to block biomolecule to surface interactions and it may be necessary to explore other AuNP to biomolecule coupling methodologies such as click chemistry, or amide coupling as previously discussed (Section 2.1.).

Whilst the gold particle has clear advantages of aqueous solubility, easy functionalisation and inert, non-toxic nature, this system is not limited to AuNPs. The use of other nanomaterials would be a very interesting comparison from how the AuNP system works in comparison to a silica or polymeric nanoparticle, which may allow for different NSB properties. Indeed, the size of the AuNP is not a limitation and the comparison of 12 nm AuNP with 100 nm AuNP could be very interesting.

6 General Experimental

6.1 General Experimental

General use of reagents

All glassware was cleaned with deionised water and acetone and oven dried prior to use.

All chemical starting materials and solvents were obtained from Sigma Aldrich UK, Fischer or Fluka and used as supplied unless otherwise stated.

Antibody and Light chain samples were supplied by Serascience.

NMR spectroscopy, FT-IR, mass spectrometry and HPLC

^{1}H NMR data was obtained on a Brüker AVIII300 at 300 or 400 MHz as stated whilst ^{13}C NMR and 2D NMR data were obtained on a Brüker AVIII400 NMR spectrometer at 101 MHz. Details of each scan are found in the appendix. Deuterated NMR solvents were used as supplied and the data was processed offline on MestReNova whereby the data was referenced to the appropriate residual peak solvent.

MS data was obtained using a micro mass liquid chromatography - TOF using the electrospray positive mode unless otherwise stated.

IR spectra were collected on a PerkinElmer Spectrum 100 FT-IR Spectrometer using an ATR attachment and processed using PerkinElmer software.

HPLC was carried out on a Dionex summit system, using a Summit P580 quaternary low pressure gradient pump. The detector was a Summit UVD 170s UV VIS multi-channel detector with a prep flow cell for semi-prep HPLC. The column used was a preparative C_{18} column with a particle size of 10 μM.

UV Vis spectroscopy

UV Vis data was obtained either on a Varian Cary 5000 or a Varian Cary 50 spectrometer at a scan rate of 300 nm / min, with a baseline correction for the appropriate solvent system. Quartz cuvettes with a 1 cm path length were used throughout.

Extinction coefficients were calculated (Equation 6.1.) with respect to the absorbance and concentration of the sample.

$$\varepsilon = \frac{A}{cl}$$

Equation 6.1.

ε, extinction coefficient; c, concentration; A, absorbance; l, path length.

The SPR wavelength of AuNPs were worked out as according to a FWHM of the curve at the point where it resembles a parabola (Figure 6.1. and Equation 6.2.).

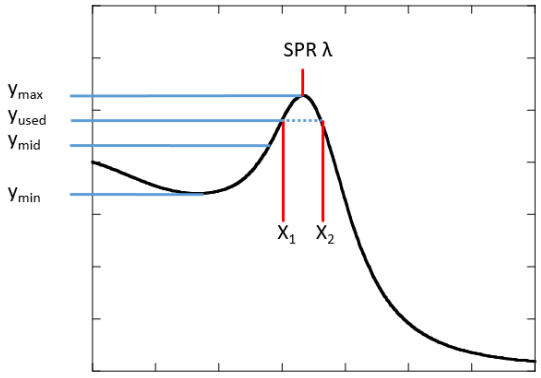

$$y_{used} = y_{max} - \left(\frac{y_{max} - y_{min}}{4}\right) \qquad x_{max} = \left(\frac{x_1 + x_2}{2}\right)$$

Figure 6.1. and Equation 6.2.

FWHM determination of AuNP SPR peak wavelength

Emission spectroscopy

Emission and excitation data was obtained on an Edinburgh Instruments FLSP920 steady state, fluorescence and phosphorescence lifetime spectrometer using a 450 W xenon arc lamp as the excitation source and Hamamatsu R928 PMT as the detection source. Appropriate cut off filters were used throughout and all data was corrected with respect to the appropriate correction file of the Hamamatsu R928 PMT and F900 software was used to record the data.

Emission quantum yield data was obtained on the spectrometer as described above with use of an integrating sphere. Quartz cuvettes with four clear faces of 1 cm^2 were used and the data processed with the F900 software.

Ln excited state lifetime measurements were carried out with the detection source as described above, using a microsecond flashlamp as the excitation source. F900 software was used to record the data and the data was analysed using the F900 software using the tail fit option and fitted to a monoexponential decay curve unless otherwise stated. All data was plotted to a χ^2 value of between 0.9 and 1.3.

NP characterisation

DLS and Zeta potential data were collected on a Malvern Zetasizer NanoZS and the data processed using the Malvern Zetasizer software.

TEM samples were imaged using Jeol 1200EX TEM and Gatan multiscan camera. Samples were air-dried onto 200 mesh formvar coated copper and images were acquired using DigitalMicrograph 1.8.

ICPMS measurments were performed on a 7500cx ICPMS at the university of Warwick. In all cases the metal concentration was determined with PlasmaCal calibration standards and the colloidal sample was dissolved in ultrapure Aqua Regia.

Synthesis of Cit@Au

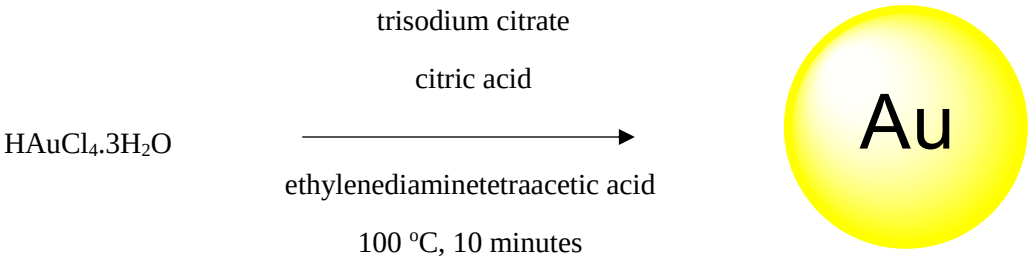

All glassware was cleaned with aqua regia (HCl : HNO_3, (3 : 1)), washed with copious amounts of deionised water and oven dried at 120 °C prior to use.

A solution of trisodium citrate dihydrate (60.6 mg, 289 μmol), citric acid monohydrate (13.3 mg, 66.5 μmol) and tetrasodium ethylenediaminetetraacetic acid monohydrate (1.0 mg, 2.25 μmol) were dissolved in deinised water (100 mL) and bought to reflux at 150 °C with rapid stirring in a round bottomed flask to create a vortex. A separate solution of chloroauric acid trihydate (8.0 mg, 20.3 μmol) in deionised water (25 mL) was prepared and heated in an oven to *ca.* 80 °C, before being added quickly to the round bottomed flask. The resulting solution was then refluxed for a further ten minutes to bring out a characteristic deep red solution and then was allowed to cool to room temperature over a period of one hour yielding **Cit@Au** at 1.6 nM.

λ_{max} SPR / nm	**Number distribution / nm**	**Intensity distribution / nm**	**PDI**
516	12 ± 3	18 ± 3	0.1

6.2 Chapter 2

Synthesis of tert-butyl (8-hydroxyquinolin-5-yl)carbamate (2)

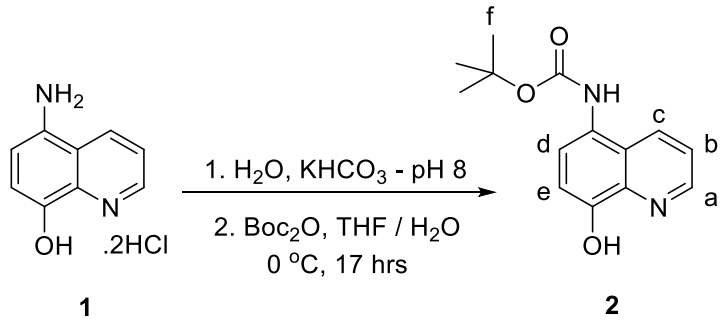

1 **2**

To a stirring solution of **1** (2.00 g, 8.58 mmol, 1.00 eq.) in water (40 mL), $KHCO_3$ (1.20 g, 12 mmol, 1.40 eq.) was added to raise the pH of the solution to 8. THF (50 mL) and water (10 mL) were added and the resulting solution left to stir under N_2 at RT for 1 hour. After this time a solution of di-tertiary butyl bicarbonate (1.96 g, 8.99 mmol, 1.05 eq.) in THF : water (1 : 1 by volume, 10 mL) was added dropwise over 30 minutes under an N_2 atmosphere. The resulting solution was then left stirring under N_2 at 0 °C which was allowed to warm to RT over 17 hours. The THF was then removed *in vacuo* and the organic material extracted with DCM (1 x 400 mL). The organic layer was then dried over anhydrous Na_2SO_4 (*ca.* 10 g), filtered, and the solvent removed *in vacuo* to give **2** as a brown solid (1.71 g, 6.58 mmol, 77%). ^{1}H NMR (300 MHz, $CDCl_3$) δ_H ppm: 8.79 (1H, dd, J = 4.2, 1.4, H_a), 8.26 (1H, dd, J = 8.6, 1.4, H_c), 7.52 (1H, br, H_d), 7.49 (1H, dd, J = 8.6, 4.2, H_b), 7.14 (1H, d, J = 8.2, H_e), 6.44 (1H, br, *NH*), 1.52 (9H, s, H_f). ^{13}C{^{1}H} PENDANT NMR (101 MHz, $CDCl_3$) δ_C ppm: 154.6 (NH<u>C</u>OC), 150.6 (Ar<u>C</u>), 148.0 (Ar<u>C</u>H), 138.3 (Ar<u>C</u>), 131.5 (Ar<u>C</u>H), 124.2 (Ar<u>C</u>H), 124.0 (Ar<u>C</u>), 121.9 (Ar<u>C</u>H), 109.4 (Ar<u>C</u>H), 80.8 (O<u>C</u>(Me)$_3$), 28.5 (OC(<u>C</u>H$_3$)$_3$). MS (ES-TOF)$^+$ *m/z*: 261.1 $[M + H]^+$. Characterisation data were in agreement with the literature.[1]

Synthesis of S-(6-bromohexyl) ethanethioate (4)

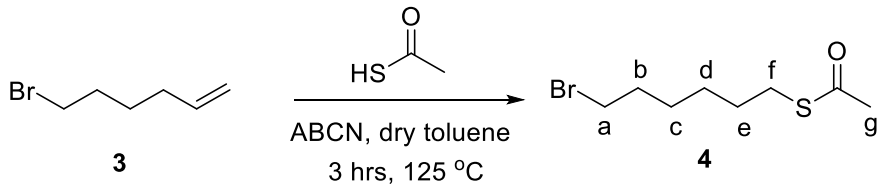

To a stirring solution of **3** (2.00 g, 12.35 mmol, 1.00 eq.) in dry toluene (15 mL), thioacetic acid (1.86 g, 24.47 mmol, 1.98 eq.) was added followed by a catalytic amount of ABCN (*ca.* 0.025 g) and the solution left to reflux at 125 °C under N_2 for 3 hours. After this time, the mixture was cooled to RT and a solution of $NaHCO_3$ (1 M, 60 mL) was added and the organic material was extracted with EtOAc (120 mL) and washed with $NaHCO_3$ (1 M, 60 mL). The organic material was then dried with anhydrous Na_2SO_4 (*ca.* 10 g), filtered, and the solvent removed *in vacuo* to yield **4** as a yellow oil (2.70 g, 11.34 mmol, 92%). ^{1}H NMR (300 MHz, $CDCl_3$) δ_H ppm: 3.40 (2H, t, J = 6.8, H_a), 2.86 (2H, t, J = 7.5, H_f), 2.32 (3H, s, H_g), 1.85 (2H, p, J = 6.8, H_b) 1.59 (2H, p, J = 7.5, H_e), 1.42 (4H, m, H_c, H_d). ^{13}C{^{1}H} NMR (101 MHz, $CDCl_3$) δ_C ppm: 196.0 (S<u>C</u>OMe), 33.8 (Br<u>C</u>$H_2$$CH_2$), 32.7 ($BrCH_2$<u>C</u>$H_2$), 30.7 (CO<u>C</u>$H_3$), 29.4 ($CH_2$<u>C</u>$H_2$S), 29.0 ($CH_2$<u>C</u>$H_2CH_2$), 28.0 ($CH_2$<u>C</u>$H_2CH_2$), 27.7 ($CH_2$<u>C</u>$H_2CH_2$). MS (ES-TOF)$^+$ *m/z*: 239.1 [M (^{79}Br)]$^+$. 241.1 [M (^{81}Br)]$^+$. Characterisation data were in agreement with the literature.[2,3]

Synthesis of S-(6-((5-((tert-butoxycarbonyl)amino)quinolin-8-yl)oxy)hexyl) ethanethioate (5)

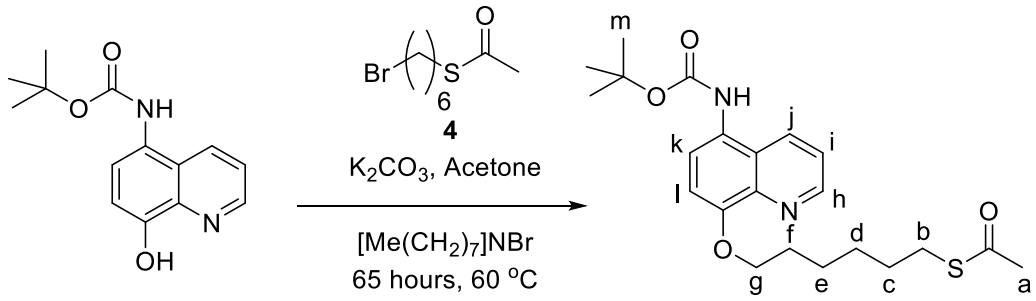

2 **5**

Compound **2** (1.00 g, 3.85 mmol, 1.00 eq.) was dissolved in acetone (45 mL), K_2CO_3 (1.53 g, 11.09 mmol, 2.88 eq.) and a catalytic amount of tetraoctylammonium bromide (*ca.* 0.025 g) were added. The solution was stirred under N_2 at 55 °C for 30 minutes after which time a solution of **4** (1.1 g, 4.62 mmol, 1.20 eq.) in acetone (15 mL) was added and the solution was stirred at 60 °C for 72 hours under N_2. The reaction mixture was then cooled to RT and the solvent removed *in vacuo* whereupon DCM (100 mL) and water (50 mL) were added. The organic material was extracted and washed with water (20 mL) and brine (20 mL), dried over anhydrous Na_2SO_4 (*ca.* 10 g), filtered and the solvent removed *in vacuo* to give a brown oil which was purified *via* column chromatography on silica (EtOAc : Hexane; 60 : 40) to yield **5** as a yellow oil (0.56 g, 1.34 mmol, 35%). ^{1}H NMR (300 MHz, $CDCl_3$) δ_H ppm: 8.93 (1H, dd, J = 4.2, 1.5, H_h), 8.22 (1H, dd, J = 8.5, 1.5, H_j), 7.54 (1H, br, H_k), 7.42 (1H, dd, J = 8.5, 4.2, H_i), 6.97 (1H, d, J = 8.5, H_l), 6.67 (1H, br, *NH*), 4.17 (2H, t, J = 7.0, H_g), 2.85 (2H, t, J = 7.2, H_b), 2.29 (3H, s, H_a), 1.95 (2H, p, J = 7.6, H_f), 1.65 – 1.35 (15H, m, H_c, H_d, H_e, H_m). ^{13}C{^{1}H} NMR (101 MHz, $CDCl_3$) δ_C ppm: 196.0 (S<u>C</u>OMe), 154.5 (NH<u>C</u>OO), 153.0 (Ar<u>C</u>), 149.2 (Ar<u>C</u>H), 140.3 (Ar<u>C</u>), 130.8 (Ar<u>C</u>H), 125.2 (Ar<u>C</u>), 122.7 (Ar<u>C</u>H), 121.5 (Ar<u>C</u>H), 121.5 (Ar<u>C</u>), 108.3 (Ar<u>C</u>H), 80.7(O<u>C</u>(Me)$_3$), 69.0 (O<u>C</u>H$_2$CH$_2$), 30.7 (CO<u>C</u>H$_3$), 29.5 (CH$_2$<u>C</u>H$_2$CH$_2$), 29.1 (CH$_2$<u>C</u>H$_2$CH$_2$), 28.9 (CH$_2$<u>C</u>H$_2$S), 28.7 (CH$_2$<u>C</u>H$_2$CH$_2$), 28.4 (C(<u>C</u>H$_3$)$_3$), 25.7 (CH$_2$<u>C</u>H$_2$CH$_2$). MS (ES-TOF)$^+$ *m/z*: 419.2 [M + H]$^+$. Characterisation data were in agreement with the literature.[4]

Synthesis of S-(6-((5-aminoquinolin-8-yl)oxy)hexyl) ethanethioate (6)

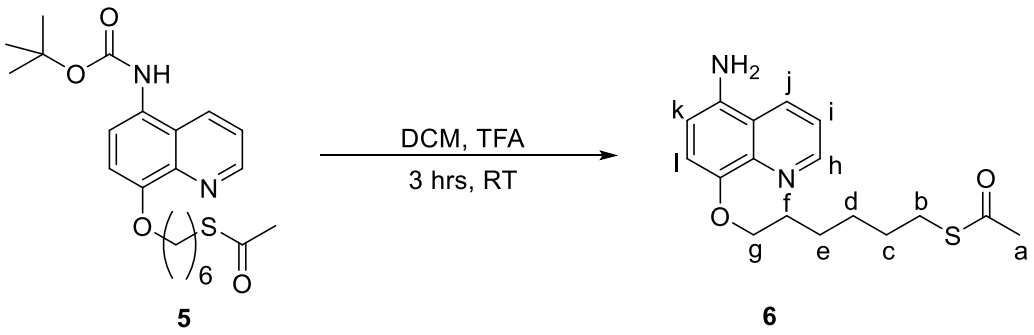

Compound **5** (0.56 g, 1.34 mmol, 1.00 eq.) was dissolved in dry DCM (23 mL) and stirred under N_2 at RT. TFA (3.40 g, 29.82 mmol, 22.25 eq.) was added over 5 minutes and the solution left to stir at RT under N_2 for 3 hours. After this time, the solvent was removed *in vacuo* whereupon DCM (100 mL) and $NaHCO_3$ (1 M, 10 mL) were added. The organic material was extracted and the aqueous material was washed with DCM (2 x 10 mL). The organic extracts were combined and dried over anhydrous Na_2SO_4 (*ca.* 10 g), filtered and the solvent removed *in vacuo* to give **6** as a red oil (0.41 g, 1.29 mmol, 97%). ^{1}H NMR (300 MHz, $CDCl_3$) δ_H ppm: 8.93 (1H, d, J = 3.8, H_h), 8.20 (1H, d, J = 8.4, H_j), 7.39 (1H, dd, J = 8.4, 3.8, H_i), 6.90 (1H, d, J = 8.2, H_l), 6.75 (1H, d, J = 8.2, H_k), 4.13 (2H, t, J = 6.9, H_g), 3.90 – 3.50 (2H, br, NH_2), 2.86 (2H, t, J = 7.2, H_b), 2.30 (3H, s, H_a), 1.95 (2H, p, J = 7.4, H_f), 1.65 – 1.35 (6H, m, H_c, H_d, H_e). ^{13}C NMR (101 MHz, $CDCl_3$) δ_C ppm: 196.1 (S<u>C</u>OMe), 149.1 (Ar<u>C</u>), 148.4 (Ar<u>C</u>), 140.6 (Ar<u>C</u>), 135.1 (Ar<u>C</u>), 130.3 (Ar<u>C</u>), 120.7 (Ar<u>C</u>), 120.3 (Ar<u>C</u>), 110.6 (Ar<u>C</u>), 110.2 (Ar<u>C</u>), 69.3 (O<u>C</u>H_2CH_2), 30.7 (CO<u>C</u>H_3), 29.5 (CH_2<u>C</u>H_2CH_2), 29.2 (CH_2<u>C</u>H_2CH_2), 29.1 (CH_2<u>C</u>H_2S), 28.7 (CH_2<u>C</u>H_2CH_2), 25.8 (CH_2<u>C</u>H_2CH_2). MS (ES-TOF)$^+$ *m/z*: 319.2 $[M + H]^+$. Characterisation data were in agreement with the literature.[4]

Synthesis of 2,2'-((((carboxymethyl)azanediyl)bis(ethane-2,1-diyl))bis((2-((8-((6-(acetylthio)hexyl)oxy)quinolin-5-yl)amino)-2-oxoethyl)azanediyl))diacetic acid (H_3QuinSAc)

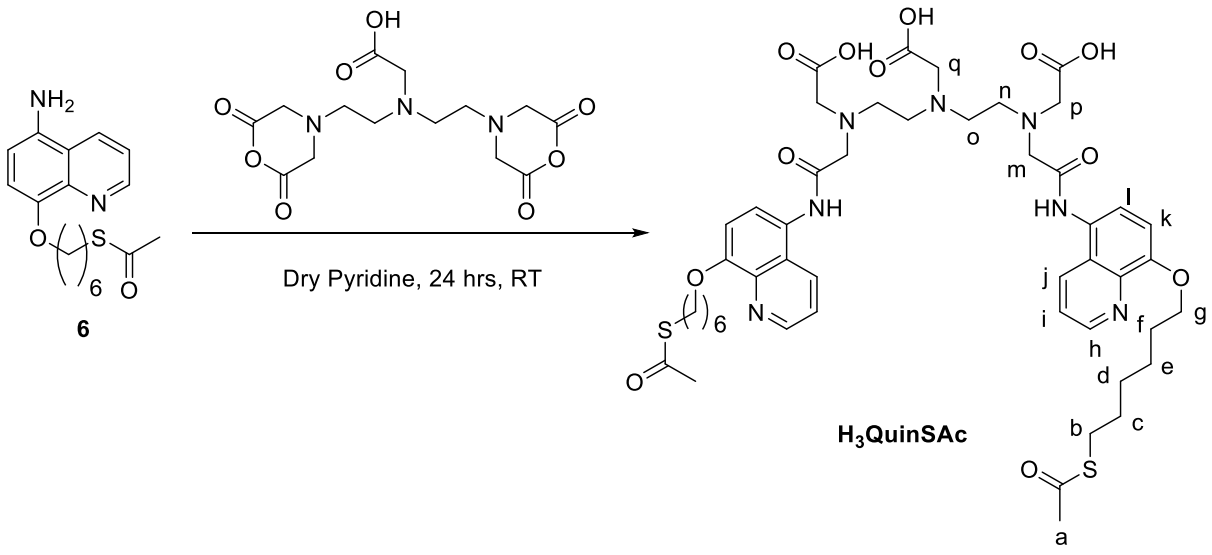

To a stirring solution of **6** (0.40 g, 1.25 mmol, 2.19 eq.) in anhydrous pyridine (25 mL), DTPA-bisanhydride (0.19 g, 0.57 mmol, 1.00 eq.) was added and the solution left to stir under N_2 for 72 hours at RT. After this time, the solvent was removed *in vacuo* and water (20 mL) was added whereupon a tarry precipitate was observed. The water was decanted off and the precipitate triturated in MeCN (20 mL) for 3 hours, filtered and washed with MeCN (10 mL) and Et_2O (10 mL) to give **H_3QuinSAc** as a light brown powder (0.30 g, 0.30 mmol, 53%). ^{1}H NMR (300 MHz, d_6-DMSO) δ_H ppm: 10.19 (2H, br, *NH*), 8.82 (2H, d, *J* = 3.8, H_h), 8.34 (2H, d, *J* = 8.4, H_j), 7.57 (2H, d, *J* = 8.2, H_l) 7.49 (2H, dd, *J* = 8.4, 3.8, H_i), 7.06 (2H, d, *J* = 8.2, H_k), 4.08 (4H, t, *J* = 6.6, H_g), 3.48 (8H, s, H_m, H_p), 3.41 (2H, s, H_q), 3.03 (4H, br, H_o), 2.92 (4H, br, H_n), 2.85 (4H, t, *J* = 7.1, H_b), 2.32 (6H, s, H_a), 1.81 (4H, t, *J* = 6.6, H_f), 1.60 – 1.35 (12H, m, H_c, H_d, H_e). ^{13}C{^{1}H} PENDANT NMR (101 MHz, d_6-DMSO) δ_C ppm: 195.7 (S<u>C</u>OMe), 173.3 (CH_2<u>C</u>OOH), 170.5 (NH<u>C</u>OCH_2), 152.3 (Ar<u>C</u>), 149.0 (Ar<u>C</u>H), 139.9 (Ar<u>C</u>), 131.6 (Ar<u>C</u>H), 125.8 (Ar<u>C</u>), 124.5 (Ar<u>C</u>), 122.6 (Ar<u>C</u>H), 121.6 (Ar<u>C</u>H), 108.9 (Ar<u>C</u>H), 68.5 (PhO<u>C</u>H_2), 58.5 (N<u>C</u>H_2CONH), 55.9 (N<u>C</u>H_2COOH), 55.5 (N<u>C</u>H_2COOH), 52.5 (N<u>C</u>H_2CH_2N), 51.9 (N<u>C</u>H_2CH_2N), 30.8 (CO<u>C</u>H_3), 29.4 (CH_2<u>C</u>H_2CH_2), 28.8 (CH_2<u>C</u>H_2CH_2), 28.6 (S<u>C</u>H_2CH_2), 28.2 (CH_2<u>C</u>H_2CH_2), 25.4 (CH_2<u>C</u>H_2CH_2). MS (ES-TOF)$^+$ *m/z*: 994.9 $[M + H]^+$, 498.0 $[M + H]^{2+}$. λ_{max} 244 nm (ε = 67000 M^{-1} cm^{-1}) and 321 nm (ε =

9000 M^{-1} cm^{-1}), mp 196 – 198 ^{O}C, ν_{max} / cm^{-1} 1688 (C=O), 2936 (C-H), 3230 (O-H). Characterisation data were in agreement with the literature.[4]

Synthesis of EuQuinSAc

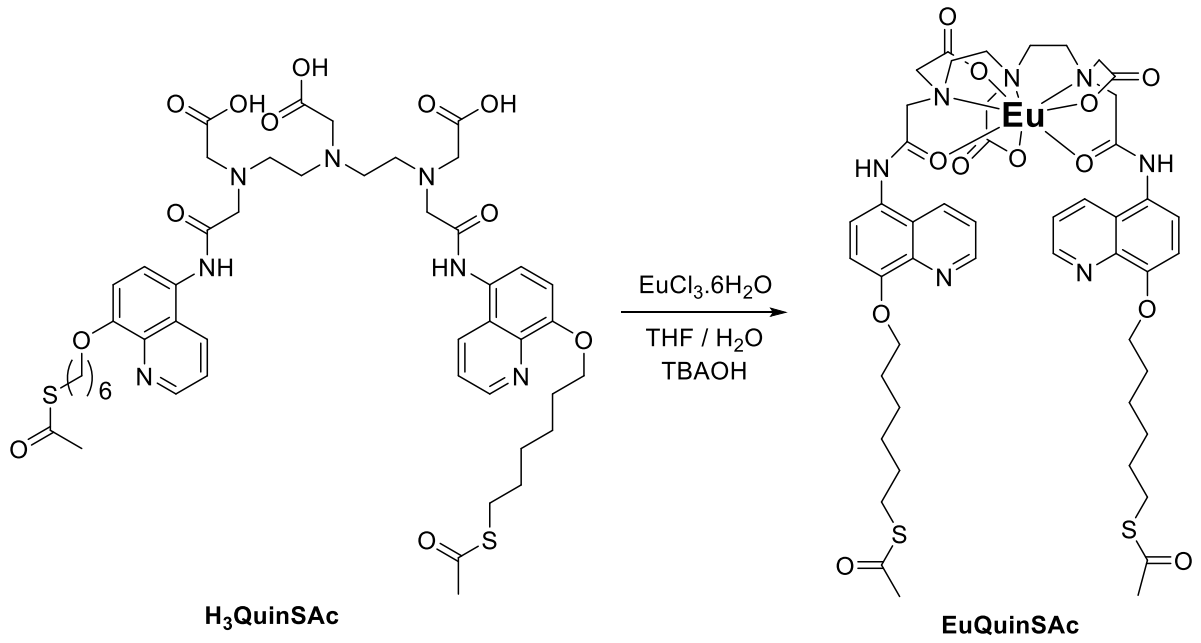

H_3QuinSAc **EuQuinSAc**

H_3QuinSAc (0.21 g, 0.21 mmol, 1.00 eq) was dissolved in THF : water (1 : 1 by volume) (20 mL) and the pH was adjusted to 6 with addition of TBAOH (40% in water). A solution of $EuCl_3.6H_2O$ (0.08 g, 0.21 mmol, 1.00 eq.) in water (4 mL) was prepared and added to the **H_3QuinSAc** solution. The vessel holding the $EuCl_3.6H_2O$ solution was washed out with water (2 x 1 mL) and this was also added to the **H_3QuinSAc** solution. The solution was left to stir for 15 minutes at RT, whereupon the THF was removed *in vacuo* and the pH was adjusted to 6 with addition of TBAOH (40% in water), which yielded a tarry precipitate. The water was decanted out and the precipitate triturated in acetone for 1 hour, filtered and further triturated with MeCN for 1 hour and filtered to give **EuQuinSAc** as a brown powder (0.17 g, 0.15 mmol, 71%). MS (ES-TOF)$^+$ *m/z*: 1144.4 [M + H (^{152}Eu)]$^+$. λ_{max} 243 nm (ε = 66000 M^{-1} cm^{-1}) and 321 nm (ε = 9000 M^{-1} cm^{-1}), mp > 300 ^oC, ν_{max} / cm^{-1} 1596 (C=O), 2933 (C-H), 3200 (N-H). Characterisation data were in agreement with the literature.

Synthesis of N-(2-((carboxymethyl)(2-((4-mercaptophenyl)amino)-2-oxoethyl)amino)ethyl)-N-(2-((carboxymethyl)(2-oxo-2-(quinolin-6-ylamino)ethyl)amino)ethyl)glycine (H_3QSH)

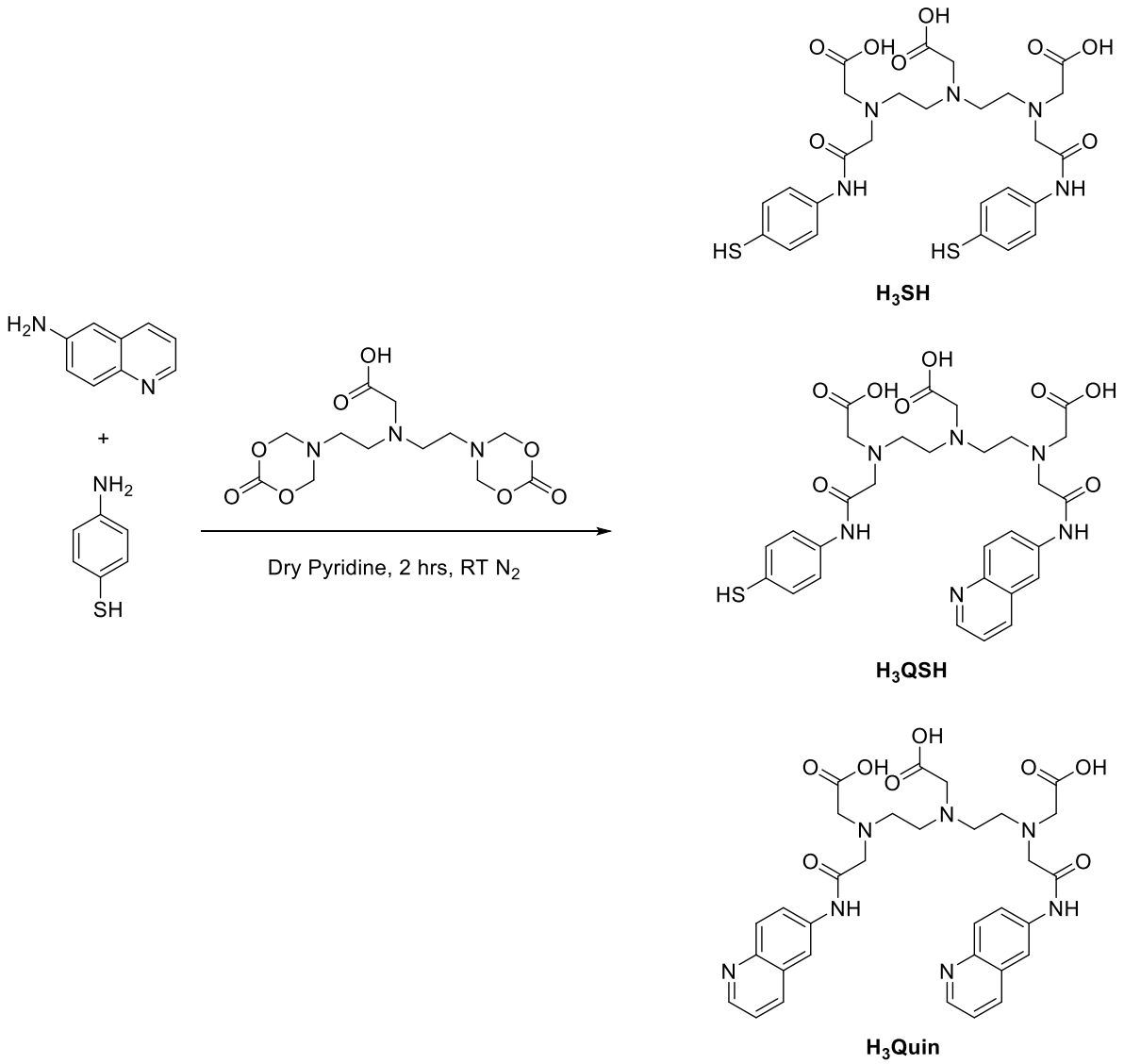

To a stirring solution of DTPA-bisanhydride (1.00 g, 3.00 mmol, 1.08 eq.) in dry pyridine (40 mL) was added 6-aminoquinoline (0.40 g, 2.78 mmol, 1.00 eq.) and the resulting solution stirred under N_2 at RT for 45 minutes. After this time 4-aminothiophenol (0.35 g, 2.80 mmol, 1.01 eq.) was added and the solution stirred at RT under an N_2 atmosphere for 2 hours. After this time, the solvent was removed *in vacuo* and the resulting yellow solid was triturated in MeCN (60 mL) for 18 hours to reveal a yellow precipitate which was collected by suction filtration and washed with Et_2O (25 mL) to leave a yellow solid (1.67 g) containing **H_3QSH** as well as the two symmetrical species **H_3Quin** and **H_3SH**.

H_3QSH was separated from **H_3Quin** and **H_3SH** *via* a preparative HPLC method. Prior to injection onto a solution of the sample was dissolved in a solution of THF : water (1 : 1 by volume) to make a 50 mg / mL solution, to which an excess of tris(2-carboxyethyl)phosphine hydrochloride (24 mg) was added to reduce any disulphide bonds within the sample. The separation was achieved using a Luna C_{18} reverse phase column with an injection size of 1 mL of the solution previously described running a water / acetone gradient method (0 – 75% over 30 minutes) whereby solvents contained 0.05% by volume TFA, were of HPLC grade and were degassed with He gas prior to use. Between each injection, the column was washed with acetone and water (10 minutes for each). Monitoring the absorbance at 210 nm and 336 nm allowed the detection of the three species whereby **H_3Quin** was eluted after 14 minutes (MS (ES-TOF)$^+$ *m/z*: 646.3 $[M + H]^+$, 668.3 $[M + Na]^+$), **H_3QSH** after 20 minutes (MS (ES-TOF)$^+$ *m/z*: 627.3 $[M + H]^+$, 649.3 $[M + Na]^+$), and **H_3SH** after 28 minutes (MS (ES-TOF)$^+$ *m/z*: 630.4 $[M + Na]^+$).

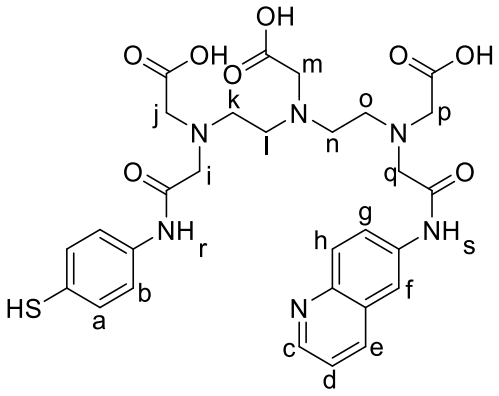

The solvent was removed from the solution containing **H_3QSH** to reveal a yellow solid which was dried under high vacuum. ^{1}H NMR (400 MHz, d_6-DMSO) δ_H ppm: 10.31 (1H, *br*, N*H*$_s$), 10.09 (1H, *br*, N*H*$_r$), 8.77 (1H, dd, *J* = 4.2, 1.5, *H*$_c$), 8.33 (1H, d, *J* = 2.2, *H*$_f$), 8.11 (1H, d, *J* = 7.9, *H*$_e$), 7.93 (1H, d, *J* = 9.1, *H*$_h$), 7.82 (1H, dd, *J* = 9.1, 2.2, *H*$_g$), 7.59 (2H, d, *J* = 8.5, *H*$_b$), 7.45 (1H, dd, *J* = 7.9, 4.2, *H*$_d$), 7.32 (2H, d, *J* = 8.5, *H*$_a$), 4.22 (2H, *br*, *H*$_i$), 3.66 (2H, *br*, *H*$_q$), 3.57 (6H, m, *H*$_j$, *H*$_m$, *H*$_p$), 3.38 (4H, *br*, *H*$_n$, *H*$_l$), 3.14 (4H, *br*, *H*$_k$, *H*$_o$). ^{13}C NMR (101 MHz, d_6-DMSO) δ_{13} ppm: 172.9 ($CH_2\underline{C}OOH$), 172.8 ($CH_2\underline{C}OOH$), 170.1 ($CH_2\underline{C}OOH$), 169.8 ($NH\underline{C}OCH_2$), 168.5 ($NH\underline{C}OCH_2$), 149.0 (Ar$\underline{C}$H), 144.6 (Ar$\underline{C}$), 138.7 (Ar$\underline{C}$), 136.5 (Ar$\underline{C}$), 135.6 (Ar$\underline{C}$H), 129.9 (Ar$\underline{C}$), 129.8 (Ar$\underline{C}$H), 129.3 (Ar$\underline{C}$H), 128.3 (Ar$\underline{C}$), 123.6 (Ar$\underline{C}$H), 121.8 (Ar$\underline{C}$H), 120.1 (Ar$\underline{C}$H), 115.3 (Ar$\underline{C}$H), 57.4 ($N\underline{C}H_2CONH$), 54.7 ($N\underline{C}H_2COOH$), 54.0 ($N\underline{C}H_2COOH$), 52.5 ($N\underline{C}H_2CH_2N$), 49.4 ($N\underline{C}H_2CH_2N$). MS (ES-TOF)$^+$ *m/z*: 627.3 [M + H]$^+$, 649.3 [M + Na]$^+$. λ_{max} 247 nm (ε = 39000 M^{-1} cm^{-1}) and 320 nm (ε = 3000 M^{-1} cm^{-1}), mp = 214 - 216 ^{o}C, ν_{max} / cm^{-1} 1671 (C=O), 3000 (C-H), 3288 (O-H). Characterisation data were in agreement with the literature.[5]

Synthesis of EuQSH

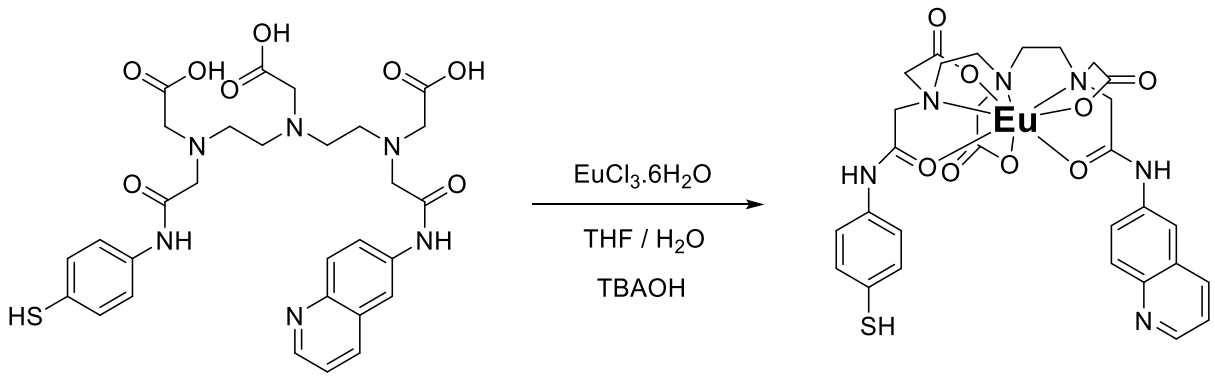

H_3QSH **EuQSH**

H_3QSH (0.060 g, 0.096 mmol, 1.00 eq) was dissolved in THF : water (1 : 1 by volume) (12 mL) and the pH was adjusted to 6 with addition of TBAOH (40% in water). A solution of $EuCl_3.6H_2O$ (0.044 g, 1.25 mmol, 1.25 eq.) in water (1 mL) was prepared and added to the **H_3QSH** solution. The vessel holding the $EuCl_3.6H_2O$ solution was washed out with water (1 mL) and this also added to the **H_3QSH** solution. The solution was left to stir for 15 minutes at RT, whereupon the THF was removed *in vacuo* and the pH was adjusted to 6 with addition of TBAOH (40% in water). The solution was reduced to 1 mL *in vacuo* and MeCN (30 mL) was added to yield a precipitate and the solution was triturated for 1 hour. After this time, the solution was filtered to give a brown solid which was washed with MeCN (10 mL) and Et_2O (10 mL) to give **EuQSH** (0.046 g, 50%). MS (ES-TOF)$^+$ m/z: 797.1 [*M* + Na (^{152}Eu)]$^+$. λ_{max} 246 nm (ε = 35000 M^{-1} cm^{-1}) and 320 nm (ε = 3000 M^{-1} cm^{-1}), mp > 300 ^{o}C, ν_{max} / cm^{-1} 1586 (C=O), 3200 (N-H). Characterisation data were in agreement with the literature.

EuL@Au (L = QSH or EuQuinSAc)

To a stirring solution of **Cit@Au** (3.2 nM, 2 mL) was added **EuL** (L = QuinSAc or QSH) (50 µL, 0.2 mM in MeOH) and stirred for 15 minutes at RT. The coated NPs were purified *via* G15 sephadex size exclusion chromatography, whereby the red band was collected and checked for no aggregation *via* UV Vis.

Sample	λ_{max} SPR / nm	Number distribution / nm	Intensity distribution / nm	PDI
EuQS@Au	521	12 ± 4	23 ± 10	0.3
EuQuinSAc@Au	520	12 ± 3	24 ± 11	0.5

xLC@Au (x = κ or λ)

To a stirring solution of **Cit@Au** (3.2 nM, 2 mL) was added xLC (x = κ or λ) (5 µL, 0.5 mg per mL in 0.001 M PBS) and stirred for 60 minutes at RT. The coated nanoparticles were purified *via* G100 sephadex size exclusion chromatography, whereby the red band was collected and checked for no aggregation *via* UV Vis.

Sample	λ_{max} SPR / nm	Number distribution / nm	Intensity distribution / nm	PDI
κstandard@Au	520	15 ± 4	56 ± 54	0.2
λstandard@Au	522	17 ± 4	47 ± 26	0.3

xLC.EuL@Au (x = κ or λ) (L = QuinSAc or QSH)

To a stirring solution of **Cit@Au** (3.2 nM, 2 mL) was added **EuL** (L = QuinSAc or QSH) (10 µL, 0.2 mM in MeOH) and stirred for 15 minutes at RT. To the stirring solution was then added xLC (x = κ or λ) (5 µL, 0.5 mg per mL in PBS) and stirred for 60 minutes at RT. The coated nanoparticles were purified *via* G100 sephadex size exclusion chromatography, whereby the red band was collected and checked for no aggregation *via* UV Vis.

Sample	**λ_{max} SPR / nm**	**Number distribution / nm**	**Intensity distribution / nm**	**PDI**
κstandard.EuQS@Au	519	14 ± 4	56 ± 54	0.4
κnew.EuQS@Au	519	14 ± 4	30 ± 13	0.3
κfur.EuQS@Au	519	16 ± 5	36 ± 17	0.3

BUCIS04-AF647

The conjugation of **BUCIS04** to **AF647** was performed using **BUCIS04** as according to instructions from the Fluoraprobe 647 kit as supplied by Life Technologies as was the lateral flow assay.

ELISA assay

To an ELISA 96 well plate was added κnew light chain antibody (100 μL, 1 μg / mL in PBS to each well) and washed with PBS (0.01 M) and Tween 20 (0.05%). Each well was then treated with BSA (100 μL, 1% in PBS to each well) and was incubated for 1 hour and then was thoroughly washed with PBS and Tween 20. To the wells was added either **BUCIS04** or **BUCIS04-AF647** (100 μL, concentration varied between 2 μg / mL and 0.1 ng / mL with a dilution factor of 0.5 each time in PBS) and the sample incubated for 1 hour and then was thoroughly washed with PBS and Tween 20. After this time, a solution of goat anti mouse IgG HRP conjugate was diluted in PBS by a factor of 4000, and this was added to the wells (100 μL in PBS per well) and left for 10 minutes. During this time a solution of TMP (1 mg) in a mixture of citric acid (5 mL, 0.1 M) and sodium phosphate buffer (5 mL, 0.2 M) to give a final pH of 5, was prepared which was then treated with H_2O_2 (50 μL). The TMP and H_2O_2 solution was then added to the wells (100 μL per well) and incubated for 5 minutes after which time H_2SO_4 (100 μL, 0.2 M per well) was added and the absorption of each well at 450 nm was measured on a 96 well plate reader.

FRET assay

To a solution of **κLC.EuL@Au** (2.7 nM, 200 μL) (in tris buffer if reported) was added **BUCIS04-AF647** (1.0 mg / mL in PBS, 4 μL) and incubated for 10 minutes after which time the FRET signal was recorded *via* time resolved spectroscopy with a λ_{exc} = 320 nm and λ_{em} = 614 nm.

Lifetime data from the PHERAstar® multimode plate reader was obtained with use of a TRF optic module. Whereby **κLC.EuL@Au** (2.7 nM, 100 μL per well) was added to the wells and **BUCIS04-AF647** (100 μg / mL in PBS, 20 μL) was added and incubated for 30 minutes. After this time, the lifetime signal was obtained with a TRF optic module with a with a λ_{exc} = 337 nm and λ_{em} = 615 nm, over a range of 2500 μs with 5 μs intervals between data points with the top optic being used. Data was processed on KaleidaGraph software whereby data was plotted to a bi-exponential decay curve.

6.3 Chapter 3

Modification of functionalised AuNPs with blocking agent

To a stirring solution of AuNPs (Either **κnew.EuQS@Au** or **EuQS@Au)** (2.7 nM, 2 ml) was added the appropriate blocking agent FCS (20 µL), BSA (100 µL of 20% solution), Tween 20 (1 µL) or Zonyl® FSA (1 µL) and the sample left to incubate for 30 minutes.

Addition of BUCIS04-AF647 to functionalised AuNPs

To a solution of AuNPs (Either **κnew.EuQS@Au** or **EuQS@Au)** at (2.7 nM, 200 µL) (in tris buffer if reported and with appropriate blocking agent modification) was added **BUCIS04-AF647** (1.0 mg / ml in PBS, 4 µL) and incubated for 10 minutes after which time the FRET signal was recorded *via* time resolved spectroscopy with a λ_{exc} = 320 nm and λ_{em} = 614 nm.

FRET assay for detection of κnew

To a solution of **BUCIS04-AF647** (1.0 mg / ml in PBS, 4 µL) was added κnew (4.9 mg / ml in PBS 5 µL) and 10 µL PBS and the solution left to incubate for 10 minutes. After this time, the solution was transferred into a solution of **κnew.EuQS@Au** (2.7 nM, 200 µL) (in tris buffer and with blocking agent present if reported) and left to incubate for 10 minutes after which time the FRET signal was recorded *via* time resolved spectroscopy with a λ_{exc} = 320 nm and λ_{em} = 614 nm.

6.4 Chapter 4

Synthesis of tert-butyl (3-acetylphenyl)carbamate (8)

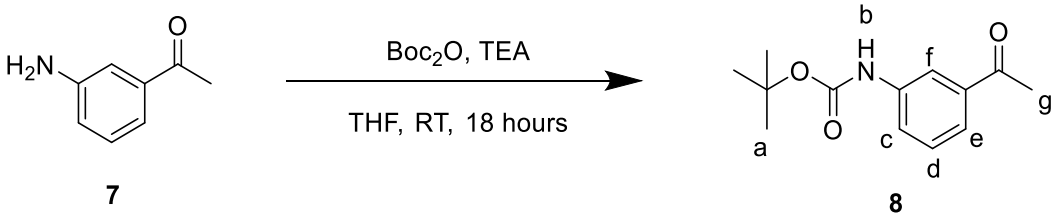

7 **8**

To a stirring solution of 3-aminoacetonpheone (2.50 g, 18.5 mmol 1.54 eq) in THF (50 mL) was added di-tertiary butyl bicarbonate (2M in THF, 6 mL, 12.00 mmol 1.00 eq) and TEA (4.2 mL) and the resulting solution was stirred at RT for 18 hours. After this time, water (100 mL) was added to the reaction mixture and the organic material was extracted with EtOAc (2 x 100 mL) which was then dried over anhydrous Na_2SO_4 (*ca.* 10 g), filtered, and the solvent removed *in vacuo* to give a yellow solid which was purified *via* column chromatography on silica (EtOAc : Hexane; 30 : 70) to yield **8** as a white solid (2.10 g, 8.94 mmol, 75%). ^{1}H NMR (400 MHz, $CDCl_3$) δ_H: 7.94 (1H, appt, J = 1.9, H_f), 7.65 (1H, d, J = 7.8, H_e), 7.60 (1H, dt, J = 7.8, 1.9, H_c), 7.38 (1H, t, J = 7.8, H_d), 6.83 (1H, *br*, H_b), 2.59 (3H, s, H_g), 1.52 (9H, s, H_a). ^{13}C{^{1}H} PENDANT NMR (101 MHz, $CDCl_3$) δ_C: 198.2 (Me<u>C</u>OPh), 152.8 (NH<u>C</u>OO), 139.1 (Ar<u>C</u>), 137.9 (Ar<u>C</u>), 129.4 (Ar<u>C</u>H), 123.1 (Ar<u>C</u>H), 123.0 (Ar<u>C</u>H), 118.2 (Ar<u>C</u>H), 81.0 (O<u>C</u>(Me)$_3$), 28.4 (OC(<u>C</u>H$_3$)$_3$), 26.8 (CO<u>C</u>H$_3$). MS (ES-TOF)$^+$ *m/z*: 258.1 [M + Na]$^+$, 180 [M - ^{t}Bu]$^+$. Characterisation data were in agreement with the literature.[6,7]

Synthesis of (Z)-1-(3-aminophenyl)-3-hydroxy-3-phenylprop-2-en-1-one (9)

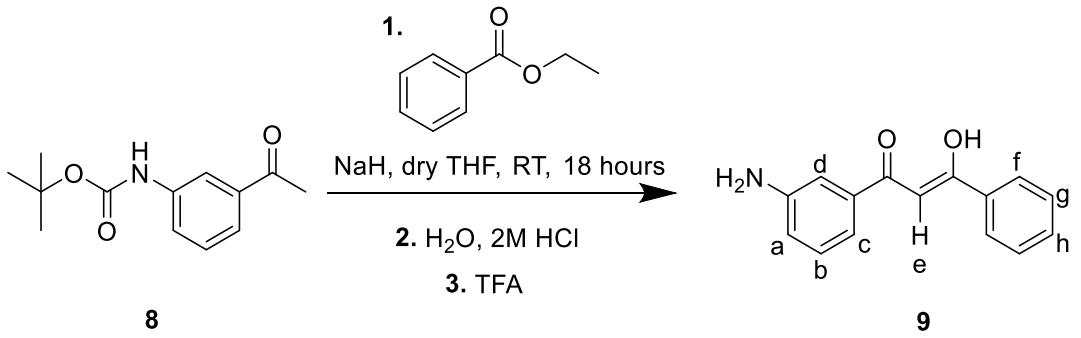

NaH (60% dispersion in mineral oil) (1.00 g, 25.0 mmol, 5.88 eq) was washed with hexane (2 x 20 mL) prior to use. To the washed NaH under N_2, was added dry THF (30 mL) and a solution of **8** (1.00 g, 4.25 mmol, 1.00 eq.) in dry THF (10 mL) and the solution stirred at RT under N_2 for 1 hour. After this time, a yellow solution was observed and a solution of ethyl benzoate (1.00 g, 6.66 mol, 1.57 eq.) in dry THF (10 mL) was added and the resulting solution was left to stir at RT for 18 hours. The remaining NaH was quenched with addition of water (5 mL) and the mixture was acidified with addition of HCl (2M, 25 mL) which afforded a yellow colour at pH 2. To this solution water (100 mL) was added and the organic material was extracted with EtOAc (2 x 100 mL) which was dried over anhydrous Na_2SO_4 (*ca.* 10 g), filtered and the was solvent removed *in vacuo* to reveal an orange oil. The resulting oil was washed with hexane (3 x 100 mL) with sonication and the resulting oil dried under high vacuum. The oil was then placed under N_2 and TFA (5 mL, 65.4 mmol) was added and the solution was stirred for 1 hour under N_2 at RT. After this time a saturated solution of $NaHCO_3$ (100 mL) was added slowly and stirred until the observed effervescence had ended and EtOAc (3 x 100 mL) was added and the organic material was extracted and dried over Na_2SO_4 (*ca.* 10 g), the solution filtered, and the solvent removed *in vacuo* to give an orange oil that was purified *via* column chromatography on silica (EtOAc : Hexane; 30 : 70) to yield **9** as a yellow oil (0.38 g, 1.59 mmol, 37%). ^{1}H NMR (400 MHz, $CDCl_3$) δ_H: 8.00 (2H, d, J = 7.1, H_f), 7.40 – 7.55 (3H, m, H_g, H_h), 7.38 (1H, dt, J = 7.8, 1.1, H_c), 7.33 (1H, appt, J = 2.2, H_d), 7.28 (1H, t, J = 7.8, H_b), 6.88 (1H, ddd, J = 7.8, 2.2, 1.1, H_a), 6.84 (1H, s, H_e), 3.60 – 4.00 (2H, br, NH_2). ^{13}C NMR (101 MHz, d_6 – $CDCl_3$) δ_C: 186.3 (PhCOCH), 185.6 (PhCOCH), 147.0 (H_2NC), 136.9 (ArC),

135.6 (Ar<u>C</u>), 132.5 (Ar<u>C</u>H), 129.7 (Ar<u>C</u>H), 128.0 (Ar<u>C</u>H), 127.3 (Ar<u>C</u>H), 119.2 (Ar<u>C</u>H), 117.6 (Ar<u>C</u>H), 113.4 (Ar<u>C</u>H), 93.2 (CO<u>C</u>HCO). *m/z*: 240.1 $[M + H]^+$, 262.1 $[M + Na]^+$.

Synthesis of (Z)-5-(1,2-dithiolan-3-yl)-N-(3-(3-hydroxy-3-phenylacryloyl)phenyl)pentanamide (DBMSS)

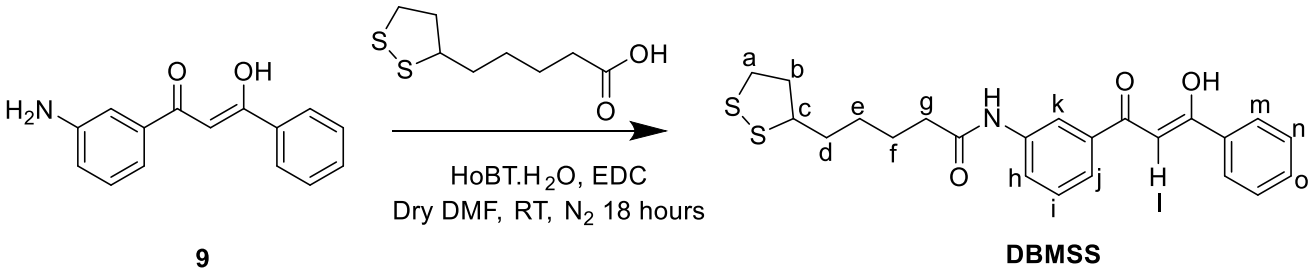

9 **DBMSS**

A solution of **9** (0.38 g, 1.59 mmol, 1.28 eq.), thioctic acid (0.26 g, 1.26 mmol, 1.02 eq.), EDC (0.24 g, 1.55 mmol, 1.25 eq.) and HoBT.H_2O (0.19 g, 1.24 mmol, 1.00 eq.) were dissolved in a solution of dry DMF (5 mL) and stirred at RT under N_2 for 18 hours. After this time, water (100 mL) was added and the organic material was extracted with EtOAc (3 x 100 mL). The organic extracts were combined and dried over anhydrous Na_2SO_4 (*ca.* 10 g), filtered and the solvent removed *in vacuo* to give an orange oil. The resulting oil was triturated in hexane (250 mL) for 18 hours after which time a yellow powder was revealed and the hexane removed *via* filtration. The yellow solid was then dissolved in the minimum amount of acetone (10 mL) and the product was precipitated with addition of hexane (100 mL) to yield **DBMSS** as a yellow solid (0.12 g, 0.28 mmol, 22%). ^{1}H NMR (400 MHz, d_6 – DMSO) δ_H: 10.13 (1H, s, *NH*), 8.28 (1H, appt, *J* = 1.8, H_k), 8.15 (2H, d, *J* = 7.3, H_m), 7.89 (2H, m, H_h, H_j), 7.67 (1H, t, *J* = 7.3, H_o), 7.58 (2H, t, *J* = 7.3, H_n), 7.49 (1H, t, *J* = 8.0, H_i), 7.25 (1H, s, H_l), 3.64 (1H, dt, *J* = 12.2, 6.2, H_c), 3.1 – 3.2 (2H, m, H_a), 2.42 (1H, dt, *J* = 6.2, 18.8, H_b), 2.35 (2H, t, *J* = 7.4, H_g), 1.88 (1H, m, H_b), 1.5 – 1.8 (4H, m, H_d, H_f), 1.42 (2H, p, *J* = 8.0, H_e). ^{13}C{^{1}H} PENDANT NMR (101 MHz, d_6 – DMSO) δ_C: 185.3 (Ph<u>C</u>O), 185.2 (Ph<u>C</u>O), 171.4 (NH<u>C</u>OCH_2), 139.9 (Ar<u>C</u>), 135.1 (Ar<u>C</u>), 134.6 (Ar<u>C</u>), 133.0 (Ar<u>C</u>H), 129.2 (Ar<u>C</u>H), 128.9 (Ar<u>C</u>H), 127.3 (Ar<u>C</u>H), 123.4 (Ar<u>C</u>H), 122.3 (Ar<u>C</u>H), 117.5 (Ar<u>C</u>H), 93.3 (CO<u>C</u>HCO), 56.1 (CH_2<u>C</u>HS), 39.5 (CH<u>C</u>H_2CH_2), 38.1 (CH_2<u>C</u>H_2S), 36.2 (CO<u>C</u>H_2), 34.2 (CH_2<u>C</u>H_2CH_2), 28.3 (CH_2<u>C</u>H_2CH_2), 24.8 (CH_2<u>C</u>H_2CH_2). MS (ES-TOF)$^+$ *m/z*: 450.1 $[M + Na]^+$. λ_{max} (MeOH) 350 nm (ε = 19900 M^{-1} cm^{-1}) and 240 nm (ε = 23200 M^{-1} cm^{-1}), mp 108 - 110 ^{O}C, ν_{max} / cm^{-1} 1652 (C=O), 2933 (C-H), 3290 (O-H).

Preparation of Eu.DBMSS.Z@Au

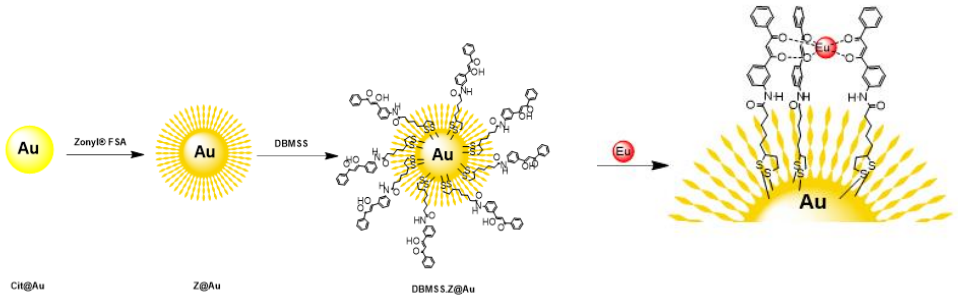

To a stirring solution of **Cit@Au** (3.2 nM, 2 mL) was added a solution of Zonyl® FSA (diluted 1 in 10 by volume in deionised water) (1 µL) and stirred for 5 minutes. Excess Zonyl® FSA was removed *via* centrifugation at 11800 RPM for 30 minutes and the supernatant was removed and the NPs were redispersed in deionised water to produce **Z.Au**. To a stirring solution of **Z.Au** (3.2 nM, 2 mL) was added **DBMSS** (0.2 mM, 120 µL in MeOH) and stirred for 15 minutes at RT. The coated NPs were purified *via* G15 Sephadex size exclusion chromatography, whereby the red band was collected and checked for no aggregation *via* UV Vis spectroscopy. To the resulting solution (2 mL), was added TEA (1 µL) and stirred with $EuCl_3.6H_2O$ (80 µM, 60 µL in water) for 20 minutes.

Sample	**λ_{max} SPR / nm**	**Number distribution / nm**	**Intensity distribution / nm**	**PDI**
Cit@Au	516	12 ± 3	18 ± 3	0.1
Z@Au	517	15 ± 3	25 ± 3	0.1
DBMSS.Z@Au	524	15 ± 4	24 ± 4	0.2
Eu.DBMSS.Z@Au	524	15 ± 3	18 ± 3	0.3

6.5 Referenced material

1 C. C. Thinnes, A. Tumber, C. Yapp, G. Scozzafava, T. Yeh, M. C. Chan, T. A. Tran, K. Hsu, H. Tarhonskaya, L. J. Walport, S. E. Wilkins, E. D. Martinez, S. Müller, C. W. Pugh, P. J. Ratcliffe, P. E. Brennan, A. Kawamura and C. J. Schofield, *Chem. Commun.*, 2015, **51**, 15458 – 15461.

2 X. Lin, G. Godeau and Mark W. Grinstaff, *New J. Chem.*, 2014, **38**, 5186 – 5189.

3 J. J. Tindale, K. L. Mouland and P.J. Ragogna, *J. Mol. Liq.*, 2010, **152**, 14 – 18.

4 S. Khan, PhD thesis, University of Birmingham, 2013.

5 A. Savage, PhD thesis, University of Birmingham, 2013.

6 X. Xiong and Y. Yeung, Angew. Chem. Int. Ed., 2016, **55**, 16101 – 16105.

7 S. Bhagwanth, A. G. Waterson, G. M. Adjabeng and K. R. Hornberger, *J. Org. Chem.* 2009, **74**, 4634 – 4637.

Appendices

Chapter 2 appendix

List of appendices

1. *^{1}H NMR of **2** in $CDCl_3$*
2. *^{13}C NMR of **2** in $CDCl_3$*
3. *MS (ES-TOF)$^{+}$ of **2***
4. *^{1}H NMR of **4** in $CDCl_3$*
5. *^{13}C NMR of **4** in $CDCl_3$*
6. *MS (ES-TOF)$^{+}$ of **4***
7. *^{1}H NMR of **5** in $CDCl_3$*
8. *^{13}C NMR of **5** in $CDCl_3$*
9. *MS (ES-TOF)$^{+}$ of **5***
10. *^{1}H NMR of **6** in $CDCl_3$*
11. *^{13}C NMR of **6** in $CDCl_3$*
12. *MS (ES-TOF)$^{+}$ of **6***
13. *^{1}H NMR of **H_3QuinSAc** in d_6 DMSO*
14. *MS (ES-TOF)$^{+}$ of **H_3QuinSAc***
15. *COSY NMR of **H_3QuinSAc** in d_6 DMSO*
16. *COSY NMR of aromatic region of **H_3QuinSAc** in d_6 DMSO*
17. *COSY NMR of aliphatic region of **H_3QuinSAc** in d_6 DMSO*
18. *HSQC NMR of aromatic region of **H_3QuinSAc** in d_6 DMSO*
19. *HSQC NMR of aliphatic region of **H_3QuinSAc** in d_6 DMSO*
20. *MS (ES-TOF)$^{+}$ of **H_3Quin***
21. *MS (ES-TOF)$^{+}$ of **H_3SH***
22. *MS (ES-TOF)$^{+}$ of **H_3QSH***
23. *^{1}H NMR of **H_3QSH** in d_6 DMSO*
24. *^{13}C NMR of **H_3QSH** in d_6 DMSO*
25. *COSY NMR of aromatic region of **H_3QSH** in d_6 DMSO*
26. *COSY NMR of alipahtic region of **H_3QSH** in d_6 DMSO*
27. *HMBC NMR of **H_3QSH** in d_6 DMSO*
28. *HSQC NMR of **H_3QSH** in d_6 DMSO*
29. *MS (ES-TOF)$^{+}$ of **EuQuinSAc***
30. *MS (ES-TOF)$^{+}$ of **EuQSH***
31. *Lifetime of **EuQSH** in H_2O, λ_{exc} = 320 nm and λ_{em} = 614 nm*

32. *Lifetime of **EuQSH** in D_2O, λ_{exc} = 320 nm and λ_{em} = 614 nm*
33. *Lifetime of **EuQSH** in MeOH, λ_{exc} = 320 nm and λ_{em} = 614 nm*
34. *Lifetime of **EuQuinSAc** in H_2O , λ_{exc} = 320 nm and λ_{em} = 614 nm*
35. *Lifetime of **EuQuinSAc** in D_2O , λ_{exc} = 320 nm and λ_{em} = 614 nm*
36. *Lifetime of **EuQuinSAc** in MeOH , λ_{exc} = 320 nm and λ_{em} = 614 nm*
37. *Lifetime of **EuQS@Au** in H_2O, λ_{exc} = 320 nm and λ_{em} = 614 nm*
38. *IRF of **Au@Cit**, λ_{exc} = 320 nm and λ_{em} = 614 nm*
39. *Lifetime of **κstandard.EuQSHc@Au** in H_2O, λ_{exc} = 320 nm and λ_{em} = 614 nm*
40. *Emission spectrum of **κLC.EuQuinSAc@Au** λ_{exc} = 320 nm, corrected for PMT response*
41. *Emission spectrum of **λLC.EuQS@Au** λ_{exc} = 320 nm, corrected for PMT response*
42. *Emission spectrum of **λLC.EuQuinSAc@Au** λ_{exc} = 320 nm, corrected for PMT response*
43. *Preparation of **κnew.EuQS@Au** as monitored via UV Vis*
44. *Emission spectrum of **κnew.EuQS@Au** λ_{exc} = 320 nm, corrected for PMT response*
45. *Preparation of **κfur.EuQS@Au** as monitored via UV Vis*
46. *Emission spectrum of **κfur.EuQS@Au** λ_{exc} = 320 nm, corrected for PMT response*
47. *ELISA assay of **BUCIS04** against κnew*
48. *ELISA assay control with **BUCIS04 – AF647** and no assay reagents*
49. *UV Vis of **κLC.EuQS@Au** in Tris HCl and PBS buffers*
50. *Emission spectrum of **BUCIS04-AF647**, λ_{exc} = 320 nm, corrected for PMT response*
51. *Lifetime of **κstandard.EuQS@Au**, λ_{exc} = 320 nm and λ_{em} = 614 nm*
52. *Lifetime of **κstandard.EuQS@Au** in tris HCl buffer, λ_{exc} = 320 nm and λ_{em} = 614 nm*
53. *Lifetime of **κstandard.EuQS@Au** and 100 nm **BUCIS04-AF647**, λ_{exc} = 320 nm and λ_{em} = 614 nm*
54. *Lifetime of **κstandard.EuQS@Au** and 100 nm **BUCIS04-AF647** in tris HCl buffer, λ_{exc} = 320 nm and λ_{em} = 614 nm*
55. *Lifetime of **κnew.EuQS@Au** , λ_{exc} = 320 nm and λ_{em} = 614 nm*
56. *Lifetime of **κnew.EuQS@Au** in tris HCl buffer, λ_{exc} = 320 nm and λ_{em} = 614 nm*
57. *Lifetime of **κnew.EuQS@Au** and 100 nm **BUCIS04-AF647**, λ_{exc} = 320 nm and λ_{em} = 614*
58. *Lifetime of **κnew.EuQS@Au** and 100 nm **BUCIS04-AF647** in tris HCl buffer, λ_{exc} = 320 nm and λ_{em} = 614 nm*
59. *Lifetime of **κfur.EuQS@Au** , λ_{exc} = 320 nm and λ_{em} = 614 nm*
60. *Lifetime of **κfur.EuQS@Au** in tris HCl buffer, λ_{exc} = 320 nm and λ_{em} = 614 nm*
61. *Lifetime of **κfur.EuQS@Au** and 100 nm **BUCIS04-AF647**, λ_{exc} = 320 nm and λ_{em} = 614*
62. *Lifetime of **κfur.EuQS@Au** and 100 nm **BUCIS04-AF647** in tris HCl buffer, λ_{exc} = 320 nm and λ_{em} = 614 nm*

INSTRUM	spect
PROBHD	5 mm PABBO BB–
PULPROG	zg30
TD	32768
SOLVENT	CDCl3
NS	32
DS	2
SWH	6009.615 Hz
FIDRES	0.183399 Hz
AQ	2.7263477 sec
RG	724
DW	83.200 usec
DE	12.89 usec
TE	290.5 K
D1	1.00000000 sec
TD0	1
======== CHANNEL f1 ========	
NUC1	1H
P1	12.80 usec
PL1	1.00 dB
PL1W	9.57725906 W
SFO1	300.1318534 MHz
SI	32768
SF	300.1300263 MHz
WDW	EM
SSB	0
LB	0.30 Hz
GB	0
PC	1.00

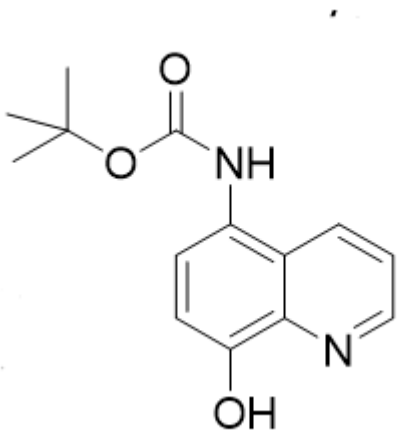

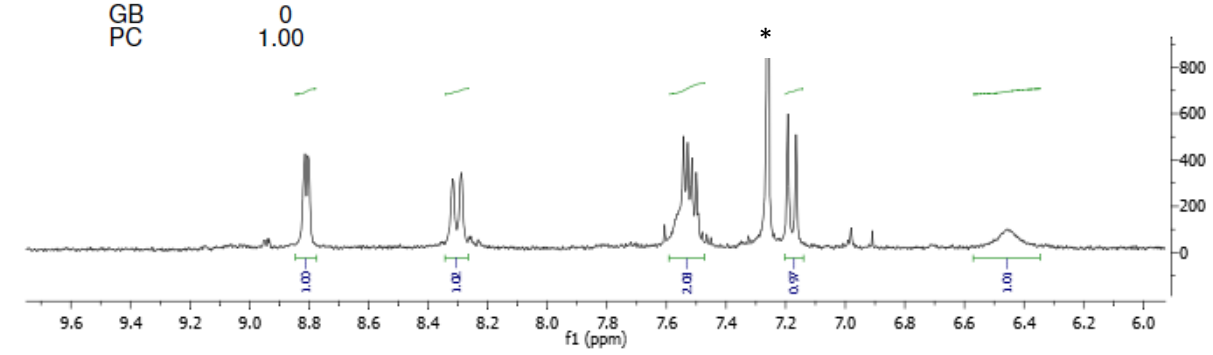

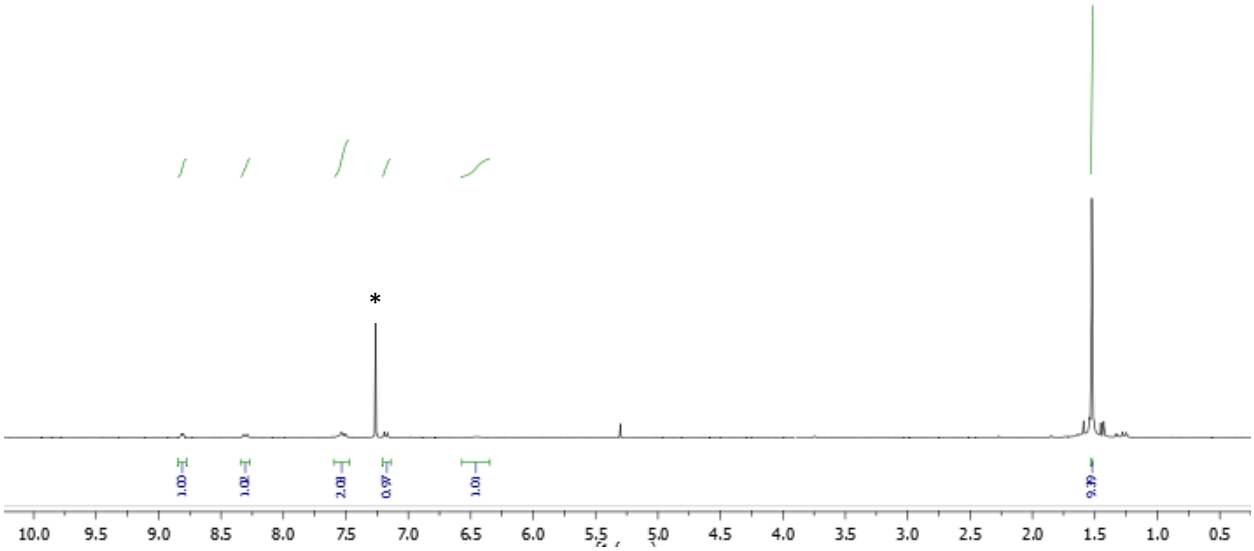

*^{1}H NMR of **2** in $CDCl_3$*

** = residual solvent resonance*

INSTRUM	spect
PROBHD	5 mm PADUL 13C
PULPROG	udeft
TD	18178
SOLVENT	CDCl3
NS	380
DS	0
SWH	25252.525 Hz
FIDRES	1.389181 Hz
AQ	0.3599744 sec
RG	2050
DW	19.800 usec
DE	8.20 usec
TE	295.0 K
D1	3.00000000 sec
D11	0.03000000 sec
D12	0.00002000 sec
D20	200.00000000 sec
TD0	380

======== CHANNEL f1 ========	
NUC1	13C
P1	8.80 usec
P12	2000.00 usec
P26	500.00 usec
PL1	–3.00 dB
PL1W	58.63890457 W
SFO1	100.6233333 MHz
SP2	6.27 dB
SP8	6.27 dB
SPNAM2	Crp60comp.4
SPNAM8	Crp60,0.5,20.1
SPOAL2	0.500
SPOAL8	0.500
SPOFFS2	0.00 Hz
SPOFFS8	0.00 Hz

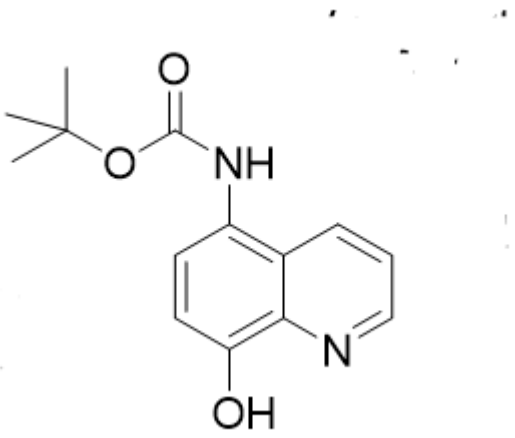

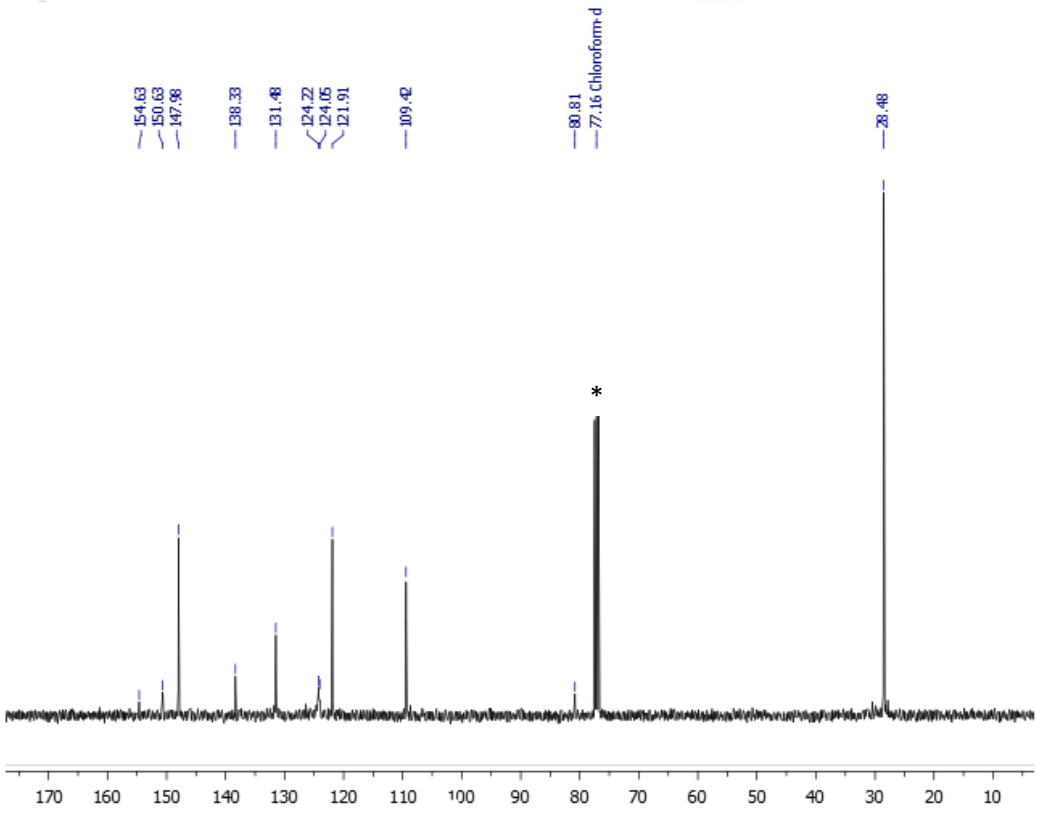

*$^{13}C\{^{1}H\}$ NMR of **2** in $CDCl_3$*

** = residual solvent resonance*

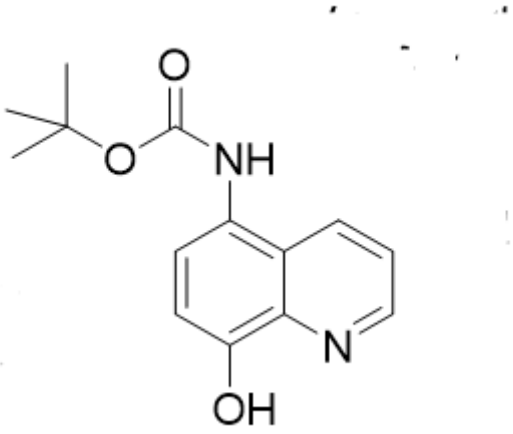
O
O
NH
N
OH

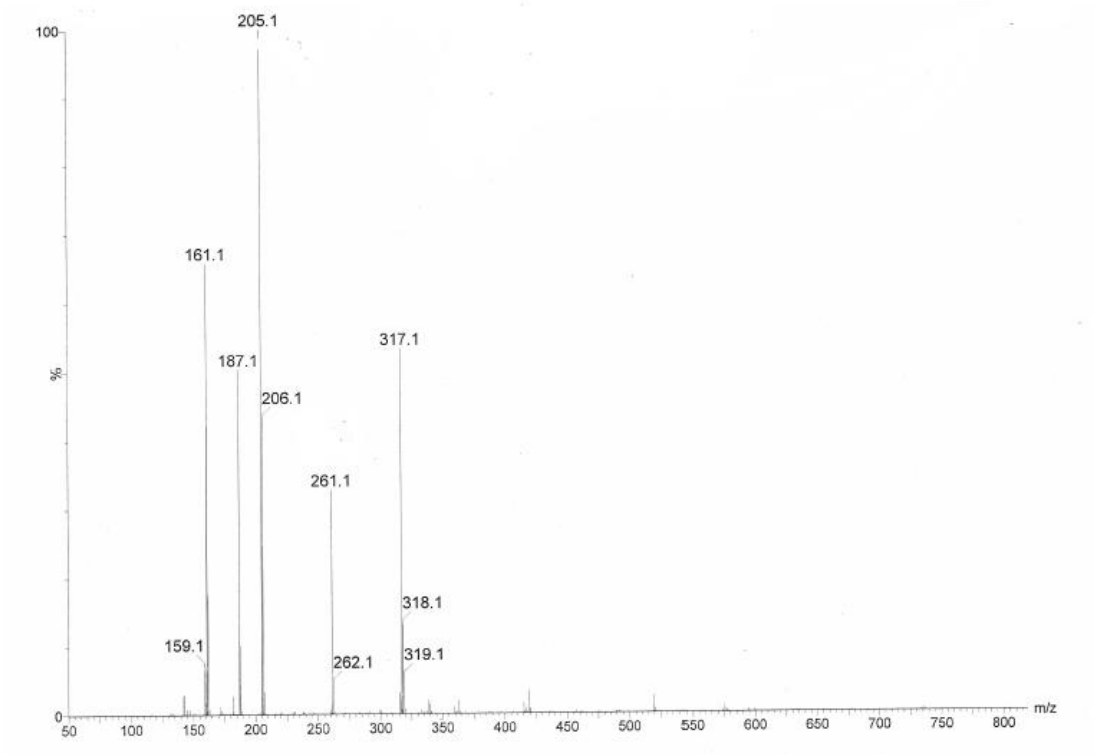
100
%
0
205.1
161.1
187.1
206.1
317.1
261.1
318.1
159.1
262.1
319.1
50
100
150
200
250
300
350
400
450
500
550
600
650
700
750
800
m/z

*MS (ES-TOF)$^+$ of **2***

INSTRUM	spect
PROBHD	5 mm PABBO BB–
PULPROG	zg30
TD	32768
SOLVENT	CDCl3
NS	32
DS	2
SWH	6009.615 Hz
FIDRES	0.183399 Hz
AQ	2.7263477 sec
RG	256
DW	83.200 usec
DE	12.89 usec
TE	290.5 K
D1	1.00000000 sec
TD0	1

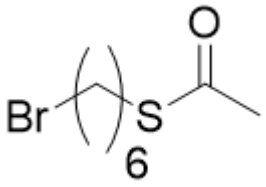

======== CHANNEL f1 ========

NUC1	1H
P1	12.80 usec
PL1	1.00 dB
PL1W	9.57725906 W
SFO1	300.1318534 MHz
SI	32768
SF	300.1300000 MHz
WDW	EM
SSB	0
LB	0.30 Hz
GB	0
PC	1.00

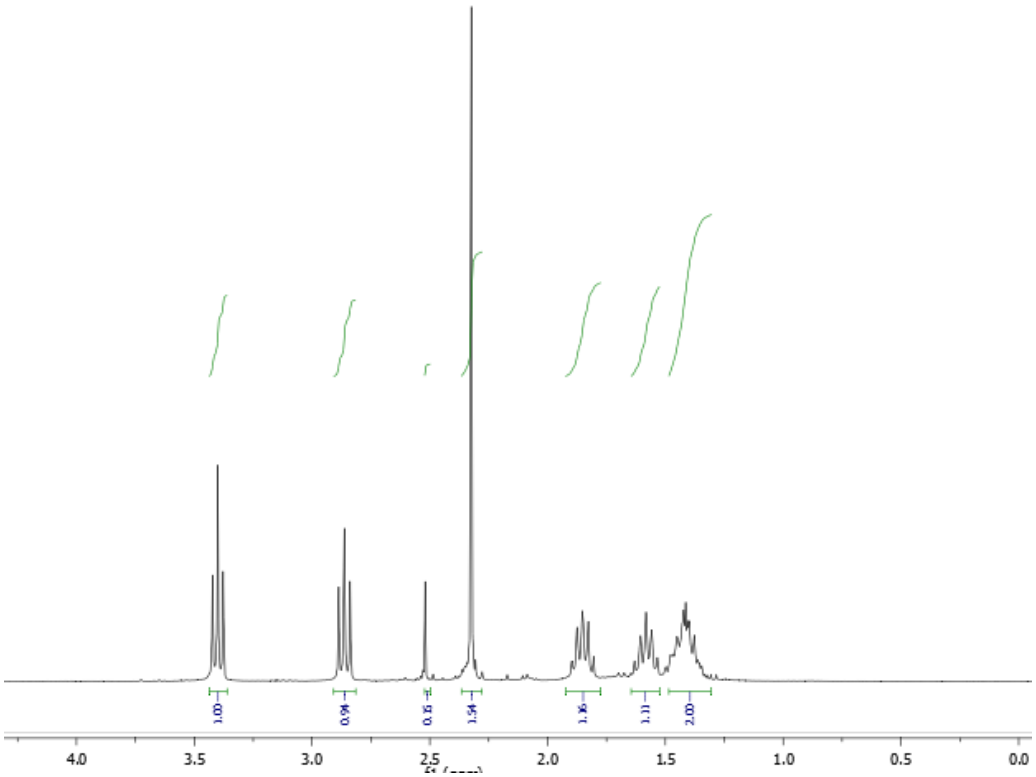

*^{1}H NMR of **4** in $CDCl_3$*

INSTRUM	spect
PROBHD	5 mm PADUL 13C
PULPROG	udeft
TD	18178
SOLVENT	CDCl3
NS	380
DS	0
SWH	25252.525 Hz
FIDRES	1.389181 Hz
AQ	0.3599744 sec
RG	2050
DW	19.800 usec
DE	8.20 usec
TE	294.4 K
D1	3.00000000 sec
D11	0.03000000 sec
D12	0.00002000 sec
D20	200.00000000 sec
TD0	380

======== CHANNEL f1 ========

NUC1	13C
P1	8.80 usec
P12	2000.00 usec
P26	500.00 usec
PL1	–3.00 dB
PL1W	58.63890457 W
SFO1	100.6233333 MHz
SP2	6.27 dB
SP8	6.27 dB
SPNAM2	Crp60comp.4
SPNAM8	Crp60,0.5,20.1
SPOAL2	0.500
SPOAL8	0.500
SPOFFS2	0.00 Hz
SPOFFS8	0.00 Hz

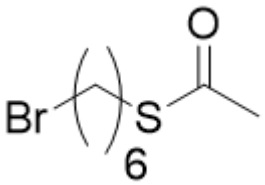

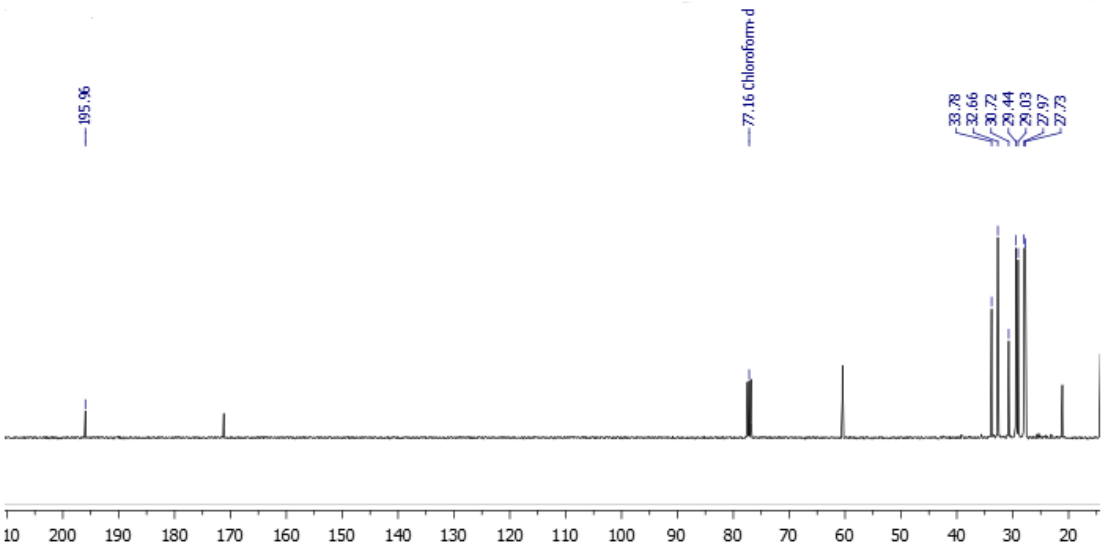

*$^{13}C\{^{1}H\}$ NMR of **4** in $CDCl_3$*

** = residual solvent resonance*

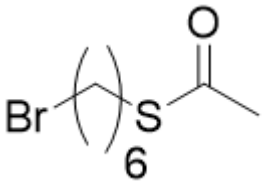
O
Br
S
6

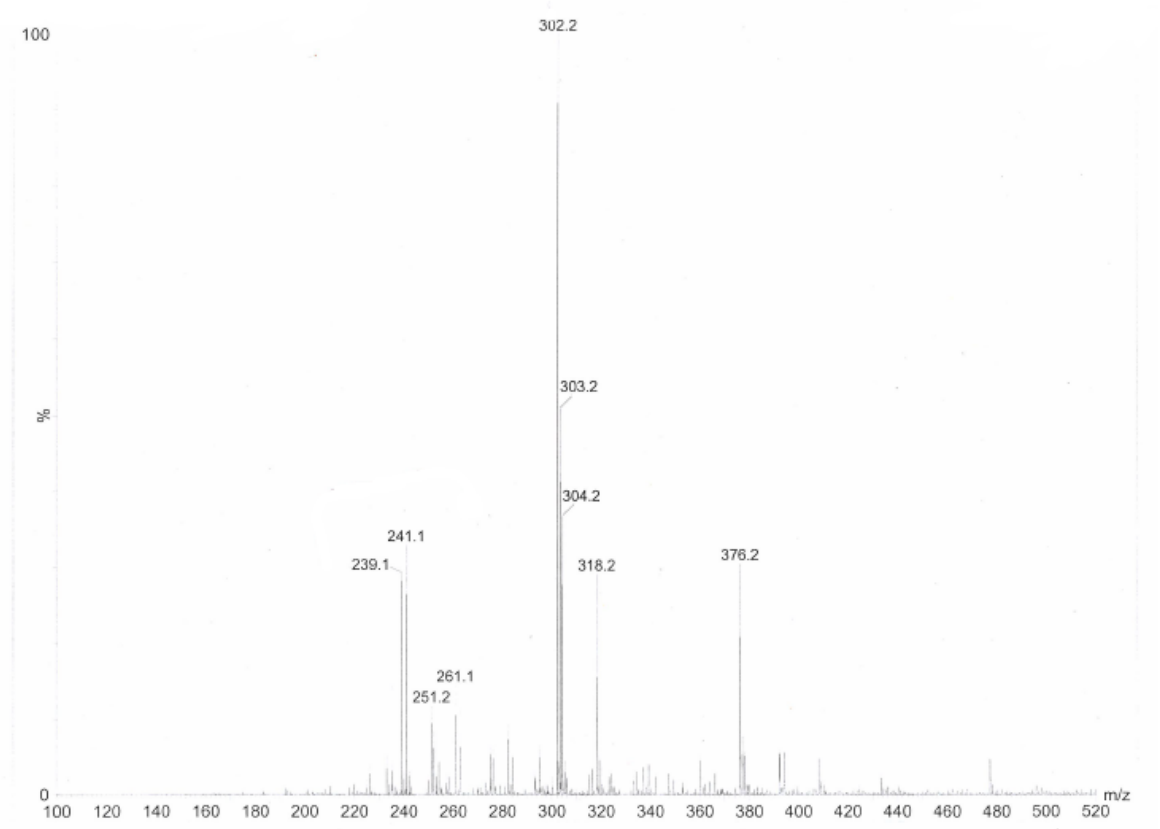
100
%
0
302.2
303.2
304.2
241.1
239.1
318.2
376.2
261.1
251.2
m/z
100 120 140 160 180 200 220 240 260 280 300 320 340 360 380 400 420 440 460 480 500 520

*MS (ES-TOF)$^+$ of **4***

```
INSTRUM          spect
PROBHD   5 mm PABBO BB-
PULPROG          zg30
TD              32768
SOLVENT          CDCl3
NS                 32
DS                  2
SWH          6009.615 Hz
FIDRES       0.183399 Hz
AQ           2.7263477 sec
RG                80.6
DW             83.200 usec
DE             12.89 usec
TE             290.5 K
D1          1.00000000 sec
TD0                1

======== CHANNEL f1 ========
NUC1               1H
P1             12.80 usec
PL1             1.00 dB
PL1W        9.57725906 W
SFO1        300.1318534 MHz
SI              32768
SF          300.1300210 MHz
WDW                EM
SSB                 0
LB              0.30 Hz
GB                  0
PC              1.00
```

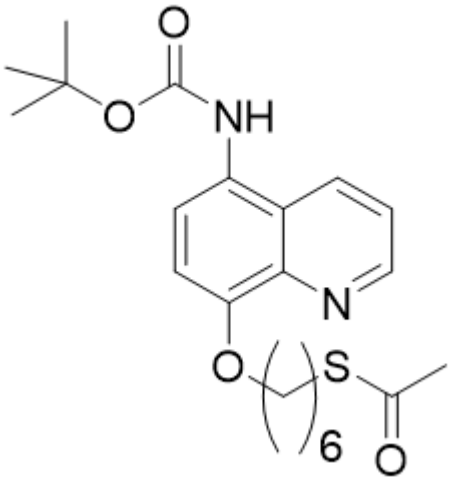

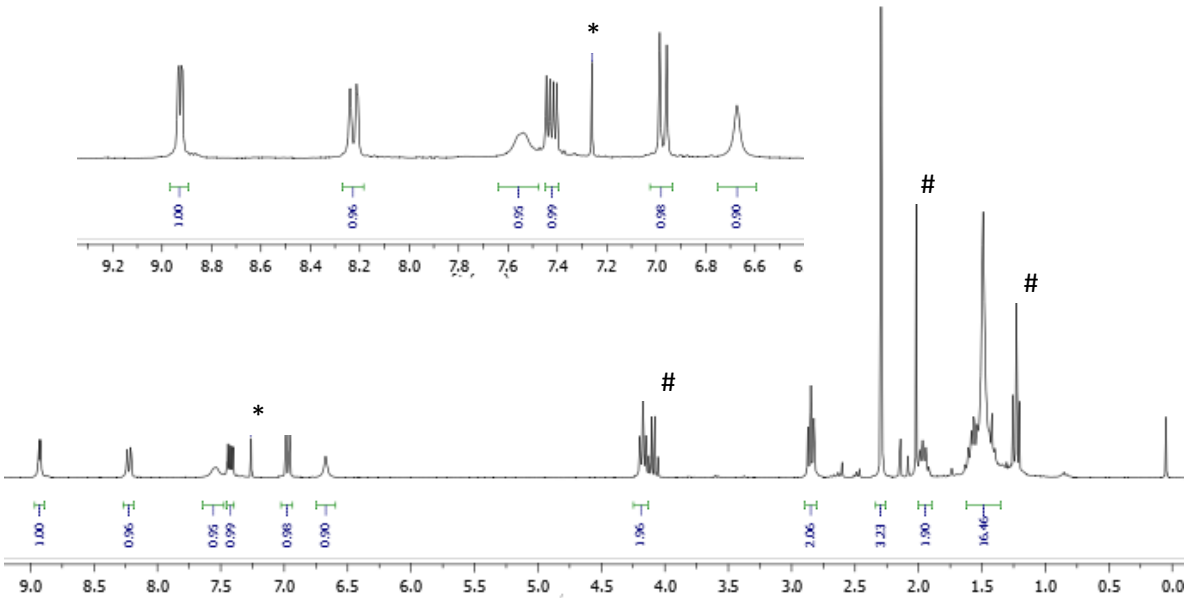

*^{1}H NMR of **5** in $CDCl_3$*

** = residual solvent resonance, # = Excess solvent resonance*

```
INSTRUM           spect
PROBHD   5 mm PADUL 13C
PULPROG           udeft
TD                18178
SOLVENT           CDCl3
NS                  380
DS                    0
SWH           25252.525 Hz
FIDRES         1.389181 Hz
AQ            0.3599744 sec
RG                 2050
DW                19.800 usec
DE                 8.20 usec
TE                294.4 K
D1           3.00000000 sec
D11          0.03000000 sec
D12          0.00002000 sec
D20        200.00000000 sec
TD0                380

======== CHANNEL f1 ========
NUC1               13C
P1                 8.80 usec
P12             2000.00 usec
P26              500.00 usec
PL1               -3.00 dB
PL1W        58.63890457 W
SFO1        100.6233333 MHz
SP2                6.27 dB
SP8                6.27 dB
SPNAM2      Crp60comp.4
SPNAM8   Crp60,0.5,20.1
SPOAL2             0.500
SPOAL8             0.500
SPOFFS2            0.00 Hz
SPOFFS8            0.00 Hz
```

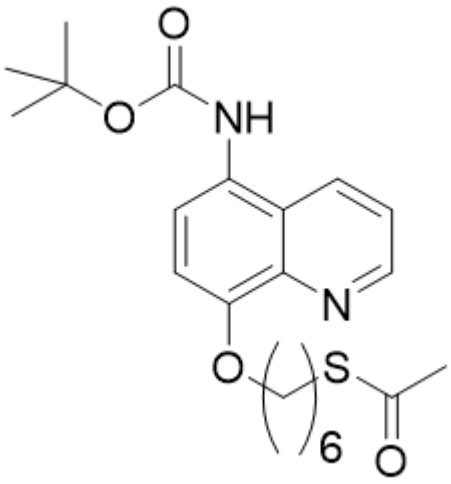

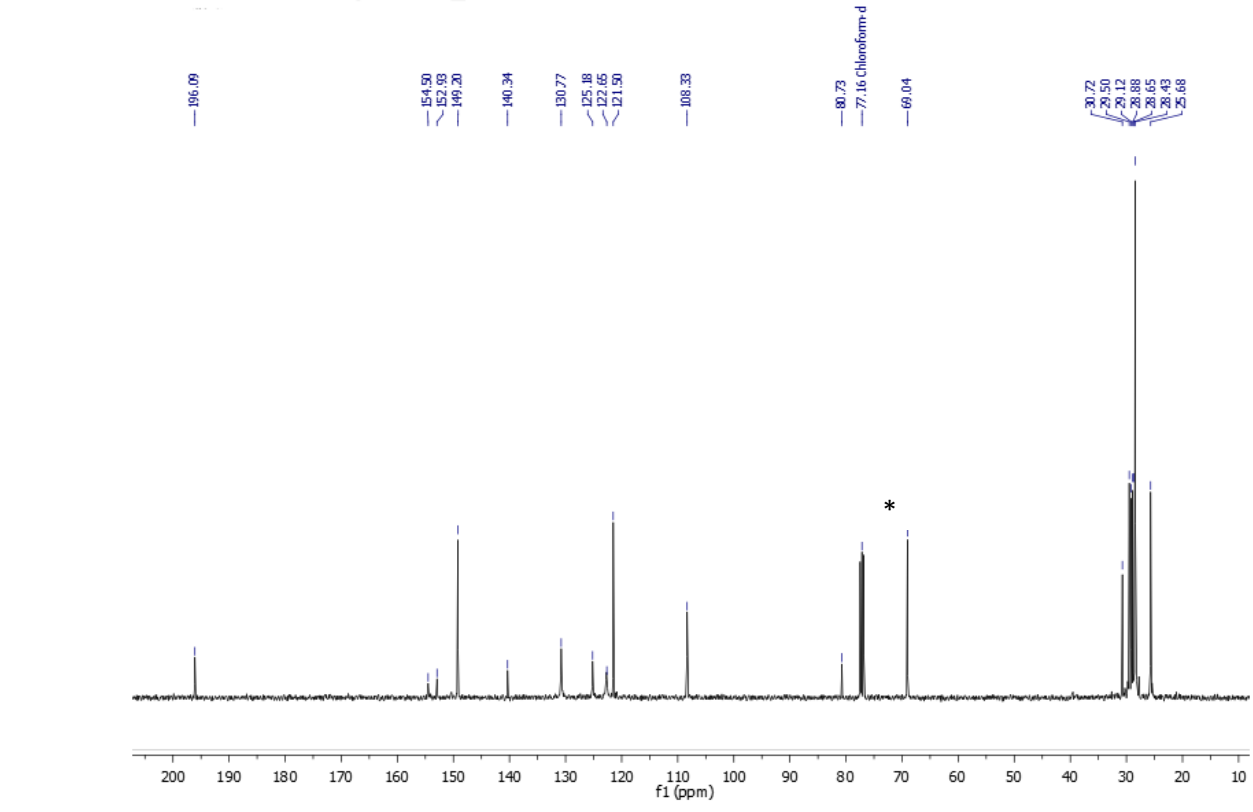

*$^{13}C\{^{1}H\}$ NMR of **5** in $CDCl_3$*

** = residual solvent resonance*

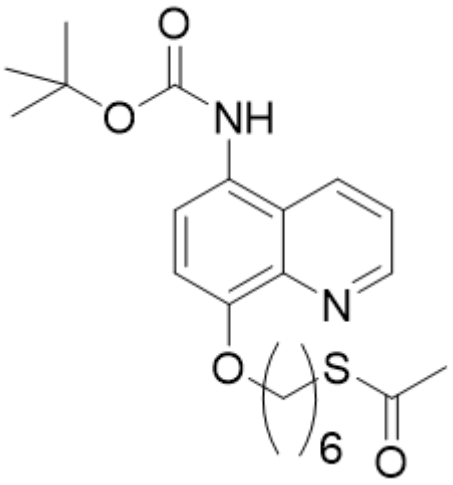
O
O
NH
N
O
S
6
O

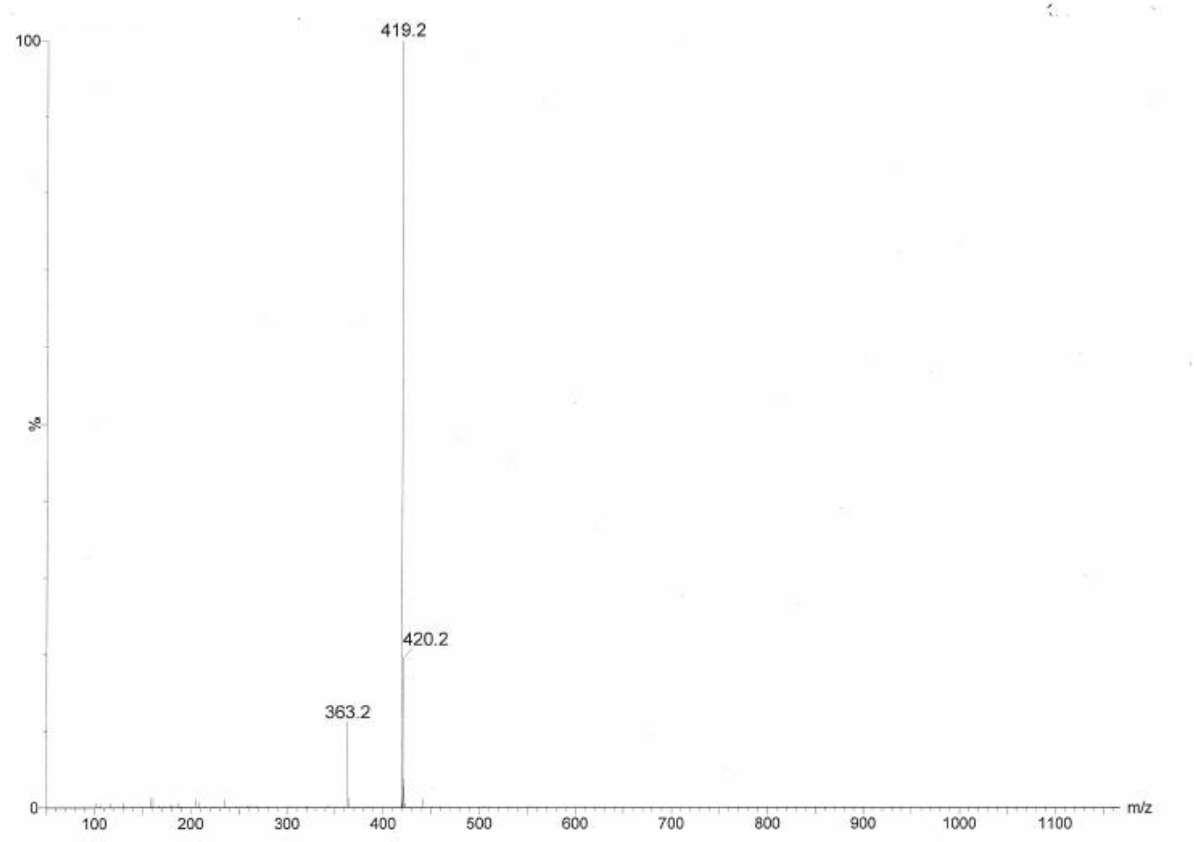
100
%
0
419.2
420.2
363.2
100
200
300
400
500
600
700
800
900
1000
1100
m/z

*MS (ES-TOF)$^+$ of **5***

INSTRUM	spect
PROBHD	5 mm PABBO BB–
PULPROG	zg30
TD	32768
SOLVENT	CDCl3
NS	32
DS	2
SWH	6009.615 Hz
FIDRES	0.183399 Hz
AQ	2.7263477 sec
RG	161
DW	83.200 usec
DE	12.89 usec
TE	290.5 K
D1	1.00000000 sec
TD0	1

======== CHANNEL f1 ========

NUC1	1H
P1	12.80 usec
PL1	1.00 dB
PL1W	9.57725906 W
SFO1	300.1318534 MHz
SI	32768
SF	300.1300242 MHz
WDW	EM
SSB	0
LB	0.30 Hz
GB	0
PC	1.00

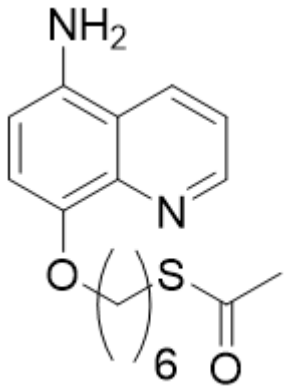

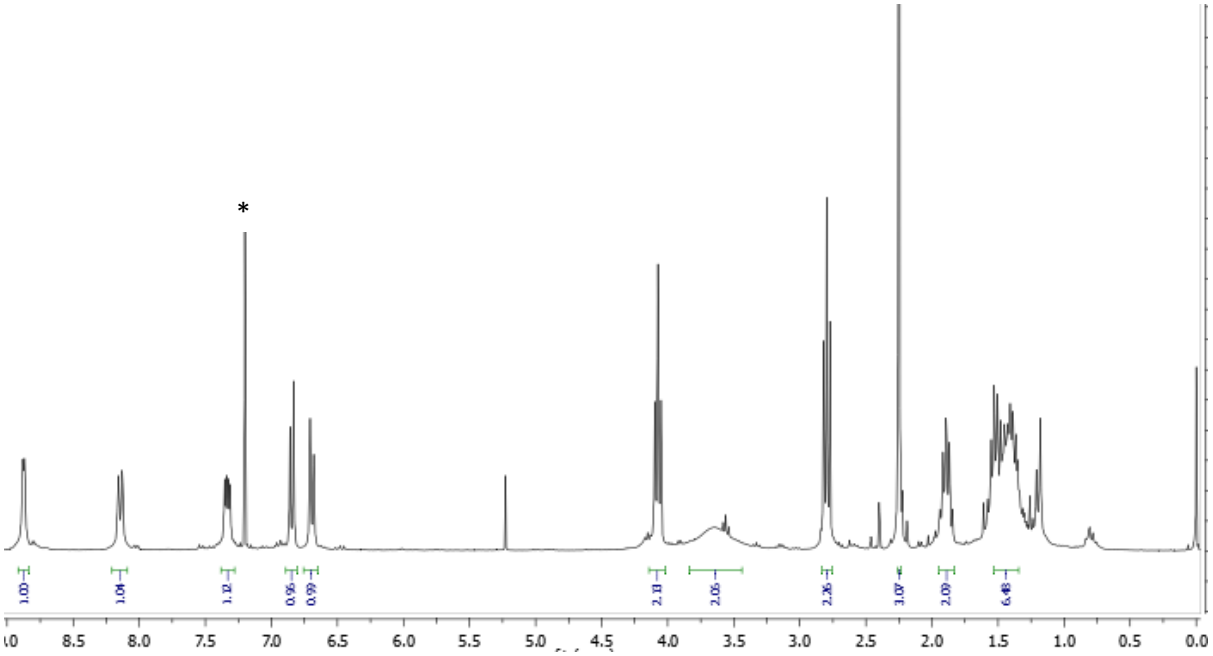

*^1H NMR of **6** in $CDCl_3$*

** = residual solvent resonance*

NAME 11-14-Pikramenou-17
EXPNO 10
PROCNO 1
Date_ 20131114
Time 23.40
INSTRUM spect
PROBHD 5 mm PADUL 13C
PULPROG udeft
TD 18178
SOLVENT CDCl3
NS 380
DS 0
SWH 25252.525 Hz
FIDRES 1.389181 Hz
AQ 0.3599744 sec
RG 2050
DW 19.800 usec
DE 8.20 usec
TE 294.3 K
D1 3.00000000 sec
D11 0.03000000 sec
D12 0.00002000 sec
D20 200.00000000 sec
TD0 380

======== CHANNEL f1 ========
NUC1 13C
P1 8.80 usec
P12 2000.00 usec
P26 500.00 usec
PL1 -3.00 dB
PL1W 58.63890457 W
SFO1 100.6233333 MHz
SP2 6.27 dB
SP8 6.27 dB
SPNAM2 Crp60comp.4
SPNAM8 Crp60,0.5,20.1
SPOAL2 0.500
SPOAL8 0.500
SPOFFS2 0.00 Hz
SPOFFS8 0.00 Hz

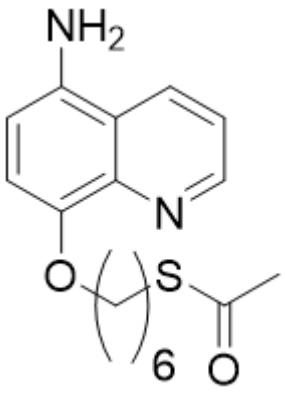

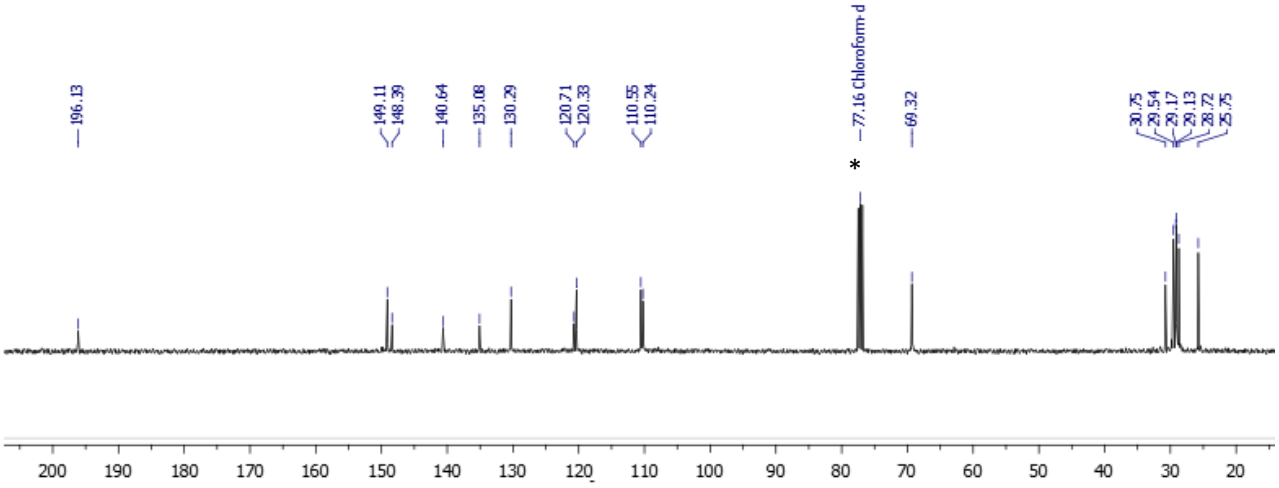

*$^{13}C\{^{1}H\}$ NMR of **6** in $CDCl_3$*

** = residual solvent resonance*

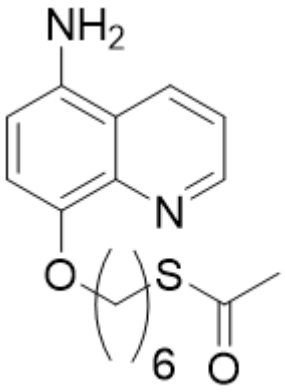
NH2
N
O
S
6
O

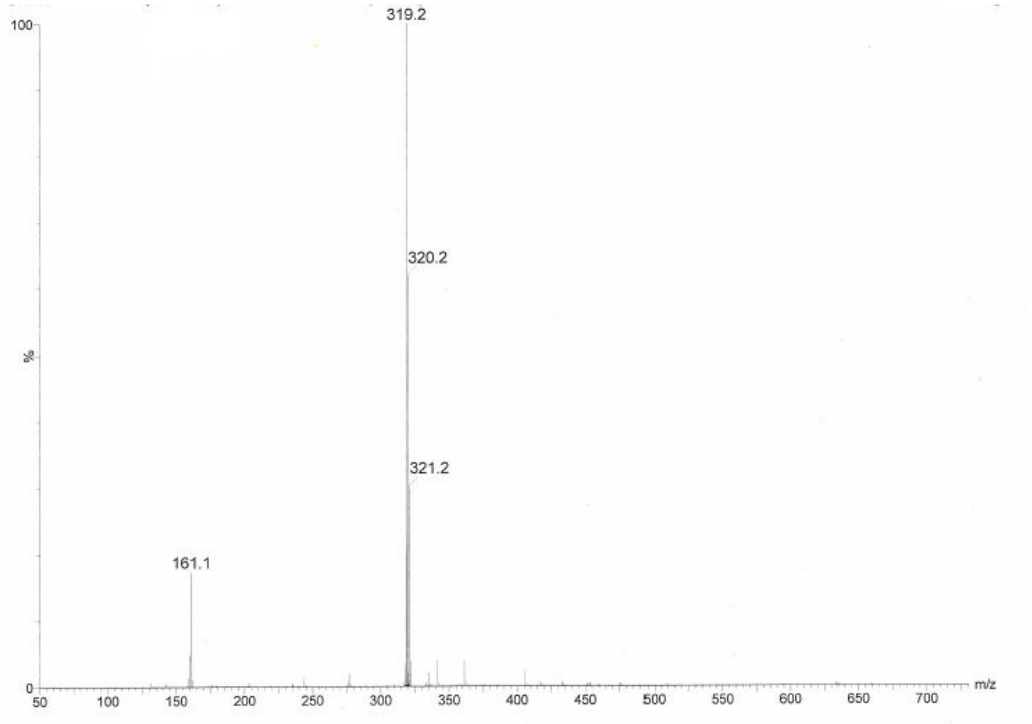
100
%
0
319.2
320.2
321.2
161.1
50
100
150
200
250
300
350
400
450
500
550
600
650
700
m/z

MS (ES-TOF)$^+$ of ***6***

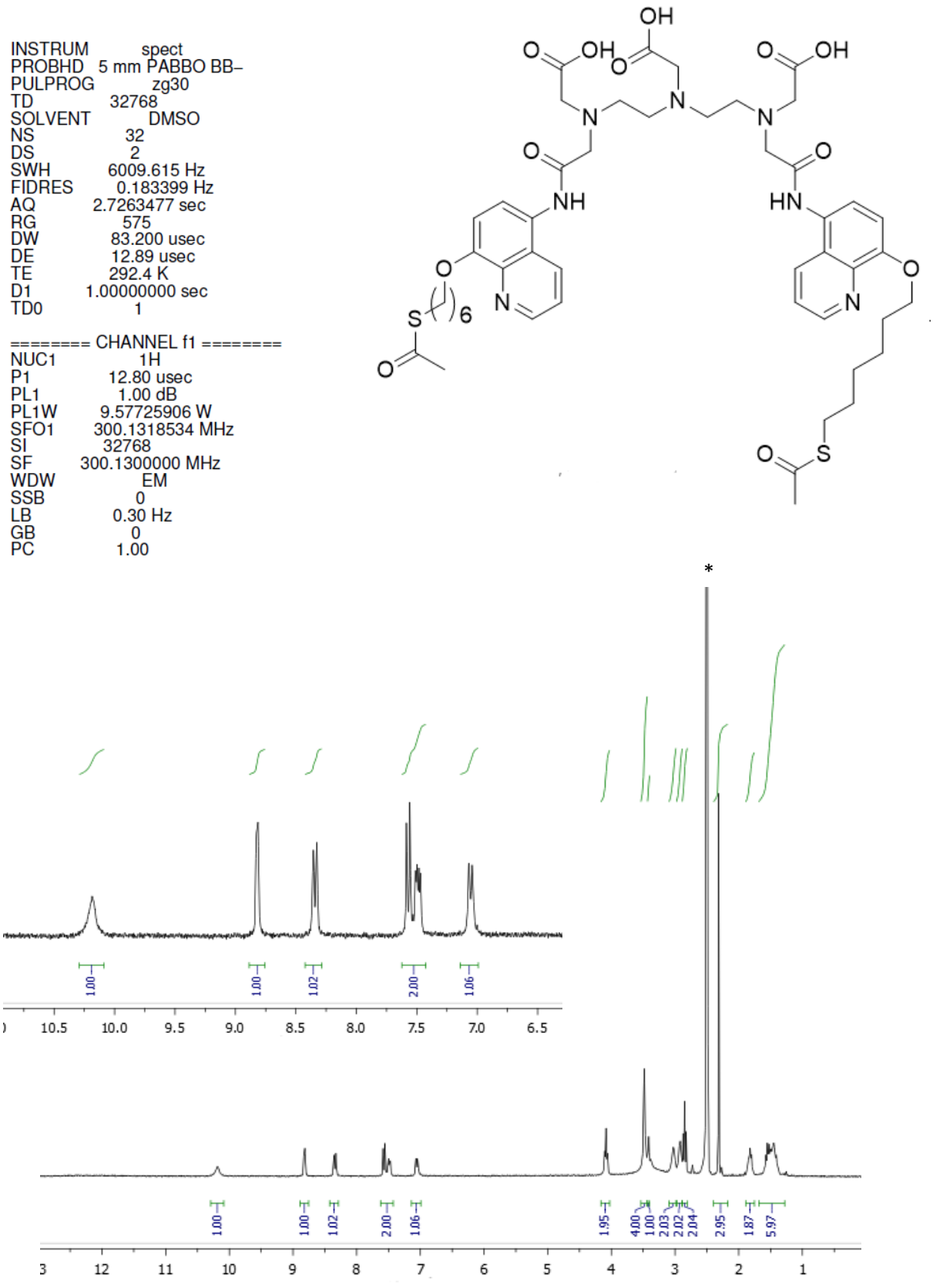

[1]H NMR of ***H₃QuinSAc*** *in d_6 DMSO*

** = residual solvent resonance*

INSTRUM	spect
PROBHD	5 mm PADUL 13C
PULPROG	pendantns
TD	65536
SOLVENT	DMSO
NS	512
DS	4
SWH	25252.525 Hz
FIDRES	0.385323 Hz
AQ	1.2976128 sec
RG	2050
DW	19.800 usec
DE	6.50 usec
TE	296.2 K
CNST2	145.0000000
CNST3	1.0000000
CNST4	5.0000000
D1	1.50000000 sec
D2	0.00172414 sec
D3	0.00431034 sec
D12	0.00002000 sec
D13	0.00000400 sec
TD0	1

======== CHANNEL f1 ========

SFO1	100.6242690 MHz
NUC1	13C
P1	8.80 usec
P2	17.60 usec
PLW1	58.63899994 W

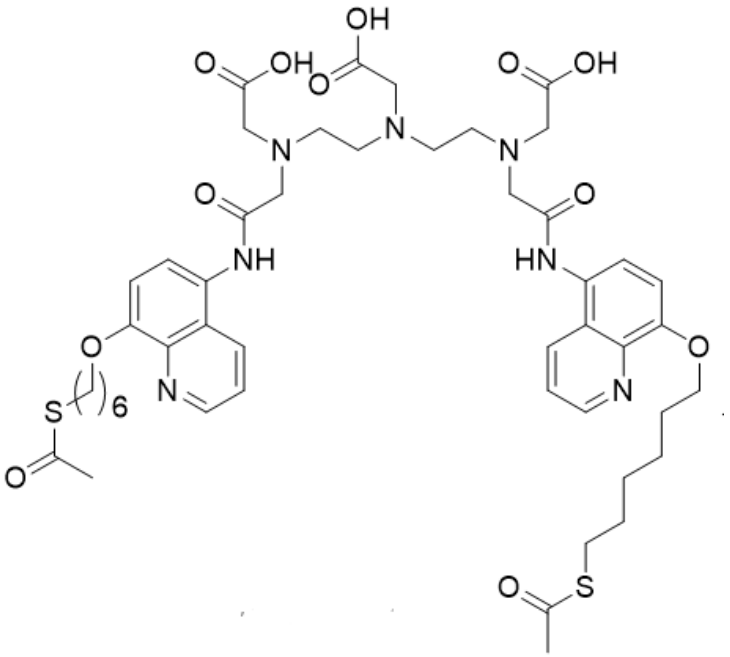

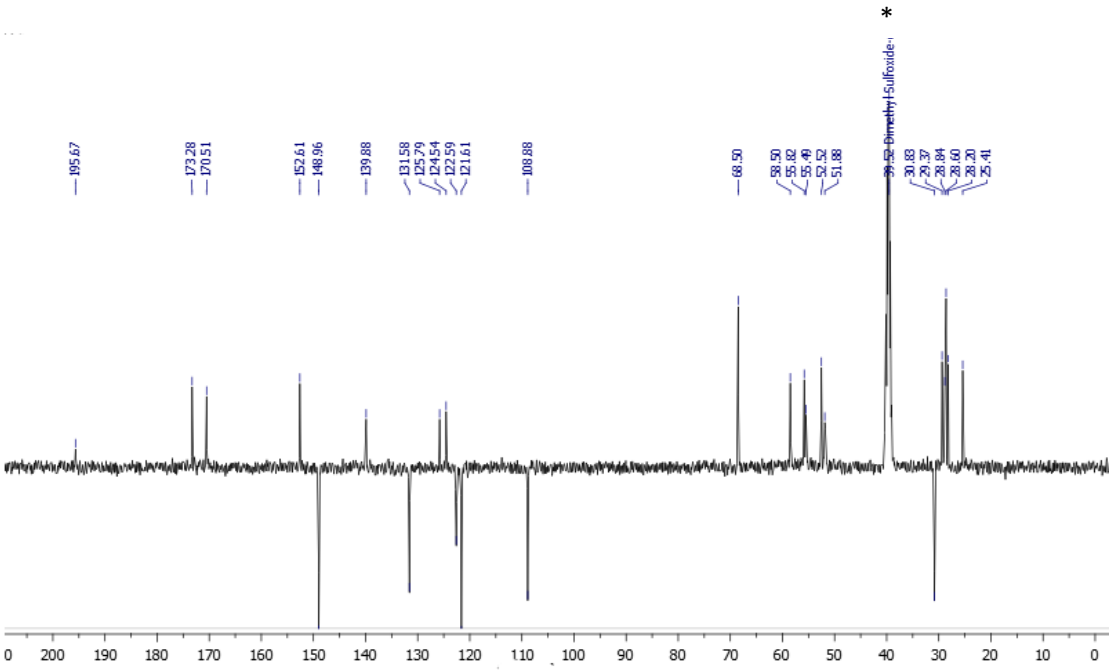

$^{13}C\{^{1}H\}$ PENDANT NMR of ***H_3QuinSAc*** *in d_6 DMSO*

** = residual solvent resonance*

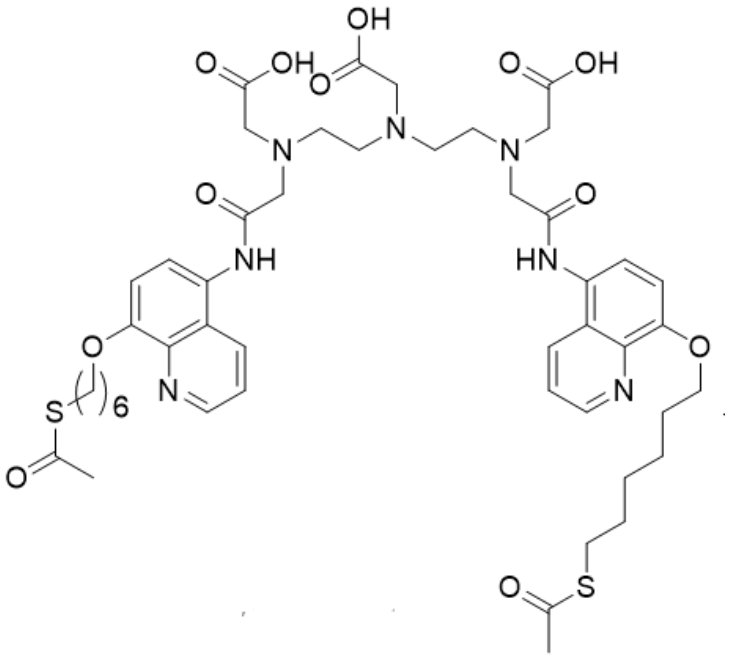

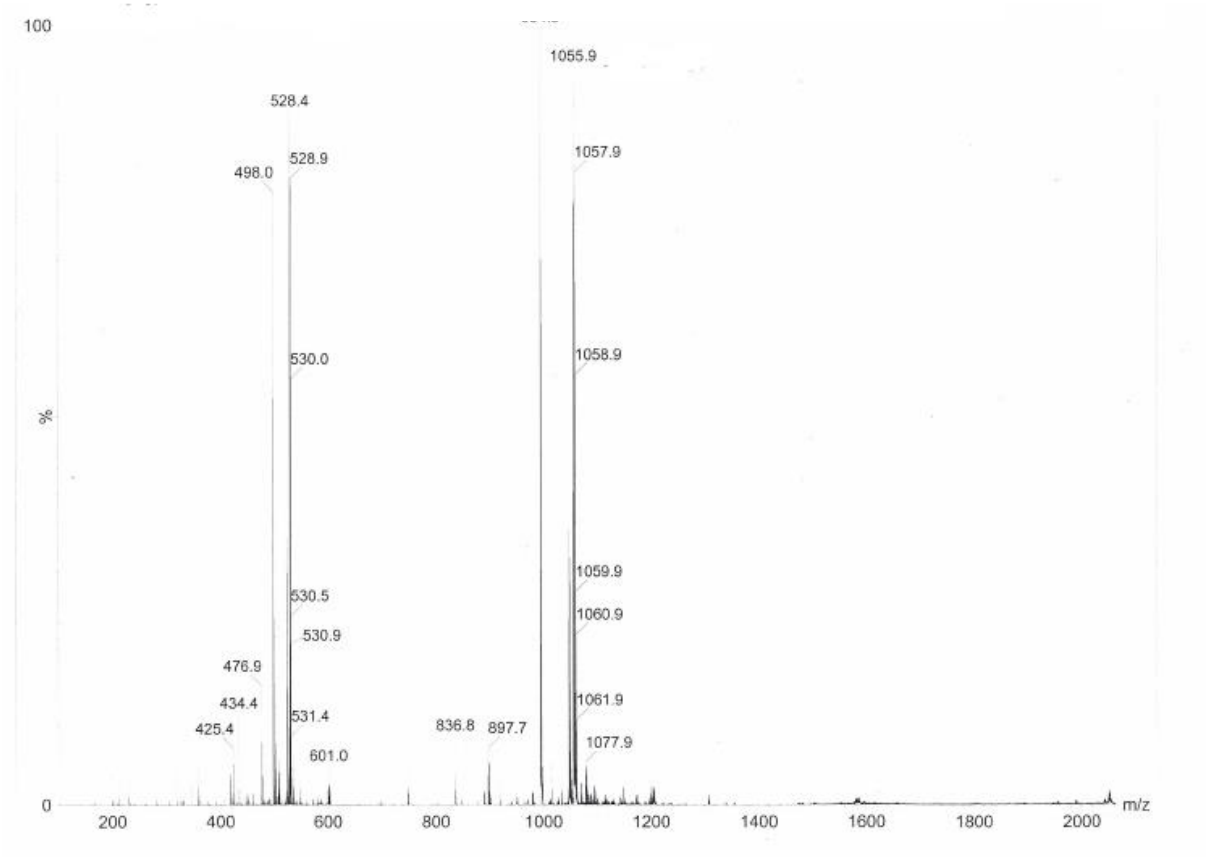

MS (ES-TOF)$^+$ of ***H_3QuinSAc***

```
INSTRUM          spect
PROBHD   5 mm PADUL 13C
PULPROG      cosygpmfqf
TD               1024
SOLVENT           DMSO
NS                  4
DS                 16
SWH          5376.344 Hz
FIDRES         5.250336 Hz
AQ          0.0952820 sec
RG                2050
DW              93.000 usec
DE               6.50 usec
TE               294.2 K
D0          0.00000300 sec
D1          1.48750603 sec
D13         0.00000400 sec
D16         0.00020000 sec
IN0         0.00018600 sec

======== CHANNEL f1 ========
NUC1                1H
P1               9.50 usec
PL1              -4.00 dB
PL1W        24.29185867 W
SFO1        400.1326835 MHz

====== GRADIENT CHANNEL =====
GPNAM1         SINE.100
GPNAM2         SINE.100
GPNAM3         SINE.100
GPZ1            16.00 %
GPZ2            12.00 %
GPZ3            40.00 %
P16           1000.00 usec
ND0                 1
TD                256
SFO1          400.1327 MHz
FIDRES         21.001345 Hz
SW             13.436 ppm
FnMODE               QF
SI                1024
SF          400.1300000 MHz
WDW               SINE
SSB                  0
LB              0.00 Hz
GB                   0
PC                1.40
SI                512
MC2                  QF
SF          400.1300000 MHz
WDW               SINE
SSB                  0
LB              0.00 Hz
GB                   0
```

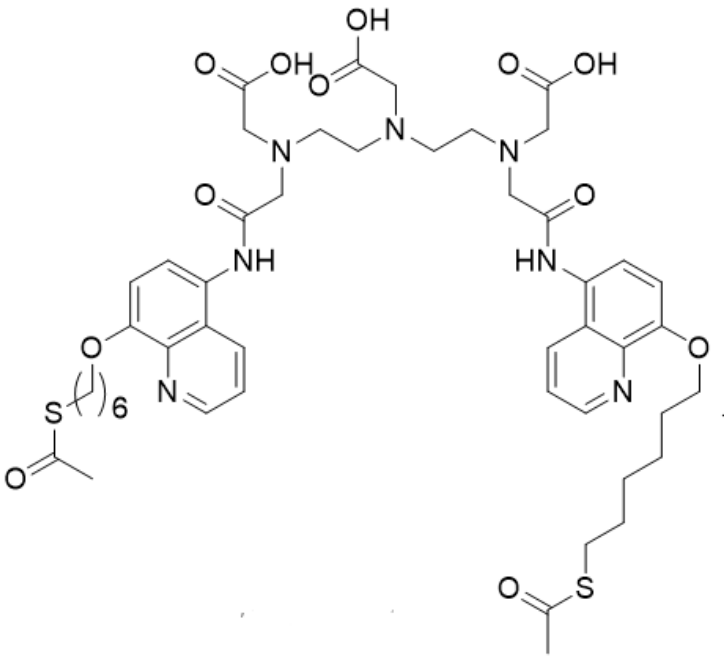

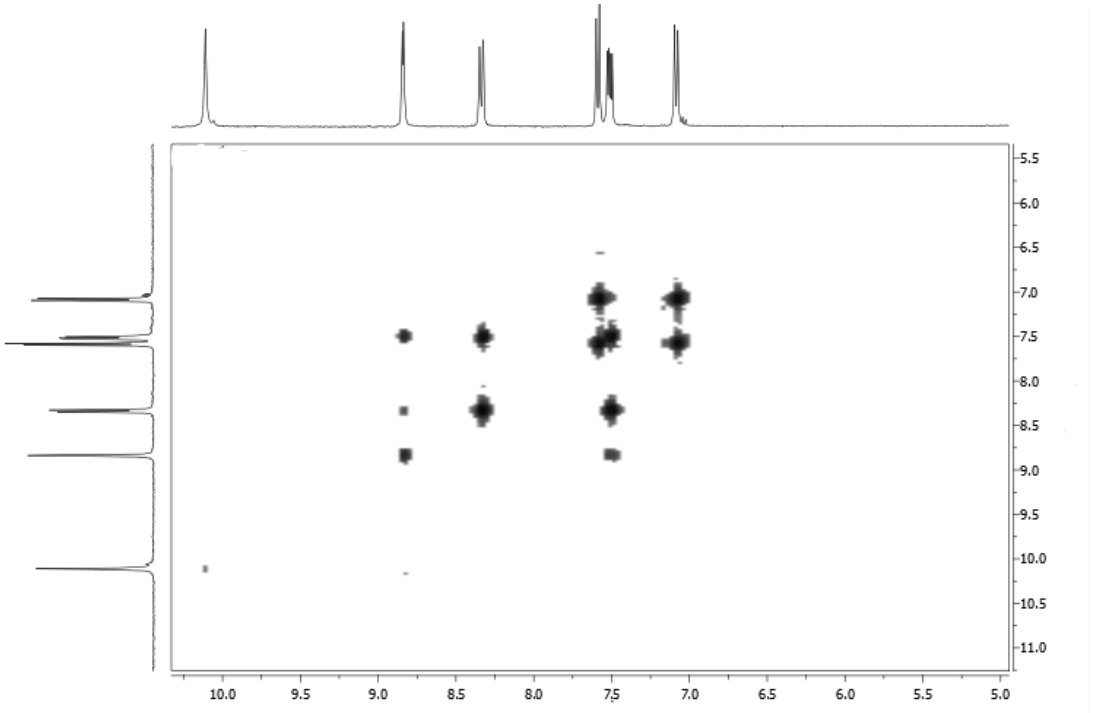

COSY NMR of aromatic region of ***H_3QuinSAc*** *in* d_6 *DMSO*

```
INSTRUM          spect
PROBHD   5 mm PADUL 13C
PULPROG      cosygpmfqf
TD               1024
SOLVENT           DMSO
NS                  4
DS                 16
SWH          5376.344 Hz
FIDRES        5.250336 Hz
AQ           0.0952820 sec
RG                2050
DW              93.000 usec
DE               6.50 usec
TE              294.2 K
D0           0.00000300 sec
D1           1.48750603 sec
D13          0.00000400 sec
D16          0.00020000 sec
IN0          0.00018600 sec

======== CHANNEL f1 ========
NUC1                1H
P1               9.50 usec
PL1              -4.00 dB
PL1W        24.29185867 W
SFO1        400.1326835 MHz

====== GRADIENT CHANNEL =====
GPNAM1         SINE.100
GPNAM2         SINE.100
GPNAM3         SINE.100
GPZ1            16.00 %
GPZ2            12.00 %
GPZ3            40.00 %
P16           1000.00 usec
ND0                 1
TD                256
SFO1         400.1327 MHz
FIDRES        21.001345 Hz
SW            13.436 ppm
FnMODE              QF
SI                1024
SF          400.1300000 MHz
WDW               SINE
SSB                  0
LB              0.00 Hz
GB                   0
PC                1.40
SI                512
MC2                 QF
SF          400.1300000 MHz
WDW               SINE
SSB                  0
LB              0.00 Hz
GB                   0
```

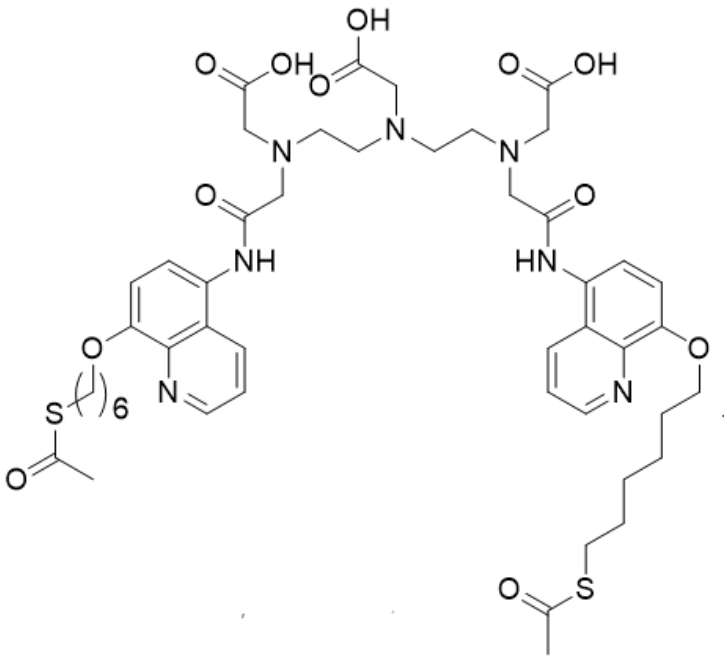

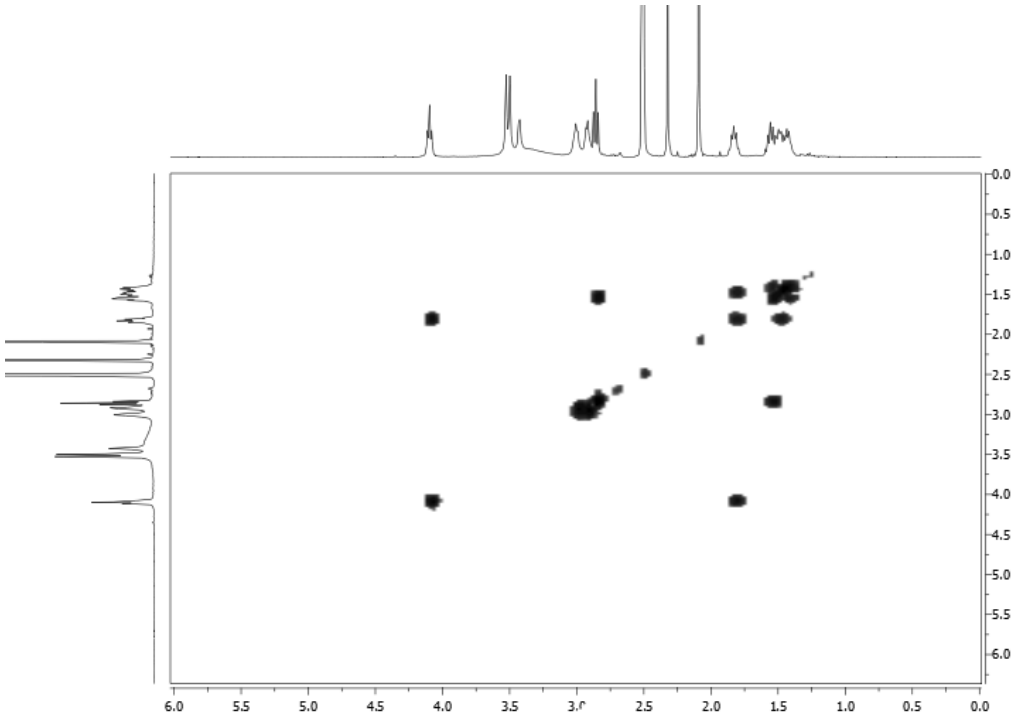

COSY NMR of aliphatic region of ***H_3QuinSAc*** *in d_6 DMSO*

INSTRUM	spect
PROBHD	5 mm PADUL 13C
PULPROG	hsqcetgp
TD	1024
SOLVENT	DMSO
NS	4
DS	16
SWH	4504.504 Hz
FIDRES	4.398930 Hz
AQ	0.1137140 sec
RG	2050
DW	111.000 usec
DE	6.50 usec
TE	295.4 K
CNST2	145.0000000
D0	0.00000300 sec
D1	1.48238695 sec
D4	0.00172414 sec
D11	0.03000000 sec
D13	0.00000400 sec
D16	0.00020000 sec
IN0	0.00003000 sec
ZGOPTNS	
---------- CHANNEL f1 ----------	
NUC1	1H
P1	9.50 usec
P2	19.00 usec
P28	0.00 usec
PL1	-4.00 dB
PL1W	24.29185867 W
SFO1	400.1322682 MHz
---------- CHANNEL f2 ----------	
CPDPRG2	garp
NUC2	13C
P3	8.90 usec
P4	17.80 usec
PCPD2	78.00 usec
PL2	-3.00 dB
PL12	16.00 dB
PL2W	58.63890457 W
PL12W	0.73822010 W
SFO2	100.6203124 MHz
---------- GRADIENT CHANNEL ----------	
GPNAM1	SINE.100
GPNAM2	SINE.100
GPZ1	80.00 %
GPZ2	20.10 %
P16	1000.00 usec
ND0	2
TD	256
SFO1	100.6203 MHz
FIDRES	65.108421 Hz
SW	165.650 ppm
FnMODE	Echo-Antiecho
SI	1024
SF	400.1300000 MHz
WDW	QSINE
SSB	2
LB	0.00 Hz
GB	0
PC	1.40
SI	512
MC2	echo-antiecho
SF	100.6127690 MHz
WDW	QSINE
SSB	2
LB	0.00 Hz
GB	0

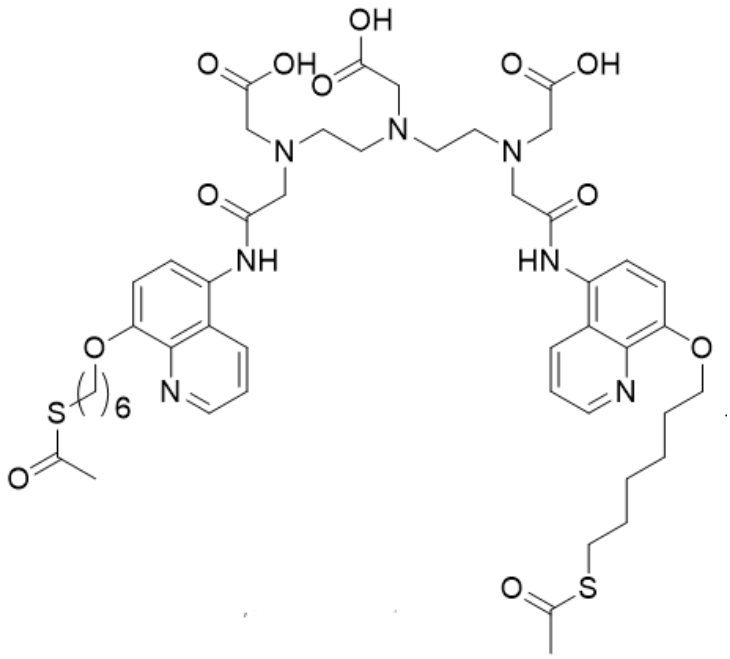

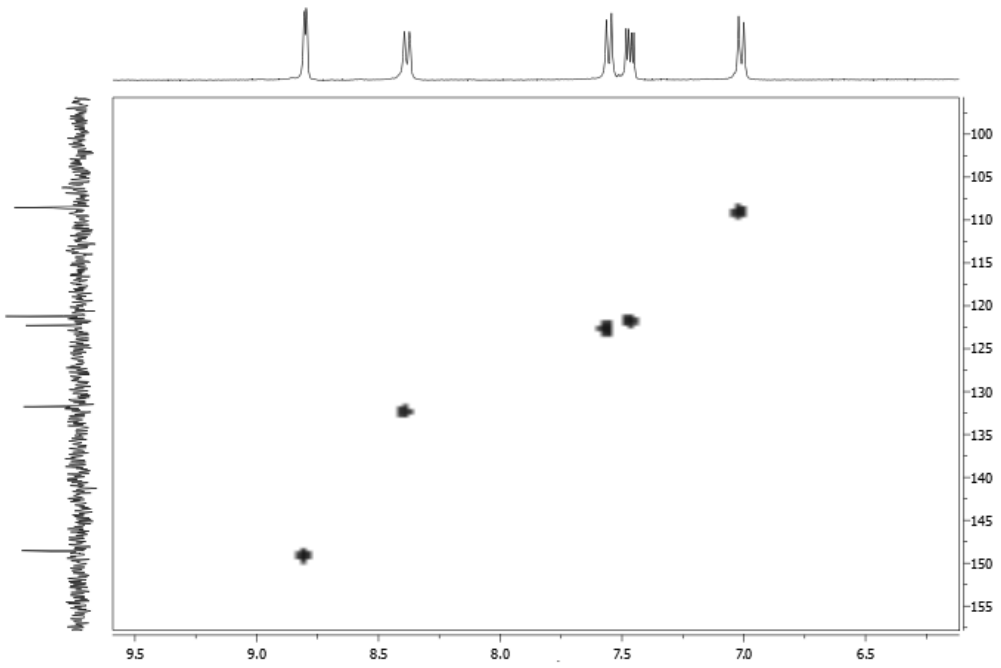

HSQC NMR of aromatic region of ***H_3QuinSAc*** *in* d_6 *DMSO*

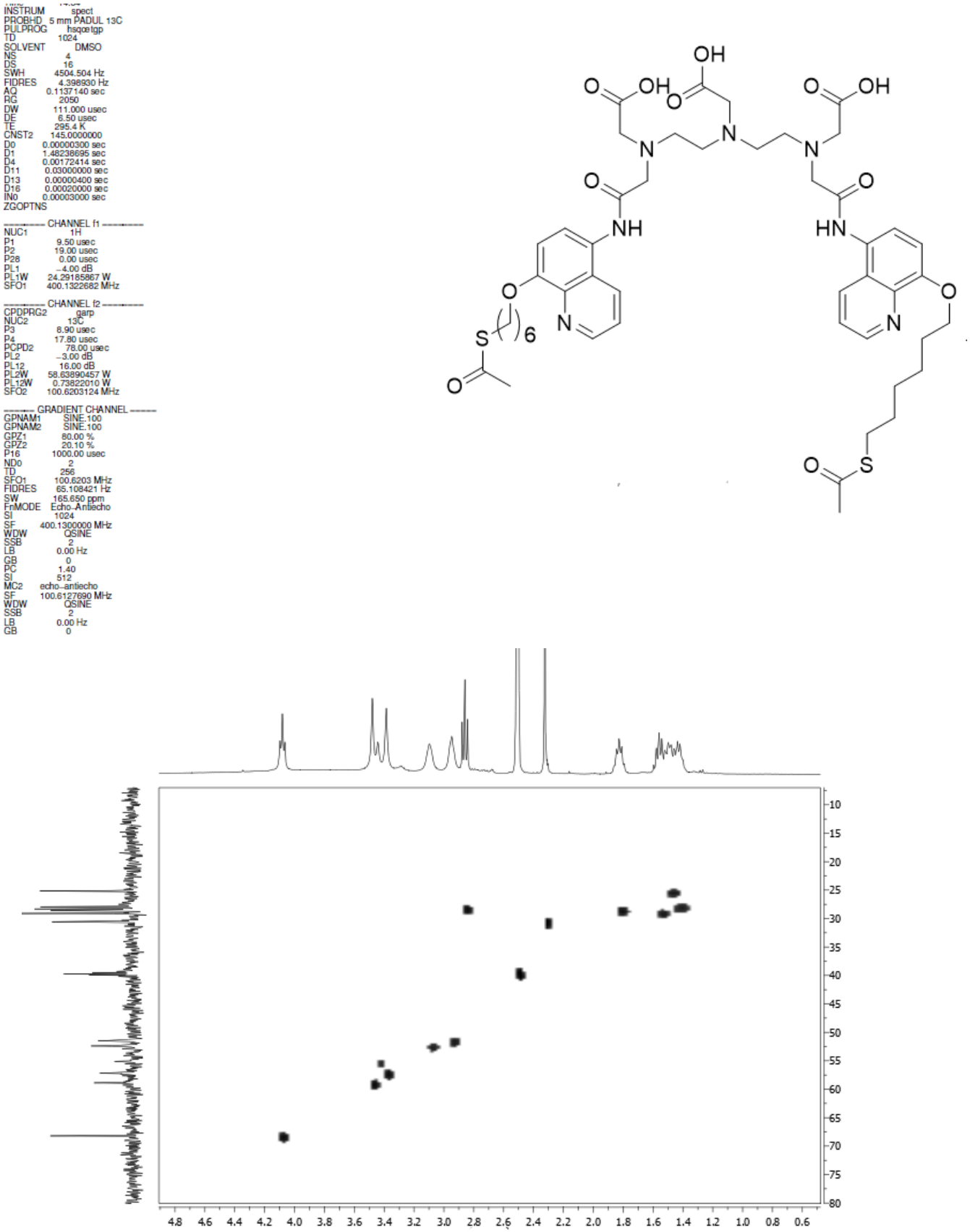

HSQC NMR of aliphatic region of ***H_3QuinSAc*** *in d_6 DMSO*

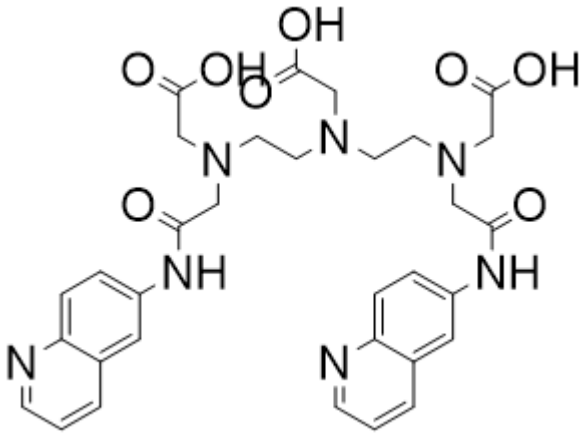

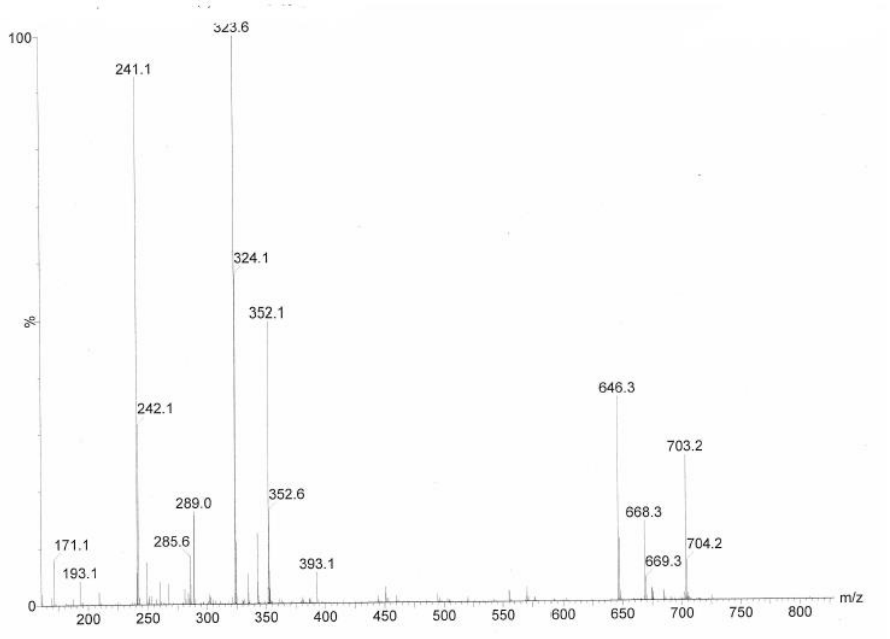

MS(ES-TOF)$^+$ of ***H_3Quin***

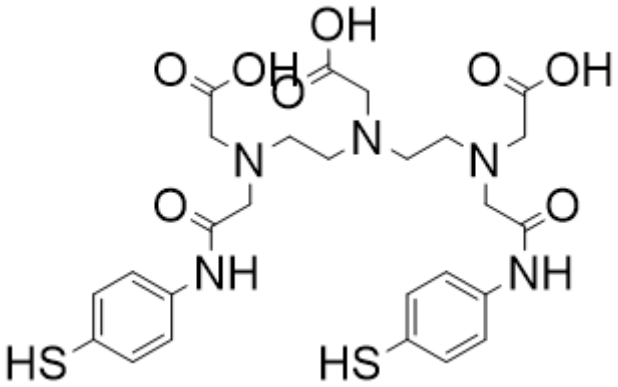

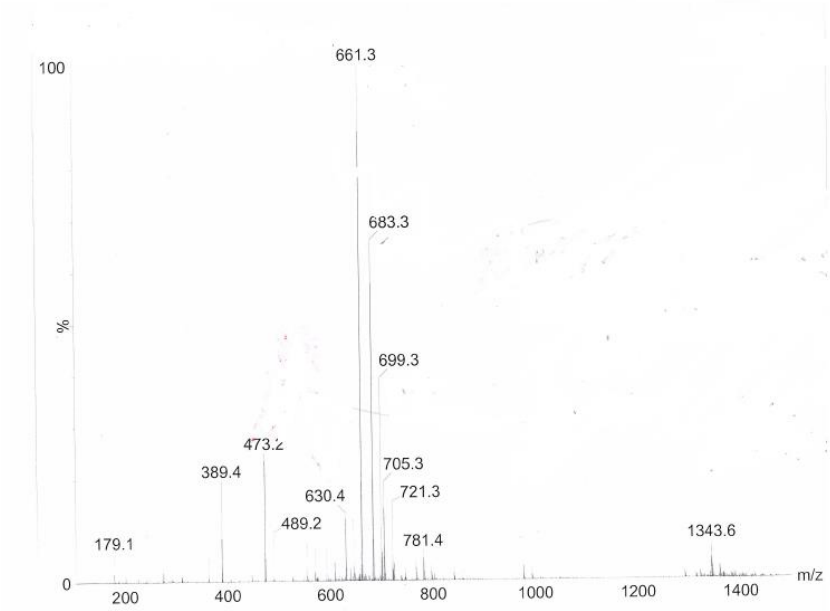

MS(ES-TOF)$^+$ of ***H_3SH***

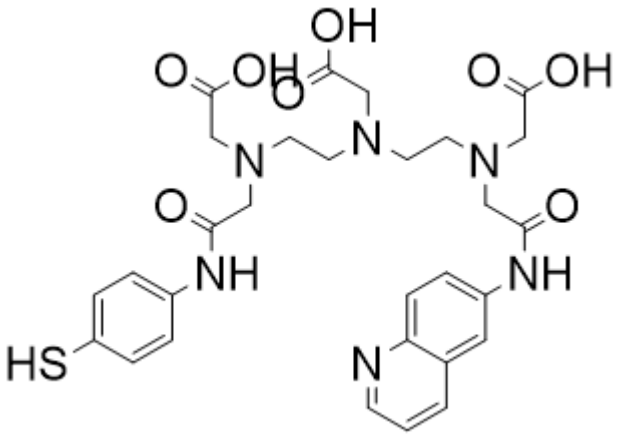

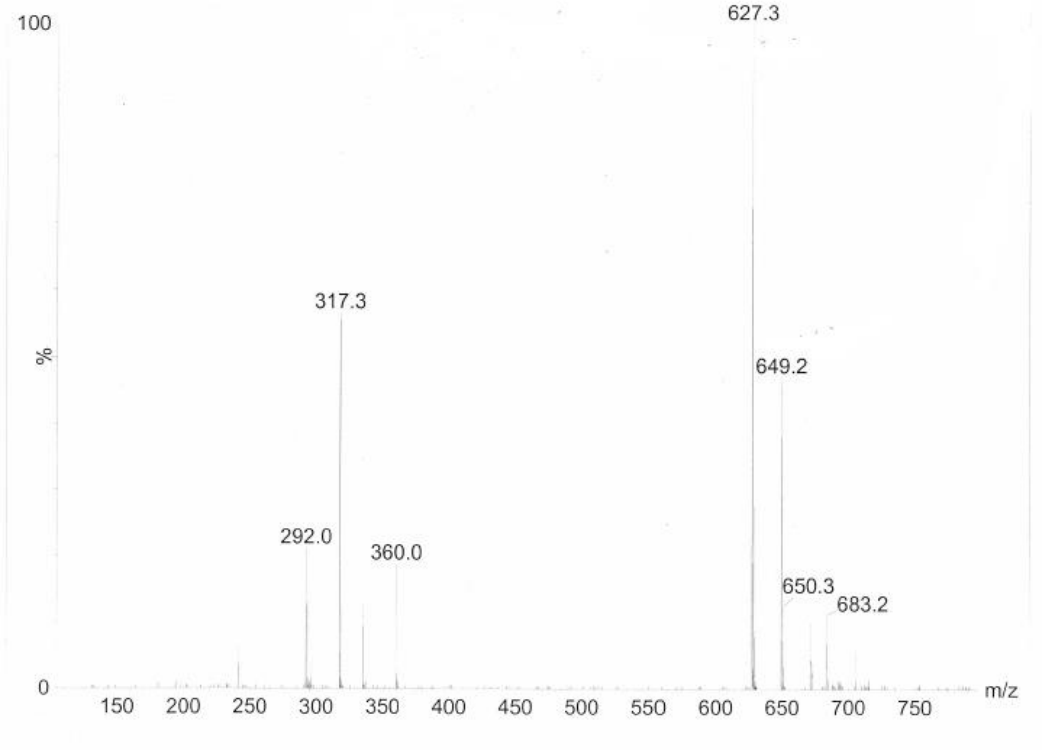

MS(ES-TOF)$^+$ of ***H_3QSH***

```
INSTRUM          spect
PROBHD   5 mm PADUL 13C
PULPROG          zg30
TD              32768
SOLVENT           DMSO
NS                 32
DS                  2
SWH          8223.685 Hz
FIDRES        0.250967 Hz
AQ           1.9922944 sec
RG                362
DW             60.800 usec
DE             16.65 usec
TE             296.0 K
D1          1.50000000 sec
TD0                1

======== CHANNEL f1 ========
SFO1       400.1324008 MHz
NUC1              1H
P1              11.06 usec
PLW1       24.29199982 W

F2 - Processing parameters
SI              32768
SF         400.1300000 MHz
WDW               EM
SSB      0
LB             0.30 Hz
GB       0
PC             1.00
```

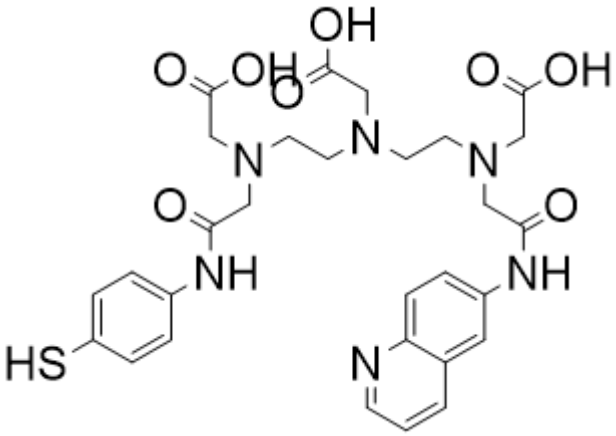

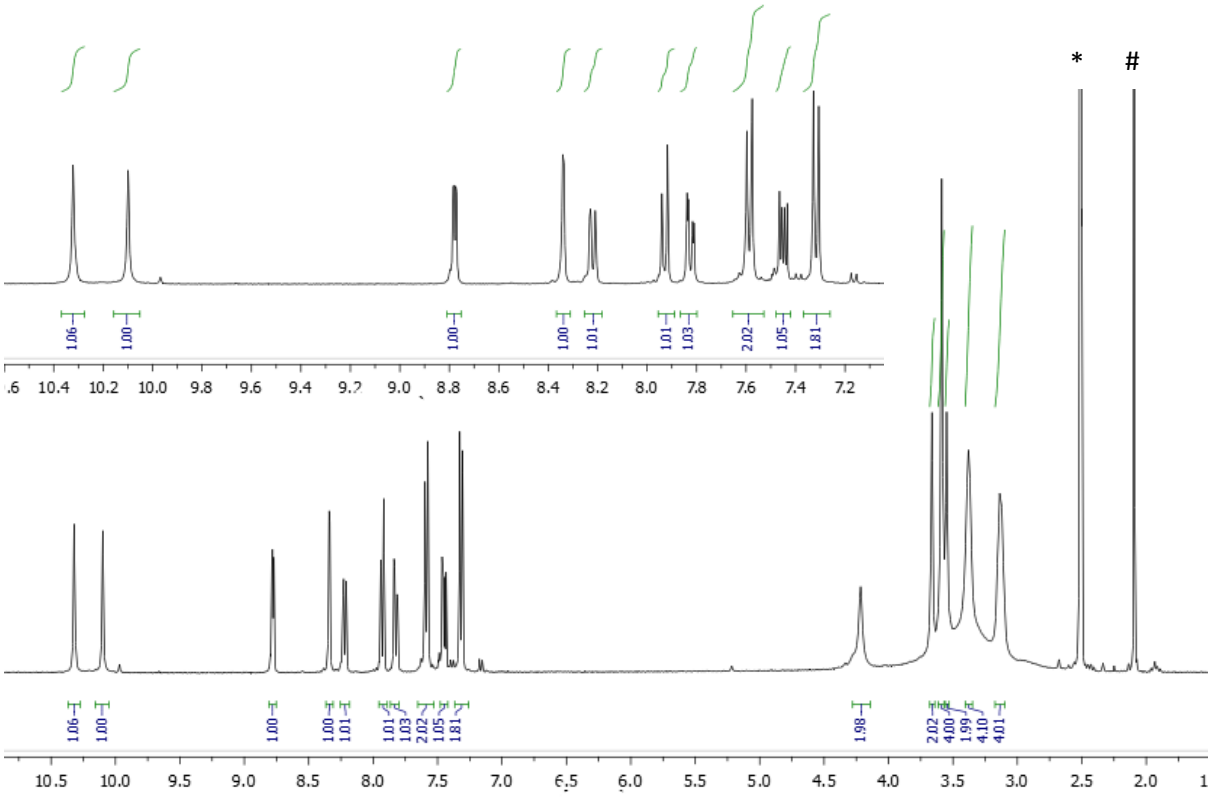

*[1]H NMR of **H_3QSH** in d_6 DMSO*

** = residual solvent resonance, # = water*

INSTRUM	spect
PROBHD	5 mm PADUL 13C
PULPROG	pendantns
TD	65536
SOLVENT	DMSO
NS	512
DS	4
SWH	25252.525 Hz
FIDRES	0.385323 Hz
AQ	1.2976128 sec
RG	2050
DW	19.800 usec
DE	6.50 usec
TE	296.1 K
CNST2	145.0000000
CNST3	1.0000000
CNST4	5.0000000
D1	1.50000000 sec
D2	0.00172414 sec
D3	0.00431034 sec
D12	0.00002000 sec
D13	0.00000400 sec
TD0	1

======== CHANNEL f1 ========

SFO1	100.6242690 MHz
NUC1	13C
P1	8.80 usec
P2	17.60 usec
PLW1	58.63899994 W

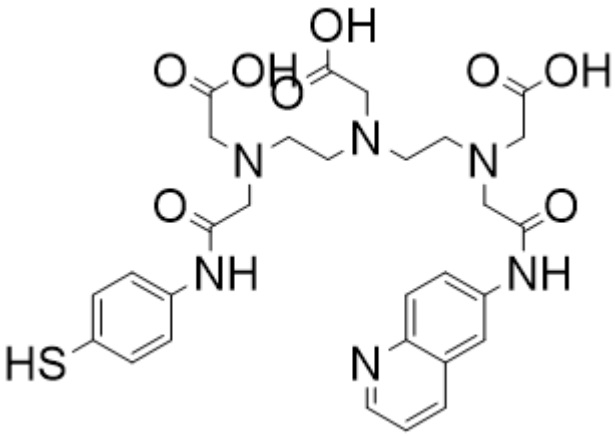

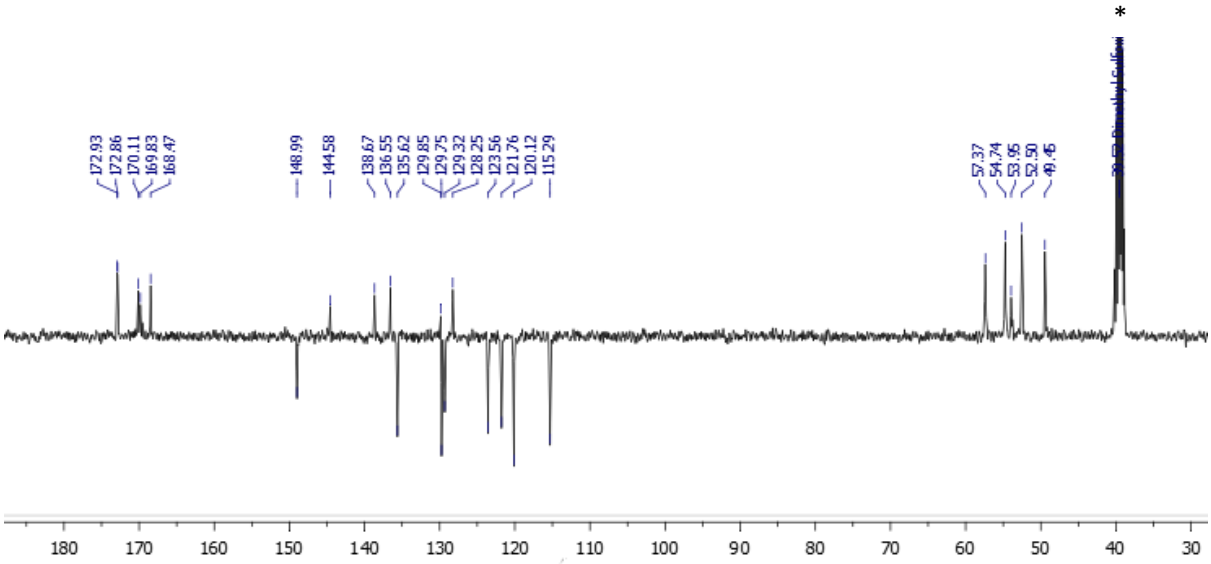

$^{13}C\{^{1}H\}$ PENDANT NMR of ***H_3QSH*** *in d_6 DMSO*

** = residual solvent resonance*

INSTRUM spect
PROBHD 5 mm PADUL 13C
PULPROG cosygpmfqf
TD 1024
SOLVENT DMSO
NS 4
DS 16
SWH 5000.000 Hz
FIDRES 4.882813 Hz
AQ 0.1024000 sec
RG 2050
DW 100.000 usec
DE 6.50 usec
TE 295.9 K
D0 0.00000300 sec
D1 1.48033798 sec
D13 0.00000400 sec
D16 0.00020000 sec
IN0 0.00020000 sec

---------- CHANNEL f1 ----------
SFO1 400.1330365 MHz
NUC1 1H
P1 11.06 usec
PLW1 24.29199982 W

-------- GRADIENT CHANNEL -------
GPNAM[1] SMSQ10.100
GPNAM[2] SMSQ10.100
GPNAM[3] SMSQ10.100
GPZ1 16.00 %
GPZ2 12.00 %
GPZ3 40.00 %
P16 1000.00 usec

F1 - Acquisition parameters
TD 256
SFO1 400.133 MHz
FIDRES 19.531250 Hz
SW 12.496 ppm
FnMODE QF

F2 - Processing parameters
SI 1024
SF 400.1300000 MHz
WDW SINE
SSB 0
LB 0 Hz
GB 0
PC 1.40

F1 - Processing parameters
SI 512
MC2 QF
SF 400.1300000 MHz
WDW SINE
SSB 0
LB 0 Hz
GB 0

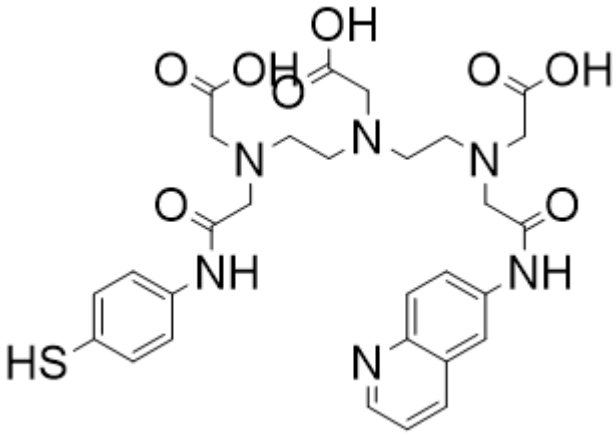

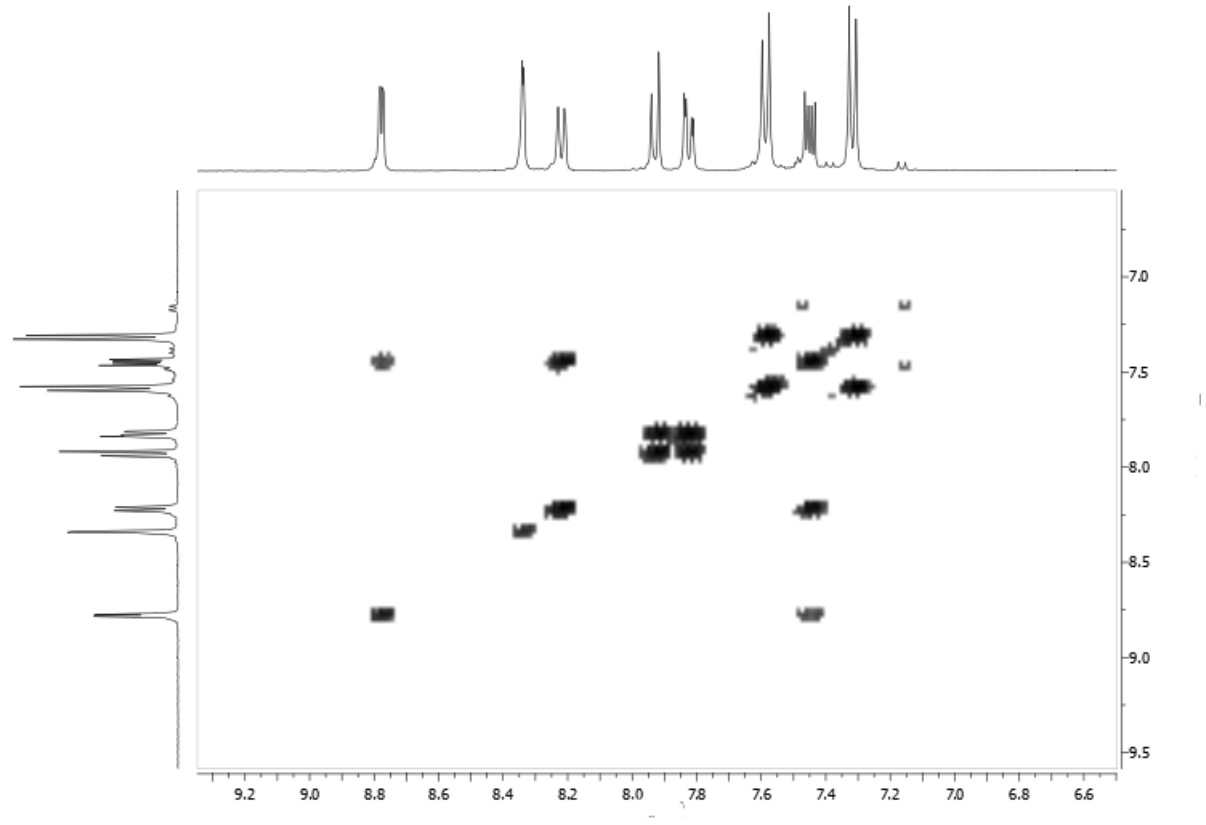

COSY NMR of aromatic region of ***H_3QSH*** *in* d_6 *DMSO*

```
INSTRUM          spect
PROBHD  5 mm PADUL 13C
PULPROG      cosygpmfqf
TD               1024
SOLVENT          DMSO
NS                  4
DS                 16
SWH          5000.000 Hz
FIDRES          4.882813 Hz
AQ           0.1024000 sec
RG                2050
DW            100.000 usec
DE              6.50 usec
TE              295.9 K
D0           0.00000300 sec
D1           1.48033798 sec
D13          0.00000400 sec
D16          0.00020000 sec
IN0          0.00020000 sec

========== CHANNEL f1 ==========
SFO1        400.1330365 MHz
NUC1               1H
P1              11.06 usec
PLW1        24.29199982 W

======== GRADIENT CHANNEL =======
GPNAM[1]    SMSQ10.100
GPNAM[2]    SMSQ10.100
GPNAM[3]    SMSQ10.100
GPZ1            16.00 %
GPZ2            12.00 %
GPZ3            40.00 %
P16          1000.00 usec

F1 - Acquisition parameters
TD                 256
SFO1        400.133 MHz
FIDRES          19.531250 Hz
SW              12.496 ppm
FnMODE             QF

F2 - Processing parameters
SI                1024
SF          400.1300000 MHz
WDW               SINE
SSB                  0
LB               0 Hz
GB                   0
PC                1.40

F1 - Processing parameters
SI                 512
MC2                QF
SF          400.1300000 MHz
WDW               SINE
SSB                  0
LB               0 Hz
GB                   0
```

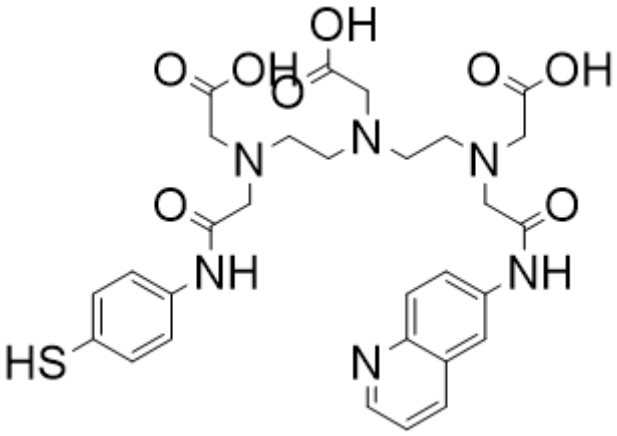

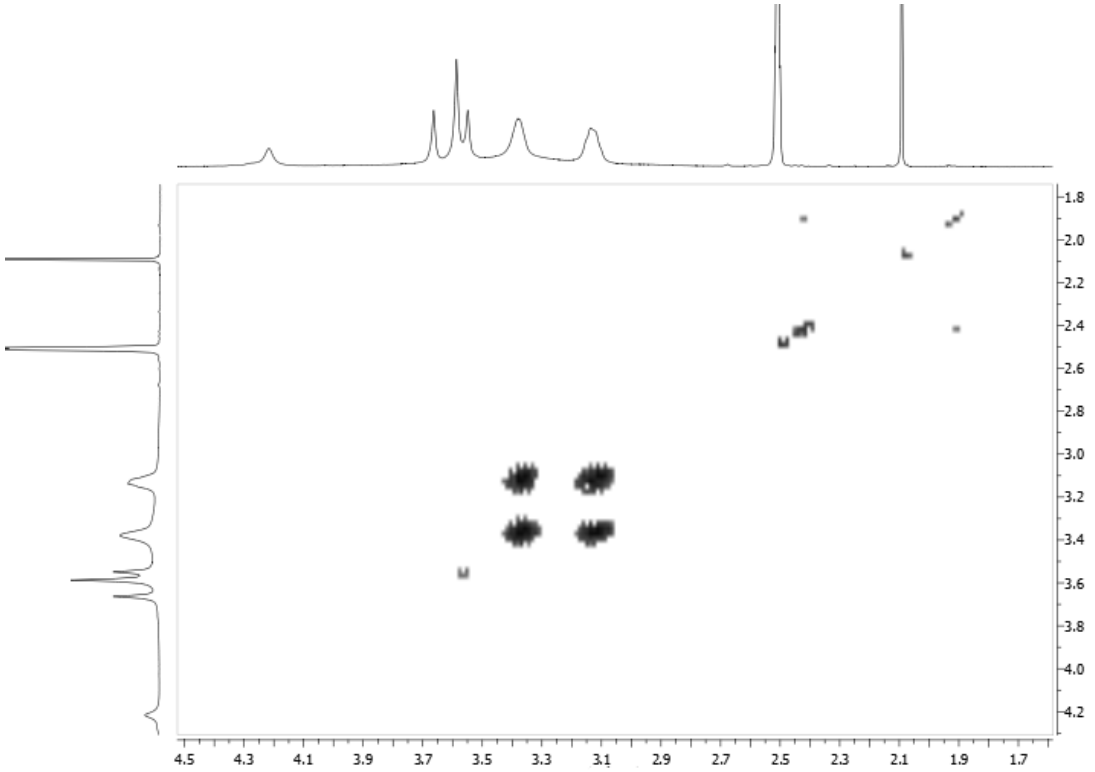

COSY NMR of aliphatic region of ***H_3QSH*** *in* d_6 *DMSO*

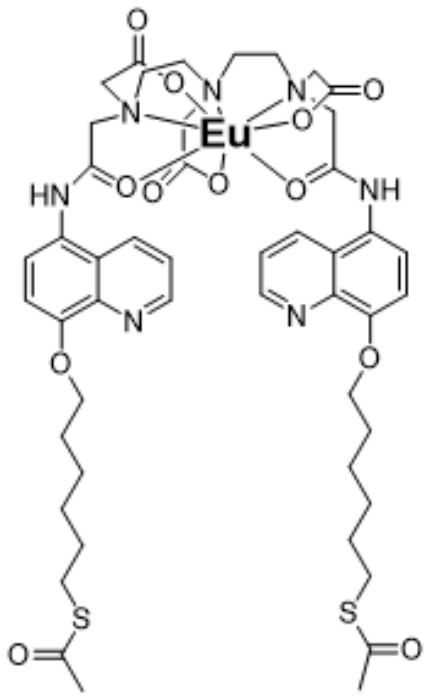

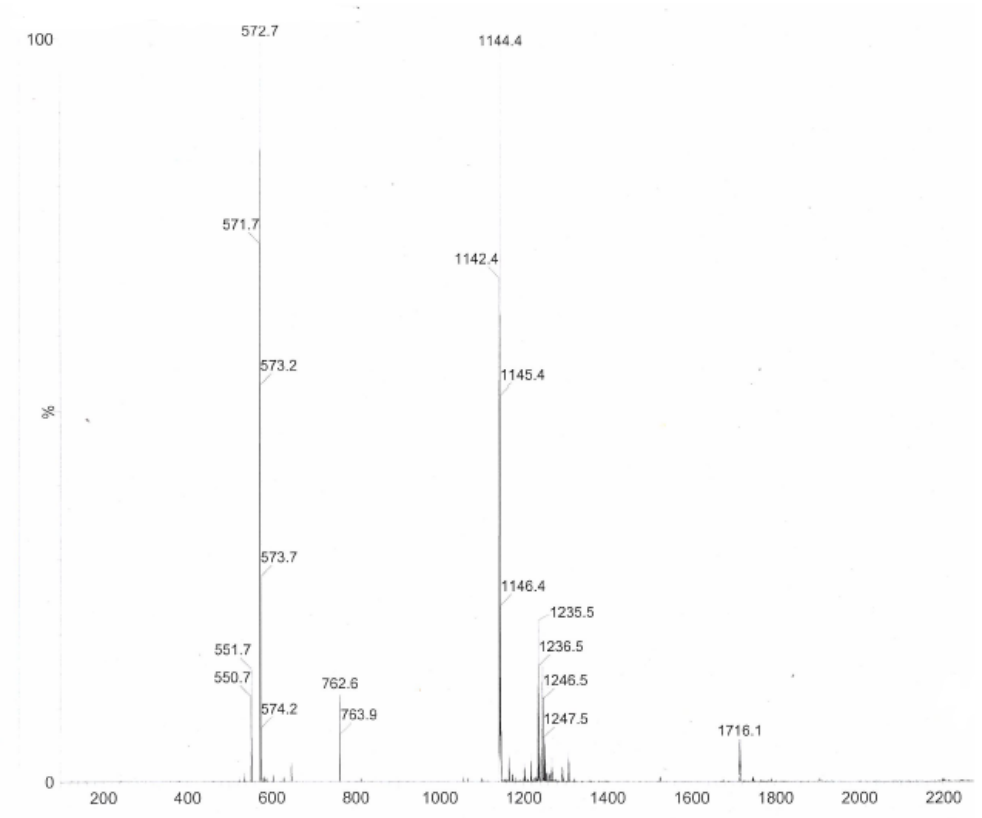

MS (ES-TOF)$^+$ of ***EuQuinSAc***

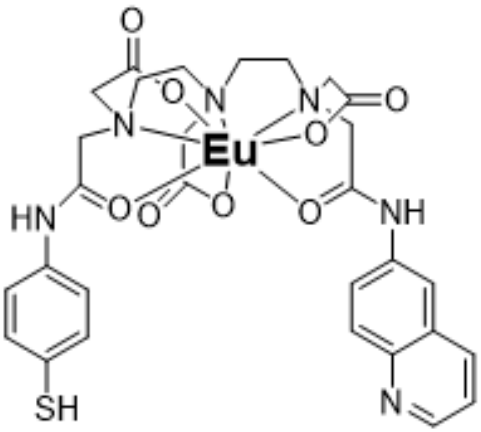

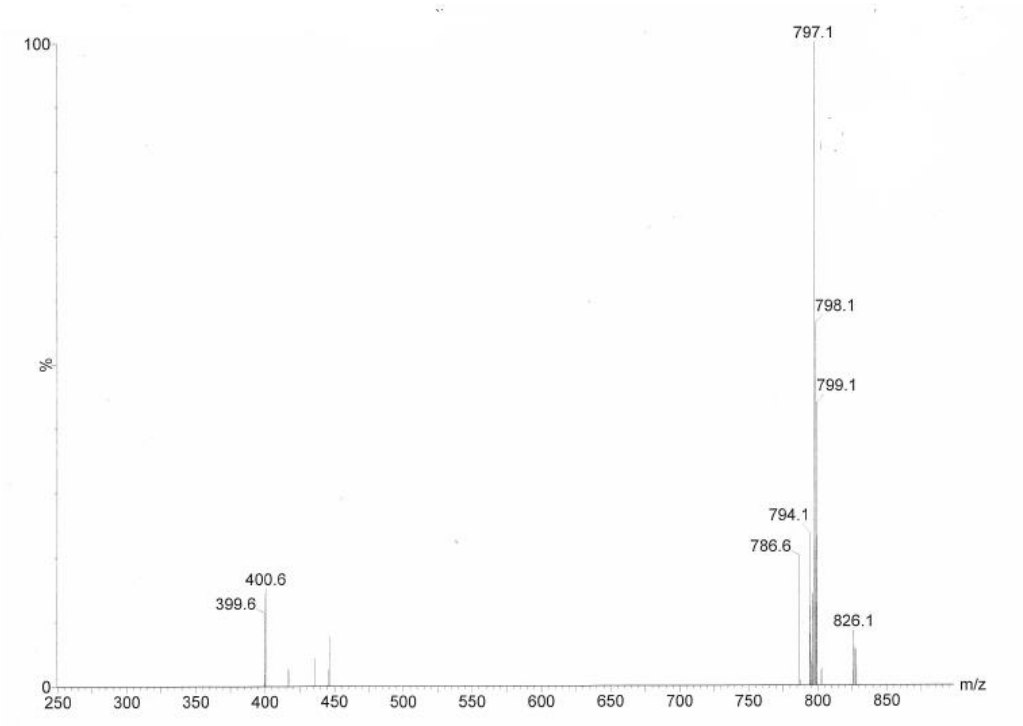

MS (ES-TOF)$^{+}$ of ***EuQSH***

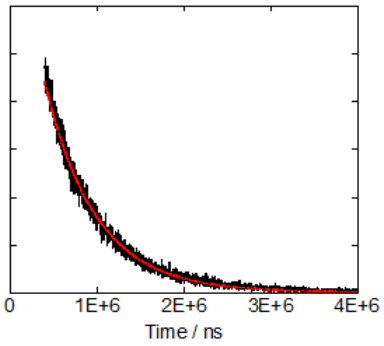

*Lifetime of **EuQSH** in H_2O, λ_{exc} = 320 nm and λ_{em} = 614 nm*

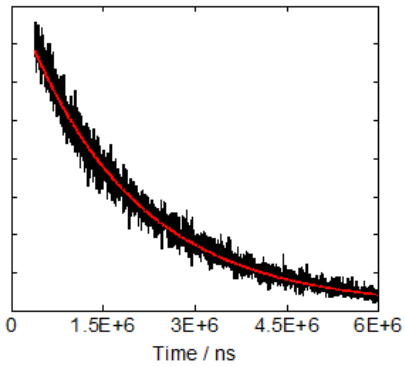

*Lifetime of **EuQSH** in D_2O, λ_{exc} = 320 nm and λ_{em} = 614 nm*

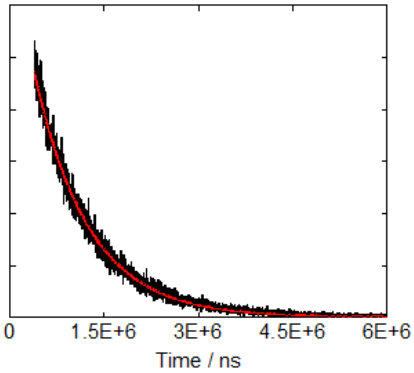

*Lifetime of **EuQSH** in MeOH, λ_{exc} = 320 nm and λ_{em} = 614 nm*

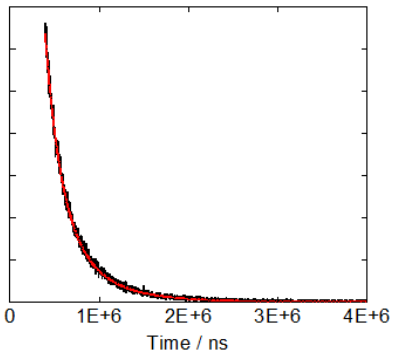

*Lifetime of **EuQuinSAc** in H_2O, λ_{exc} = 320 nm and λ_{em} = 614 nm*

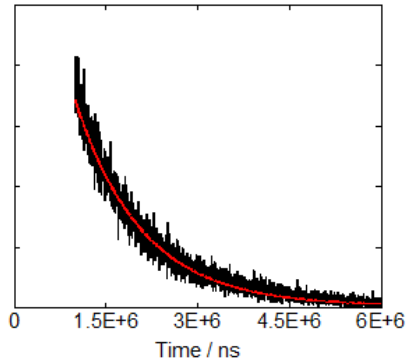

*Lifetime of **EuQuinSAc** in D_2O, λ_{exc} = 320 nm and λ_{em} = 614 nm*

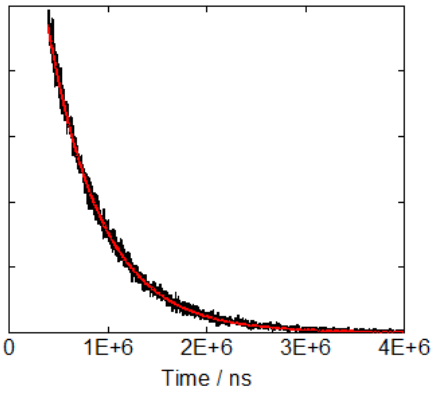

*Lifetime of **EuQuinSAc** in MeOH, λ_{exc} = 320 nm and λ_{em} = 614 nm*

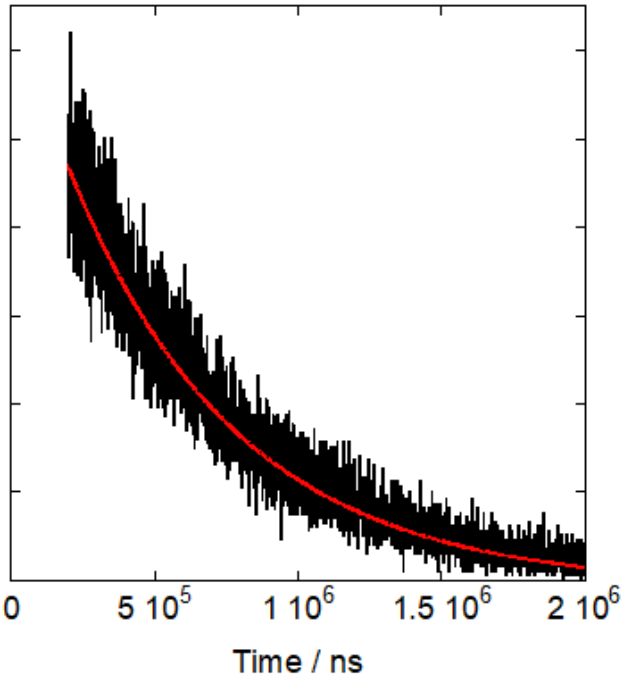

*Lifetime of **EuQS@Au** in H_2O, λ_{exc} = 320 nm and λ_{em} = 614 nm*

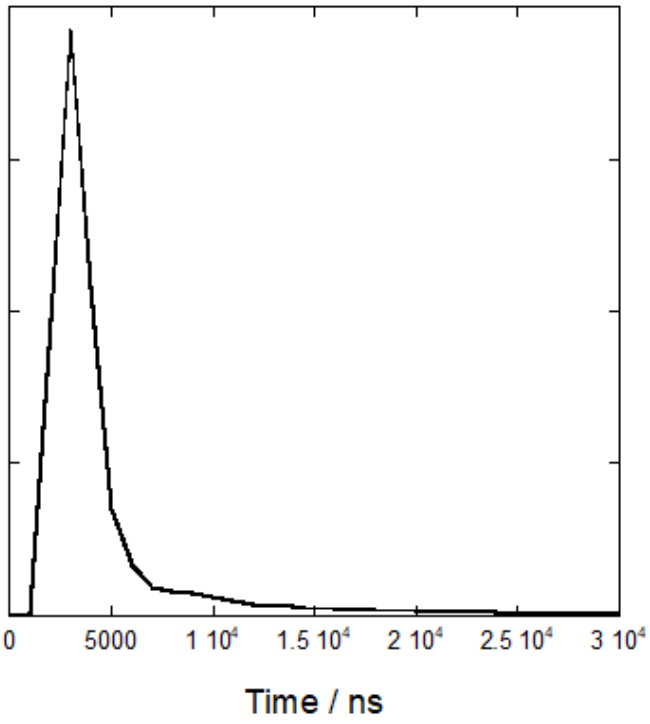

*Lifetime of IRF **Cit@Au** in H_2O, λ_{exc} = 320 nm and λ_{em} = 614 nm*

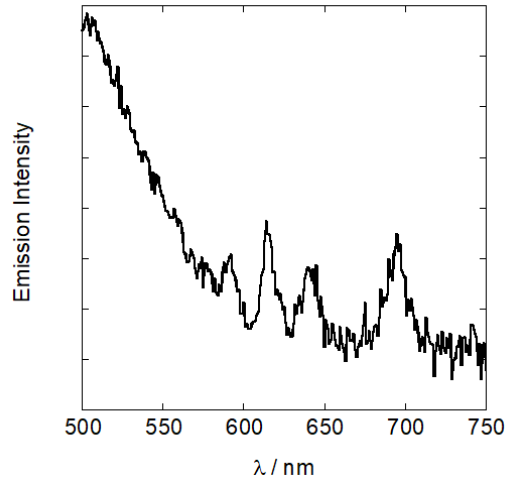

Emission spectrum of ***κstandard.EuQuinSAc@Au****.* λ_{exc} *= 320 nm, corrected for PMT response*

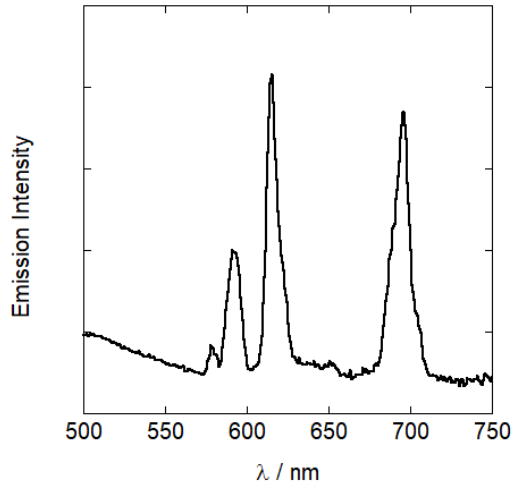

Emission spectrum of ***λstandard.EuQS@Au,*** λ_{exc} *= 320 nm, corrected for PMT response*

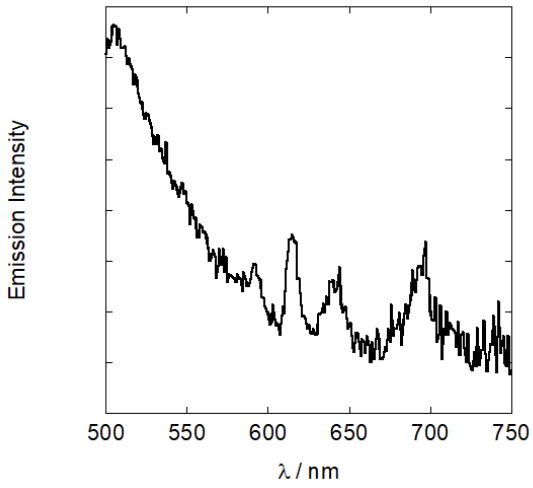

Emission spectrum of ***λstandard.EuQuinSAc@Au,*** λ_{exc} *= 320 nm, corrected for PMT response*

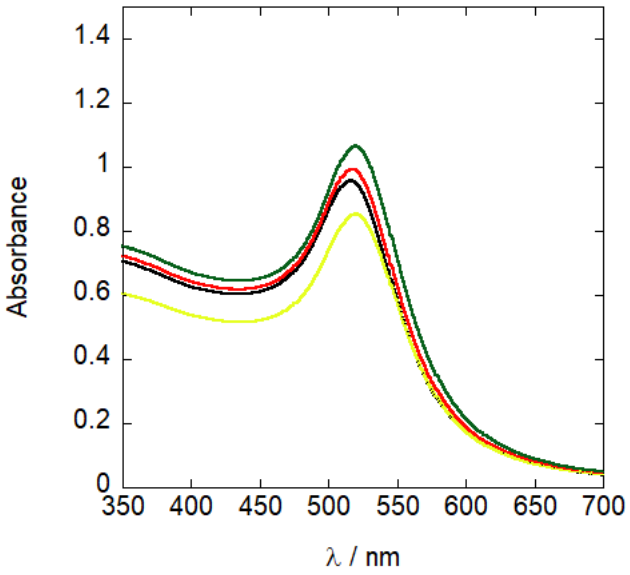

*Preparation of **κnew.EuQS@Au** as monitored via UV Vis*

*Change in SPR of **Cit@Au** (3.2 nM in water) as a methanolic solution of **EuQSH** is added in to a final concentration of 1 μM, followed by the addition of a solution of κnew in 0.001 M PBS to a final concentration of 60 nM. The yellow curve is post gel filtration to show that no aggregation occurs from the purification method*

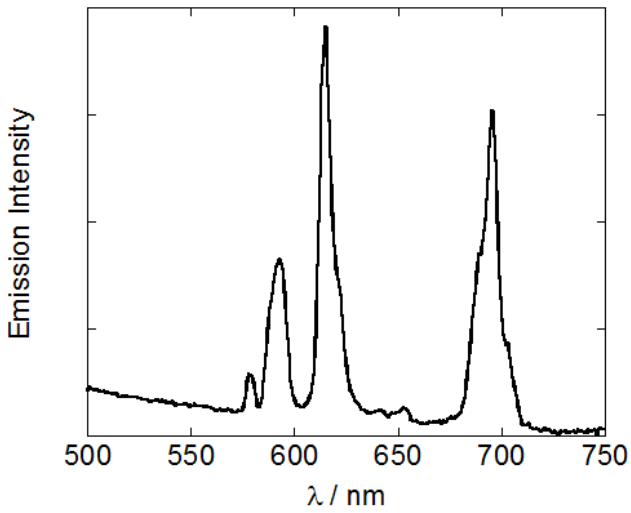

*Emission spectrum of **κnew.EuQS@Au,** λ_{exc} = 320 nm, corrected for PMT response*

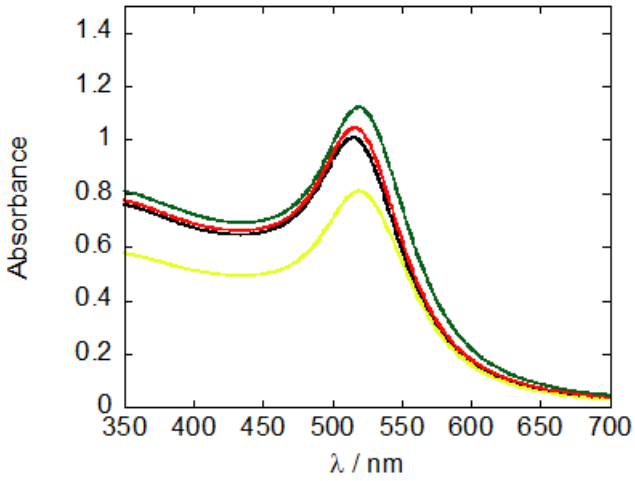

*Preparation of **κfur.EuQS@Au** as monitored via UV Vis*

*Change in SPR of **Cit@Au** (3.2 nM in water) as a methanolic solution of **EuQSH** is added in to a final concentration of 1 μM, followed by the addition of a solution of κfur in 0.001 M PBS to a final concentration of 60 nM. The yellow curve is post gel filtration to show that no aggregation occurs from the purification method*

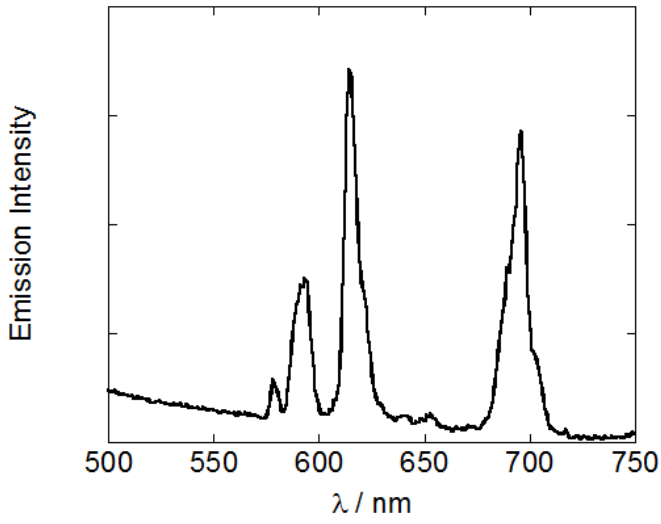

*Emission spectrum of **κfur.EuQS@Au,** λ_{exc} = 320 nm, corrected for PMT response*

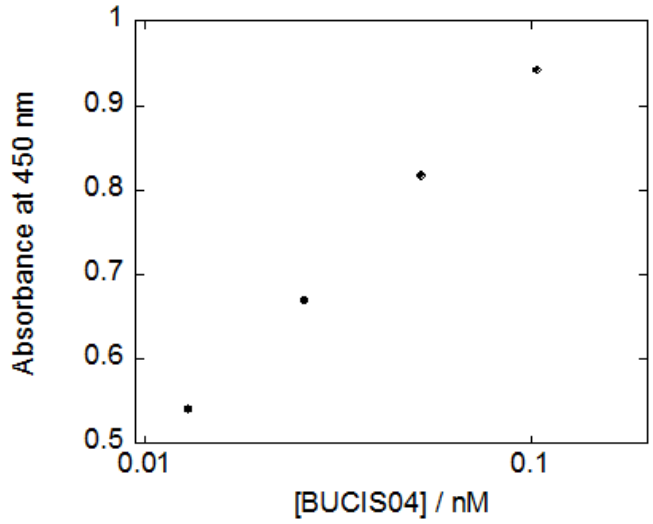

*ELISA assay of **BUCIS04** against surface immobilised κnew as measured via the absorbance signal obtained with TMP and HRP*

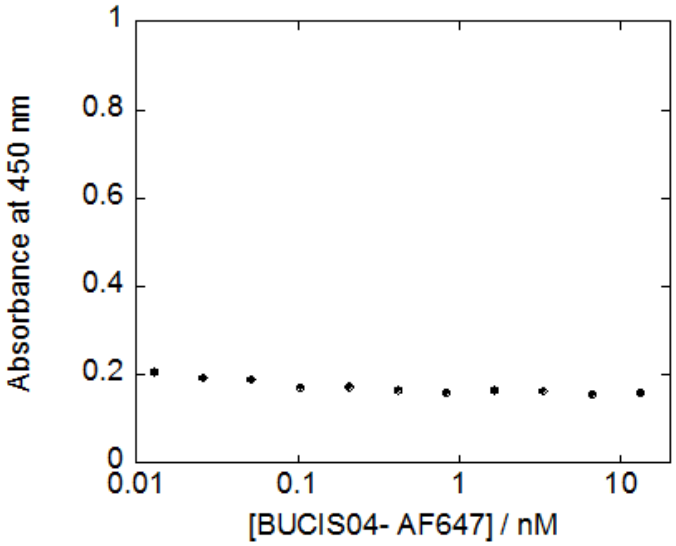

*Blank ELISA assay of **BUCIS04 – AF647** showing the absorption signal with increasing concentrations of **BUCIS04 – AF647***

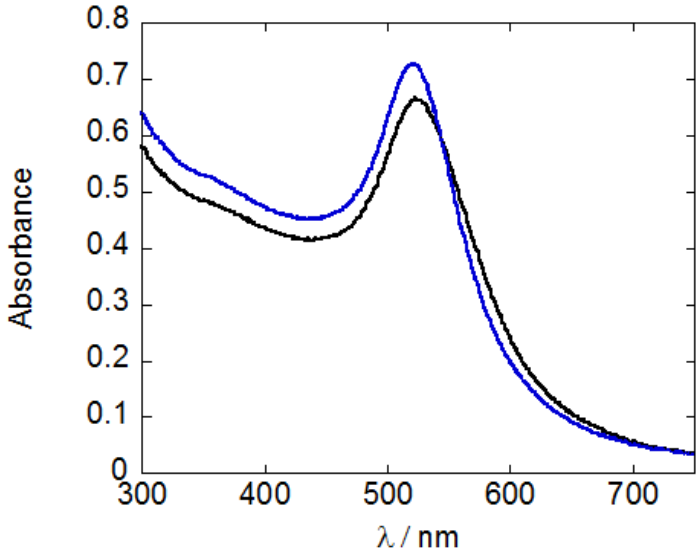

Absorption spectrum of ***κstandard.EuQS@Au*** *in Tris HCl (50 mM) (blue) and PBS (0.01 M) (black)*

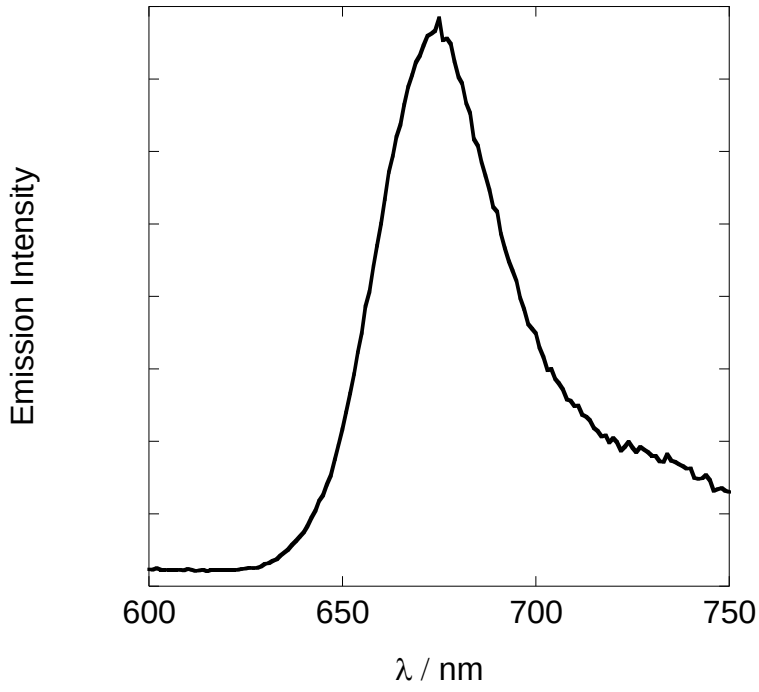

Emission spectrum of ***BUCIS04-AF647****,* λ_{exc} *= 320 nm, corrected for PMT response*

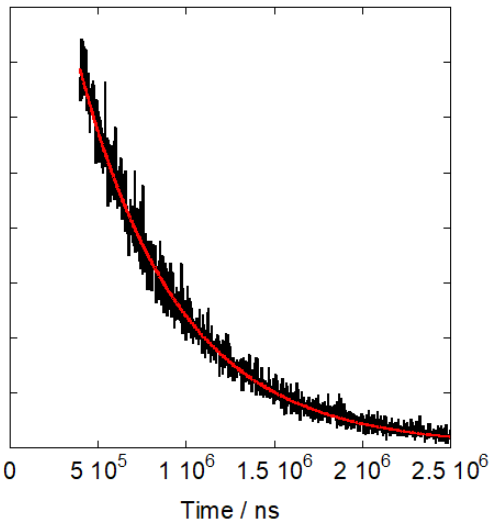

Lifetime of ***κstandard.EuQS@Au*** *in water,* λ_{exc} *= 320 nm and* λ_{em} *= 614 nm*

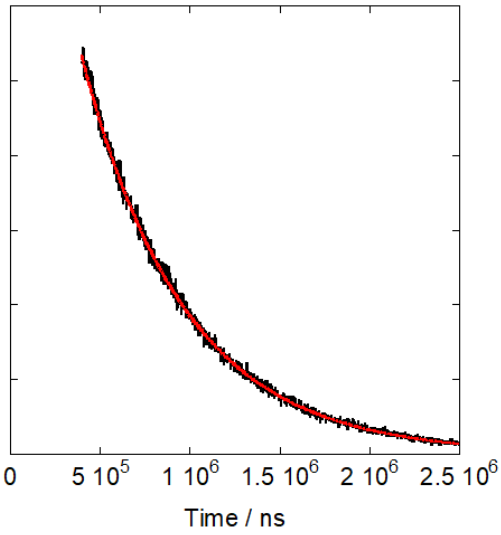

Lifetime of ***κstandard.EuQS@Au*** *in tris HCl buffer,* λ_{exc} *= 320 nm and* λ_{em} *= 614 nm*

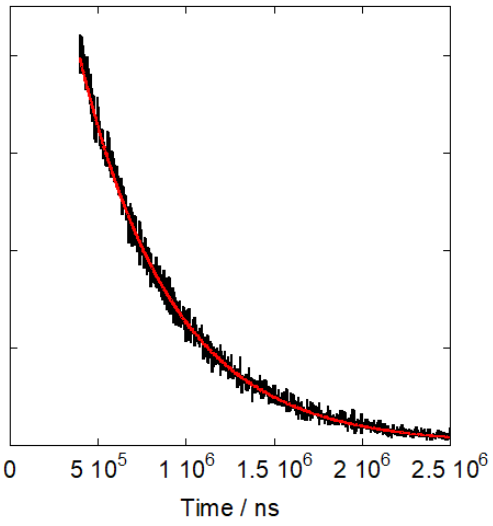

Lifetime of ***κstandard.EuQS@Au*** *with* ***BUCIS04-AF647****,* λ_{exc} *= 320 nm and* λ_{em} *= 614 nm*

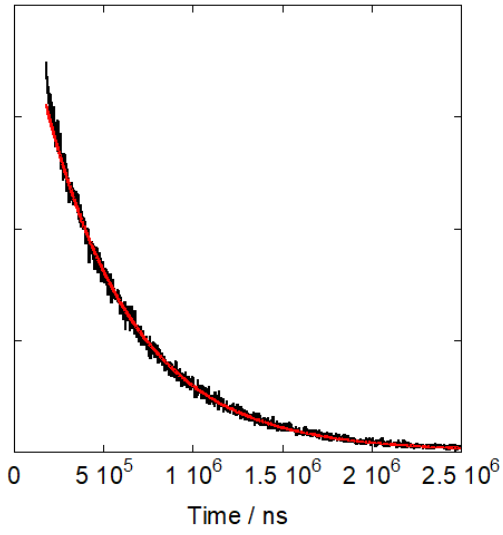

Lifetime of ***κstandard.EuQS@Au*** *with* ***BUCIS04-AF647*** *in tris HCl buffer,* λ_{exc} *= 320 nm and* λ_{em} *= 614 nm*

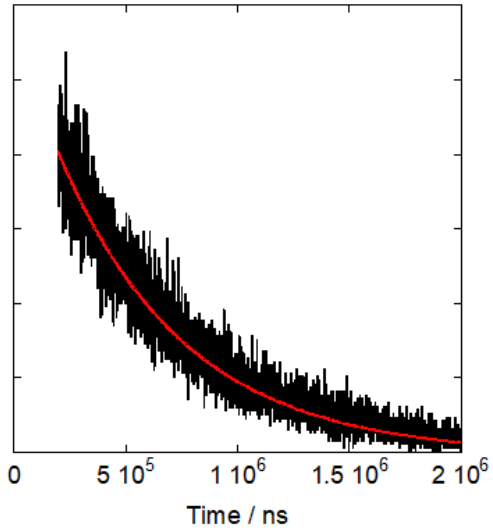

Lifetime of ***κnew.EuQS@Au,*** λ_{exc} *= 320 nm and* λ_{em} *= 614 nm*

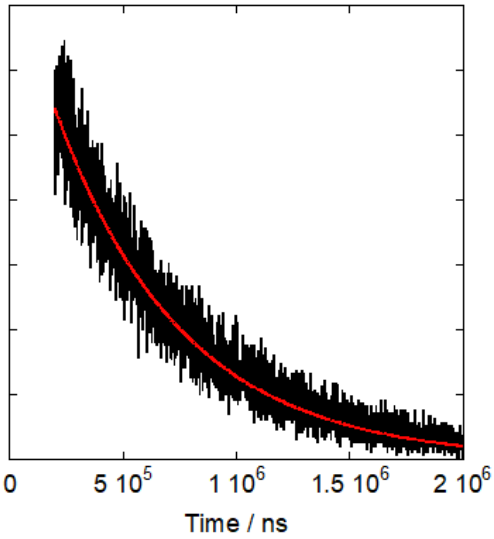

Lifetime of ***κnew.EuQS@Au*** *in tris HCl buffer,* λ_{exc} *= 320 nm and* λ_{em} *= 614 nm*

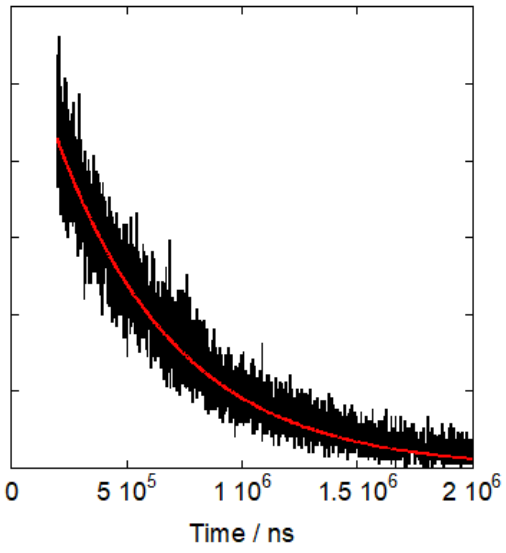

Lifetime of ***κnew.EuQS@Au*** *with* ***BUCIS04-AF647****,* λ_{exc} *= 320 nm and* λ_{em} *= 614 nm*

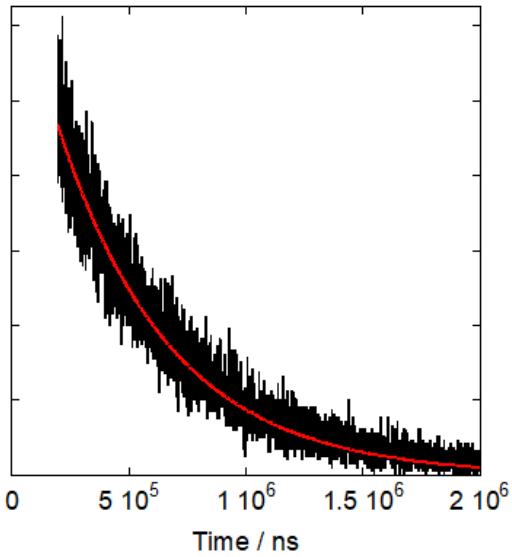

Lifetime of ***κnew.EuQS@Au*** *with* ***BUCIS04-AF647,*** *in tris HCl buffer* λ_{exc} *= 320 nm and* λ_{em} *= 614 nm*

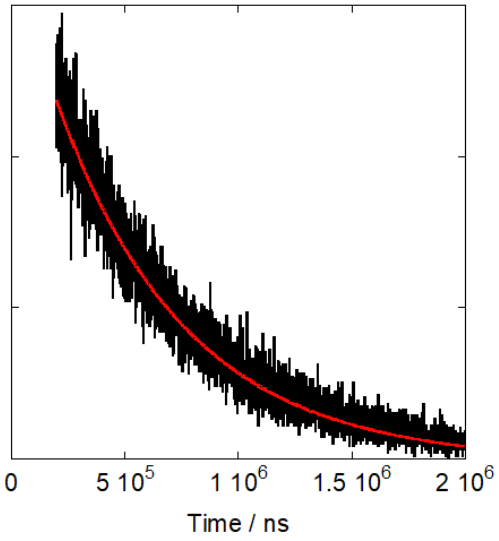

Lifetime of ***κfur.EuQS@Au****,* λ_{exc} *= 320 nm and* λ_{em} *= 614 nm*

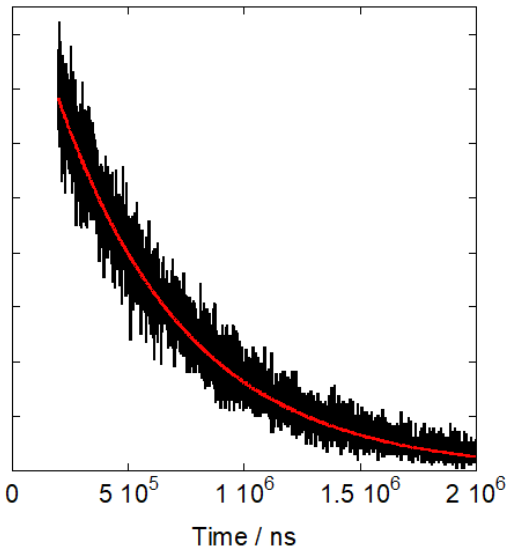

Lifetime of ***κfur.EuQS@Au*** *in tris HCl buffer,* λ_{exc} *= 320 nm and* λ_{em} *= 614 nm*

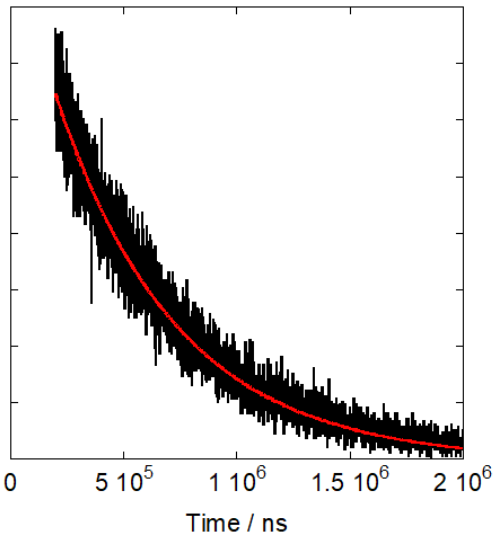

Lifetime of ***κfur.EuQS@Au*** *with* ***BUCIS04-AF647****,* λ_{exc} *= 320 nm and* λ_{em} *= 614 nm*

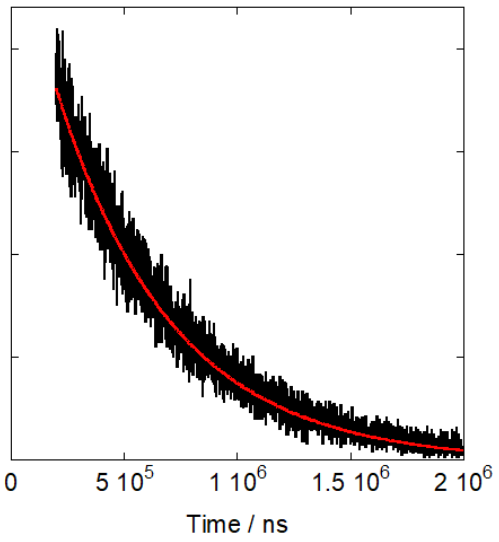

Lifetime of ***κfur.EuQS@Au*** *with* ***BUCIS04-AF647,*** *in tris HCl buffer* λ_{exc} *= 320 nm and* λ_{em} *= 614 nm*

Chapter 3 appendix

List of appendices

All Lifetime data was gathered with, λ_{exc} = 320 nm and λ_{em} = 614 nm.

1. *Lifetime of **EuQS@Au** in water*
2. *Lifetime of **EuQS@Au** in tris HCl*
3. *Lifetime of **EuQS@Au** in water incubated with **BUCIS04-AF647***
4. *Lifetime of **EuQS@Au** in tris HCl incubated with **BUCIS04-AF647***
5. *Lifetime of **EuQS@Au** in 1% BSA*
6. *Lifetime of **EuQS@Au** in 1% BSA in tris HCl*
7. *Lifetime of **EuQS@Au** in 1% BSA incubated with **BUCIS04-AF647***
8. *Lifetime of **EuQS@Au** in 1% BSA in tris HCl incubated with **BUCIS04-AF647***
9. *Lifetime of **EuQS@Au** in 1% FCS*
10. *Lifetime of **EuQS@Au** in 1% FCS in tris HCl*
11. *Lifetime of **EuQS@Au** in 1% FCS incubated with **BUCIS04-AF647***
12. *Lifetime of **EuQS@Au** in 1% FCS in tris HCl incubated with **BUCIS04-AF647***
13. *Lifetime of **EuQS@Au** in with 0.05% Tween 20*
14. *Lifetime of **EuQS@Au** in with 0.05% Tween 20 in tris HCl*
15. *Lifetime of **EuQS@Au** in with 0.05% Tween 20 incubated with **BUCIS04-AF647***
16. *Lifetime of **EuQS@Au** in with 0.05% Tween 20 in tris HCl incubated with **BUCIS04-AF647***
17. *Lifetime of **EuQS@Au** in 0.05% Zonyl FSA*
18. *Lifetime of **EuQS@Au** in 0.05% Zonyl FSA in tris HCl*
19. *Lifetime of **EuQS@Au** in 0.05% Zonyl FSA incubated with **BUCIS04-AF647***
20. *Lifetime of **EuQS@Au** in 0.05% Zonyl FSA in tris HCl incubated with **BUCIS04-AF647***
21. *Lifetime of **κnew.EuQS@Au** in 1% BSA*
22. *Lifetime of **κnew.EuQS@Au** in 1% BSA in tris HCl*
23. *Lifetime of **κnew.EuQS@Au** in 1% BSA incubated with **BUCIS04-AF647***
24. *Lifetime of **κnew.EuQS@Au** in 1% BSA in tris HCl incubated with **BUCIS04-AF647***
25. *Lifetime of **κnew.EuQS@Au** in 1% FCS*
26. *Lifetime of **κnew.EuQS@Au** in 1% FCS in tris HCl*
27. *Lifetime of **κnew.EuQS@Au** in 1% FCS incubated with **BUCIS04-AF647***
28. *Lifetime of **κnew.EuQS@Au** in 1% FCS in tris HCl incubated with **BUCIS04-AF647***
29. *Lifetime of **κnew.EuQS@Au** incubated with premixed κnew and **BUCIS04-AF647***
30. *Lifetime of **κnew.EuQS@Au** incubated with premixed κnew and **BUCIS04-AF647** in tris HCl*
31. *Lifetime of **κnew.EuQS@Au** incubated with premixed κnew and **BUCIS04-AF647** in 1% BSA*

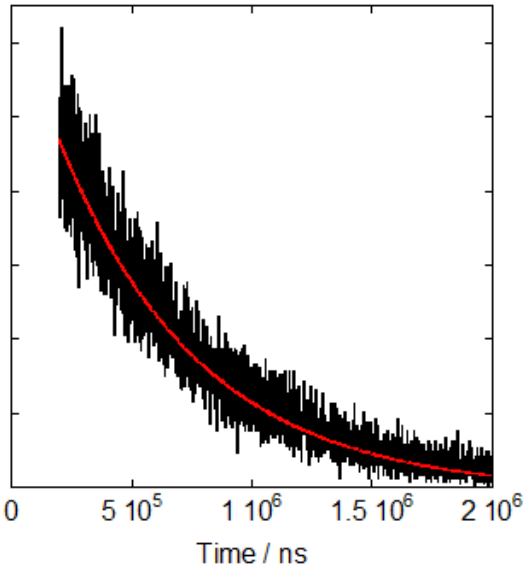

*Lifetime of **EuQS@Au** in water*

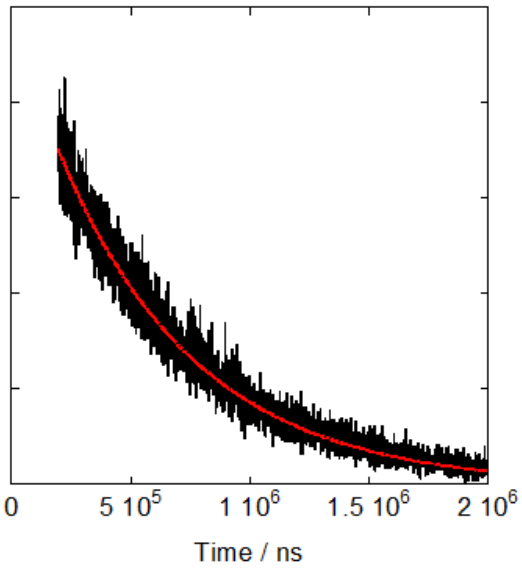

*Lifetime of **EuQS@Au** in tris HCl*

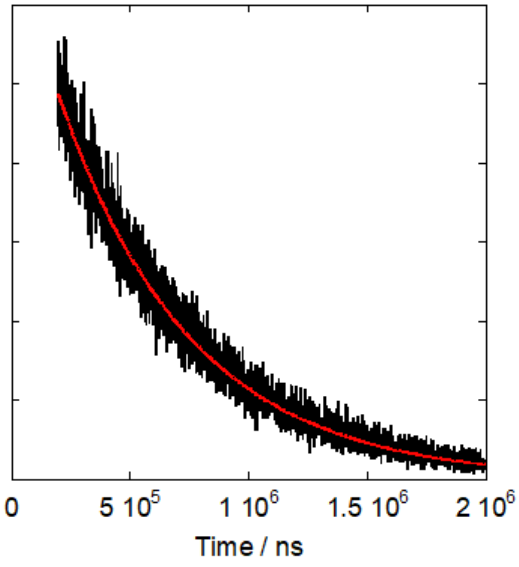

*Lifetime of **EuQS@Au** and **BUCIS04-AF647***

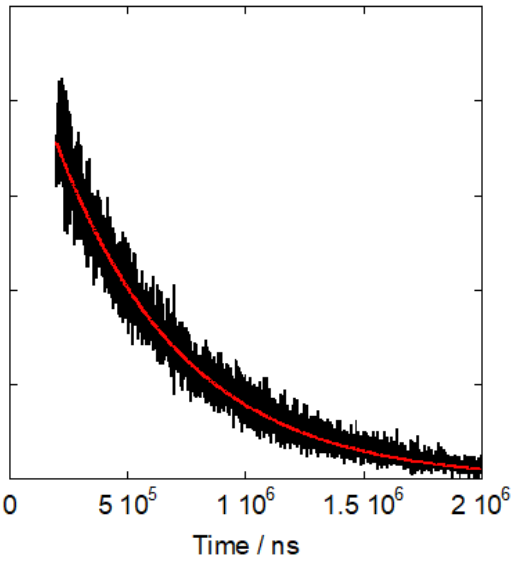

*Lifetime of **EuQS@Au** and **BUCIS04-AF647** in tris HCl buffer*

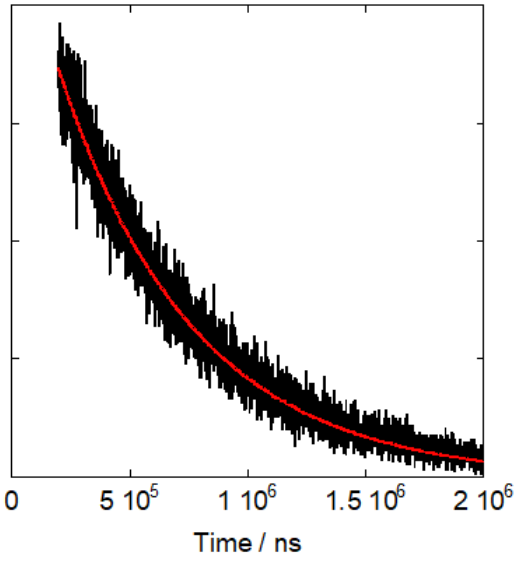

*Lifetime of of **EuQS@Au** in 1% BSA*

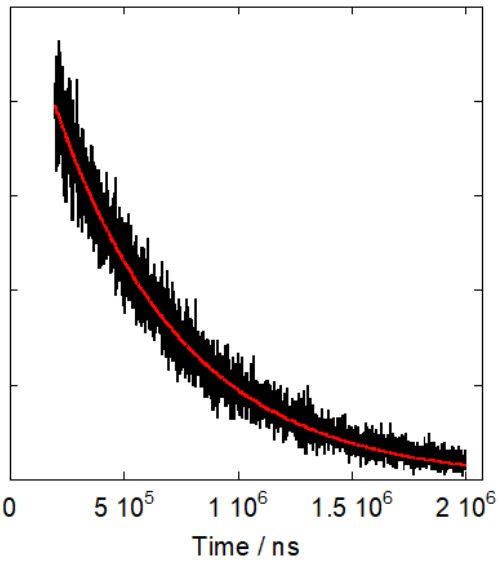

*Lifetime of of **EuQS@Au** in 1% BSA in Tris HCl*

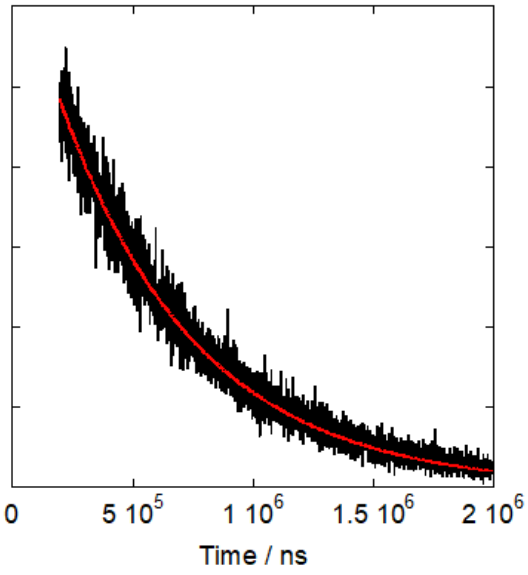

*Lifetime of of **EuQS@Au** in 1% FCS*

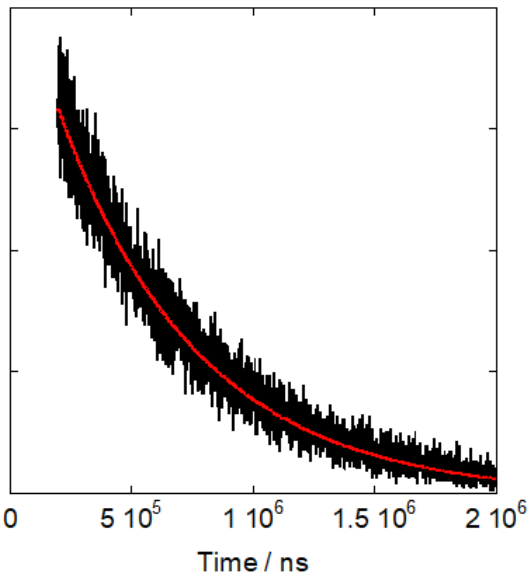

*Lifetime of **EuQS@Au** in 1% FCS in Tris HCl*

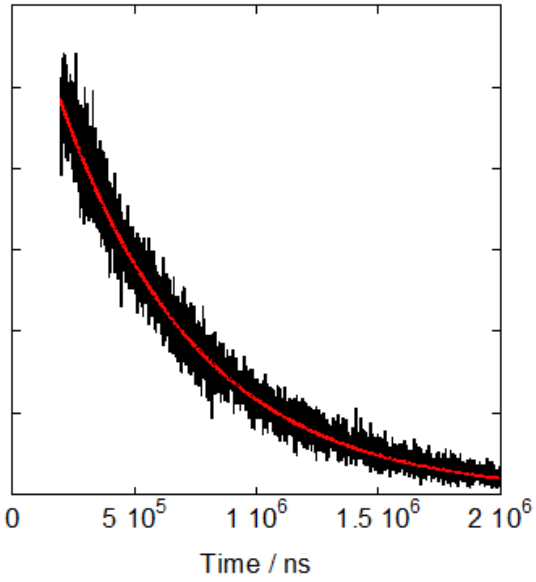

*Lifetime of **EuQS@Au** in 1% BSA incubated with **BUCIS04-AF647***

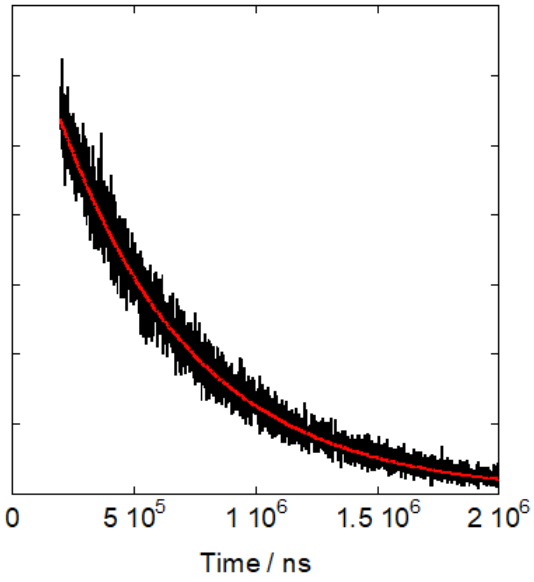

*Lifetime of **EuQS@Au** in 1% BSA in Tris HCl incubated with **BUCIS04-***

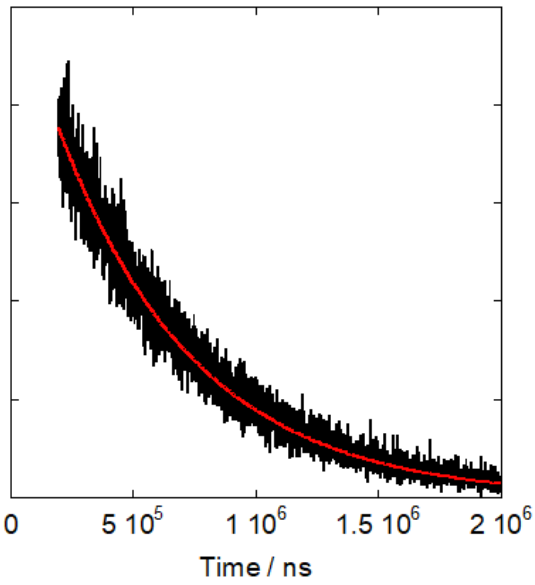

*Lifetime of **EuQS@Au** in 1% FCS incubated with **BUCIS04-AF647***

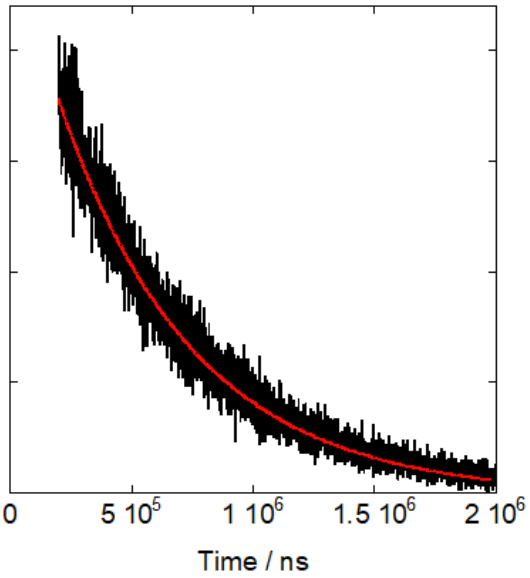

*Lifetime of **EuQS@Au** in 1% FCS in Tris HCl incubated with **BUCIS04-AF647***

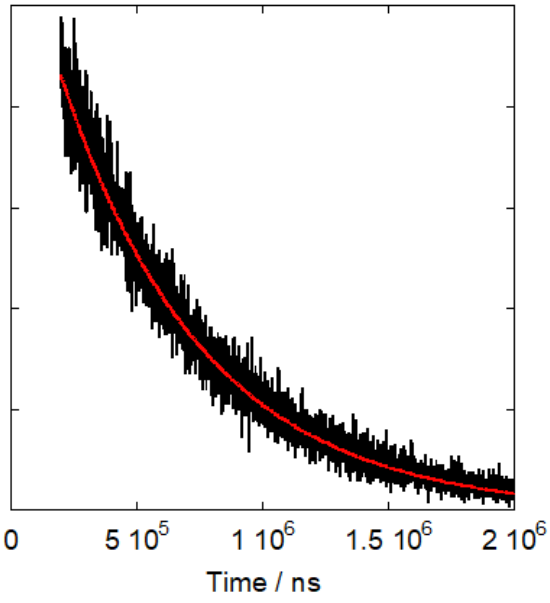

*Lifetime of **EuQS@Au** in 0.05 % Zonyl FSA*

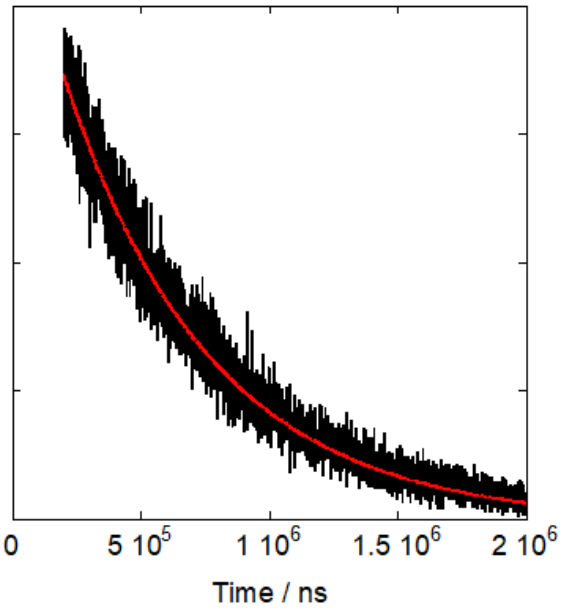

*Lifetime of **EuQS@Au** in 0.05 % Zonyl FSA in Tris HCl*

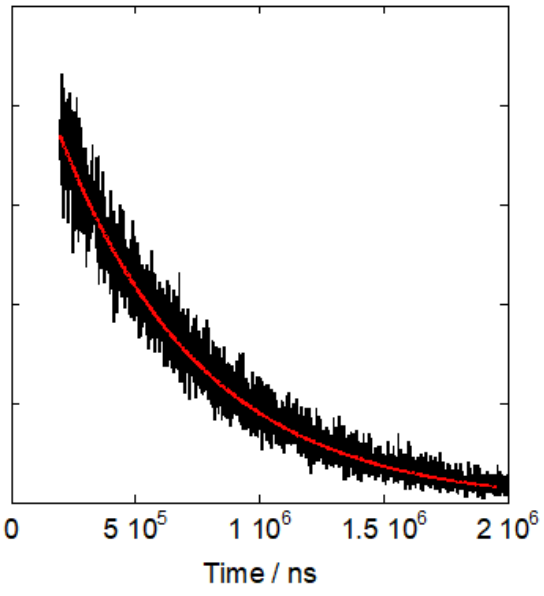

*Lifetime of **EuQS@Au** in 0.05% Tween 20*

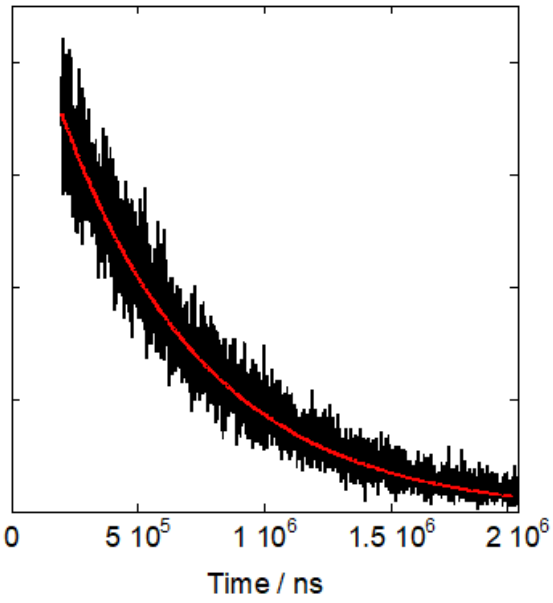

*Lifetime of **EuQS@Au** in 0.05% Tween 20 in Tris HCl*

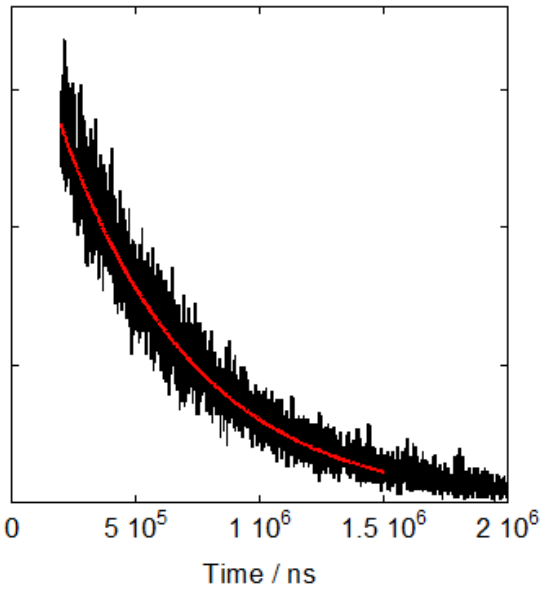

*Lifetime of **EuQS@Au** in 0.05 % Zonyl FSA incubated with **BUCIS04-AF647***

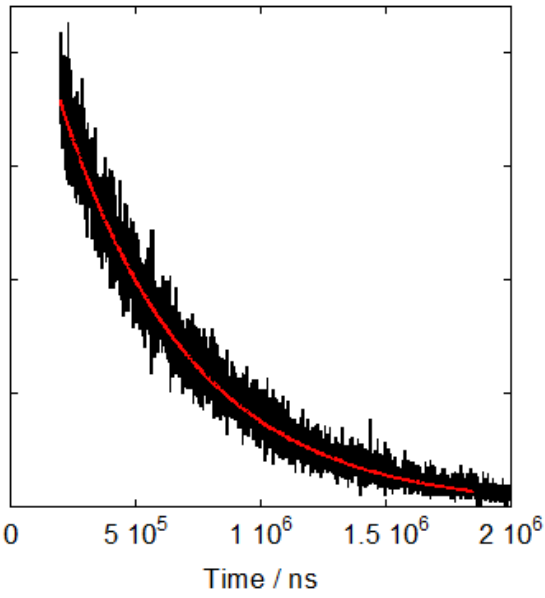

*Lifetime of **EuQS@Au** in 0.05 % Zonyl FSA in Tris HCl incubated with **BUCIS04-AF647***

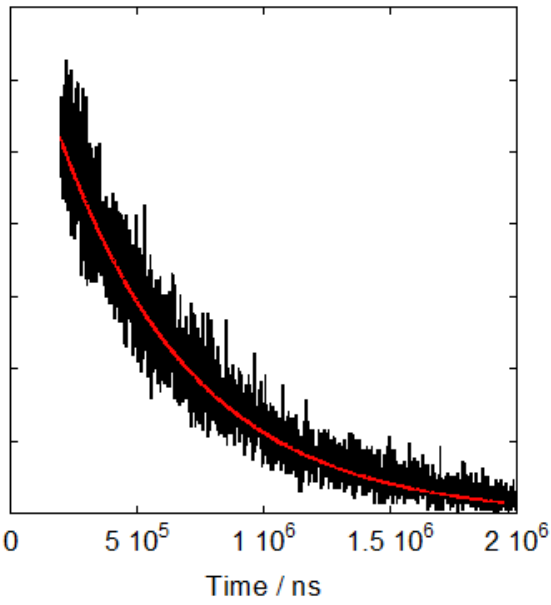

*Lifetime of **EuQS@Au** in 0.05% Tween 20 incubated with **BUCIS04-AF647***

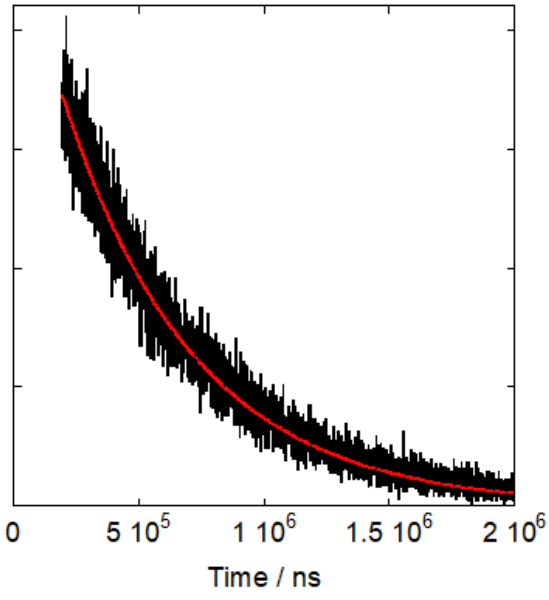

*Lifetime of **EuQS@Au** in 0.05% Tween 20 in Tris HCl incubated with **BUCIS04-AF647***

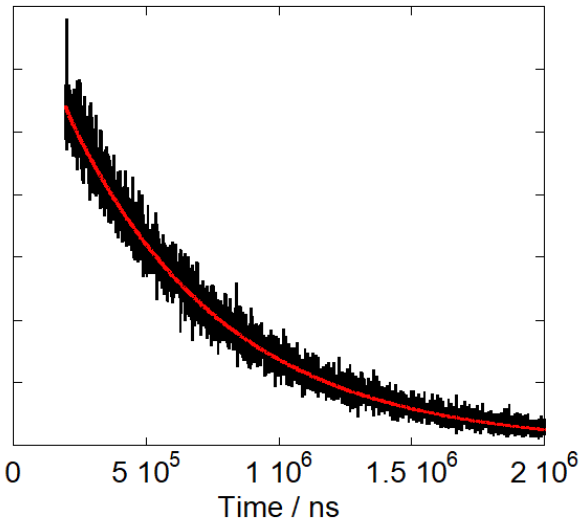

*Lifetime of **κnew.EuQS@Au** in 1% BSA*

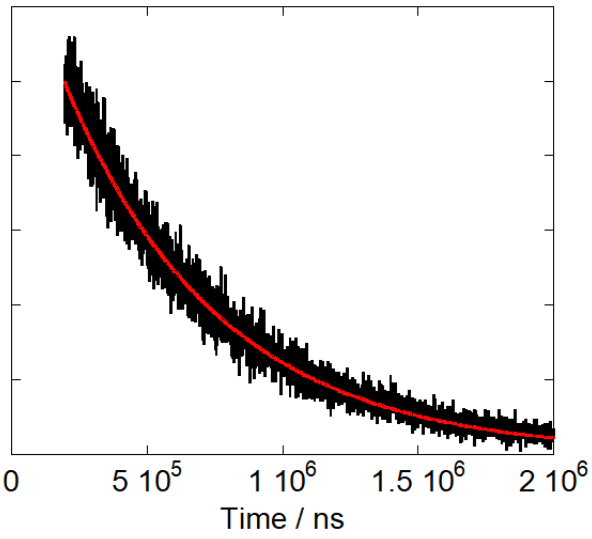

*Lifetime of **κnew.EuQS@Au** in 1% BSA in Tris HCl*

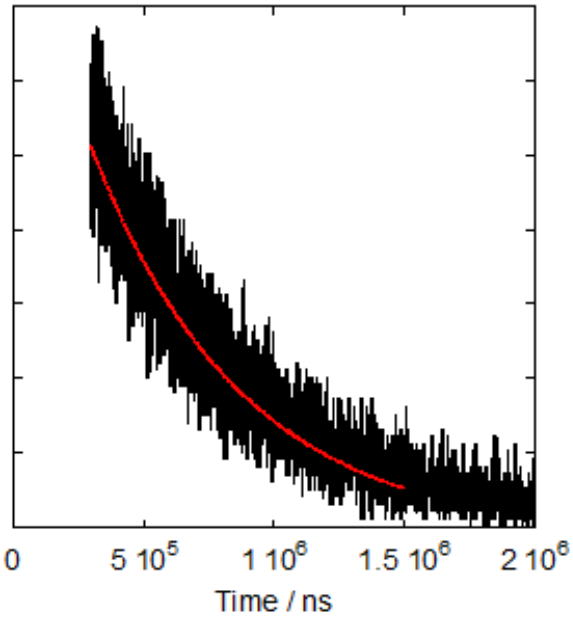

*Lifetime of **κnew.EuQS@Au** in 1% FCS*

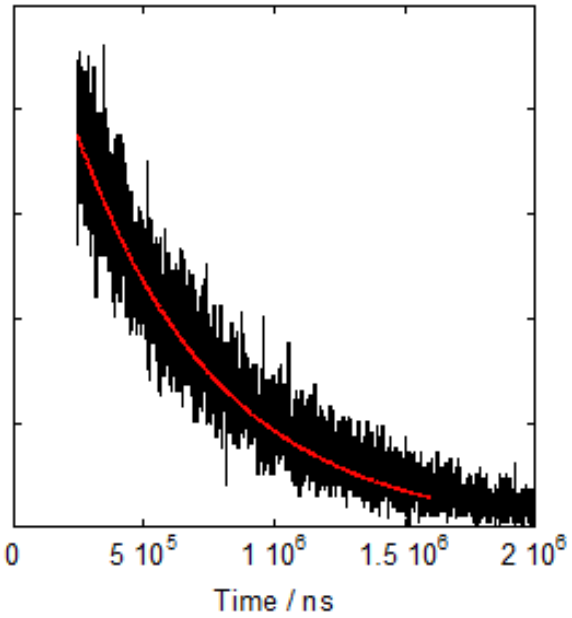

*Lifetime of **κnew.EuQS@Au** in 1% FCS in Tris HCl*

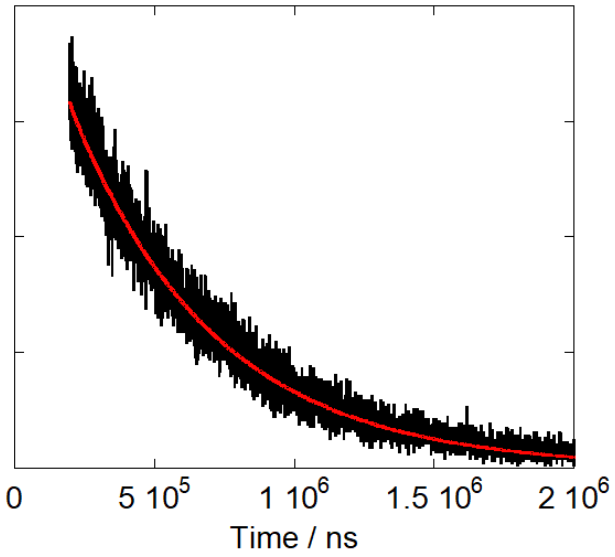

*Lifetime of **κnew.EuQS@Au** in 1% BSA incubated with **BUCIS04-AF647***

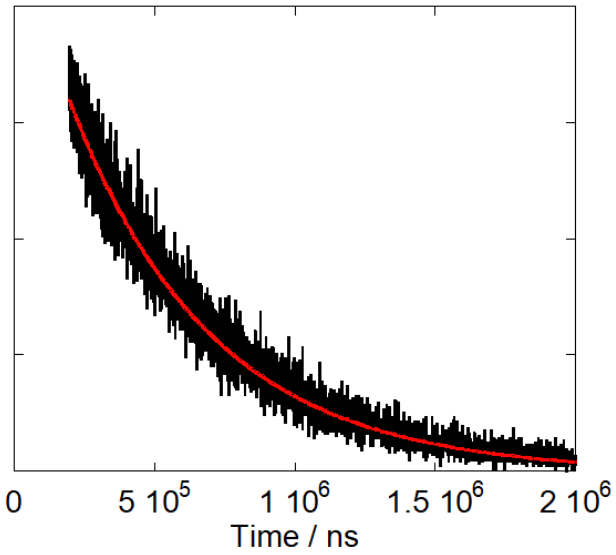

*Lifetime of **κnew.EuQS@Au** in 1% BSA in Tris HCl incubated with **BUCIS04-AF647***

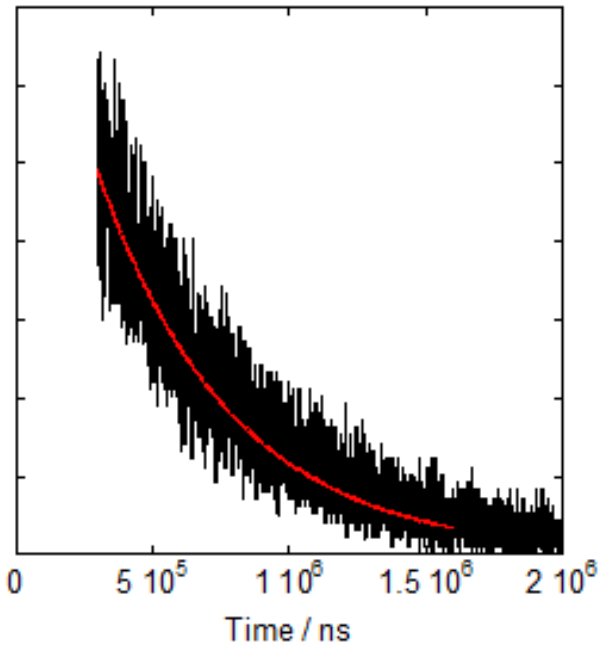

*Lifetime of **κnew.EuQS@Au** in 1% FCS incubated with **BUCIS04-AF647***

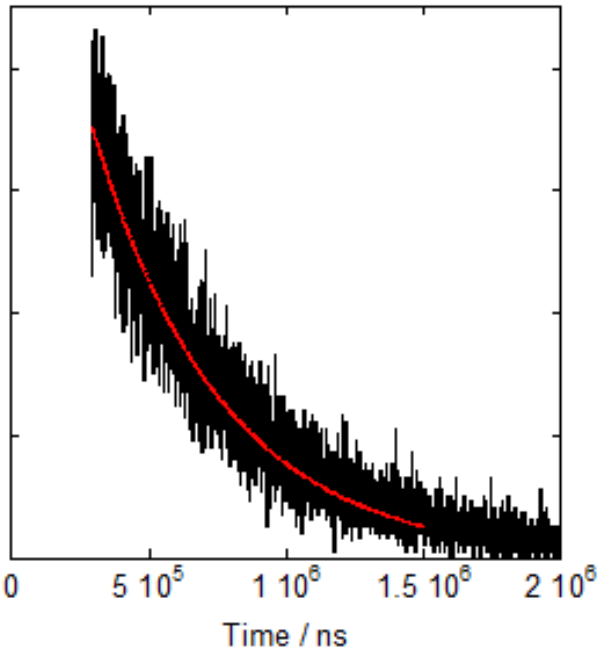

*Lifetime of **κnew.EuQS@Au** in 1% FCS in Tris HCl incubated with **BUCIS04-AF647***

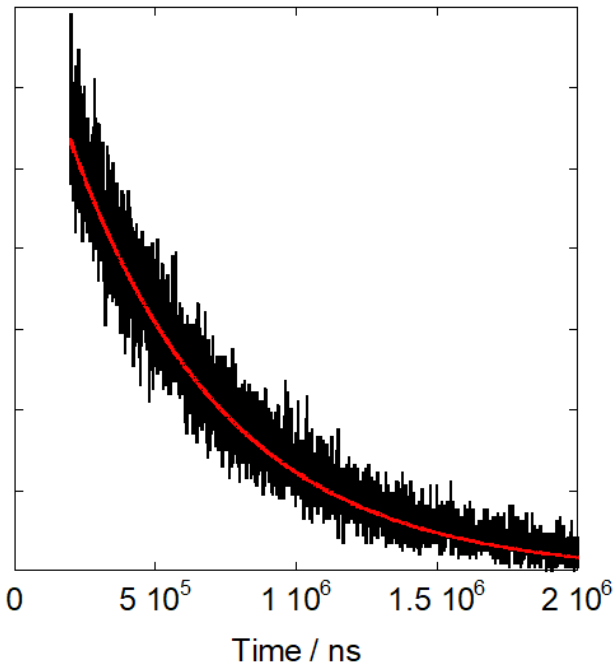

*Lifetime of **κnew.EuQS@Au** with premixed κnew and **BUCIS04-AF647***

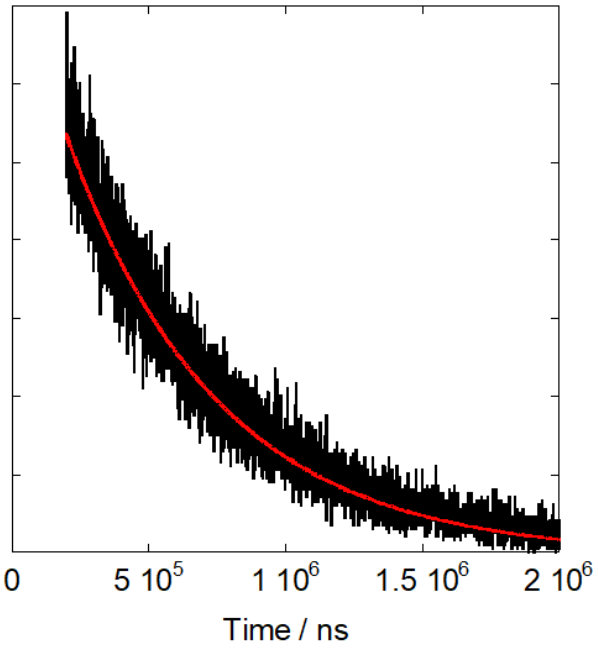

*Lifetime of **κnew.EuQS@Au** with premixed κnew and **BUCIS04-AF647** in tris HCl*

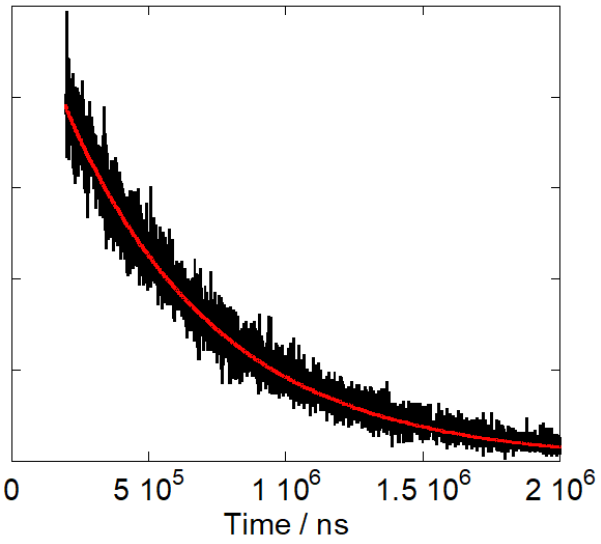

*Lifetime of **κnew.EuQS@Au** in 1% BSA with premixed κnew and **BUCIS04-AF647***

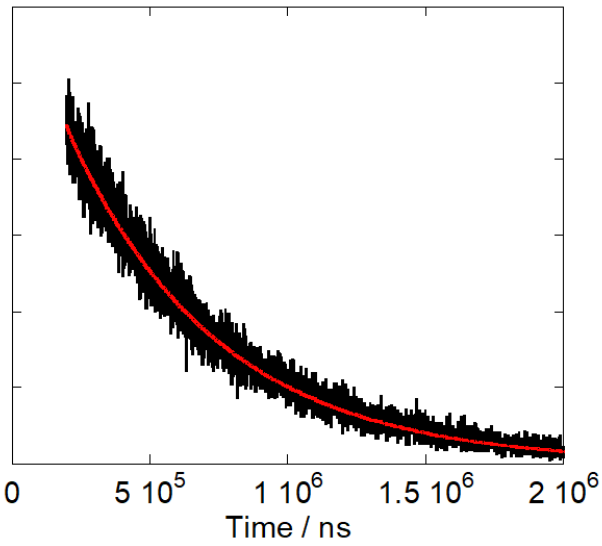

*Lifetime of **κnew.EuQS@Au** in 1% BSA with premixed κnew and **BUCIS04-AF647** in tris HCl*

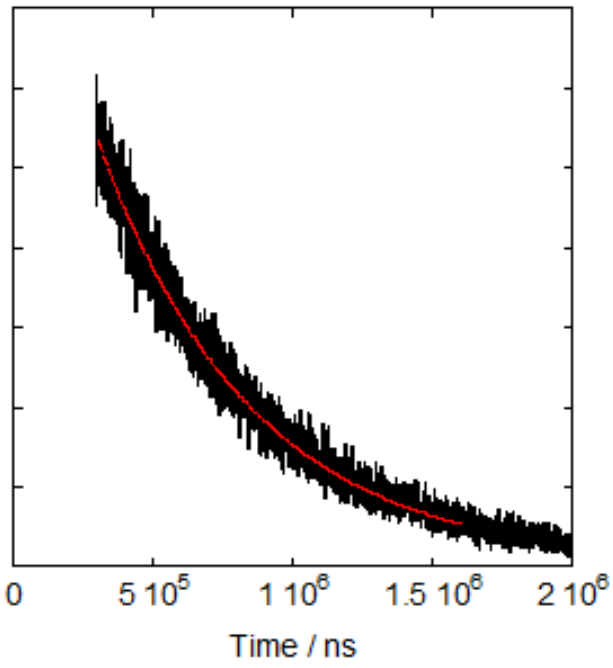

*Lifetime of **κnew.EuQS@Au** in 1% FCS with premixed κnew and **BUCIS04-AF647***

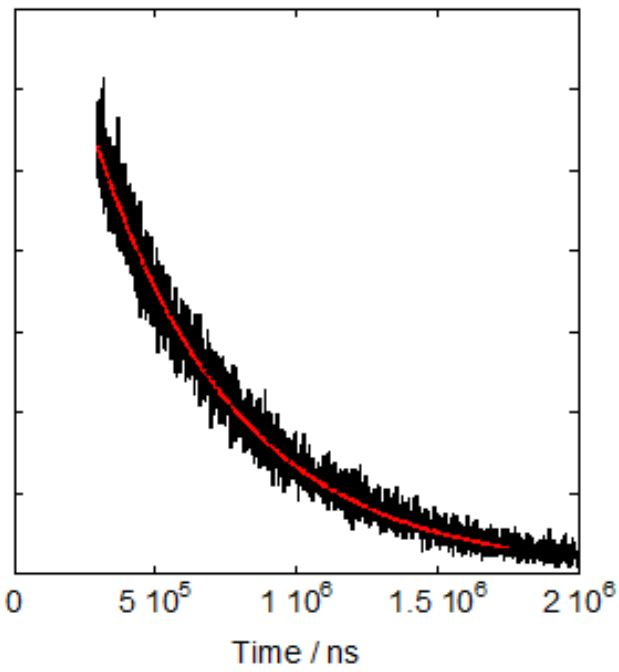

*Lifetime of **κnew.EuQS@Au** in 1% FCS with premixed κnew and **BUCIS04-AF647** in tris HCl*

Chapter 4 appendix

List of appendices

1. *^{1}H NMR of **8** in $CDCl_3$*
2. *^{13}C NMR of **8** in $CDCl_3$*
3. *MS (ES-TOF)$^{+}$ of **8***
4. *^{1}H NMR of **9** in $CDCl_3$*
5. *^{13}C NMR of **9** in $CDCl_3$*
6. *MS (ES-TOF)$^{+}$ of **9***
7. *^{1}H NMR spectrum of **DBMSS** in d_6-DMSO.*
8. *^{13}C NMR spectrum of **DBMSS** in d_6-DMSO.*
9. *MS (ES-TOF)$^{+}$ of **DBMSS***
10. *HSQC of aromatic region of **DBMSS** in d_6 DMSO*
11. *HSQC of aliphatic region of **DBMSS** in d_6 DMSO*
12. *HMBC of **DBMSS** in d_6 DMSO*
13. *HMBC of aromatic region of **DBMSS** in d_6 DMSO*
14. *HMBC of aliphatic region of **DBMSS** in d_6 DMSO*
15. *Lifetime of **Eu(DBMSS)$_3$** in MeOH, λ_{exc} = 350 nm and λ_{em} = 614 nm.*
16. *Lifetime of **Eu(DBMSS)$_3$** in MeOD, λ_{exc} = 350 nm and λ_{em} = 614 nm.*
17. *Lifetime of **Eu.DBMSS.Z@Au** H_2O, λ_{exc} = 350 nm and λ_{em} = 614 nm.*

INSTRUM spect
PROBHD 5 mm PADUL 13C
PULPROG zg30
TD 32768
SOLVENT CDCl3
NS 32
DS 2
SWH 8223.685 Hz
FIDRES 0.250967 Hz
AQ 1.9922944 sec
RG 128
DW 60.800 usec
DE 16.65 usec
TE 295.8 K
D1 1.50000000 sec
TD0 1

======== CHANNEL f1 ========
SFO1 400.1324008 MHz
NUC1 1H
P1 11.06 usec
PLW1 24.29199982 W

F2 - Processing parameters
SI 32768
SF 400.1300352 MHz
WDW EM
SSB 0
LB 0.30 Hz
GB 0
PC 1.00

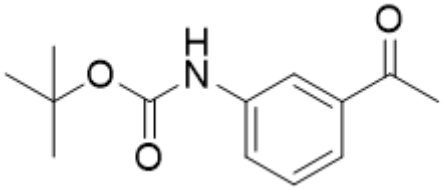

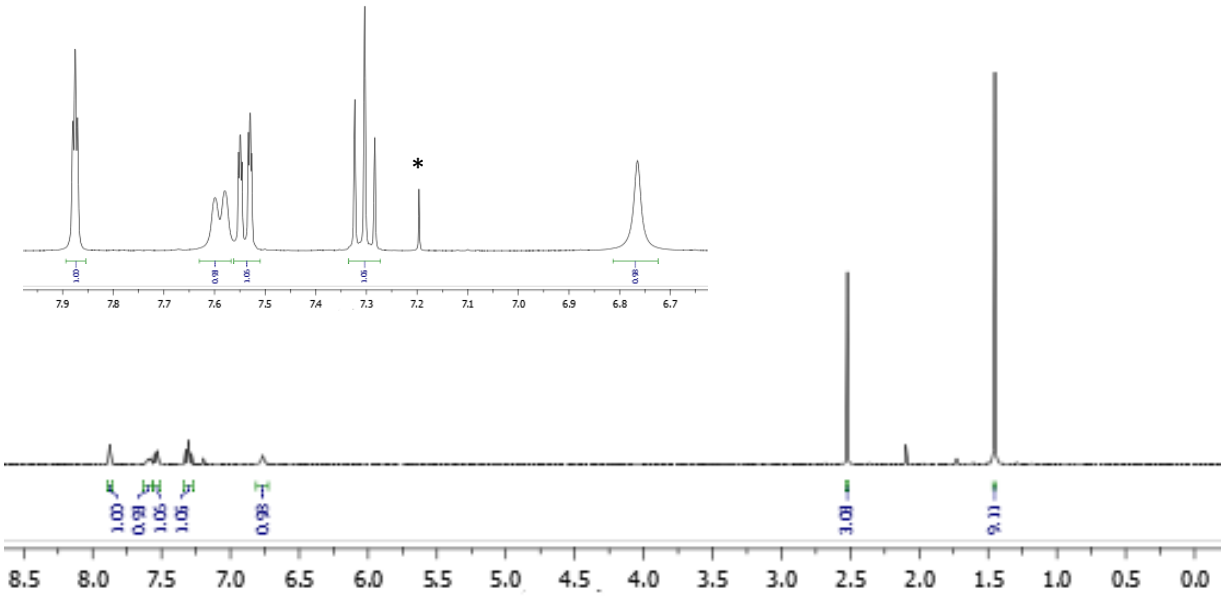

*^{1}H NMR of **8** in $CDCl_3$*

** = residual solvent resonance*

INSTRUM	spect
PROBHD	5 mm PADUL 13C
PULPROG	pendantns
TD	65536
SOLVENT	CDCl3
NS	512
DS	4
SWH	25252.525 Hz
FIDRES	0.385323 Hz
AQ	1.2976128 sec
RG	2050
DW	19.800 usec
DE	6.50 usec
TE	296.2 K
CNST2	145.0000000
CNST3	1.0000000
CNST4	5.0000000
D1	1.50000000 sec
D2	0.00172414 sec
D3	0.00431034 sec
D12	0.00002000 sec
D13	0.00000400 sec
TD0	1

======== CHANNEL f1 ========	
SFO1	100.6242690 MHz
NUC1	13C
P1	8.80 usec
P2	17.60 usec
PLW1	58.63899994 W

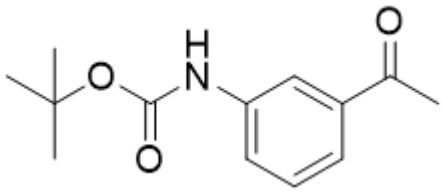

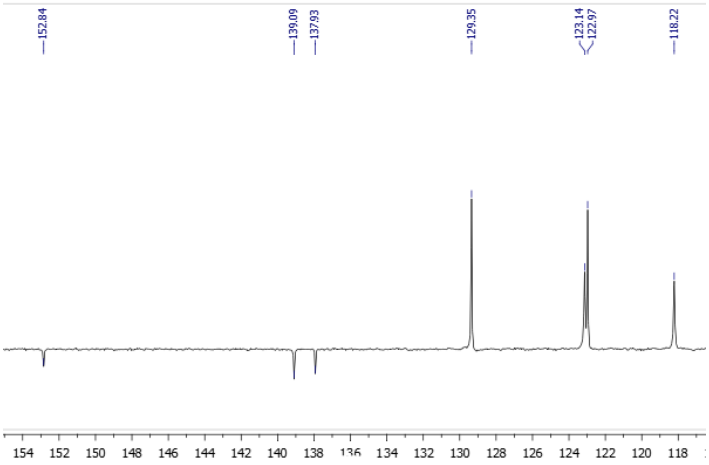

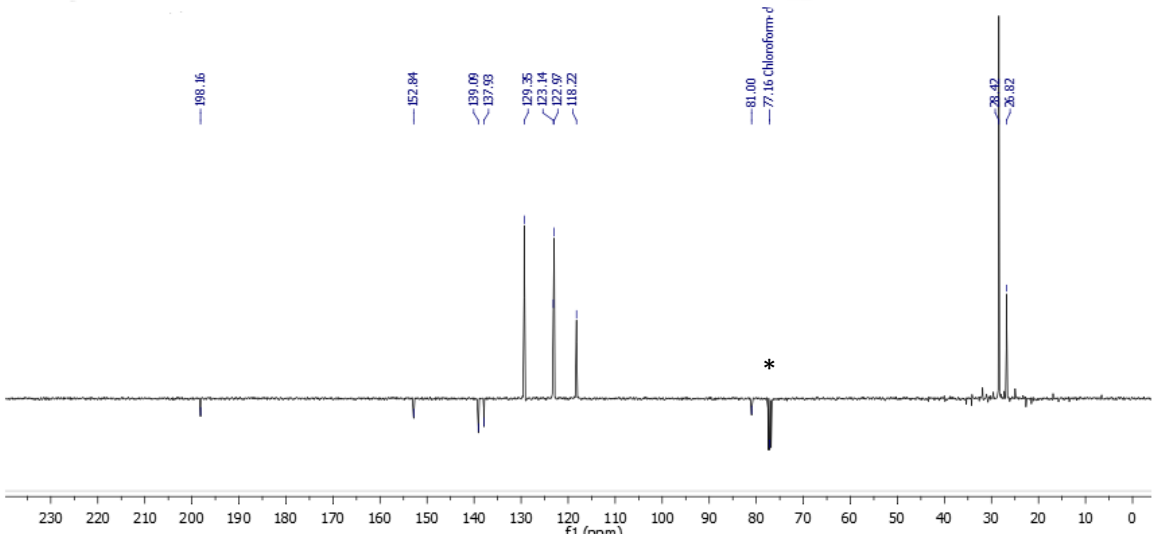

*$^{13}C\{^{1}H\}$ PENDANT NMR of **8** in $CDCl_3$*

** = residual solvent resonance*

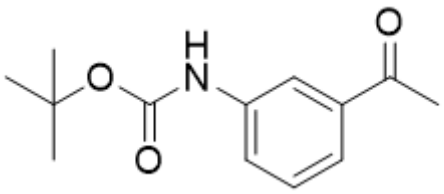
O
H
N
O
O

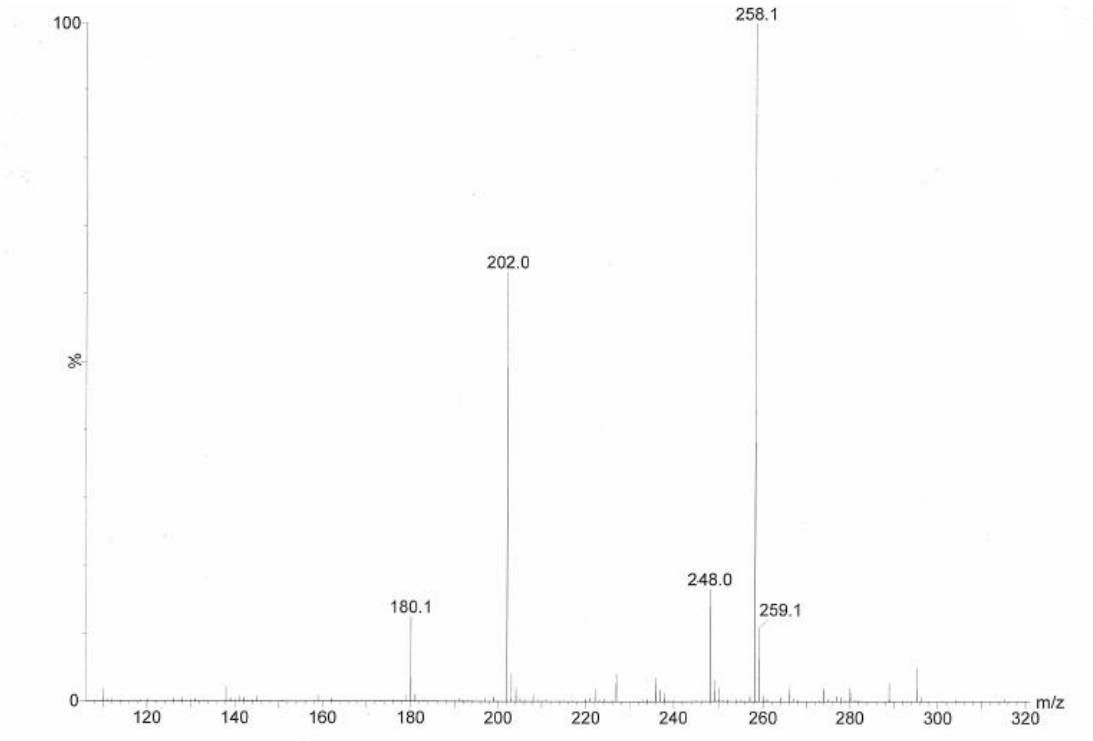
100
%
0
258.1
202.0
248.0
180.1
259.1
120
140
160
180
200
220
240
260
280
300
320
m/z

*MS (ES-TOF)$^+$ of **8***

INSTRUM spect
PROBHD 5 mm PADUL 13C
PULPROG zg30
TD 32768
SOLVENT CDCl3
NS 32
DS 2
SWH 8223.685 Hz
FIDRES 0.250967 Hz
AQ 1.9922944 sec
RG 287
DW 60.800 usec
DE 16.65 usec
TE 295.8 K
D1 1.50000000 sec
TD0 1

======== CHANNEL f1 ========
SFO1 400.1324008 MHz
NUC1 1H
P1 11.06 usec
PLW1 24.29199982 W

F2 - Processing parameters
SI 32768
SF 400.1300000 MHz
WDW EM
SSB 0
LB 0.30 Hz
GB 0
PC 1.00

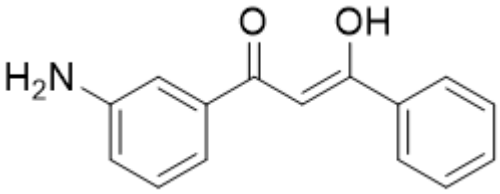

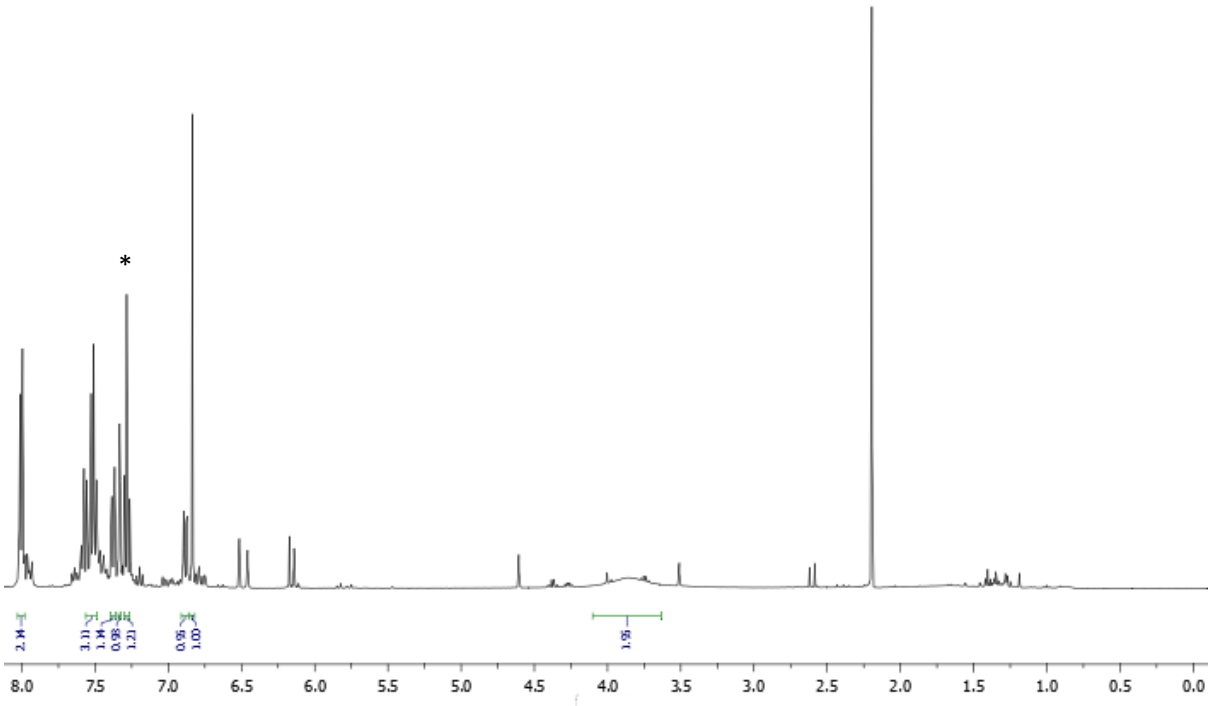

*[1]H NMR of **9** in $CDCl_3$*

** = residual solvent resonance*

INSTRUM	spect
PROBHD	5 mm PADUL 13C
PULPROG	pendantns
TD	65536
SOLVENT	CDCl3
NS	512
DS	4
SWH	25252.525 Hz
FIDRES	0.385323 Hz
AQ	1.2976128 sec
RG	2050
DW	19.800 usec
DE	6.50 usec
TE	296.2 K
CNST2	145.0000000
CNST3	1.0000000
CNST4	5.0000000
D1	1.50000000 sec
D2	0.00172414 sec
D3	0.00431034 sec
D12	0.00002000 sec
D13	0.00000400 sec
TD0	1
======== CHANNEL f1 ========	
SFO1	100.6242690 MHz
NUC1	13C
P1	8.80 usec
P2	17.60 usec
PLW1	58.63899994 W

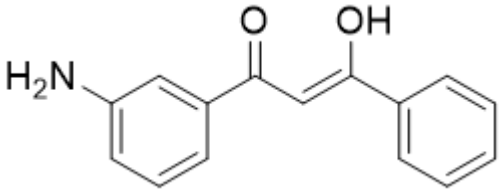

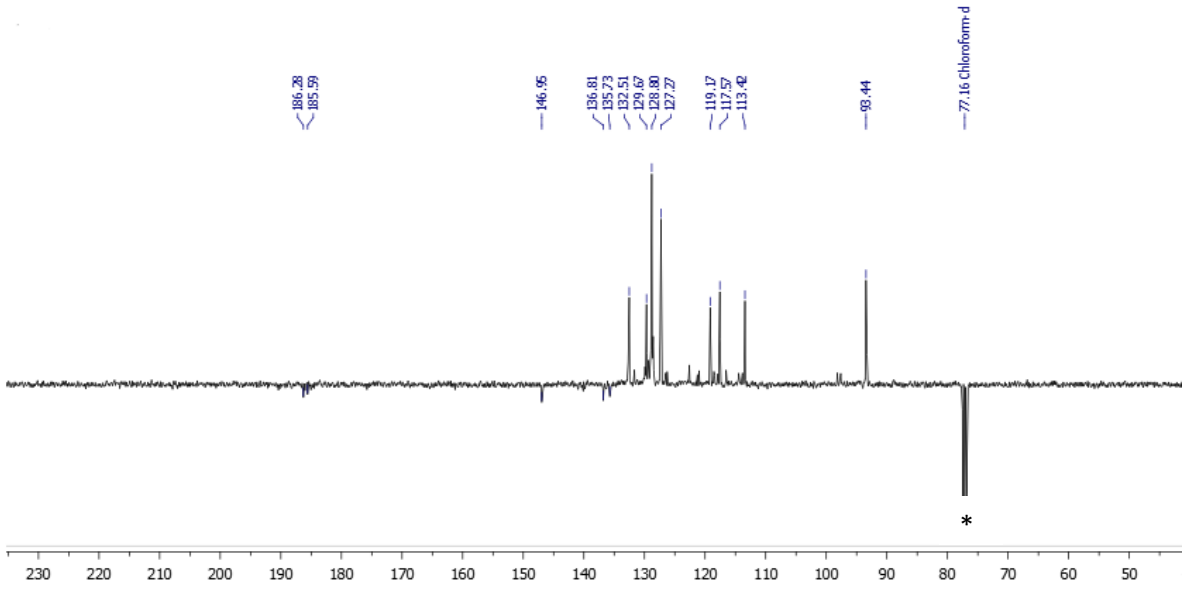

*$^{13}C\{^{1}H\}$ PENDANT NMR of **9** in $CDCl_3$*

** = residual solvent resonance*

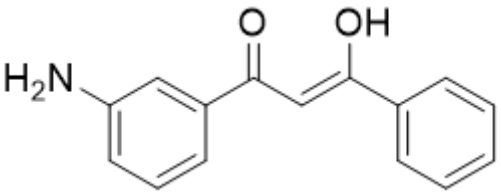
O
OH
H_2N

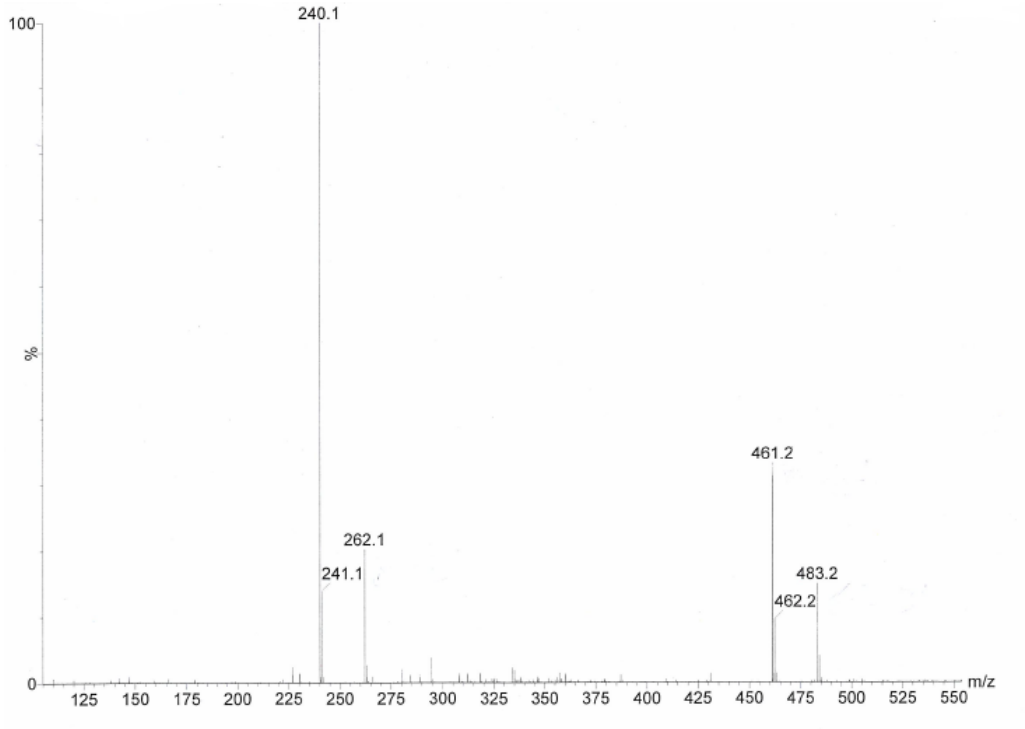
100
%
0
240.1
461.2
262.1
241.1
483.2
462.2
m/z
125 150 175 200 225 250 275 300 325 350 375 400 425 450 475 500 525 550

MS (ES-TOF)$^+$ of ***9***

```
INSTRUM         spect
PROBHD   5 mm PADUL 13C
PULPROG          zg30
TD              32768
SOLVENT           DMSO
NS                 32
DS                  2
SWH          8223.685 Hz
FIDRES        0.250967 Hz
AQ          1.9922944 sec
RG                406
DW             60.800 usec
DE             16.65 usec
TE             294.3 K
D1          1.50000000 sec
TD0                1

======== CHANNEL f1 ========
SFO1       400.1324008 MHz
NUC1               1H
P1              11.06 usec
PLW1       24.29199982 W

F2 - Processing parameters
SI              32768
SF         400.1300000 MHz
WDW                EM
SSB     0
LB              0.30 Hz
GB      0
PC              1.00
```

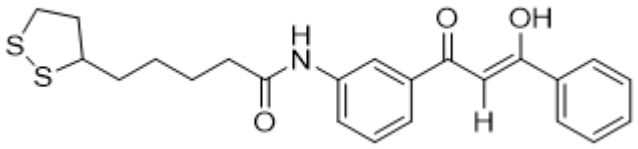

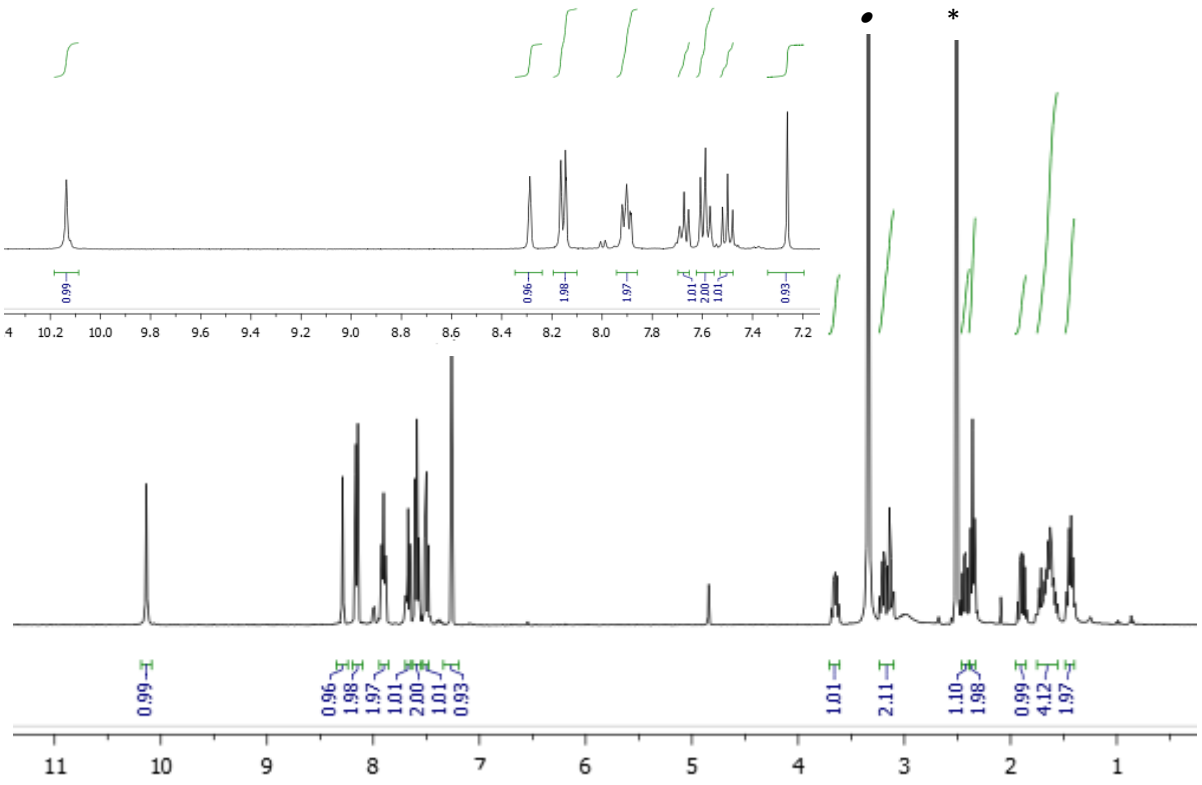

*[1]H NMR spectrum of **DBMSS** in d_6-DMSO.*

**= residual solvent resonance; • = water.*

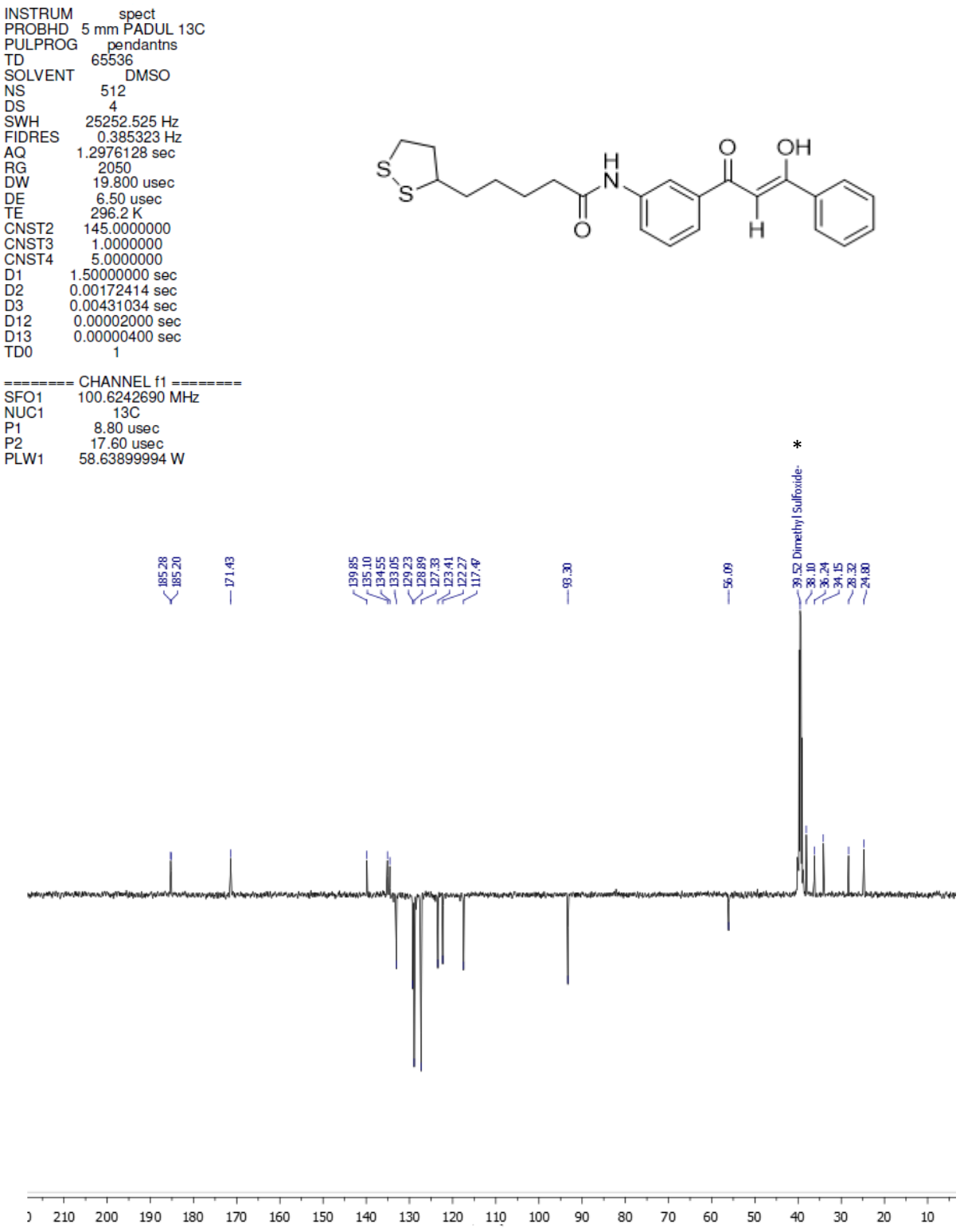

*^{13}C NMR spectrum of **DBMSS** in d_6-DMSO.*

**= residual solvent resonance.*

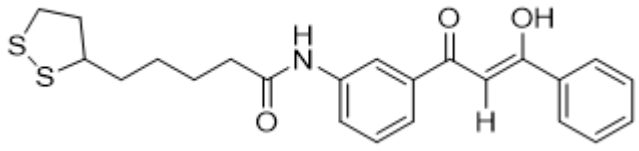

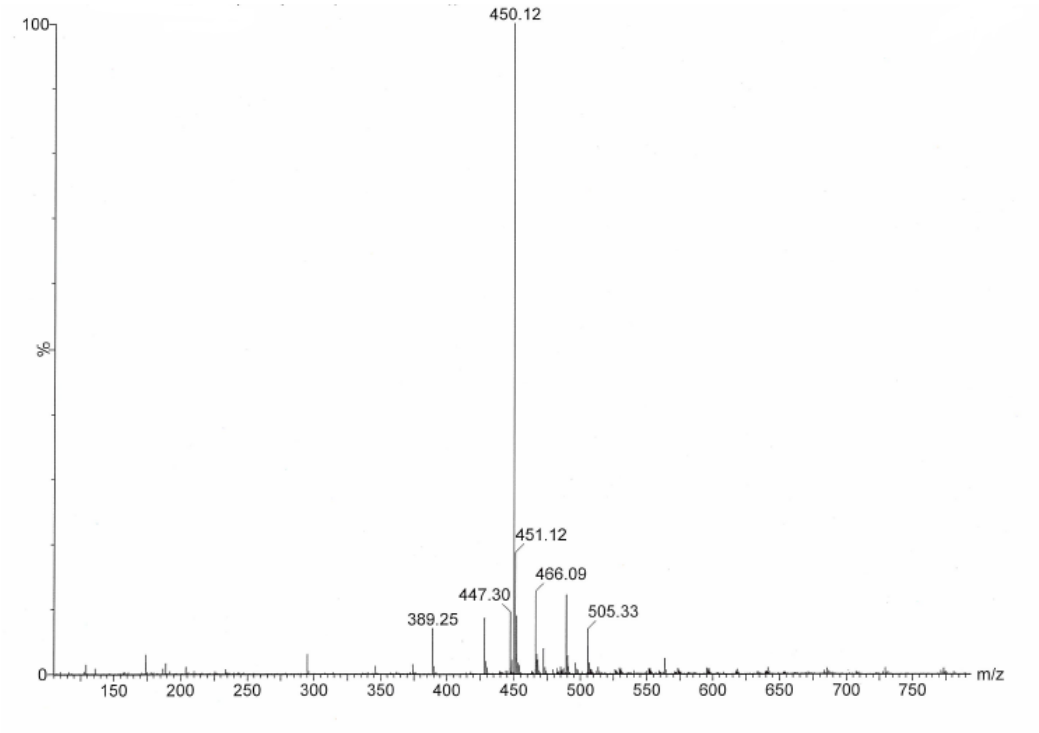

MS (ES-TOF)$^{+}$ of ***DBMSS***

F2 - Acquisition Parameters
Date 20160624
Time 1.26
INSTRUM spect
PROBHD 5 mm PADUL 13C
PULPROG hsqcetgp
TD 1024
SOLVENT DMSO
NS 4
DS 16
SWH 4310.345 Hz
FIDRES 4.209321 Hz
AQ 0.1187840 sec
RG 2050
DW 116.000 usec
DE 6.50 usec
TE 294.4 K
CNST2 145.0000000
D0 0.00000300 sec
D1 1.47726703 sec
D4 0.00172414 sec
D11 0.03000000 sec
D16 0.00020000 sec
IN0 0.00003000 sec
ZGOPTNS

-------- CHANNEL f1 --------
SFO1 400.1322009 MHz
NUC1 1H
P1 11.06 usec
P2 22.12 usec
P28 1000.00 usec
PLW1 24.29199982 W

-------- CHANNEL f2 --------
SFO2 100.6203124 MHz
NUC2 13C
CPDPRG[2 garp
P3 8.90 usec
P4 17.80 usec
PCPD2 80.00 usec
PLW2 58.63899994 W
PLW12 0.72575003 W

-------- GRADIENT CHANNEL -----
GPNAM[1] SMSQ10.100
GPNAM[2] SMSQ10.100
GPZ1 80.00 %
GPZ2 20.10 %
P16 1000.00 usec

F1 - Acquisition parameters
TD 256
SFO1 100.6203 MHz
FIDRES 65.104164 Hz
SW 165.639 ppm
FnMODE Echo-Antiecho

F2 - Processing parameters
SI 1024
SF 400.1300000 MHz
WDW QSINE
SSB 2
LB 0 Hz
GB 0
PC 1.40

F1 - Processing parameters
SI 512
MC2 echo-antiecho
SF 100.6127690 MHz
WDW QSINE
SSB 2
LB 0 Hz
GB 0

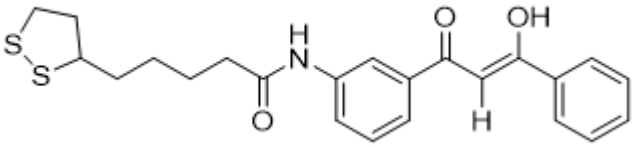

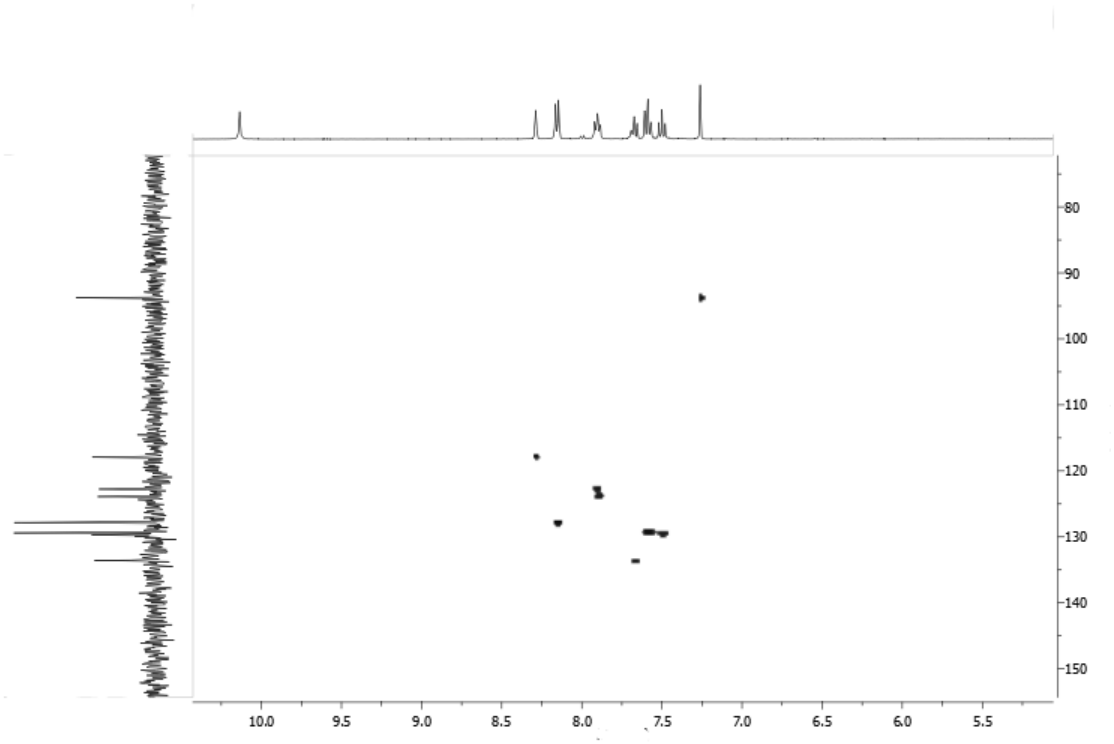

*HSQC of aromatic region of **DBMSS** in d_6 DMSO*

F2 - Acquisition Parameters
Date 20160624
Time 1.26
INSTRUM spect
PROBHD 5 mm PADUL 13C
PULPROG hsqcetgp
TD 1024
SOLVENT DMSO
NS 4
DS 16
SWH 4310.345 Hz
FIDRES 4.209321 Hz
AQ 0.1187840 sec
RG 2050
DW 116.000 usec
DE 6.50 usec
TE 294.4 K
CNST2 145.0000000
D0 0.00000300 sec
D1 1.47726703 sec
D4 0.00172414 sec
D11 0.03000000 sec
D16 0.00020000 sec
IN0 0.00003000 sec
ZGOPTNS

-------- CHANNEL f1 --------
SFO1 400.1322009 MHz
NUC1 1H
P1 11.06 usec
P2 22.12 usec
P28 1000.00 usec
PLW1 24.29199982 W

-------- CHANNEL f2 --------
SFO2 100.6203124 MHz
NUC2 13C
CPDPRG[2 garp
P3 8.90 usec
P4 17.80 usec
PCPD2 80.00 usec
PLW2 58.63899994 W
PLW12 0.72575003 W

-------- GRADIENT CHANNEL -----
GPNAM[1] SMSQ10.100
GPNAM[2] SMSQ10.100
GPZ1 80.00 %
GPZ2 20.10 %
P16 1000.00 usec

F1 - Acquisition parameters
TD 256
SFO1 100.6203 MHz
FIDRES 65.104164 Hz
SW 165.639 ppm
FnMODE Echo-Antiecho

F2 - Processing parameters
SI 1024
SF 400.1300000 MHz
WDW QSINE
SSB 2
LB 0 Hz
GB 0
PC 1.40

F1 - Processing parameters
SI 512
MC2 echo-antiecho
SF 100.6127690 MHz
WDW QSINE
SSB 2
LB 0 Hz
GB 0

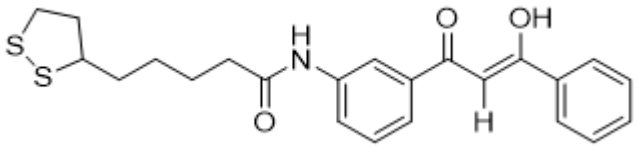

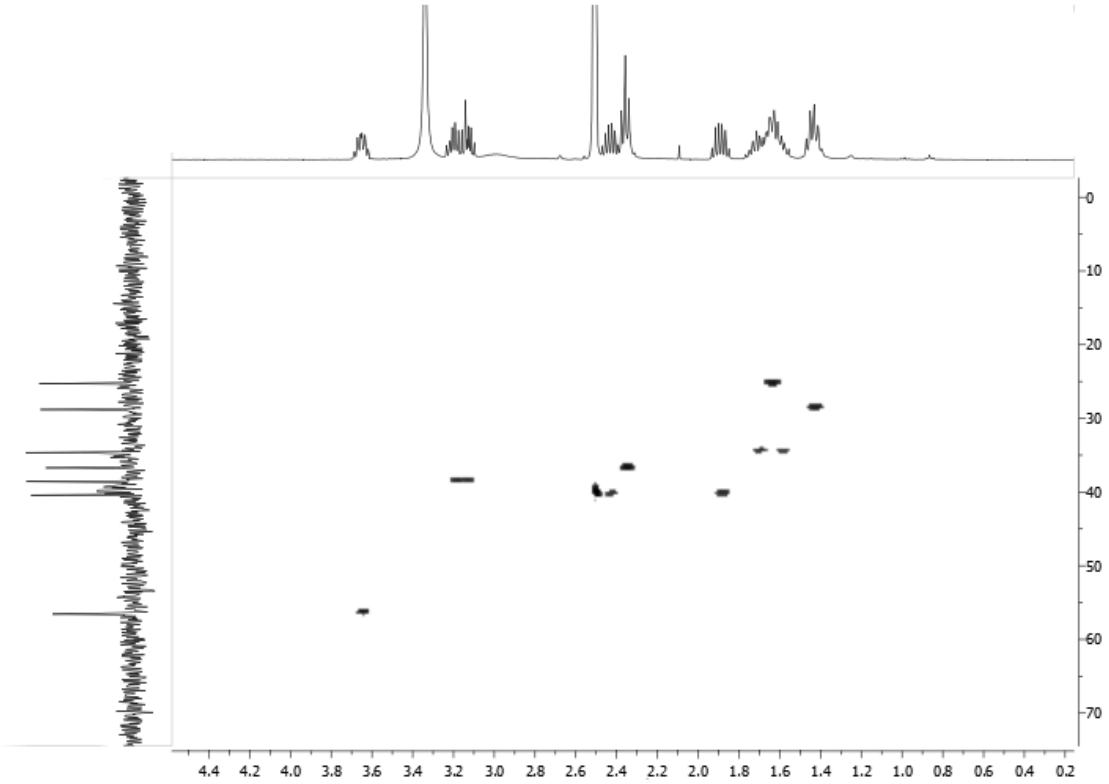

*HSQC of aliphatic region of **DBMSS** in d_6 DMSO*

F2 - Acquisition Parameters
Date_ 20160624
Time 0.27
INSTRUM spect
PROBHD 5 mm PADUL 13C
PULPROG hmbcgplpndqf
TD 1024
SOLVENT DMSO
NS 4
DS 16
SWH 4310.345 Hz
FIDRES 4.209321 Hz
AQ 0.1187840 sec
RG 2050
DW 116.000 usec
DE 6.50 usec
TE 294.9 K
CNST2 145.0000000
CNST13 5.0000000
D0 0.00000300 sec
D1 1.47951996 sec
D2 0.00344828 sec
D6 0.10000000 sec
D16 0.00020000 sec
IN0 0.00002240 sec

------ CHANNEL f1 ------
SFO1 400.1322009 MHz
NUC1 1H
P1 11.06 usec
P2 22.12 usec
PLW1 24.29199982 W

------ CHANNEL f2 ------
SFO2 100.6228138 MHz
NUC2 13C
P3 8.90 usec
PLW2 58.63899994 W

------ GRADIENT CHANNEL ------
GPNAM[1] SMSQ10.100
GPNAM[2] SMSQ10.100
GPNAM[3] SMSQ10.100
GPZ1 50.00 %
GPZ2 30.00 %
GPZ3 40.10 %
P16 1000.00 usec

F1 - Acquisition parameters
TD 256
SFO1 100.6228 MHz
FIDRES 87.193077 Hz
SW 221.833 ppm
FnMODE QF

F2 - Processing parameters
SI 1024
SF 400.1300000 MHz
WDW QSINE
SSB 2
LB 0 Hz
GB 0
PC 1.40

F1 - Processing parameters
SI 512
MC2 QF
SF 100.6127690 MHz
WDW QSINE
SSB 2
LB 0 Hz
GB 0

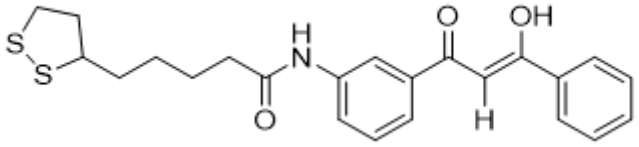

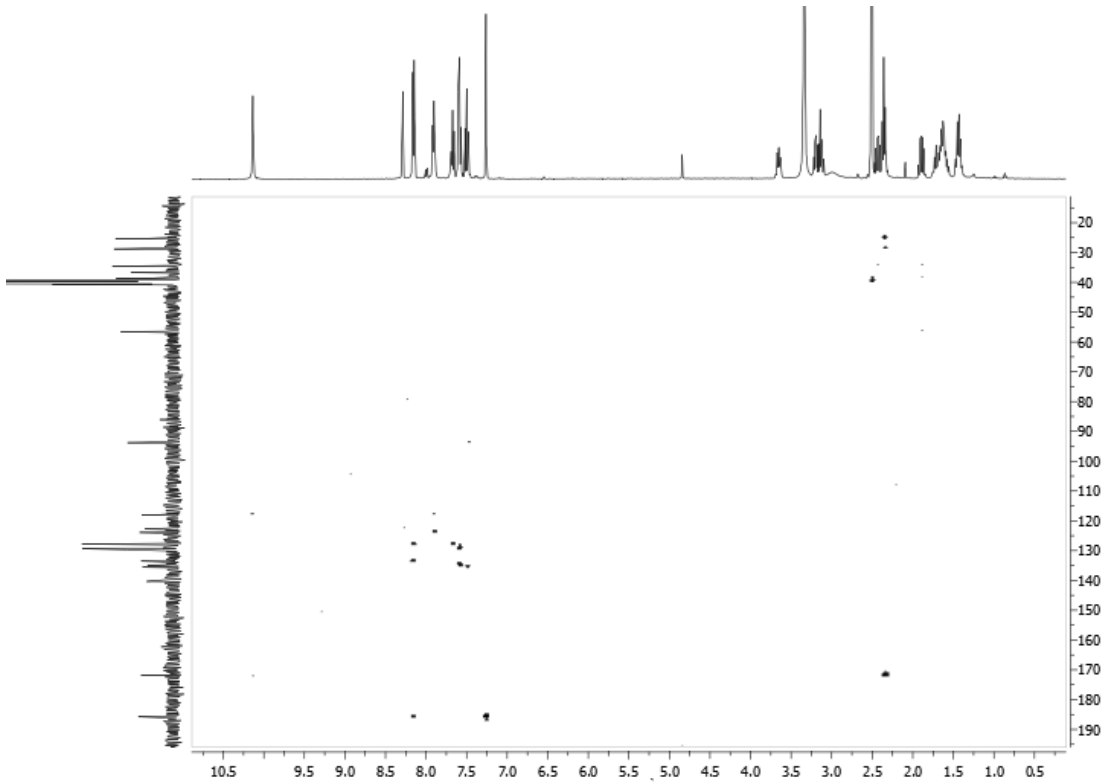

*HMBC of **DBMSS** in d_6 DMSO*

F2 - Acquisition Parameters
Date 20160624
Time 0.27
INSTRUM spect
PROBHD 5 mm PADUL 13C
PULPROG hmbcgplpndqf
TD 1024
SOLVENT DMSO
NS 4
DS 16
SWH 4310.345 Hz
FIDRES 4.209321 Hz
AQ 0.1187840 sec
RG 2050
DW 116.000 usec
DE 6.50 usec
TE 294.9 K
CNST2 145.0000000
CNST13 5.0000000
D0 0.00000300 sec
D1 1.47951996 sec
D2 0.00344828 sec
D6 0.10000000 sec
D16 0.00020000 sec
IN0 0.00002240 sec

------ CHANNEL f1 ------
SFO1 400.1322009 MHz
NUC1 1H
P1 11.06 usec
P2 22.12 usec
PLW1 24.29199982 W

------ CHANNEL f2 ------
SFO2 100.6228138 MHz
NUC2 13C
P3 8.90 usec
PLW2 58.63899994 W

------ GRADIENT CHANNEL ------
GPNAM[1] SMSQ10.100
GPNAM[2] SMSQ10.100
GPNAM[3] SMSQ10.100
GPZ1 50.00 %
GPZ2 30.00 %
GPZ3 40.10 %
P16 1000.00 usec

F1 - Acquisition parameters
TD 256
SFO1 100.6228 MHz
FIDRES 87.193077 Hz
SW 221.833 ppm
FnMODE QF

F2 - Processing parameters
SI 1024
SF 400.1300000 MHz
WDW QSINE
SSB 2
LB 0 Hz
GB 0
PC 1.40

F1 - Processing parameters
SI 512
MC2 QF
SF 100.6127690 MHz
WDW QSINE
SSB 2
LB 0 Hz
GB 0

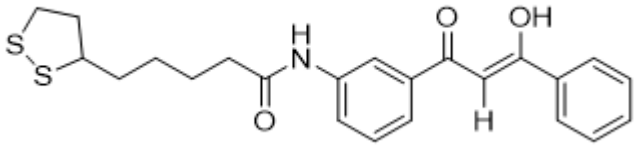

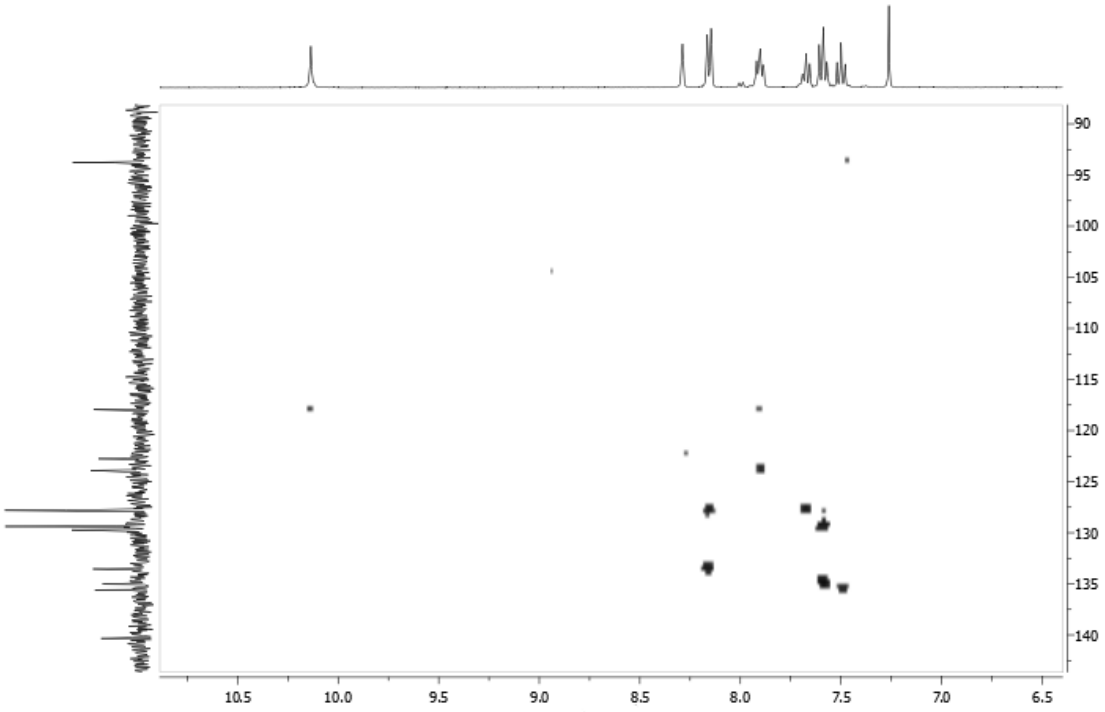

*HMBC of aromatic region of **DBMSS** in d_6 DMSO*

F2 - Acquisition Parameters
Date 20160624
Time 0.27
INSTRUM spect
PROBHD 5 mm PADUL 13C
PULPROG hmbcgplpndqf
TD 1024
SOLVENT DMSO
NS 4
DS 16
SWH 4310.345 Hz
FIDRES 4.209321 Hz
AQ 0.1187840 sec
RG 2050
DW 116.000 usec
DE 6.50 usec
TE 294.9 K
CNST2 145.0000000
CNST13 5.0000000
D0 0.00000300 sec
D1 1.47951996 sec
D2 0.00344828 sec
D6 0.10000000 sec
D16 0.00020000 sec
IN0 0.00002240 sec

-------- CHANNEL f1 --------
SFO1 400.1322009 MHz
NUC1 1H
P1 11.06 usec
P2 22.12 usec
PLW1 24.291999982 W

-------- CHANNEL f2 --------
SFO2 100.6228138 MHz
NUC2 13C
P3 8.90 usec
PLW2 58.63899994 W

------ GRADIENT CHANNEL -----
GPNAM[1] SMSQ10.100
GPNAM[2] SMSQ10.100
GPNAM[3] SMSQ10.100
GPZ1 50.00 %
GPZ2 30.00 %
GPZ3 40.10 %
P16 1000.00 usec

F1 - Acquisition parameters
TD 256
SFO1 100.6228 MHz
FIDRES 87.193077 Hz
SW 221.833 ppm
FnMODE QF

F2 - Processing parameters
SI 1024
SF 400.1300000 MHz
WDW QSINE
SSB 2
LB 0 Hz
GB 0
PC 1.40

F1 - Processing parameters
SI 512
MC2 QF
SF 100.6127690 MHz
WDW QSINE
SSB 2
LB 0 Hz
GB 0

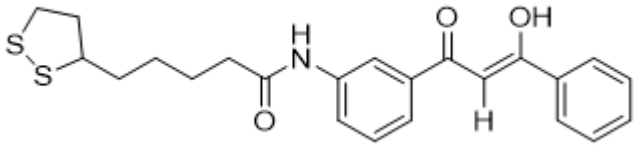

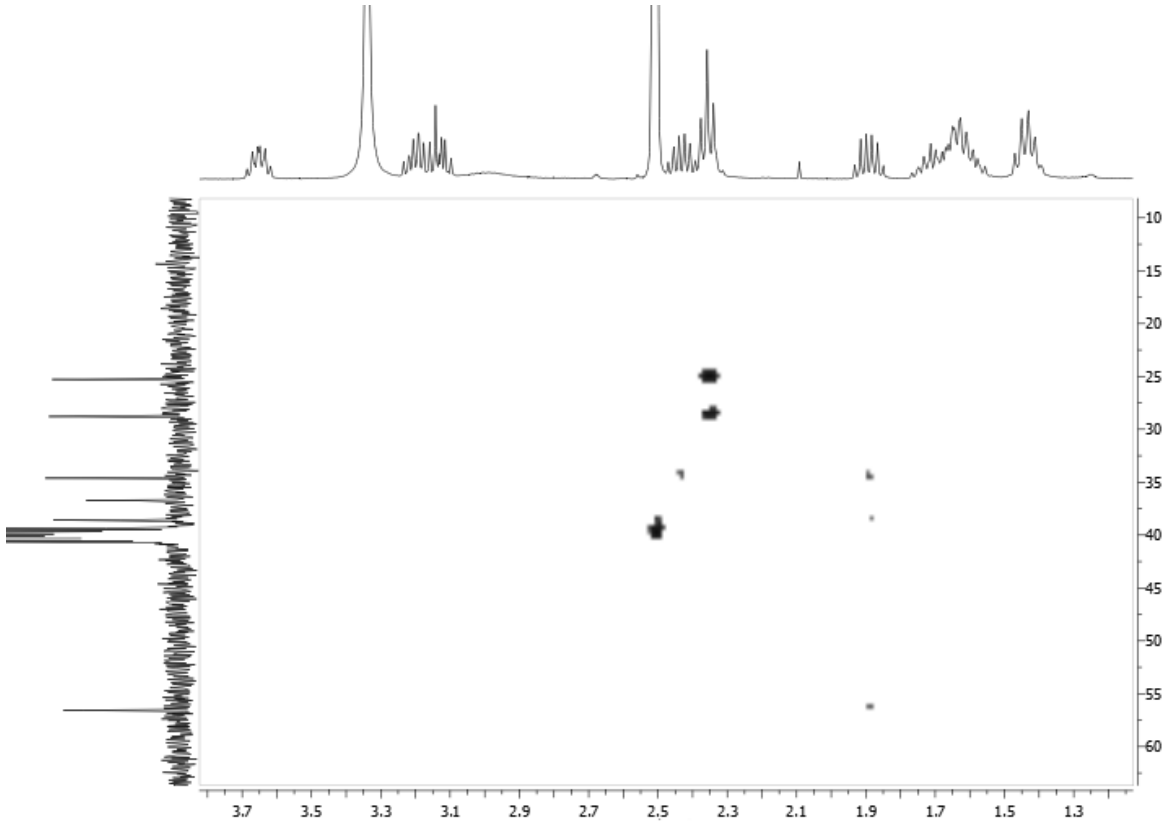

*HMBC of aliphatic region of **DBMSS** in d_6 DMSO*

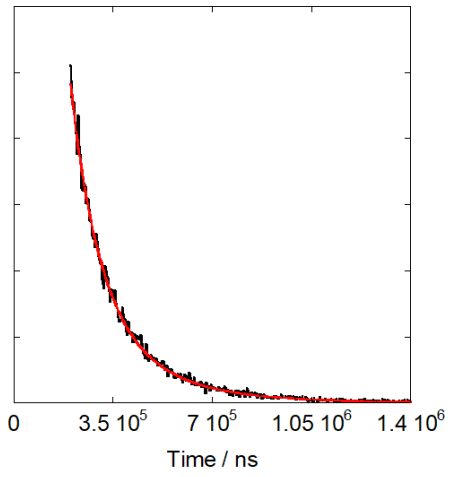

Lifetime of ***Eu(DBMSS)$_3$*** *in MeOH, λ_{exc} = 350 nm, λ_{exc} = 614 nm.*

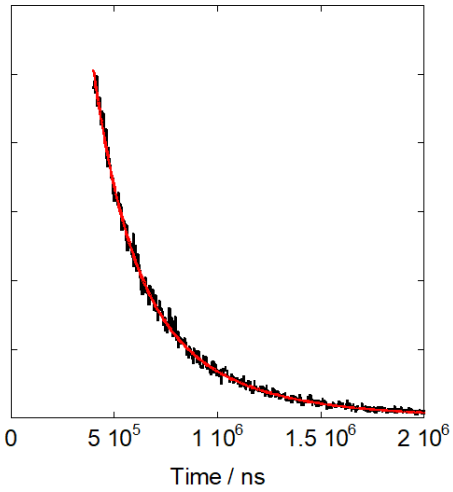

Lifetime of ***Eu(DBMSS)$_3$*** *in MeOD, λ_{exc} = 350 nm, λ_{exc} = 614 nm.*

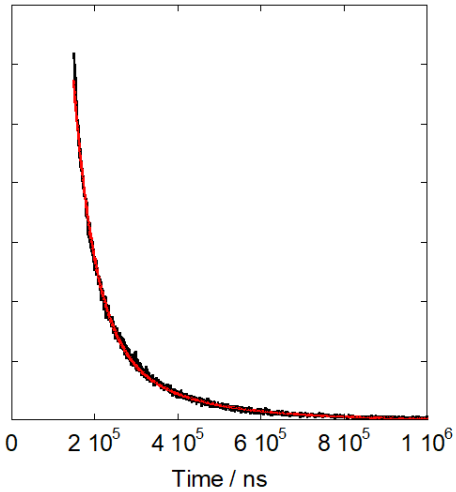

Lifetime of ***Eu.DBMSS.Z@Au*** *in H_2O, λ_{exc} = 350 nm, λ_{exc} = 614 nm.*